The role of oxidative stress in photoreceptor degeneration

Dafni Vlachantoni

PhD

The University of Edinburgh

2006

Declaration

I declare that this thesis was composed by myself. The contributions of others to the work are clearly indicated. This work has not been submitted for any other degree or professional qualification.

Dafni Vlachantoni
July 2006

Acknowledgements

First of all, I would like to thank my supervisor, Alan Wright, for giving me the opportunity to work on this project. I would literally not be writing this if it weren't for his constant faith in me, support and guidance, especially when things were not going according to plan!

It has been a great pleasure working in Alan's group and I would especially like to thank Brian Tulloch, Xinhua Shu, Alan Lennon, Kevin Chalmers, Julie Ferguson, Morad Ansari and Fern Slinsgby for advice and support throughout the project. Thank you also to Caroline and Veronique and the remaining members of the Population Genetics Group for their support.

Thank you to Veronica van Heyningen for her support and interest in this project, to everyone in the office and to members of the E2 lab for contributing to a supportive, collaborative and enjoyable lab atmosphere.

I am grateful to Doug Turnbull at the University of Newcastle and to members of his lab, especially Rob Taylor, Martin Barron, Langping He, Laura Greaves and Ali McGill, for helping me to set up various experimental methods and for allowing me to use their spectrophotometer (quite a lot!).

A big thank you to Lisa McKie, Ian Jackson, Alan Hart and Sally Cross for advice on and help with animal breeding. To Paul Perry for support (and patience!) with microscopy work. To Allyson Ross for advice on histology work. To Mary O'Connell for advice on scintillation counting. To Peter Teague for statistical advice and to Sandy Bruce for help with photography and binding. Also to Linda and Davy from the BRF for taking care of the mouse colonies.

I would also like to thank Mike Murphy, from the MRC Dunn- Unit and from Antipodean Pharmaceuticals, for providing the MitoQ and for advice and suggestions on various MitoQ-related experimental procedures. Graeme Pettigrew from the University of Edinburgh for advice and support on setting up enzyme assays. Sebastian Calligaris, from Italy, for providing the protocol for GSH measurements and advice on its optimization.

During the past few years numerous friends have been a source of unconditional support and good distraction! I would like to particularly thank Andrea, Lorna, Fabio, Sahdia, Marit, Julie, David and Kyra for being there, for believing that I could get to the stage of writing my acknowledgements and for motivating me, especially during writing up! Thank you also to the 'Hillviewers' Maija, Tim, Julie, Hugo and Pierre for making home a nice place to go to after a long day in the lab!

Thanks to Alan, Kevin, Brian and Andrea for discussing and/or reading parts of this thesis. I'd also like to thank my sister Athina who, from a Social Policy and Politics background, read the whole thesis and at the end asked whether GSH, whose levels were decreased in some mutants, stands for Good Sense of Humour!

Finally, I cannot thank enough my family, Nina, Theodore, Iris and Athina, who even from a long distance provided continuous and unconditional support and encouragement

Table of contents

Abstract

Reactive oxygen species (ROS) are constitutively produced by mitochondria and represent the major cellular source of oxidative stress. ROS are capable of attacking molecules such as DNA, proteins and lipids, and of compromising either the structural and functional integrity or the survival of cells. Mitochondria also play a key role in apoptosis, the major mechanism of cell death in retinitis pigmentosa (RP), which is a diverse group of inherited human retinal dystrophies associated with progressive degeneration of photoreceptor cells. Mutations in numerous genes have been implicated in RP, which have distinct pathophysiological mechanisms and lead to retinal degeneration at different rates. The aim of this thesis was to investigate the role of oxidative stress in disease progression using mouse models of human RP.

The mouse mutants retinal degeneration 1 (*rd1/rd1*), atypical retinal degeneration 1 (*atrd1/atrd1*), rhodopsin knockout ($Rho^{-/-}$) and peripherin/retinal degeneration slow (*rds/rds*) were firstly investigated for evidence of oxidative damage by analysis of oxidative stress markers. Secondly, the mutants were crossed to a superoxide dismutase 2 heterozygous mouse ($Sod2^{+/-}$), with decreased mitochondrial antioxidant activity, to examine the effect on disease progression. Thirdly, mutants were treated with a mitochondrially targeted ubiquinone derivative (MitoQ), which is a powerful antioxidant, to try and slow the rate of retinal degeneration. MitoQ was administered orally during pregnancy and for an extended postnatal period and uptake, toxicity, breeding behaviour and survival were assessed. Rates of photoreceptor degeneration were estimated by morphometric and apoptosis assays, while the cellular redox status was assessed by glutathione assays and by measuring the activities of the mitochondrial enzymes NADH:ubiquinone oxidoreductase (complex I), which is oxidative stress-sensitive, compared with citrate synthase, which is oxidative stress-insensitive.

All retinal degeneration mutants were found to show significantly reduced complex I activities, while citrate synthase was unchanged, indicating mitochondrial oxidative stress. Rates of photoreceptor degeneration were unchanged either by crossing to a $Sod2^{+/-}$ genetic background or by MitoQ administration. Only the *rds/rds* mutant, with the slowest rate of degeneration, showed a significant increase in complex I activity after MitoQ administration. Although mitochondrial oxidative stress is shown to be present in all of the retinal degeneration mutants, altering the oxidative status of the retina had no effect on photoreceptor survival.

LIST OF ABBREVIATIONS

8-oxoG	7,8-dihydrox-8-oxoguanosine
AAV	Adeno-associated virus
ALS	Amyotrophic lateral sclerosis
ANT	Adenine nucleotide translocator
APS	Adenosine 5'-phosphosulfate, sodium salt
ATP	Adenosine triphosphate
atrd1	Atypical retinal degeneration 1 mutant mouse (*pde6b*^{atrd1})
BCG	Bacillus Calmette-Guerin
BSA	Bovine serum albumin
BSO	L-buthionine-(S,R)-sulfoximine
cAMP	Cyclic adenosine 3' 5' monophosphate
CAT	Catalase
CI	Complex I (NADH:ubiquinone oxidoreductase)
CoQ	Coenzyme Q (Ubiquinone)
COX	Cytochrome *c* oxidase
CS	Citrate synthase
DAPI	Diamidino-2-phenyl-indol
DBD	DNA binding domain
DNA	Deoxyribonucleic acid
dNTP	Deoxynucleotide triphosphate
DTNB	Dithionitrobenzoic acid
EDTA	Ethylenediaminetetraacetic acid
EGTA	Ethyleneglycoltetraacetic acid
ELISA	Enzyme-Linked Immunosorbent Assay
ENU	N-ethyl-N-nitrosourea
ER	Endoplasmic reticulum
ERG	Electroretinography
ETC	Electron transport chain
$FADH_2$	Flavin adenine dinucleotide (reduced)
FCCP	Carbonyl cyanide p-trifluotomethoxyphenylhydrazone
Fe^{2+}	Ferrous ion

FITC	Fluorescein isothiocyanate
FRDA	Friedreich's ataxia
GC	Ganglion cells
GPX	Glutathione peroxidase
GR	Glutathione reductase
GSH	Glutathione (reduced)
GSSG	Glutathione (oxidised)
GTP	Guanosine triphosphate
H&E	Haematoxylin and Eosin
H_2O_2	Hydrogen peroxide
HIF	Hypoxia inducible factor
HNE	4-Hydroxynonenal
IBM	Inner boundary membrane
IBTP	4-Iodobutyl-triphenylphosphonium
IMS	Intermembrane space
INL	Inner nuclear layer
IPL	Inner plexiform layer
IR	Ischemia-reperfusion
IS	Inner segment
KCN	Potassium cyanide
KO	Knock out
LHON	Leber's hereditary optic neuropathy
LP	Lipid peroxidation
MDA	Malondialdehyde
$MgCl_2$	Magnesium chloride
MIM	Mitochondrial inner membrane
MnTBAP	Manganese 5,10,15,20-tetrakis (4-benzoic acid) porphyrin
MOM	Mitochondrial outer membrane
MSS	Mutant steady state
mtDNA	Mitochondrial DNA
NADH	Nicotinamide adenine dinucleotide (reduced)
NADPH	Nicotinamide adenine dinucleotide phosphate (reduced)

NBT	Nitro blue tetrazolium chloride
NMDA	*N*-methyl-D-aspartic acid
NO	Nitric oxide
Ntyr	Nitrotyrosine
O_2-·	Superoxide anion
OAA	Oxaloacetate
·OH	Hydroxyl radical
ONH	Optic nerve head
ONL	Outer nuclear layer
ONOO-	Peroxynitrite
OPL	Outer plexiform layer
OS	Outer segment
OXPHOS	Oxidative phosphorylation
PARP	Poly (ADP-ribose) polymerase
PBS	Phosphate buffered saline
PCR	Polymerase chain reaction
PDE	3'-5' cyclic guanosine monophosphate phosphodiesterase
PFA	Paraformaldehyde
Pi	Phosphate inorganic
PM	Plasma membrane
PS	Phosphatidylserine
PTP	Permeability transition pore
PUFAs	Polyunsaturated fatty acids
rd1	Retinal degeneration 1 mutant mouse ($Pde6b^{atrd1}$)
rds	Retinal degeneration slow mutant mouse ($Prph2^{rds}$)
REDOX	Reduction/oxidation
Rho	Rhodopsin mutant mouse
ROS	Reactive oxygen species
RP	Retinitis pigmentosa
RPE	Retinal pigment epithelium
RT	Room temperature
RT-PCR	Reverse transcribed polymerase chain reaction

S/n	Supernatant
SDH	Succinate dehydrogenase
SDS	Sodium dodecyl sulfate
SOD	Superoxide dismutase
SSC	Saline-sodium citrate
TBARS	Thiobarbituric acid reactive substances
TBE	Tris/Borate/EDTA
TEA	Triethanolamine
TNFα	Tumour necrosis factor-alpha
TPMP	Methyltriphenylphosphonium
TUNEL	Terminal deoxynucleotidyl transferase-mediated dUTP-biotin nick end-labelling
UV	Ultraviolet
VDAC	Voltage-dependent anion channel
VitE	Vitamin E

LIST OF FIGURES

LIST OF TABLES

CHAPTER 1

INTRODUCTION

1.1. Oxidative stress

1.1.1. Definition

Cells aim to achieve a state of chemical equilibrium so that fundamental processes, such as development, growth, metabolism and death, can be carried out efficiently. The reduction (= gain of electrons)/oxidation (= removal of electrons) (REDOX) state of the intracellular environment is crucial for the functioning of many enzymes and its distortion towards the oxidative state can cause problems that lead to cellular dysfunction and, ultimately, to cell death. If the relative amounts of oxidants and antioxidants change in favour of the former, then oxidative stress is generated. Oxidative stress has been broadly defined as the imbalance between the rate of formation of reactive oxygen species and their elimination by antioxidants (Halliwell & Gutteridge, 1999; Koutsilieri *et al.*, 2002). 'Reactive oxygen species' (ROS) is an umbrella term used to describe potentially toxic by-products of reduced oxygen. ROS can be either free radicals - i.e. chemical species capable of independent existence with at least one unpaired electron in their outer orbit (Beatty *et al.,* 2000) - or molecules with their full complement of electrons, but in an unstable or reactive state (Winkler *et al.,* 1999; Beatty *et al.,* 2000; Freitas *et al.,* 2002). Consequently, an antioxidant has been defined as a mechanism, enzyme or compound that counteracts a defined oxidant.

Most free radicals are very reactive molecules, because of their unstable electron configuration and their search for stability through the acquisition of another electron. This electron needs to be 'stolen' from a stable molecule, which in turn becomes a free radical itself. Therefore, a chain of reactions commences, in which molecules attack each other. Not all free radicals are oxidants, for instance molecular oxygen has two unpaired electrons, and also not all oxidants are free radicals, for example hydrogen peroxide (Winkler *et al.,* 1999).

The most common metabolites of oxygen are superoxide anions ($O_2^{-\bullet}$), hydrogen peroxide (H_2O_2) and hydroxyl radicals ($^{\bullet}OH$), mentioned in order both of formation, as intermediates during the partial one-electron-at-a-time reduction of oxygen to water (**Figure 1**), and of increased reactivity. In brief, superoxide anion is generated by the univalent reduction of molecular oxygen. Although it is not very reactive and cannot diffuse through cell membranes, it can react with

nitric oxide (NO) to generate the oxidant peroxynitrite ($ONOO^-$) (Rego *et al.*, 2000). Addition of one more electron to superoxide anion can give rise to the next most reactive oxygen species, hydrogen peroxide. Although hydrogen peroxide has no unpaired electrons, and hence is not very reactive (Lledias *et al.*, 1998), its oxidising properties can kill bacteria. Its most dangerous property lies in its slow reactivity in the absence of ferrous ion (Fe^{2+}), which gives it time to diffuse into more distant cellular compartments (Barbouti *et al.*, 2002). In the presence of transition metals, however, H_2O_2 can participate in the Fenton reaction, which results in the formation of the most reactive of all free radicals, the hydroxyl radical, ($^{\bullet}OH$). Hydroxyl radicals can also be formed by the reaction of superoxide anion and hydrogen peroxide (Haber-Weiss reaction) and it is virtually impossible to stop them from reacting with the first molecule in their path (Halliwell & Gutteridge, 1999).

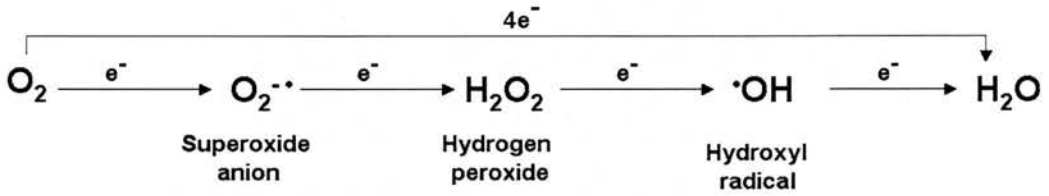

Figure 1: Reactive Oxygen Species

Addition of four electrons to molecular oxygen leads to its full reduction to water. Sequential addition of single electrons results in the partial reduction of oxygen and the generation of the reactive oxygen species (ROS) superoxide anion, hydrogen peroxide and hydroxyl radical.

1.1.2. Generation of oxidative stress

1.1.2.1. Mitochondria

The main source of endogenous ROS is the mitochondrion, although is also known to occur in other organelles (Esposito *et al.*, 1999; Melov *et al.*, 1999; Hansen *et al.*, 2006). Mitochondria are intracellular organelles found in all eukaryotic cells. It is widely accepted that their ancestors are α-proteobacteria that lived in primitive eukaryotic cells as intracellular parasites (Larsson & Luft, 1999;

Rivera & Lake, 2004) and were later transformed into organelles that are dependent on the nucleus for their function and replication.

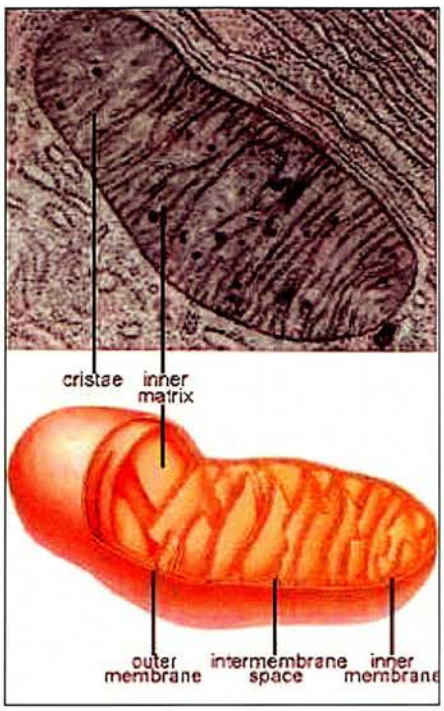

Figure 2: The structure of a mitochondrion

Mitochondria are typically rod-shaped organelles of about 1-10 μm in length. They have two specialised membranes, the inner (MIM) and outer membranes (MOM), which divide the organelle into a narrow inter-membrane space (IMS) and a much larger internal matrix. The surface of the inner membrane is increased by a large number of infoldings called cristae. [Image from http://www.spiralnotebook.org/ingraphicdetail]

The structure of mitochondria (**Figure 2**) is well established (reviewed in Frey & Mannella, 2000). They are bound by two membranes, the mitochondrial outer (MOM) and inner (MIM) membranes, which are separated by the inter-membrane space (IMS) that is about 28 nm wide (Perkins *et al.,* 1997). These membranes enclose the mitochondrial matrix, which includes proteins and DNA. Pioneering work by Palade (1953) showed that the MIM is itself further divided into two components whose surfaces are contiguous; the inner boundary membrane (IBM) and the cristae. Although the latter, which increase the surface of the MIM several fold, were initially thought to be broad foldings of the MIM

(Palade, 1953), it is now clear that they have a mean diameter of about 31 nm and are connected to the IBM via narrow, 28 nm in diameter, tubular openings called cristae junctions (Perkins *et al.,* 1997). The MOM is the physical barrier, separating the cytoplasmic from the mitochondrial metabolic processes, and the flux of molecules through it is mediated by the pore-forming protein voltage-dependent anion channel (VDAC) (Mannella *et al.,* 1992). The MIM is more selective in its permeability and allows substances to flow through it only via tightly regulated transporters, complexes and pumps. The shape and copy number of mitochondria are determined by ongoing mitochondrial fusion and fission events, which can vary between different cells and over time (Bleazard *et al.,* 1999). Even within the same cell, mitochondrial shape can range from spherical organelles to branched tubular networks (Bereiter-Hahn *et al.,* 1994).

Mitochondria have their own DNA (referred to as mtDNA), which is a circular double stranded molecule of 16,569 base pairs in length in humans and can be present in anything from tens to tens of thousands of copies per cell (Larrson & Luft, 1999; GOBASE at http://gobase.bcm.umontreal.ca/index.php). MtDNA encodes 37 genes and has a compact structure containing overlapping genes and no introns (Montoya *et al.,* 1983; Rose *et al.,* 2002). The transcription products of 13 of these are mRNAs, 22 are tRNAs, and 2 are rRNAs (Anderson *et al.,* 1981). Therefore, only a small fraction of the ~1500 proteins required for normal mitochondrial functioning is encoded by mtDNA (Wallace, 2005). Most mitochondrial proteins are synthesised in the cytosol and then targeted to the mitochondrion by short peptide signal sequences (Chinnery & Turnbull, 2000).

1.1.2.2. The oxidative phosphorylation system

Mitochondria have been called the powerhouses of the cell as they produce cellular energy, in the form of adenosine 5'-triphosphate (ATP), by oxidative phosphorylation (OXPHOS) (Kim *et al.,* 2002; Nijtmans *et al.*, 2004). The mammalian OXPHOS system resides in the MIM and comprises the four

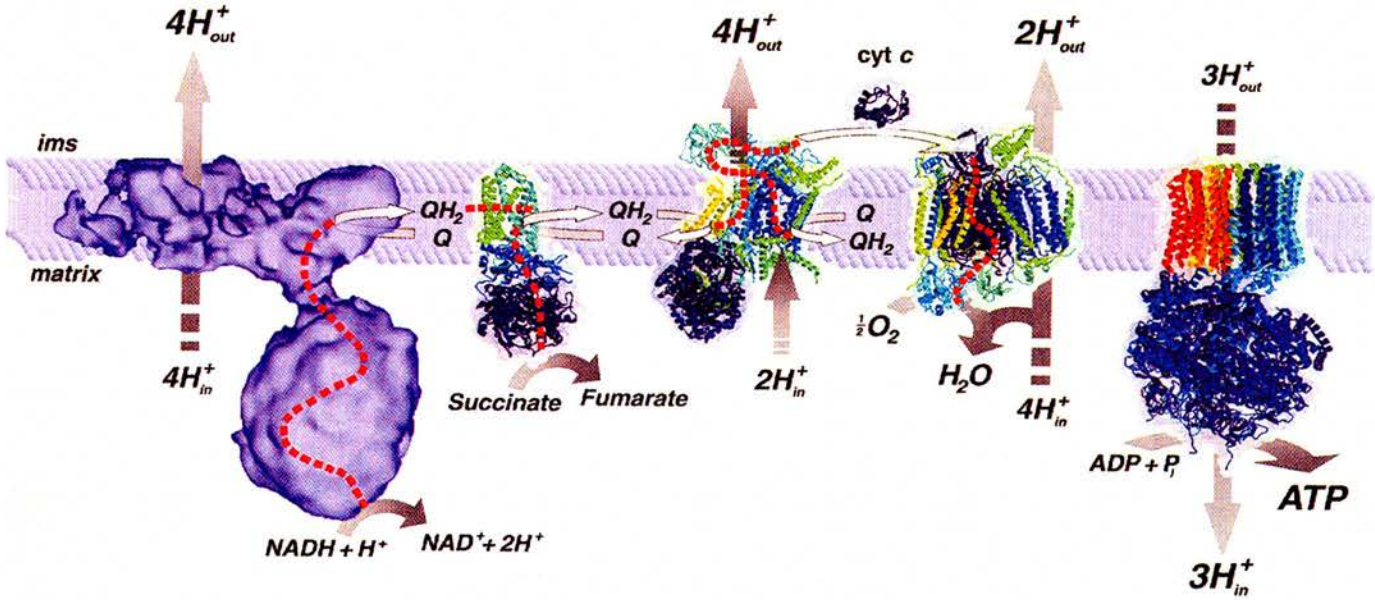

	complex I	complex II	complex III	complex IV	complex V
Name	NADH:ubiquinone oxidoreductase	Succinate:ubiquinone oxidoreductase	Ubiquinol:cytochrome c oxidoreductase	Cytochrome c oxidase	ATP synthase
# of subunits	46	4	11	13	14
mtch : nuclear	7:39	0:4	1:10	3:10	2:12
Inhibitors	Rotenone Piercidin A	Malonate	Antimycin Myxothiazone	Cyanide	Oligomycin

Figure 3: Oxidative phosphorylation

Oxidative phosphorylation (OXPHOS) comprises the four complexes (I-IV) of the respiratory chain and ATP synthase (complex V). As indicated by the red dotted lines, electrons flow through the respiratory chain to eventually reduce molecular oxygen to water.At the same time, protons are translocated from the matrix to the intermembrane space (ims), generating an electrochemical gradient across the mitochondrial inner membrane. This gradient is then used by ATP synthase to form ATP from ADP and Pi. Each of the complexes of the OXPHOS system consists of multiple subunits, some of which are encoded by mitochondrial DNA (mtch) and some by nuclear DNA. Finally, the inhibitors that are specific to each complex are also shown. [Image taken from Nijtmans *et al.*, 2004]

mitochondrial respiratory chain complexes (complexes I-IV) and ATP synthase (complex V) (**Figure 3**). They are collectively composed of at least 90 different polypeptide subunits, 13 of which are mitochondrially encoded (Nijtmans *et al.*, 2004). Animals release energy from their diet, which includes proteins, lipids and carbohydrates, by oxidising them to CO_2 and H_2O. The Krebs cycle is responsible for most of these oxidation reactions and the energy yield is conserved in the form of the reduced electron-accepting coenzymes nicotinamide adenine dinucleotide phosphate (NADH) and a reduced form of flavin adenine dinucleotide ($FADH_2$) (Nijtmans *et al.*, 2004). The electrons of these coenzymes can be used to reduce molecular oxygen to H_2O via the respiratory chain (Beatty *et al.*, 2000). The 4 multi-subunit complexes of the ETC are (Larsson & Luft, 1999; Nijtmans *et al.*, 2004):

Complex I (CI): NADH: ubiquinone oxidoreductase (EC 1.6.5.3)
Complex II (CII): succinate: ubiquinone oxidoreductase (EC 1.3.5.1)
Complex III (CIII): ubiquinol: cytochrome *c* reductase (EC 1.10.2.2)
Complex IV (CIV): cytochrome *c* oxidase (EC 1.9.3.1)

The generation of energy through OXPHOS is a complicated process that involves electron flow through the respiratory chain (Nijtmans *et al.*, 2004). The latter is also therefore referred to as electron transport chain (ETC) (**Figure 3**). Electrons are donated from NADH to CI or from succinate to CII, and are then passed on to coenzyme Q (CoQ) to generate ubisemiquinone (CoQH) and then ubiquinol ($CoQH_2$). Electrons are further donated to CIII, which transfers them via cytochrome c to CIV. Eventually they are used to reduce O_2 to H_2O. During the transport of electrons, protons (H^+) are pumped from the matrix out to the IMS via complexes I, III and IV, giving rise to both a pH and an ionic gradient across the MIM. This electrochemical gradient ($\Delta\psi$) has been named the proton-motive force and is used by the last complex of the OXPHOS system, the ATP synthase, to generate ATP from ADP and inorganic phosphate (Pi). ADP and Pi can enter the mitochondrion through ATP Synthase and act as substrates for ATP generation on the matrix side of the MIM. This ATP is then exchanged for cytosolic ADP through an adenine nucleotide translocator (ANT) located in the MIM (Rose *et al.*, 2002; Genova *et al.*, 2003).

1.1.2.3. Leakage of electrons and free radical formation

About 90% of the oxygen consumed by the cell is used by the ETC for ATP production, while the remaining 10% is used by reactions involving oxidases and oxygenases (Beatty *et al.*, 2000; Raza *et al.*, 2002). Of this 90%, about 0.4-4% of the respired oxygen undergoes incomplete reduction to superoxide anion, the first ROS to be formed (Melov *et al.*, 2001; Noor *et al.*, 2002). The main sites of electron leakage, and hence of superoxide anion formation, are CI and CIII (Herrero & Barja, 1997; Nulton-Persson & Szweda, 2001; Genova *et al*, 2003). $O_2^{-\bullet}$ is then rapidly converted to H_2O_2 by superoxide dismutase (SOD). As noted earlier, H_2O_2 can readily react with Fe^{2+} and participate in the Fenton reaction to generate the most reactive of all ROS, $^{\bullet}OH$ (Bilinski *et al.*, 1985; Nulton-Persson & Szweda, 2001). This series of reactions is shown in **Figure 4**.

Leakage of electrons occurs even under normal physiological conditions and hence ROS production is a constitutive cellular event. However, the low percentage of partially reduced oxygen can be increased if the ETC is inhibited or cannot counteract the concentration of oxidants present within the cell.
This can be the result of:

a) Inhibition of an ETC complex

Inhibition of one of the complexes of the ETC results in the accumulation of electrons at complex I and ubiquinone (UQ) pool sites (Nulton-Persson & Szweda, 2001; Pitkanen & Robinson, 1996). Some specific inhibitors for each of the complexes are given in **Figure 3**.

b) Inhibition of a Krebs cycle enzyme

If the progress of the Krebs cycle is disrupted, then there are not enough substrates (namely, NADH and $FADH_2$) for electron transport to take place along the ETC. For example, aconitase can be inhibited by fluoroacetate and *N*-methyl-D-aspartic acid (NMDA). Oxidative stress can both result from Krebs cycle inhibition, and it can also be the cause of it. The enzymes implicated in the cycle have different sensitivities to oxidants. Aconitase, which catalyses the conversion of citrate to cis-aconitate, is very sensitive to $O_2^{-\bullet}$, but much less so to H_2O_2. It has a $[4Fe\text{-}4S]^{2+}$ active centre that can be readily converted by $O_2^{-\bullet}$ to

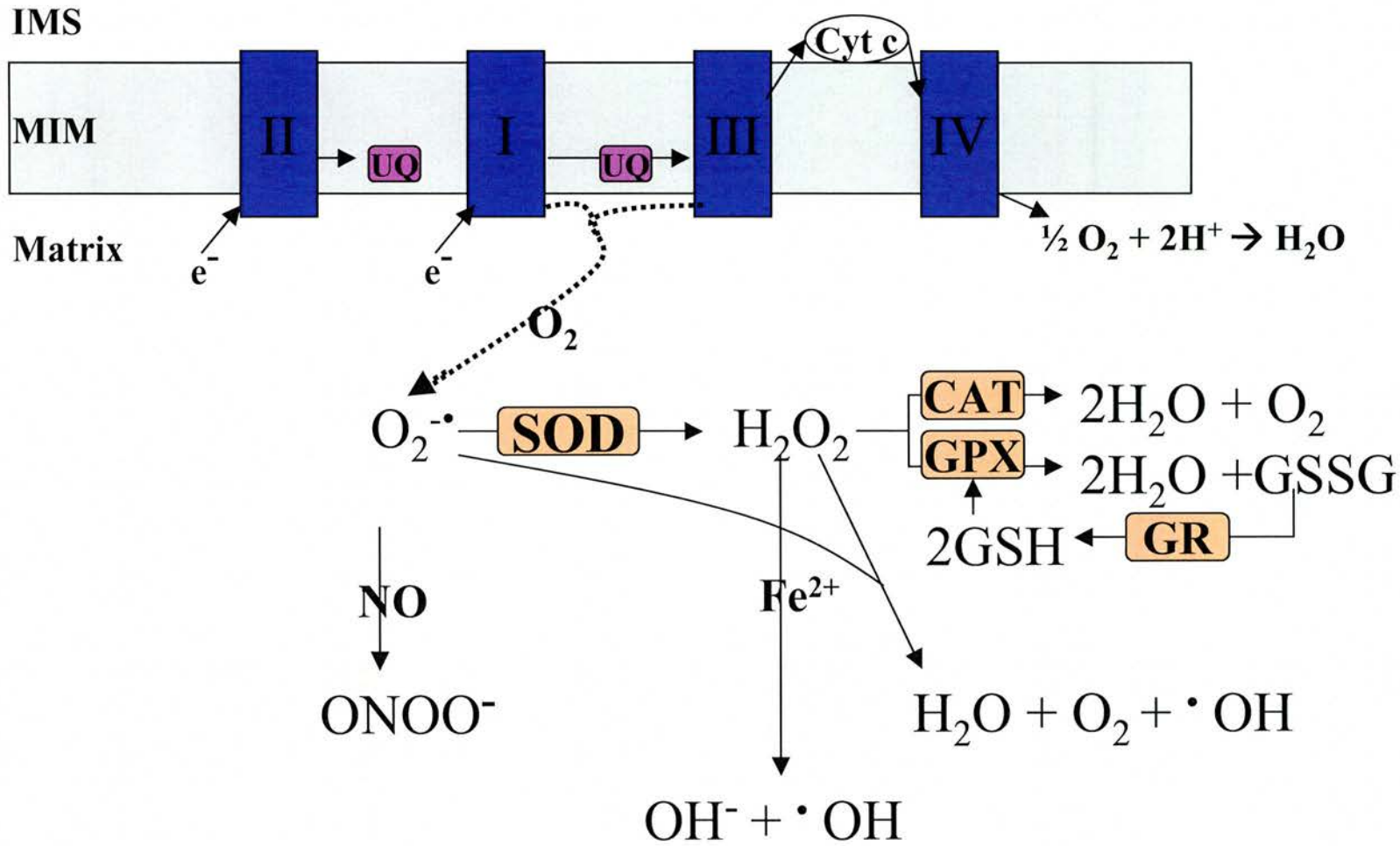

Figure 4: ROS production and antioxidant enzymes

Electrons flow through the four complexes of the electron transport chain that resides in the mitochondrial inner membrane (MIM) to eventually reduce molecular oxygen to water. Leaking electrons from complexes I and II partially reduce molecular oxygen to superoxide anion ($O_2^{-\bullet}$). This can react with nitric oxide (NO) and generate peroxynitrite ($ONOO^-$). The antioxidant enzyme superoxide dismutase (SOD) dismutates superoxide anions to hydrogen peroxide (H_2O_2), which is then detoxified by either catalase (CAT) or glutathione peroxidase (GPX). Hydrogen peroxide can react with either transition metals (Fenton reaction) or superoxide anions to generate hydroxyl radicals ($^{\bullet}OH$).

the inactive $[3Fe\text{-}4S]^+$ (Gardner *et al.,* 1994; 1995; Nulton-Persson & Szweda, 2001). The activity of the enzyme is often an indirect measure of the degree of oxidative stress in the cell.

c) Inhibition of ADP/ATP translocator

If ANT is blocked, it results in a depletion of intra-mitochondrial ADP, which in turn shuts down ATPase (Esposito *et al.,* 1999). This leads to the depletion of H^+ in the mitochondrial matrix and their accumulation in the IMS. As a result, the ETC is blocked, no electron flow takes place and electrons accumulate at the matrix-side of complexes I and III. These electrons are then available for converting molecular oxygen to superoxide radicals.

1.1.3. Damaging actions of reactive oxygen species

The extensive production of free radicals is regarded as a type of cellular stress. As mentioned earlier, free radicals, whether with complete electronic configurations or not, are in an unstable, and thus reactive, state. In order to achieve stability, they extract electrons from other molecules, which are themselves rendered unstable (Beatty *et al.,* 2000). Therefore, a cytotoxic oxidative chain reaction begins which can only be terminated either if two radicals react with each other and their unpaired electrons pair up, or if the new free radical generated is so poorly reactive that it is virtually harmless (Halliwell & Gutteridge, 1999). However, unless one of these two events takes place, ROS initiate a large number of oxidative reactions in cellular systems that lead to the oxidation of macromolecules like DNA, proteins and lipids (Winkler *et al.,* 1999; Freitas *et al.,* 2002; Koutsilieri *et al.,* 2002; Sverko *et al.,* 2002).

DNA is very sensitive to damage by H_2O_2 through Fenton-type reactions, which can result in base modifications, single-strand or double-strand breaks and/or sister chromatid exchanges (Barbouti *et al.,* 2002). The proximity of the mtDNA to the source of free radicals, the absence of protective histones and the limited repair mechanisms available make it a primary target for free radicals (Esposito *et al.,* 1999). As a result, mtDNA has at least a 10-fold higher mutation rate compared to the nuclear genome (Yakes & Van Houten, 1997). The identification of oxidant lesions in either nuclear or mtDNA has been performed by HPLC-electrochemical detection (Yakes & Van Houten, 1997). Such studies

have suggested that the most important DNA lesion produced during oxidative stress is the 7,8-dihydro-8-oxoguanine (8-oxoG), which, if not repaired, results in mutagenesis due to G:C to T:A transversions during DNA synthesis (Yakes & Van Houten, 1997; Soultanakis *et al.,* 2000). In addition, a good marker for mutations in mtDNA is the frequency of a common 4977bp-deletion (Wallace, 2005).

Proteins are also oxidatively damaged by free radicals, since post-translational modifications can impair their functions or inhibit them altogether. Not all proteins are uniformly susceptible to oxidative damage, but those that are include the Krebs cycle enzyme aconitase and complex I of the ETC, in part due to their close proximity to oxidative stress sources and to the presence of iron-sulphur clusters (Nulton-Person & Szweda, 2001; Beal, 2002). The most widely studied marker of protein oxidation is a protein carbonyl group, which is formed by direct oxidation of the side chains of lysine, arginine, proline and threonine residues (Levine *et al.,* 1990; Beal, 2002). The reaction of these groups with carbonyl-specific reagents, such as 2,4-dinitrophenylhydrazine, provides a method for detecting and quantifying protein oxidation (Frank *et al.,* 2000). Another marker of protein oxidation is a change in the protein's mass, which can be measured by mass spectrometry. A common example is the targeting of tyrosine residues by peroxynitrite, converting them to 3-nitrotyrosine and resulting in a 45 Da mass shift (Leeuwenburgh *et al.,* 1998; Nakagawa *et al.,* 2001; Sarver *et al.,* 2001; Beal, 2002).

Finally, polyunsaturated fatty acids (PUFAs) are particularly susceptible to oxidative stress (Kuhn & Borchert, 2002), because their conjugated double bonds are convenient sources of hydrogen atoms, which contain one free electron. The lipid radical formed then tries to capture an electron from another PUFA, in order to achieve stability. Thus, a cascade of reactions is initiated which results in the consumption of valuable PUFAs and the impairment of membrane structures.

Each of these damaging effects of ROS at the DNA, protein and lipid level, will be further discussed in Chapter III, where the methods for detecting and measuring oxidative damage are outlined.

1.1.4. Antioxidant defences

1.1.4.1. General

There are different endogenous antioxidant mechanisms, by which the cell is able to defend itself against free radical production. In general, these include lowering the steady-state concentration of free radical species, counteracting sources that generate cellular oxidants and/or limiting the likelihood that oxidative damage will occur (reviewed in Halliwell & Gutteridge, 1999).

Firstly, there are proteins, like haem oxygenase, that minimise the availability of pro-oxidants. Haem oxygenase is found in the endoplasmic reticulum (ER) and catalyses the breakdown of the pro-oxidant, haem. As haemoglobin undergoes slow oxidation to form biliverdin, ferrous ions (Fe^{2+}) and carbon monoxide are released and superoxide anions and ferric ions (Fe^{3+}) are also formed. There are also proteins capable of protecting against oxidative damage to proteins, for instance heat shock proteins. Their expression has been shown to increase in response to protein damage, facilitating rapid repair and recovery of damaged sites (Calderwood, 2005). In addition, there are low molecular mass agents, like glutathione and ascorbic acid, which are able to scavenge ROS and reactive nitrogen species (RNS). Lastly, cells have agents that catalytically remove free radicals and other reactive molecules. Examples of the latter are the antioxidant enzymes superoxide dismutase, glutathione peroxidase and catalase.

It is clear therefore that there is a range of ways in which the cell is able to cope with the production of ROS. These defence mechanisms are highly tissue-, cell type- and/or cellular localisation-specific. Depending on the physiology and metabolism of organelles, cells or tissues, different antioxidant defence mechanisms prevail, and often work in conjunction with each other. An example is the cellular compartmentalisation of catalase and glutathione peroxidase, discussed in section **1.1.4.2**.

1.1.4.2. Antioxidant enzymes

The primary antioxidant enzymes in mammalian cells are superoxide dismutase (SOD), glutathione peroxidase (GPX) and catalase (CAT) (Yen *et al.,* 1996) (**Figure 4**). Glutathione peroxidases are antioxidant enzymes involved in the primary defence against ROS. There are at least 4 isoforms of GPX, namely cytosolic GPX1, intestinal GPX2, plasma GPX3 and mitochondrial phospholipid hydroperoxide GPX4 (Ursini *et al.,* 1995, Esworthy *et al.,* 1997; Ho *et al.,* 1997; de Haan *et al.,* 1998; Singh & Shichi, 1998; Brigelius-Flohe, 1999; Esposito *et al.,* 2000; Melov, 2000). All are selenium-dependent homotetramers, which catalyse the reaction:

$H_2O_2 + 2GSH \rightarrow GSSG + 2H_2O$

Glutathione (GSH) is present in distinct cytoplasmic and mitochondrial pools (Griffith & Meister, 1985) and is oxidised to its stable oxidised form GSSG. Reduction of the latter by the enzyme glutathione reductase (GR) replenishes glutathione, maintaining high cellular levels of this antioxidant (van Remmen *et al.,* 1999). *Gpx1*$^{-/-}$ mice are healthy, fertile, show no histopathological abnormality for at least 15 months and are in general very similar to wild-type animals in the absence of oxidative challenge (de Haan *et al.,* 1998; Brigelius-Flohe, 1999).

Similar to GPX, CAT can also detoxify H_2O_2 to H_2O. It is an iron-dependent enzyme whose activity is regulated by zinc (Beatty *et al.,* 2000) and by the concentration of H_2O_2 (Yang *et al.,* 1998). Homozygous catalase knockout mice develop normally and show no gross abnormalities (Ho *et al.*, 2004).

As mentioned above, GPX and CAT have different cellular localisations and a series of studies have been concerned with their relative importance in detoxifying H_2O_2. These two enzymes catalyse the same reaction, namely the conversion of hydrogen peroxide to water and oxygen. They differ however in that catalase is found predominantly in peroxisomes and is absent from mitochondria (with the exception of heart mitochondria), whereas glutathione peroxidase is more abundant in mitochondria, as well as being present in a number of different cellular compartments, including the cytoplasm and the nucleus (Halliwell & Gutteridge, 1999; Melov, 2000). It has been reported that glutathione peroxidase is the main antioxidant enzyme used for scavenging

hydrogen peroxide, and its capacity for doing so depends also on the activity of glutathione reductase, on the rate of NADPH supply and on the glutathione content. In cellular compartments where both enzymes are present and active, glutathione peroxidase has the predominant role (Halliwell & Gutteridge, 1999), while catalase becomes more important in removing hydrogen peroxide as the latter's concentration increases. The main difference is that detoxification of H_2O_2 by CAT does not represent a stress to the cell, because it is converted to oxygen and H_2O, while detoxification by GPX generates energetic stress, since it is only accomplished by the oxidation of glutathione (Antunes *et al.,* 2002). The GSH redox cycle however is the primary means of protection against H_2O_2-induced damage at low concentrations of H_2O_2. When H_2O_2 concentrations rise, the importance of CAT in detoxifying this ROS increases (Halliwell & Gutteridge, 1999; Winkler *et al.,* 1999; Reddy *et al.,* 2001) since its efficiency is such that it cannot be saturated by H_2O_2 at any concentration (Lledias *et al.,* 1998). Surprisingly, no change in CAT activity has been detected in *gpx1*$^{-/-}$ mice (Forgione *et al.,* 2002).

1.1.4.2.1. Superoxide dismutase

Superoxide dismutase is one of the key antioxidant enzymes as it detoxifies superoxide anion to generate hydrogen peroxide. This reaction is very fast and is followed by the detoxification of hydrogen peroxide to water and oxygen by GPX and/or CAT. There are three isoforms of superoxide dismutase, SOD1, SOD2 and SOD3, all of which catalyse the same reaction, but differ in, amongst other things, their cellular localisation.

The first isoform of superoxide dismutase to be characterised was SOD1 (Halliwell & Gutteridge, 1999; Zelko *et al.,* 2002). The gene for SOD1 is on human chromosome 21 and on mouse chromosome 16. The human and mouse genes each have 5 exons, are 567 and 459 base pairs long respectively and show 81% homology at the DNA level. The translation products of the gene are 155 amino acids in the human and 153 amino acids in the mouse, which are 83% homologous. SOD1 (CuZnSOD) uses copper and zinc as its co-factors. It is the predominant SOD in most cells, as it accounts for 70-90% of the total cellular SOD activity, and is mainly cytosolic (Crapo *et al.,* 1992; van Remmen *et al.,*

2001; Matsui *et al.,* 2003). It is a 32 kDa homodimer that can be specifically inhibited by cyanide. Mutations in *SOD1* resulting in decreased SOD1 activity can cause progressive loss of motor neurons in familial amyotrophic lateral sclerosis (ALS) (Rosen *et al.,* 1993; Rothstein *et al.,* 1994).

The gene for the second isoform of superoxide dismutase, SOD2 (MnSOD), is on human chromosome 6 and on mouse chromosome 17 (Halliwell & Gutteridge, 1999). It has 5 exons in each species and the transcripts are 1026 and 1179 base pairs long, respectively, which are 78% homologous. The SOD2 protein in both species is 222 amino acids long and they are 90% homologous in human and mouse. Manganese is required as a co-factor for SOD2 and the protein, a 25kDa homotetramer, is strictly mitochondrial. SOD2 accounts for 10-20% of cellular SOD activity (van Remmen *et al.,* 2001) and cannot be inhibited by cyanide, which is often used to distinguish between the two isoforms.

The third isoform of superoxide dismutase, SOD3, is a homotetrameric CuZnSOD. The *SOD3* gene is on human chromosome 4 and on mouse chromosome 5 (Halliwell & Gutteridge, 1999). *SOD3* has 3 and 2 exons in human and mouse respectively, with transcripts that are 1816 and 1984 base pairs long, which are 64% homologous. The SOD3 protein is 240 amino acids in human and 251 amino acids long in the mouse and they are 64% homologous to each other. Copper and zinc are the cofactors for SOD3, which shows an extracellular localisation.

The relative importance of the intracellular isoforms SOD1 and SOD2 is reflected by the differing severity of the phenotypes in animals that have altered expression of these genes. Studies on *Sod2* null mice, both *in vitro* (Huang *et al.,* 1997) and *in vivo* (Reaume *et al.,* 1996), have shown that lack of the SOD1 isoform of superoxide dismutase does not confer a lethal phenotype. There have been contradictory results on the effect of decreased *Sod1* expression on lifespan. Mutant or knockout mice for *Sod1* produced by homologous recombination (Reaume *et al.,* 1996), which are totally devoid of CuZnSOD activity, are apparently normal and live into adulthood. More recent studies however, showed that *Sod1*$^{-/-}$ mice do indeed have reduced lifespans, when compared to controls (Elchuri *et al.,* 2005). Although it is unclear if decreased CuZnSOD affects lifespan, it is apparent that Sod*1*$^{-/-}$ animals are more sensitive to different types of acute oxidative stress (Phillips *et al.,* 1989). For example, increased development

of neurological phenotypes and occurrence of cancers with increased age have been observed (Busutti *et al.*, 2005; Elchuri *et al.*, 2005). Homozygous *Sod1*$^{-/-}$ animals and cells are significantly more sensitive to different types of oxidative stress than heterozygotes or wild-type mice, with a clear correlation between the amount of active Sod1 and the sensitivity to the insult.

Mice that are deficient for the extracellular isoform of superoxide dismutase also develop normally and are healthy for at least 14 months (Carlsson *et al.*, 1995). This is not surprising since the localisation of Sod3 makes it a minor defence mechanism against what is primarily intracellularly generated oxidative stress. This would also explain the relatively limited attention Sod3 has received in the research field of oxidative stress.

In contrast, however, to both *Sod1* and *Sod3* null mice, mice completely devoid of Sod2 activity have a severe lethal phenotype (Melov *et al.*, 1999). Two independent groups have produced MnSOD gene knockout mice. Li *et al.* (1995) deleted the third exon of *Sod2*. Homozygous mutants on a C57BL/6 background were smaller and paler, and exhibited a hypotonic and hypothermic state compared with wild-type or heterozygous mice. Although they appeared to fatigue more rapidly, their behaviour was otherwise normal. By the time of death at P10, they did not show any motor disturbances, central nervous system injury, ultrastructural evidence of mitochondrial injury or gross mtDNA re-arrangements. However, on a CD1 background, *Sod2* homozygotes died within 10 days post birth with dilated cardiomyopathy (enlarged hearts with a dilated left ventricular cavity and reduced left ventricular wall thickness). Accumulation of lipid, both in the liver and the skeletal muscle, and metabolic acidosis were also present.

Lebovitz *et al.* (1996) deleted exons 1 and 2 of the *Sod2* gene. At birth, the homozygous mutants could not be distinguished from their littermate controls, but had a diminished growth rate and, on a mixed genetic background, survived for up to 18 days. They also exhibited severe anaemia, degeneration of neurons in the basal ganglia and brain stem, and progressive motor disturbances characterised by weakness, rapid fatigue, and circling behavior. Mice surviving for more than 7 days exhibited extensive mitochondrial injury within degenerating neurons and cardiac myocytes. Only 10% of these mice had dilated cardiomyopathy.

A number of different groups have since phenotypically analysed these homozygous *Sod2* mutants and/or the heterozygotes, in attempts to elucidate the

role of oxidative stress in a wide variety of physiological and metabolic processes and diseases. From the phenotypes of the different *Sod2* mutants it was apparent that there was a discrepancy in the survival rates of the mice depending on the background of the animals. The biochemistry of $Sod2^{-/-}$ mice that were on a CD1 background was compared to that of littermate heterozygous and control mice (Melov *et al.*, 1999). Tissue mitochondrial samples prepared from 4 to 6-day old homozygous mutants showed decreased succinate dehydrogenase, complex I and aconitase activities, while fumarase activity, which is insensitive to oxidative stress, remained unchanged. Organic acid abnormalities, like increased levels of 3-methylglutaconic, 2-hydroxyglutaric acids, and 3-hydroxy-3-methylglutaryl (HMG)-CoA lyase deficiency were also reported in urine and liver, respectively. Finally, the genomic DNA was oxidatively damaged in the homozygous mutants, with over 20 different types of DNA lesions detected in different tissues, including a 3-fold increase in 8-oxo-guanine, -adenine and -cytosine, in the heart and brain.

Huang *et al.* (2001) investigated the role of the genetic background on the phenotype conferred by MnSOD deficiency. MnSOD deficient mice on the outbred CD1 strain background developed severe metabolic acidosis and dilated cardiomyopathy by 5 days of age and died within 10 days, while another mutant on a mixed C57BL/6 (B6) and 129/Sv genetic background survived for up to 18 days, with only 10% of the mice developing severe dilated cardiomyopathy. Huang *et al.* (2001) generated congenic $Sod2^{tm1}$*Cje* mice on a C57BL/6 (B6), DBA/2J (D2) and B6D2F1 (= B6 female x D2 male, 1 backcross) background to achieve genetic uniformity and compared the phenotypic differences among the $Sod2^{-/-}$ mice bred on these different genetic backgrounds. They firstly observed marked differences in lifespan, with mice on a B6, D2 and B6D2F1 background surviving for increasing lengths of time. Mice on a B6 background were mostly dying prenatally (between E15 and P1), whereas those on a B6D2F1 background survived for up to 3 weeks. Dilated cardiomyopathy was evident only in B6 mice. D2 mutants showed increased signs of metabolic acidosis and B6D2F1 mice had milder metabolic acidosis and developed neurological problems. It was concluded that lifespan is greatly influenced by as yet unknown genetic modifiers, and that allowing *Sod2* mutants to survive longer, brings to the surface phenotypes that would not be apparent had the animals died earlier. This latter point was further

supported by subsequent work in which SOD2 mimetics were administered to *Sod2* null mice (Melov *et al.,* 1998; 2000). Melov *et al.* (1998) reported that treatment with the SOD mimetic manganese 5, 10, 15, 20-tetrakis (4-benzoic acid) porphyrin (MnTBAP) rescued Sod2 $^{-/-}$ mutants from the pathology described above and significantly prolonged their survival. Surviving animals developed a pronounced movement disorder, which progressed to complete impairment of strength by 3 weeks of age. Neuropathologic evaluation showed spongiform degeneration of the cortex and specific brainstem nuclei, associated with gliosis and intramyelinic vacuolisation, both of which are phenotypic characteristics previously observed in disorders associated with inherited mitochondrial abnormalities such as Leigh disease. Melov *et al.*, (1998) suggested that it was the failure of MnTBAP to cross the blood-brain barrier that caused the progressive neuropathology, as the mimetic failed to prevent excessive mitochondrial production of ROS within the brain.

Asikainen *et al.* (2002) investigated the sensitivity, lung histopathology and biochemistry of *Sod2* null mice subjected to hyperoxia. Taking advantage of their increased survival rate on the mixed genetic background, the mice showed increased mortality rates and decreased body and lung weights, when compared to wild-type animals. Also, the plasma glutathione levels were decreased, while the mRNA levels and activity of glutathione peroxidase were increased, possibly reflecting a compensatory response to decreased MnSOD activity.

The limited lifespan of *Sod2* null mice makes it difficult to study the importance of the mitochondrial isoform of superoxide dismutase in longer-term experiments and to analyse in more detail the effects that its absence would have in phenotypes, such as retinal degeneration, that take longer than 3 weeks to become apparent. Also, the limited lifespan of these mice means that they do not reach a fertile age, which in turn prohibits the generation of compound mutants, for investigating the role of oxidative stress in different diseases. One solution is the use of *Sod2* heterozygous mice that have decreased levels of Sod2, but not to the extent that this becomes lethal. An increasing number of studies have focused on analysing Sod2$^{+/-}$ mice and using them to understand the involvement of oxidative stress, and particularly *Sod2*'s role in a range of disorders, including neurodegenerative diseases. Heterozygous *Sod2* mice on a C57BL/6 background and aged 2-4 months were initially analysed (Tsan *et al.,* 1998; Williams *et al.,*

1998; van Remmen *et al.,* 1999; 2001). Decreased Sod*2* expression and protein levels were confirmed in all tissues analysed. The animals survived well following exposure to 100% oxygen and, with some exceptions, the mRNA and protein levels of Sod1, Cat and Gpx were unchanged (Tsan *et al.,* 1998; van; Williams *et al.,* 1998). In the heart however, there was an increase of Sod1 and Gpx activities, possibly reflecting a compensatory response to decreased Sod2 levels (Tsan *et al.,* 1998). The mRNA level of *Gpx* in the muscle also showed a significant decrease (van Remmen *et al.,* 1999). Moreover, in the heterozygous animals there was a 30% decrease both in total glutathione levels of liver mitochondria, and in the specific activities of the mitochondrial and oxidative stress-sensitive enzymes aconitase and complex I. Increased levels of 8-oxoG residues in the DNA and of increased protein oxidation, suggested increased oxidative damage in $Sod2^{+/-}$ mice (Williams *et al.,* 1998).

Subsequent studies focused on longer-term experiments. Andreassen *et al.* (2001) evaluated the susceptibility of $Sod2^{+/-}$ animals, on a CD1 background, to exposure to different sources of oxidative stress. Animals were subjected to 1-methyl-4-phenyl-1, 2, 5, 6-tetrahydropyridine (MPTP), malonate and 3-nitropropionic acid (3NP) treatments, all of which are neurotoxins commonly used for generation of animal models of Parkinson's and Huntington's diseases (Bove *et al.,* 2005; Brouillet *et al.,* 2005). No neuropathological features were evident for 6 months. Malonate-induced brain lesions were however larger in the heterozygotes, compared to wild-types, and neuronal loss was increased following 3NP treatment. Finally, van Remmen *et al.* (2003) studied the *Sod2* heterozygotes for up to 26 months of age. Although their lifespan was identical to that of control animals, they showed increased 8-oxoG levels in their DNA, as well as a 100% increased tumour incidence.

1.1.4.3. Antioxidants in disease treatment

In addition to work on genetically modified animals, the importance of Sod2 has been demonstrated by the exogenous administration of chemical analogues that serve as potential treatments for diseases in which oxidative stress has been implicated. Rong *et al.* (1999) pre-treated rats with EUK-134, a synthetic superoxide dismutase-catalase (Sod-Cat) mimetic, and showed decreased levels of

protein nitration and neuronal damage after kainate-induced seizure activity. Also, Izumi *et al.* (2002) observed decreased organ injury in haemorrhagic shock induced in anaesthetised rats, after they were treated with EUK-8, another Sod-Cat mimetic. Finally, Melov *et al.* (2000) increased the level of antioxidant systems in *C. elegans* by administration of either EUK-8 or EUK-134, and observed a 44% increase in the worm's life span.

1.1.5. Drug development and mitochondrial targeting

It is therefore an attractive idea to design drugs that are targeted to mitochondria, which, based on the *Sod2* studies, are the principal sites of ROS formation in the cell. The effectiveness of such a drug depends on a number of points, as discussed by Murphy & Smith (2000). A bioactive molecule needs to find its way to the correct intracellular location, in specific cell types of a specific organ. Once there, the drug should be able to manipulate specific metabolic processes without compromising neighbouring ones. Also, the drug should be cleared from the system, to ensure the lack of its accumulation in target tissues, hence avoiding potential problems such as overdose and overloading. For some drugs, depending on where they are being targeted to, it is also essential to cross the blood-brain barrier (BBB). This has been discussed in a recent paper by Pardridge (2005), in which it was pointed out that 98% and 100% of small and large molecule drugs respectively do not cross the BBB. For a small-molecule drug to be able to do so in pharmacologically significant amounts, the molecule must have a molecular mass of less than 500 Da and a high lipid solubility (Pardridge, 2001). In central nervous system (CNS) disorders, where the primary phenotype resides in neurons, this is a major issue that needs to be overcome. Finally, the drug delivery and role-execution procedure should be done with minimal side effects that do not compromise the vital functions of the cells or their survival.

1.1.5.1. Candidates for mitochondrial targeting

The beneficial effects of a number of natural antioxidants have been studied and verified, making them potentially good drug candidates in disorders where mitochondrial function is impaired. Antioxidants like vitamin E (VitE) (Meydani,

1995) and SOD mimetics have been shown to offer some protection against oxidative damage. Extensive work, both *in vitro* and *in vivo,* has demonstrated beneficial effects. The best clinical evidence supporting the protective role of VitE against ischemia/reperfusion injury comes from VitE pretreatment of patients undergoing cardiopulmonary bypass surgery (Coghlan *et al.,* 1993; Meydani, 1995). If not pre-treated with the antioxidant, the decreased levels of the vitamin observed during bypass surgery lead to increased levels of oxidative damage. Also, treatment with the SOD mimetic MnTBAP significantly ameliorated both dilated cardiomyopathy and hepatic lipid accumulation and increased the mean lifespan of *Sod2* null mice (Melov *et al.,* 2001).

1.1.5.1.1. Ubiquinone

Ubiquinol derivatives are also promising antioxidants to target to mitochondria, as work by both Matthews *et al.* (1998) and Laas *et al.* (1999) has demonstrated. Ubiquinones (UQ) are a group of homologous quinones, all of which contain a 2, 3-dimethoxy-5-methylbenzoquinone nucleus with a phenyl side chain (Clane & Barr 1971). It is the length of this chain that differs between different quinones (**Figure 5**), which are also known as coenzymes Q (CoQ) (Bhagavan & Chopra, 2006). They are the most widely distributed quinones in nature, and are found in the mitochondria of plants, animals and bacteria. In humans, the most prevalent isoform is coenzyme Q_{10} (CoQ_{10}), with a 10-carbon chain, and is present in all human tissues in varying amounts (Bhagavan & Chopra, 2006). The distribution of ubiquinone is usually correlated with energy requirement and metabolic activity, which agrees well with its involvement as a coenzyme in the cytochrome-containing terminal respiratory system. As reported by Bhagavan & Chopra (2006), the heart, kidney, liver and muscle contain the highest CoQ_{10} concentrations in humans.

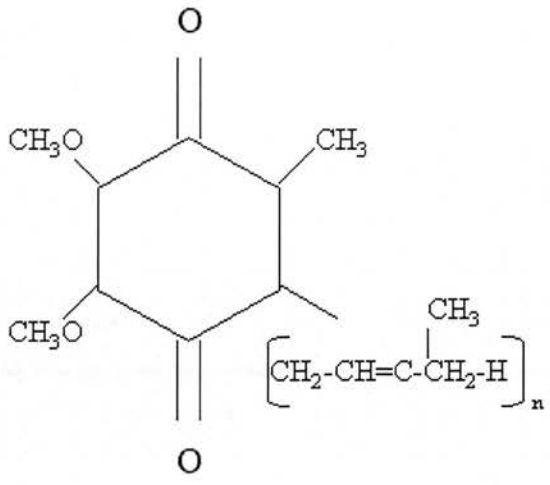

Figure 5: Ubiquinone structure

General chemical structure of ubiquinones. They all contain a 2,3-dimethoxy-5-methylbenzoquinone nucleus with a prenyl side chain in the 6-position, but differ in the length of this side chain.

UQ can exist in different redox forms in the cell. It is buried within the lipid core of the MIM and can stably exist in either an oxidized form (UQ) or a reduced form called ubiquinol (UQH_2) (Ernster & Dallner, 1995). The conversion from UQ to UQH_2 is catalysed by ubiquinone reductases and the UQH_2/UQ ratio is determined by the electron flow through the ETC, shifting to a reduced state when the flow is decreased (James *et al.*, 2004). *In vivo*, the ubiquinone pool is highly reduced and in humans, about 95% of CoQ_{10} exists as ubiquinol (Bhagavan & Chopra, 2006).

Ubiquinone is an essential cofactor in the ETC, where it accepts electron from CI and CII, becoming reduced to ubiquinol, and donates them to CIII. In addition to its electron carrier role, ubiquinol is a potent antioxidant, as it has been shown to reduce lipid peroxidation within the MIM (Beyer & Ernster, 1990, Ingold *et al.*, 1993, Kelso *et al.*, 2001). Its antioxidant role is exerted by the donation of a hydrogen atom to a lipid peroxyl radical, and the subsequent formation of a ubisemiquinone radical ($UQH^{\bullet}$). The latter can react with oxygen to form ubiquinone and $O_2^{-\bullet}$, which gets detoxified by the antioxidant enzyme superoxide dismutase (Maguire *et al.*, 1989; Ingold *et al.*, 1993; Kelso *et al.* 2001).

1.1.5.2. Targeting antioxidants to mitochondria

There is a drawback, however, in using the previously described antioxidants as drugs. Only a small proportion of the administered antioxidant manages to reach the mitochondrion, where it is able to reduce ROS formation. Orally administered CoQ_{10} has a poor efficiency of absorption due to its insolubility in water and relatively large molecular weight (Bhagavan & Chopra, 2006). This has been confirmed in a study with rats, where only 2-3% of orally administered CoQ_{10} was absorbed (Zhang *et al.*, 1995). As a result, patients need to be treated with large amounts of these natural antioxidants to be able to obtain a beneficial effect, at which point undesired side effects attributed to over-dosage become apparent. It is therefore essential to be able to target these antioxidants directly to mitochondria, where they can accumulate and exert their beneficial effects. Extensive work by Murphy, Smith and colleagues has been dedicated to investigating the development and potential use of mitochondrially-targeted antioxidants (Smith *et al.*, 1999, 2003; Kelso *et al.*, 2001; Asin-Cayuela *et al.*, 2004).

A common way of targeting compounds to mitochondria has been to attach a specific 25-amino acid signal peptide to the N-terminus of the compound of interest. This is not always straightforward, as the addition of this peptide can interfere with the structure and function of the molecule. The structural, physiological and metabolic characteristics of mitochondria can be exploited in drug targeting. The MIM is selective in its permeability and allows substances to pass through it only via tightly regulated transporters, complexes and pumps. For example, only complexes I, III and IV of the ETC are able to pump protons out through the MIM during respiration. Similarly, it is only through the ATP synthase that protons can re-enter into the mitochondrial matrix. During respiration, the selective flux of protons generates a concentration gradient, which in turn constitutes a major part of the proton-motive force driving respiration. In living, respiring cells, a membrane potential is established across the MIM. In cultured cells, this is 180-200 mV (negative inside), while *in vivo* it is 130-150 mV. This drop is attributed to the use of some of the electrochemical potential for respiration, ATP production and ion translocation. It has been shown that some

cations are able to use this electrochemical potential to their advantage and to accumulate within mitochondria against a concentration gradient (**Figure 6**). Indeed, 90% of intracellular lipophilic cations are located within mitochondria (Kauppinen, 1983), as they can easily pass through the lipid bilayer, since their

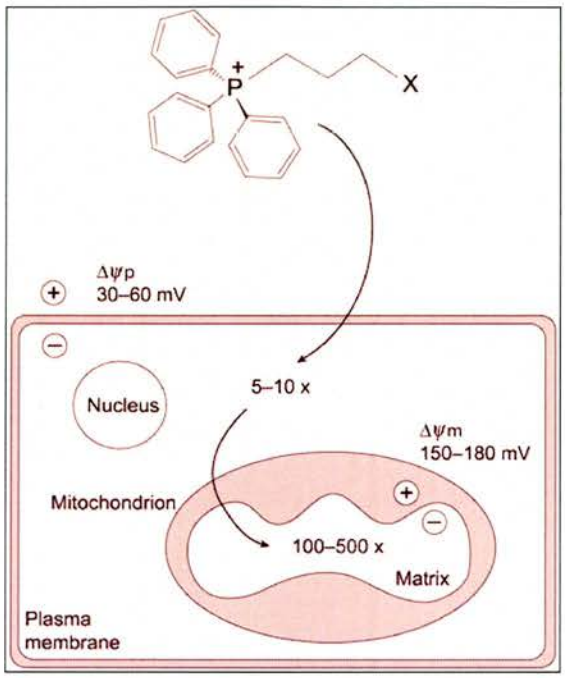

Figure 6: Uptake of alkyltriphenylphosphonium cations by mitochondria within cells

The lipophilic triphenylphosphonium cation, which is covalently attached to a biologically active molecule (X), is accumulated 5- to 10-fold into the cytoplasm from the extracellular space by the plasma membrane potential ($\Delta\psi p$) and then further accumulated 100- to 500-fold into the mitochondrial matrix by the mitochondrial membrane potential ($\Delta\psi m$) [Image from Smith *et al.*, 2003]

positive charge is shielded (Murphy & Smith, 2000). This accumulation is described by the Nernst equation:

$$\text{Membrane potential (mV)} = 61.5 \log_{10} \{[\text{cation}]_{in}/[\text{cation}]_{out}\}$$

according to which every 61.5 mV increase in the membrane potential causes a 10-fold increase in the mitochondrial accumulation of lipophilic cations. This

property of the lipophilic cations has been successfully used for targeting toxic substances to cancer cells in order to induce their death (Rideout *et al.*, 1989).

1.1.5.2.1. Mitochondrially targeted antioxidant compounds

Murphy and co-workers developed a number of mitochondrially-targeted compounds, by taking advantage of these properties of lipophilic cations.

IBTP (4-iodobutyl-triphenylphosphonium) (**Figure 7**) is a lipophilic cation that is able to accumulate one hundred-fold within mitochondria and specifically to label mitochondrial proteins (Lin *et al.* 2002). Inside mitochondria, protein thiolates displace the iodo functional group of IBTP to form stable phosphonium thioethers. These can in turn be identified by immunoblotting using anti-triphenylphosphonium antiserum. The selectivity of IBTP for mitochondrial proteins is high, since the pKa values of protein thiols (about 8-8.5) mean that the mitochondrial pH of 8 is more appropriate for a fast reaction than the cytosolic pH of 7.2. Therefore, protein modifications attributed to formation of mixed disulfides, *S*-nitrosylation, or oxidation can result in an altered recognition pattern of IBTP.

MitoQ (**Figure 7**) is a ubiquinone derivative targeted to mitochondria. It is a mixture of mitoquinone and mitoquinol, the two charged forms of ubiquinone, which are covalently attached to a lipophilic triphenylphosphonium cation through an aliphatic carbon chain. The properties of MitoQ as a targeted antioxidant are often verified by comparison with idebenone. The latter is a short chain analogue of CoQ_{10}, which has been shown to decrease oxidative damage in Friedreich's ataxia (FRDA) patients (Mariotti *et al.*, 2003). It is an artificial ubiquinone with better bioavailability and pharmacokinetic properties than exogenous CoQ_{10}, and has been shown to have beneficial effects in clinical studies (Rustin *et al.*, 2002). Other compounds that have been synthesised using the same principle, and which will be mentioned occasionally in this project, are ^{3}H-MitoQ, a tritium-labelled form of MitoQ and TPMP (methyltriphenylphosphonium cation), which is very similar structurally to the above compounds, but does not have an antioxidant capacity.

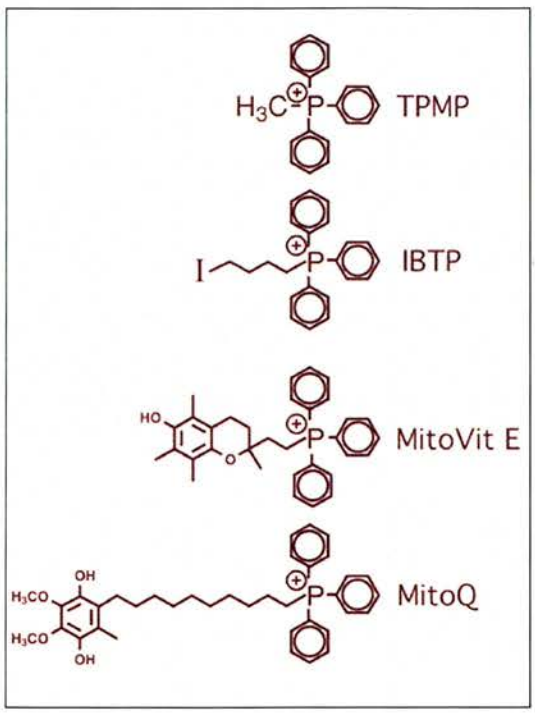

Figure 7: Mitochondrially targeted antioxidant compounds

Chemical structures of mitochondrially targeted compounds. They are all covalently attached to a lipophilic triphenylphosphonium cation. TPMP has no antioxidant function, whereas IBTP, MitoVitE and MitoQ do. [Image from Smith *et al.*, 2003]

1.1.5.2.2. Evaluating mitochondrially targeted antioxidants

Having developed these mitochondrially targeted compounds, the next step was to assess *in vitro* their efficiency in mitochondrial accumulation and effectiveness as antioxidants. Because of their very similar chemical structures, inferences were often made on results using a single targeted compound.

The efficient targeting of these antioxidants into isolated mitochondria was verified. Kelso *et al.* (2001) energised isolated mitochondria by incubating them with KCl buffer including succinate and rotenone. Subsequent treatment with ^{3}H-MitoQ, allowed the uptake of this compound by mitochondria and was verified by scintillation counting. The specificity of the uptake was confirmed by the use of the respiration uncoupler carbonyl cyanide p-

trifluoromethoxyphenylhydrazone (FCCP), which blocked the uptake and prevented the antioxidant's accumulation in the organelles. Lin *et al.* (2002) demonstrated the uptake of IBTP by isolated mitochondria, following a similar protocol that included detection of the compound by an anti-IBTP antibody. Finally, Kelso *et al.* (2001) showed that once ^{3}H-MitoQ was taken up by energised mitochondria, it was largely adsorbed to the matrix side of the MIM.

Having demonstrated the uptake of the targeted antioxidants by isolated mitochondria, it was important to confirm that this was also the case within isolated cells. Kelso *et al.* (2001) treated isolated cells with ^{3}H-MitoQ for 40 minutes prior to cellular fractionation and showed a 50% enrichment of the tritium-label in the mitochondrial fraction, compared to the cytosolic one. The specificity of this accumulation was verified by treatment with the uncoupler FCCP, which disrupts the membrane potential.

The mechanism of action of MitoQ as an antioxidant was also investigated by Kelso *et al.* (2001). MitoQ can be reduced and oxidized by complexes of the ETC. Depletion of endogenous ubiquinone or use of a yeast strain deficient in ubiquinone biosynthesis verified that MitoQ redox changes were not attributed to the endogenous ubiquinone pool. The antioxidant role of MitoQ was clarified by using parinaric acid, which fluoresces when in lipid bilayers but loses this fluorescence under lipid peroxidation. Incubation of mitochondria with ferrous iron resulted in a decreased membrane potential and increased levels of lipid peroxidation. Treatment with MitoQ however, prevented oxidation of parinaric acid by ferrous iron, blocked the accumulation of the lipid peroxidation marker malondialdehyde (MDA) and restored mitochondrial function. The antioxidant properties of MitoQ, which seem to lie in its ubiquinol moiety, were abolished upon malonate and rotenone treatment. These are inhibitors of complex II and complex I, respectively, which blocked the reduction of MitoQ and prevented it from successfully inhibiting lipid peroxidation.

The toxicity of MitoQ in cells was assessed by Kelso *et al.* (2001). The authors demonstrated that MitoQ doses of less than 10 μM had little effect on mitochondrial membrane potential and no effect on cell viability. However when the concentration was increased to 25-50 μM, a decreased membrane potential and an increase in cell death was observed.

As mentioned above, for a drug to be efficient, it should be cleared from the biological system in which it is introduced. This was confirmed for TPMP and it was therefore assumed that MitoQ would have a similar clearance rate from mitochondria (Kelso *et al.*, 2001).

The necessity of targeting antioxidant compounds to mitochondria was illustrated by a comparison between idebenone and MitoQ. Idebenone is evenly distributed between intra- and extra-cellular compartments, without being concentrated in the mitochondria. Jauslin *et al.* (2003) used fibroblasts that had been isolated from Friedreich's ataxia (FRDA) patients which were then exposed to the glutathione synthesis inhibitor L-buthionine-(S,R)-sulfoximine (BSO) to induce cell death by increased endogenous oxidative stress. Comparing the treatments with Idebenone and MitoQ, the authors showed that the latter was up to 800-fold more effective at preventing cell death at a much lower concentration than the former. This difference was abolished upon treatment with the uncoupler FCCP.

1.1.5.2.3. *In vitro* studies of MitoQ

Since the development of MitoQ as a targeted antioxidant, a number of studies have demonstrated its efficiency as an antioxidant. Kelso *et al.* (2001) investigated *in vitro* the role of MitoQ in apoptosis. Incubating Jurkat cells with H_2O_2 activated the caspase cascade and increased cell death within 4-6 hours of exposure. Pre-incubation of the cells however with 1μM MitoQ completely blocked caspase activation and decreased the number of dying cells following H_2O_2 treatment. It is worth noting however that this did not occur when the non-targeted, but evenly distributed, coenzyme Q_1 was administered, highlighting the importance of targeting. Similarly, the level of apoptosis induced by staurosporin or tumor necrosis factor-alpha (TNFα) were also decreased upon MitoQ treatment (Kelso *et al.*, 2001).

The effect of MitoQ on telomere shortening and lifespan has been examined under mild oxidative stress. Telomere shortening, which is a marker of ageing, is attributed either to the inability of DNA polymerases to replicate the ends of chromosomes or to the specific accumulation of oxidative damage in the

DNA. Saretzki *et al.* (2003) observed a 50% decrease in hyperoxia-induced peroxide formation in human fibroblast cultures treated with MitoQ. They also showed that the replicative lifespan of fibroblasts, which lack telomerase, was increased by 40% and that telomere shortening was minimised in the presence of the antioxidant. Also, Sanjuan-Pla *et al.* (2005) investigated the role of mitochondrially-produced ROS in the hypoxic signalling of hypoxia inducible factor 1 alpha (HIF-1α). The latter is a transcription factor which is a key regulator of the cellular responses to reduced oxygen concentrations. HIF consists of an oxygen-sensitive α subunit and a constitutively active β subunit. The former is targeted for ubiquitination and proteasome degradation under normoxic conditions (21% oxygen), but is stabilised under hypoxia (0-5% oxygen) so that it can transactivate target genes. In this study, the authors found that mitochondrial ROS are required for HIF-1α stabilisation since addition of MitoQ led to disruption of mitochondrial ROS formation, destabilisation of HIF1α and subsequent loss of its transcriptional activity. MitoQ was therefore used to highlight the involvement of ROS and oxidative stress in important cellular processes like telomere integrity, transcriptional activation and apoptosis.

1.1.5.2.4. *In vivo* studies of MitoQ

Based on the results of *in vitro* studies, MitoQ appeared to be a promising targeted antioxidant that could potentially be used as a therapeutic drug in mitochondrial diseases. In order to become clinically useful drugs, targeted antioxidants should work as efficiently *in vivo* as they have been shown to do *in vitro*. The *in vivo* studies of MitoQ have not yet been as extensive, since the antioxidant has only recently become available, but the results so far have been promising. Work by Smith *et al.* (2003) was the first attempt to investigate the delivery and distribution of TPMP, MitoVitE and MitoQ *in vivo*. These authors used Swiss-Webster mice to compare three methods of administering these compounds; intraperitoneal (i.p.) injection, intravenous (i.v.) injection and orally through the drinking water. Single injections (i.p. or i.v.) of TPMP or MitoVitE up to 300 nmol were not toxic for at least 7 days after administration. Toxicity was however evident at 500 nmol within 12 hours of injection. For MitoQ,

injections of up to 750 nmol were well tolerated by the animals, but toxic side effects were evident at doses above 1000 nmol. It was concluded that the maximum tolerated dose of MitoQ for administration by injection was 20 mg/kg.

The figures were somewhat different when the substances were administered to the animals through their drinking water. At concentrations of 500 μM, 1 mM and 5 mM, TPMP showed no toxic effects for at least 43 days, toxic effects at 26 days and toxic effects at 6 days, respectively. MitoVitE doses of 500 μM caused no side effects for at least 14 days of administration. These data translate into maximum tolerated doses of 97 ± 13 μmol/kg/day and 105 ± 9.2 μmol/kg/day for TPMP and MitoVitE, respectively. MitoQ concentrations of 500 μM and 1mM had no toxic effects for at least 26 days, but doses of 2 or 5 mM had toxic effects after 10 days of treatment. It was also noted that at these concentrations, food consumption by the animals was 65-80% and 20-30% that of control animals. The maximum tolerated dose for MitoQ was concluded to be 346 μmol/kg/day.

It is apparent that the toxicity of these compounds depends on the method of administration, so that oral administration is less toxic than injection. This may be because lipophilic cations can be toxic at high concentrations, as their excessive uptake can result in the disruption of ATP synthesis by mitochondria. It was also noted that it is the lipophilic cations that are toxic to the cell and not the side chains of the compounds, as indicated by the similar maximum tolerated doses observed for TPMP and MitoVitE, whose side chains are very different.

The uptake of these substances into tissues was investigated by the use of tritium-labelled analogues. ^{3}H-TPMP and ^{3}H-MitoVitE, administered to mice by i.p. injections, were efficiently taken up by the heart, liver and kidney, but not by the brain, within an hour of injection. All tissues absorbed the substances following i.v. injection. Similarly, all organs also absorbed TPMP and MitoVitE after 7-10 and 4 days of oral administration through the drinking water, respectively. Administration of 500 μm MitoQ for 10 days was sufficient for uptake by all the organs tested. The tissue concentrations recorded were however lower than for TPMP or MitoVitE, probably reflecting MitoQ's higher hydrophobicity.

The hydrophobicity of these compounds is a key issue that can greatly affect their efficiency as drugs. Work by Asin-Cayuela *et al.* (2004) investigated this by using alkyltriphenylphosphonium (TPP) cations. TPP cations enter mitochondria as follows: they first bind the outer surface of the MIM and then permeate the hydrophobic phospholipid bilayer, which potentially acts as an energy barrier. They then bind to the matrix side of the MIM, from where they are distributed throughout the mitochondrial matrix. Eventually, equilibrium is reached between the cations free in solution and those adsorbed as a monolayer on the membrane surface. It is conceivable that the more hydrophobic the alkyl chain of the targeted compound, the higher the proportion of the cation that is membrane-bound, leaving only a smaller proportion available in the matrix. This point was illustrated by the same group, who modified the size of the alkyl chain that joins the TPP and ubiquinol moieties. They compared $MitoQ_3$, $MitoQ_5$, $MitoQ_{10}$ and $MitoQ_{15}$, (with 3, 5, 10 and 15 carbons in their alkyl chains, respectively) to find that there was a perfect correlation between the chain length and adsorption. The antioxidant efficacy of these MitoQ analogues depends both on their reduction by the ETC and on their accumulation within the mitochondria. As shown by thiobarbituric acid reactive substances (TBARS) and other lipid peroxidation markers, the antioxidant efficacy of the MitoQ analogues correlated positively with the size of the alkyl chain. It is conceivable therefore that a balance needs to be achieved between the availability of the compound and its antioxidant efficacy. $MitoQ_{10}$ is the analogue that has been most extensively used in both *in vitro* and *in vivo* experiments.

The key property of these targeted MitoQ analogues is their ability to accumulate in the mitochondria. It is difficult to confirm this *in vivo*, using tritium-labelled sub-analogues, as they are rapidly re-distributed upon loss of membrane potential. For this reason IBTP, which shows covalent binding to proteins and for which an antibody has been designed, is used. (Lin *et al.*, 2002). Within mitochondria, the iodo moiety of IBTP is slowly displaced by protein thiols, binding the butyltriphenylphosphonium cation to mitochondrial proteins by a stable thioether linkage. This covalent association is stable even under tissue homogenisation, making its detection by immunoblotting possible. Therefore, Kelso *et al.* (2001) injected IBTP intravenously into mice, and 4 hours later were able to confirm its accumulation in heart mitochondrial fractions. The integrity of

the targeted antioxidants within the mitochondria, following uptake, was assessed by mass spectrometry. It was confirmed that the MitoVitE mass was not altered upon targeting. The same authors also confirmed the clearance of TPMP at a reasonable rate, with a half-life of 1.54 days. Inferences therefore were made regarding the integrity and clearance of MitoQ following its administration *in vivo*.

The effects of administration of these targeted substances on the breeding capacity of animals were also investigated. In addition, it was necessary to determine whether the targeted antioxidants reach the embryos and whether they can accumulate in different embryonic organs. By orally administering ^{3}H-TPMP to the mouse dam during days 1-17 of pregnancy, Smith *et al.* (2003) showed substantial TPMP accumulation in the embryos. Additionally, administration of ^{3}H-TPMP throughout pregnancy, up to postnatal day 7 (P7) of the neonate, confirmed its distribution in all organs of the neonate.

Based on the TPMP results, Smith *et al.* (2003) suggested the following pharmacokinetic model. Orally administered TPMP is absorbed by the gut and enters the bloodstream eventually to be taken up by all tissues. This occurs by non-mediated movement through the lipid bilayer of the cell plasma membrane (PM), driven by the PM potential. Once in the cytosol, cations are further concentrated in mitochondria, this time driven by the membrane potential across the MIM. After several days of oral administration, the cations reach a steady state concentration within the mitochondria that is several hundred-fold higher than the concentration in the bloodstream. At this point, the rate of absorption of these cations matches that of its clearance into the urine and bile.

In summary, the studies of Smith *et al.* (2003) established that MitoQ can be used effectively *in vivo*. Oral administration of MitoQ at a maximum tolerated dose of 346 μmol/kg/day for at least 26 days is safe for the animals. It was confirmed that MitoQ, driven by membrane potentials, can enter tissues and cells and accumulate within mitochondria. The delivery of MitoQ from parents to embryos and fetuses after oral administration is also confirmed. Once it has entered the mitochondria, MitoQ remains structurally intact and can exert its antioxidant role, which has since been verified *in vivo* in a number of different model systems.

Adlam *et al.* (2005) used MitoQ in an *in vivo* model of cardiac ischemia-reperfusion (IR) injury. During IR, the coronary blood supply to the heart is temporarily reduced or stopped, preventing oxygen, glucose and fatty acids from reaching the muscle. OXPHOS is inactivated and a number of different physiological changes point to the disruption of mitochondrial function. These include loss of cytochrome *c*, build up of phosphates and lactic acid and increased intracellular Ca^{2+} concentrations. Upon reperfusion, molecular oxygen interacts with the now damaged respiratory chain to produce ROS. Rats were administered MitoQ orally, through their drinking water, at a dose of 74-99 μmol/kg/day for 14 days. Following IR injury Adlam *et al.* (2005) showed that MitoQ protects cardiac function, as assayed by heart rate and coronary blood flow, against tissue damage during IR injury. The extent of IR injuries was measured by transmission electron microscopy and lactate dehydrogenase leakage into the perfusate. MitoQ also protected against disruption of mitochondrial function, as assessed by the respiratory control ratio.

1.2. Photoreceptor degeneration

1.2.1. The structure of the eye

The mammalian eye is a specialised organ concerned with photoreception. Light enters the eye from the external environment and generates a series of physicochemical reactions that result in vision. The structure of the eye is highly organised and is well conserved among vertebrates (Rodieck, 1973).

The mouse eye (**Figure 8**) is a sphere a few millimetres in diameter, with distinct anterior and posterior segments. The anterior segment of the eye includes the conjuctiva, cornea, anterior chamber, aqueous drainage structures, iris, ciliary body and lens (Smith *et al.*, 2002b). The posterior segment includes the vitreous body, posterior uvea (choroid), retina, optic nerve, orbit and extraocular muscles (Smith *et al.*, 2002a). The eye is composed of three major layers; the scleral layers (sclera and cornea), the uveal structures (choroid, ciliary body and iris) and the neural layers.

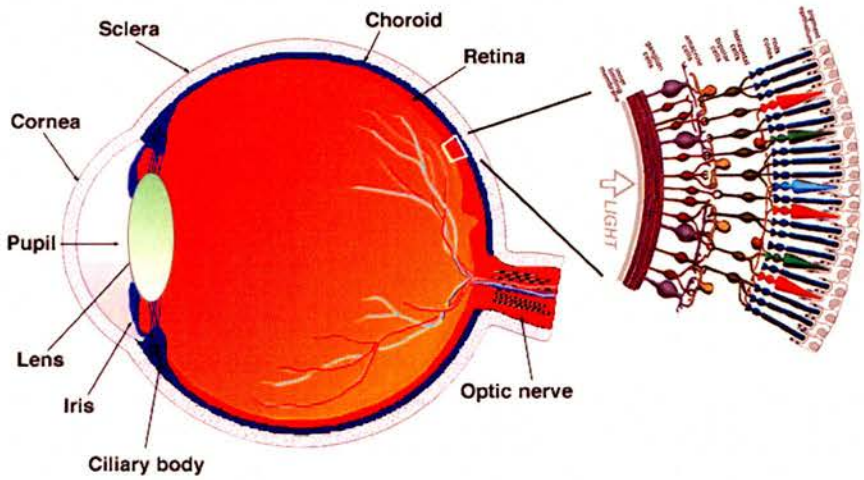

Figure 8: Structure of the eye

Diagrammatic version of an eye sectioned at the vertical plane. The distinct features of the posterior and anterior parts of the eye are indicated, with a focus on the retinal layer. [Image from http://webvision.med.utah.edu/sretina.html]

1.2.1.1. The retina

The retina (**Figure 9**) is a thin sheet of interconnected nerve cells that lines the inner surface of the posterior part of the eye (Smith *et al.*, 2002a). It has two main components; the neurosensory retina, which contains the photoreceptor cells, and the retinal pigment epithelium (RPE). The neurosensory retina is organised in layers, which are, in order from the outside of the eye, the nerve fibre layer, the ganglion cell layer, the inner plexiform layer, the inner nuclear layer, the outer plexiform layer, the outer nuclear layer and the outer segments of the photoreceptor cells (Smith *et al.*, 2002a).

Almost all vertebrate retinas are duplex, in that they contain two types of photoreceptor cells; cones and rods (Carter-Dawson & La Vail, 1979a). Both are long cells which contain a nucleus, axon, synaptic terminal, inner segment (IS) and the outer segment (OS), which are closer to and further away from the centre of the hemispherical retina, respectively (Rodieck, 1973) (**Figure 9**). The IS and OS are connected by a thin structure called the connecting cilium. In the mouse retina, the IS of the cone is shorter and larger in diameter (3-4 μm) than that of the rod, whose diameter is about 2 μm. Also, the cone OS is conically shaped and its

length is about 13.4 μm, whereas the rod OS has a uniform diameter across its ~23.6 μm length (Carter-Dawson & La Vail, 1979a). The outer segments are densely packed with well-organised stacked disk membranes that contain abundant photopigments; rhodopsin in rods and short and medium wavelength cone opsins in cones. The OS, although of constant length, is continually renewed. This is done by shedding the older portion at the tip as a result of phagocytosis by retinal pigment epithelium (RPE) cells and by adding new membranes at the base of the OS (LaVail, 1983).

The nuclei of photoreceptor cells are in the outer nuclear layer. Cone nuclei are oval shaped, with horizontal and vertical diameters of 4.3 and 7.3 μm respectively, and have at least one clump of heterochromatin and a large amount of euchromatin. In contrast, rod nuclei are much smaller -at least half the size of cone nuclei- and are round with a diameter of about 4.5 μm. They have a single heterochromatin clump that is surrounded by a small amount of euchromatin.

The distribution of rods and cones in the retina varies at different developmental stages, but the tissue gradually reaches a more-or-less fixed composition during early postnatal life. In an extensive study by Carter-Dawson & La Vail (1979b), the genesis of rod and cone cells in C57BL/6 mouse retinas was studied by autoradiography using tritiated thymidine. It was shown that in the posterior retina, all cones are generated during the foetal period, while only a minority of rods is generated during the same period. The majority of the rods are formed postnatally. In the peripheral retina, cones are again generated before birth while rods extend their formation up to postnatal day P8. In the mouse retina, the total number of photoreceptors decreases slightly from the posterior pole to the periphery and only about 4% of them are cones (Carter-Dawson *et al.,* 1979a). This low percentage of cone cells in the retina remains constant with age and their nuclei are confined to the outer half of the outer nuclear layer.

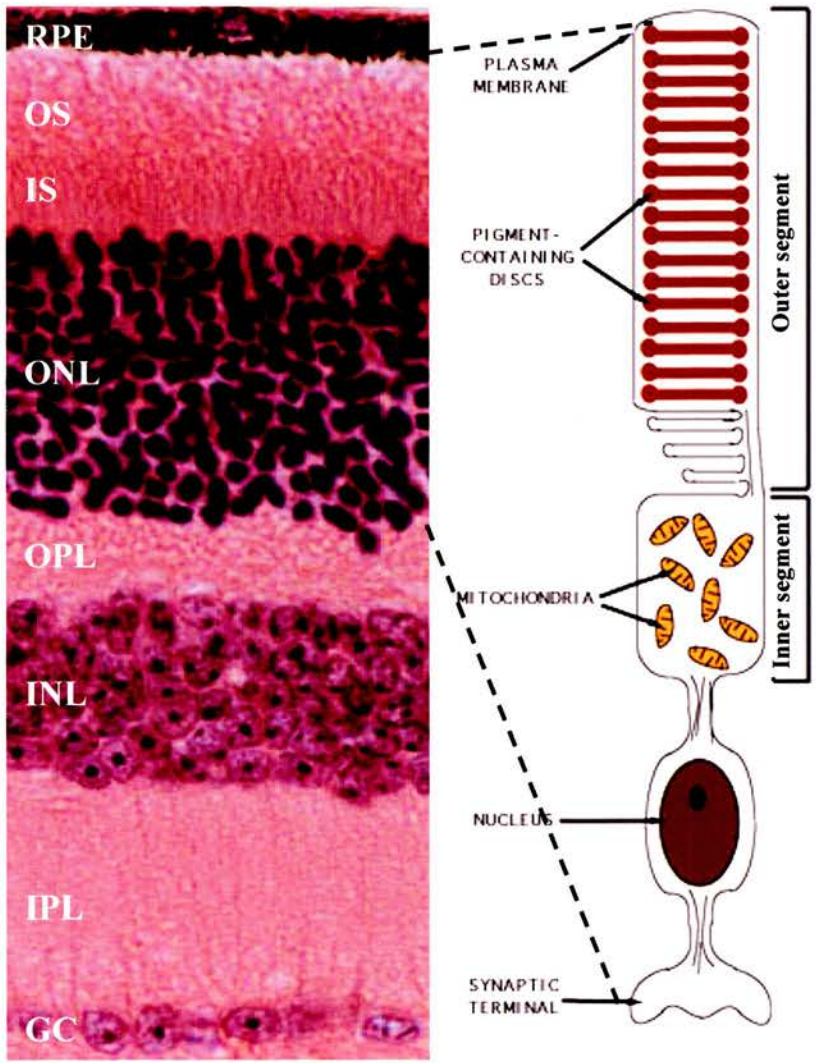

Figure 9: The structure of the retina

(**A**) The retina is organised in different layers. Starting from the equatorial retina (bottom) the layers are; a single layer of ganglion cells (GC), the inner plexiform layer (IPL), the inner nuclear layer (INL), the outer plexiform layer (OPL), the outer nuclear layer (ONL), the inner segments (IS) and the outer segments (OS) of the photoreceptor cells and the retinal pigment epithelium (RPE). (**B**) Schematic diagram of a photoreceptor cell. The outer segment, which is composed of stacked membranous disks, is connected to the inner segment by the connecting cilium. The inner segment accomodates different organelles including mitochondria. [Image from http://www.chemistry.wustl.edu/~edudev/LabTutorials/Vision/images/Rodcell.jpg]

Cones and rods are also functionally different. Cones are used for the distinction of spatial details and the detection of colour, while rods detect brightness, contrast and motion (Baylor, 1987). The underlying mechanism by which these functions are carried out is common to both rods and cones and involves phototransduction. Phototransduction is a cascade of protein activation and inactivation, ion channel opening and closure, which together alter the intracellular ion concentrations and affect the polarisation of the photoreceptor membrane. In the dark, when photoreceptor cells are not stimulated, there is Na^+ influx at the OS and K^+ efflux at the IS, which set the inner membrane potential at –40mV. This depolarising current is known as the dark current. The normal gradients for these ions are maintained by Na^+K^+ ATPase pumps, which are located in the PM of the IS (Steinberg, 1987). Upon illumination, a photon of light is absorbed by rhodopsin and activates it by isomerisation of 11-*cis* retinal to the all-*trans* form. A single activated rhodopsin molecule can then propagate and amplify the signal by activating 500 transducin molecules by means of GDP/GTP exchange. Transducin in turn activates cGMP phosphodiesterase, which lowers cGMP concentrations and so controls the open or closed status of cyclic nucleotide gated ion channels residing in the outer segment plasma membrane. In the light, cGMP-gated Na^+ channels close, while the K^+ and Ca^{2+} effluxes in the IS continue as normal. As a result, the interior becomes increasingly more negative until the membrane becomes hyperpolarised.

1.2.2. Retinitis pigmentosa

Defects in components of the phototransduction cascade can lead to a large number of retinal diseases, mediated by both rod and cone dystrophies, many of which result from impairment of the visual cycle and/or disruption of photoreceptor OS maintenance (van Soest *et al.*, 1999; Rivolta *et al.*, 2002). Many of the defects in genes whose products are involved in photoreceptor-specific functions result in progressive degeneration of rods and cones, and eventually impaired vision and blindness. These include retinitis pigmentosa.

Retinitis pigmentosa (RP) is the term used to collectively describe a group of inherited progressive retinal dystrophies characterised by retinal pigmentary deposition and diminished rod electroretinograms (Rivolta *et al*, 2002). RP is the

most prevalent group of retinopathies in the western world, affecting about 1 in 3000 people, and is both genetically and clinically heterogeneous (Rivolta *et al.*, 2002). It is typically a monogenic disorder, which may be inherited in an autosomal dominant, autosomal recessive or X-linked fashion, and for which there have occasionally been reports of digenic inheritance (Fan *et al.*, 2006).

Regardless of the mode of inheritance of RP, the phenotype is characterised by, initially, the development of night blindness followed by gradual loss of peripheral vision -referred to as tunnel vision- and eventually loss of complete vision in many cases (Humphries *et al.*, 1992; Olson *et al.*, 1992). Photoreceptors are most commonly the retinal cells primarily affected by the disease (Berson *et al.*, 1968; Kolb & Gouras, 1974), but RP can also result from a primary RPE defect, which causes secondary photoreceptor cell death (Mullen & LaVail, 1976). In RP, rod photoreceptors degenerate first, leading to night blindness, whereas the cone dysfunction and death follows at a later stage, when daytime vision becomes noticeably impaired. As RP progresses and pathological changes develop, the retinal pigment epithelium becomes thinner and deposits of pigment often accumulate on the retinal surface, a phenomenon that gives RP its name. Nevertheless, long before these visual problems become apparent, eletrophysiological changes may be detectable in the retina by electroretinography (ERG), which measures the electrical activity generated by the retina in response to flashes of light. Reduced amplitude and/or delayed response to the stimulus are indications of impaired photoreceptor cell function (Berson *et al.*, 1968, 1969).

1.2.2.1. Genes implicated in retinitis pigmentosa

More than 37 genes have been implicated in RP to date (**Table 1**) (RetNet at http://www.sph.uth.tmc.edu/Retnet/home.htm). Some examples of genes in which mutations lead to RP in humans are shown in Table 1. These genes include rod cGMP phosphodiesterase 6 beta subunit (*PDE6B*), rhodopsin (*RHO*) and peripherin 2/retinal degeneration slow (*PRPH2/RDS*). Mouse models for these three RP mutations are described below.

1.2.2.1.1. Rod cGMP phosphodiesterase 6b: the retinal degeneration 1 mutation (*Pde6b*^{rd1})

The retinal degeneration 1 (*rd1*) mutation in the *Pde6β* gene is a naturally occurring, autosomal recessive mutation first reported by Sidman & Green in the C3H mouse strain in 1965. In the retina of homozygous *rd1* mice there is defective postnatal development of photoreceptor cells, leading to their complete loss, as well as to loss of some bipolar cells, by the 3rd postnatal week (Farber & Lolley, 1974; Lolley *et al.,* 1974). The morphology of the inner layers of the retina appears to be unaffected by the disease but biochemical adjustments to the loss of photoreceptor cells, like elevated glucose and glycogen levels, have been reported (Lolley, 1972). The mutant phenotype has been attributed to the defective activity of rod cGMP phosphodiesterase (PDE). The latter appears to be deficient before the onset of photoreceptor degeneration and its levels are very low throughout postnatal life (Schmidt & Lolley, 1973). A number of other biochemical abnormalities are apparent in *rd1/rd1* retinas (Lolley *et al.,* 1974). Retinas in the *rd1/rd1* mouse were found to accumulate large amounts of cGMP, attributed to abnormally low cGMP PDE activity, strongly implicating defective cGMP metabolism in photoreceptor
degeneration. *In vitro* studies by Lolley *et al.* (1977) demonstrated the deleterious effects of increased cGMP levels to retinal photoreceptors. Raised cGMP in toad cultured cells, caused by addition of the unspecific PDE inhibitor 3-isobutyl-1-methylxanthine (IBMX) in the culture medium, induced photoreceptor degeneration. It therefore became necessary to elucidate the role of cGMP in the visual cycle, in order to understand why photoreceptor cells degenerate in the *rd/rd1* mouse.

Although a retinal degeneration mutation was long known to be present in the C3H mouse strain, it was not until 1990 that Bowes *et al.* found that the mouse *rd1* locus encodes the β subunit of the rod photoreceptor 3' 5' cGMP phosphodiesterase (Pde6b). The product of Pde6b contributes to the rod heterotetrameric phosphodiesterase complex (PDE α, β, γ, γ) (Deterre *et al.,* 1986; Fung *et al.,* 1990), which regulates cytoplasmic cGMP levels in rod

Gene symbol	Mode of Inheritance	Protein	Location
CERKL	Recessive	ceramide kinase-like protein	2q31.3
ABCA4	Recessive	ATP-binding cassette transporter - retinal	1p22.1
CA4	Dominant	carbonic anhydrase IV	17q23.2
CNGA1	Recessive	rod cGMP-gated channel alpha subunit	4p12
CRB1	Recessive	crumbs homolog 1	1q31.3
CRX	Dominant	cone-rod otx-like photoreceptor homeobox transcription factor	19q13.32
GUCA1B	Dominant	guanylate cyclase activating protein 1B	6p21.1
IMPDH1	Dominant	inosine monophosphate dehydrogenase 1	7q32.1
LRAT	Recessive	lecithin retinol acyltransferase	4q32.1
MERTK	Recessive	c-mer protooncogene receptor tyrosine kinase	2q13
NRL	Dominant, recessive	neural retina lucine zipper	14q11.2
PDE6A	Recessive	cGMP phosphodiesterase alpha subunit	5q33.1
PDE6B	Recessive	rod cGMP phosphodiesterase beta subunit	4p16.3
PRPF3	Dominant	human homolog of yeast pre-mRNA splicing factor 3	1q21.2
PRPF31	Dominant	human homolog of yeast pre-mRNA splicing factor 31	19q13.42
PRPF8	Dominant	human homolog of yeast pre-mRNA splicing factor C8	17p13.3
RDS	Dominant	peripherin 2	6p21.2
RGR	Recessive	RPE-retinal G protein-coupled receptor	10q23.1
RHO	Dominant, recessive	rhodopsin	3q22.1
RLBP1	Recessive	cellular retinaldehyde-binding protein	15q26.1
ROM1	Dominant	rod outer segment membrane protein 1	11q12.3
RP1	Dominant, recessive	RP1 protein	8q12.1
RP2	X-linked	RP2 protein similar to human cofactor C	Xp11.23
RP22	Recessive	not identified	16p12.3-p12.1
RP23	X-linked	not identified	Xp22
RP24	X-linked	not identified	Xq26-q27
RP25	Recessive	not identified	6cen-q15
RP28	Recessive	not identified	2p16-p11
RP29	Recessive	not identified	4q32-q34
RP31	Dominant	not identified	9p22-p13
RP32	Recessive	not identified	1p34.3-p13.3
RP33	Dominant	not identified	2cen-q12.1
RP6	X-linked	not identified	Xp21.3-p21.2
RP9	Dominant	PIM1-kinase associated protein 1	7p14.3
RPE65	Recessive	pigment epithelium-specific 65 kD protein	1p31.2
RPGR	X-linked	retinitis pigmentosa GTPase regulator	Xp11.4
SAG	Recessive	arrestin (s-antigen)	2q37.1
SEMA4A	Dominant	semaphorin 4A	1q22
TULP1	Recessive	tubby-like protein 1	6p21.31
USH2A	Recessive	usherin	1q41

Table 1: Genes implicated in non-syndromal forms of retinitis pigmentosa

photoreceptors in response to light. On light stimulation, PDE is activated by the removal of the two inhibitory γ subunits, resulting in decreased cGMP levels and the hyperpolarisation of the rod cell. Failure to form a normal PDE complex compromises the enzyme's activity, reducing cGMP hydrolysis and leading to increased cGMP concentration and rod degeneration (Hussain *et al.*, 1992). The destructive effect of mutated rod cGMP PDE on photoreceptor survival is further highlighted by the fact that more than 95% of retinal cGMP is present in photoreceptor cells (Cohen, 1984). An equally high percentage of cGMP in the cells' outer segments may be bound to the cGMP enzyme PDE (Pugh & Lamb, 1990). Therefore, as discussed by Hussain *et al.* (1992), defective PDE, which has a higher Km and, hence, a lower affinity for cGMP, results in an increased free concentration of cGMP in the outer segments. The cGMP-gated cation channels therefore remain permanently open, which increases the intracellular levels of several ions, including calcium. The latter has been implicated in a number of disease phenotypes, and can influence guanylate cyclase, rhodopsin and/or PDE activities. It can also potentially modulate both the function and survival of photoreceptor cells, including the light-response recovery, rod sensitivity and light adaptation (Pepe *et al.*, 1986; Wagner *et al.*, 1989). Ultimately the ionic imbalance observed in mutated photoreceptors may lead to their death by apoptosis.

1.2.2.1.2. Rod cGMP phosphodiesterase 6b: the atypical retinal degeneration 1 mutation (*Pde6b*^{atrd1})

As part of the MRC Harwell ENU mutagenesis program, new models of retinal degeneration were identified. N-ethyl-N-nitrosourea (ENU) is an alkylating agent that, when injected into mouse spermatogonial stem cells, acts as a powerful mutagen by creating point mutations at random across the genome (Justice *et al.*, 1999). Its ethyl group can be transferred to oxygen or nitrogen radicals in DNA and, if not repaired, result in mispairing or base pair substitutions, inducing many different types of mutant alleles (Justice *et al.*, 1999). The mutagenesis programme involves mating of ENU-mutagenised male BALB/C mice to C3H females, to produce F1 progeny that are then screened for the phenotype of

interest, in this case, eye defects (Thaung *et al.,* 2002). Because C3H mice are homozygous for the *Pde6b*^{rd1} allele, all the F1 mice screened were heterozygous for the recessive *Pde6b*^{rd1} allele, which enabled Thaung *et al.* (2002) to identify seven mutant lines that carried new recessive alleles of *Pde6b.* The phenotype of four of these lines was indistinguishable from that of the *rd1* allele in C3H, and these were named retinal degeneration 1, 1-4 Harwell (*Pde6b*$^{rd1\text{-}1\text{-}4H}$). On fundus examination, the remaining three new mutant lines appeared to have a near-normal retina at 3 weeks of age compared with the degenerated retina observed in age-matched C3H mice. These lines were named atypical retinal degenerations (*atrd*) 1-3 (*Pde6b*$^{atrd1\text{-}3}$). Subsequent work by the same group analysed the timescale of retinal degeneration in these new models of RP. Indeed, the *atrd* mutants showed slower onset of retinal degeneration as determined by visual acuity testing (the mice responded well to a rotating drum at 3.5 weeks, but were effectively blind by 10 weeks), fundus examination (near normal fundus at 3.5 weeks, discolouring of optic disks by 6 weeks and indistinguishable from *rd1* homozygotes by 10 weeks) and histology (mild cell loss at 3.5 weeks but rapid progression thereafter) (Hart *et al.,* 2005).

1.2.2.1.3. Rhodopsin knockout mouse

The involvement of rhodopsin in the process of vision has been postulated from as early as the 19th century, and a large amount of research has established its central role in phototransduction.

The structure of the mouse rhodopsin gene (*Rho*), as well as that of its transcription and translation products, were analysed by Baehr *et al.* (1988) and the protein's function has been reviewed by Garriga & Manyosa (2002). The gene is found on mouse chromosome 6, is just over 3 kilobases long and has 5 exons. Despite a difference in the length of the introns, the length of the exons is identical between the species homologues. At the nucleotide level, the mouse sequence of rhodopsin is 62% and 59% identical to the human and bovine sequences, respectively. Rhodopsin consists of the 348-amino-acid protein opsin and the 11-*cis*-retinal chromophore, which are covalently attached. It belongs to the G-protein coupled receptor superfamily, members of which share a seven-transmembrane helical structure and activate G-proteins upon ligand binding. In

the case of the visual system, the G-protein is transducin. Rhodopsin is the main protein component of the rod OS disks in vertebrate retina, comprising about 70% of the total protein (Baehr *et al.,* 1988). The amino-terminus of the protein resides within the lumen of the disk, whereas the carboxy-terminus is in the cytoplasm (Humphries *et al.,* 1992).

Light activation triggers a cascade of events that result in cell signalling. Upon exposure to light, the 11-*cis*-retinal attached to opsin isomerises to all-*trans*-retinal, which leads to the activation of transducin, by the exchange of GDP for GTP. The signal is considerably amplified during propagation until hyperpolarisation of the cell occurs and a reduction in the rate of photoreceptor neurotransmission that is perceived as light (Baehr *et al.,* 1988).

Although initial research focused on understanding the function of rhodopsin, it was not until after the gene was cloned (Nathans & Hogness, 1984) and an autosomal dominant RP gene was mapped to this locus (Humphries *et al.,* 1992) that mutations in its sequence were identified (Dryja *et al.,* 1990a, 1990b, 1991). This subsequently led to the association of rhodopsin with visual impairment. Indeed mutations in *RHO,* residing on human chromosome 3, account for 25-30% of autosomal dominant RP (RetNet at http://www.sph.uth.tmc.edu/Retnet/home.htm). Experimentally-induced or genetically-inherited mutations in rhodopsin have thrown light on the importance of rhodopsin, not only in terms of its biochemical role in visual transduction but also in maintaining the integrity of the retina. Different laboratories have therefore produced mouse lines expressing rhodopsin either at different levels or with different mutations (Olsson *et al.*, 1992; Naash *et al.*, 1993).

Olsson *et al.* (1992) made a transgenic mouse line that carried a mutant (P23H) human allele. The animals showed marked photoreceptor degeneration by P20, although the inner retinal layers appeared normal. Also, Naash *et al.* (1993) established a transgenic mouse line that carried a mutated mouse opsin gene in addition to the endogenous opsin gene. Three amino-acid substitutions were made (V20G, P23H, P27L) near the N-terminus of rhodopsin in exon 1. The heterozygous animals appeared initially to develop normal photoreceptors but these failed to reach full length. The number of both rods and cones decreased with age, which was reflected also by the gradual decrease in light-evoked ERG responses.

Humphries *et al.* (1997) produced a rhodopsin knockout (KO) mouse by targeted disruption of the *Rho* gene by homologous recombination. They introduced a neomycin resistance cassette within the second exon of the gene, which resulted in reduced levels of rhodopsin mRNA and protein as detected by reverse transcription-polymerase chain reaction (RT-PCR) and immunohistochemistry, respectively. Since this is one of the retinal degeneration models used in this project, its phenotype will be described in more detail. At P24, homozygous mutant animals had normal numbers of rod nuclei, normal ONL thickness but no rod OS. The ONL began to thin at P30 and was absent by P90. Preliminary ERGs showed that there was no dark-adapted (rod) response at 8 weeks, whereas substantial light-adapted responses were present in younger animals. The mice otherwise developed normally. The heterozygotes retained the majority of their photoreceptors but the IS and OS displayed some structural disorganisation, the OS becoming shorter with age. Analysis of retinal sections at 4 months of age revealed that heterozygotes had thinner ONL and shorter OS. They appeared otherwise normal, although there was evidence of some disorganisation. The homozygous mutants showed a declining number of photoreceptor cells with age. At P48, the ONL was reduced to 4-5 rows of nuclei and the inner and outer segments were even thinner. Finally by P90, a single layer of nuclei was left in the ONL, indicating completion of the photoreceptor degeneration. Degeneration was relatively uniform from the periphery to the central retina. Electron microscopy on 27-day old rhodopsin mutant eyes revealed that the region between the outer limiting membrane (between IS and OS) and the RPE contains material primarily of IS origin, including cilia, basal bodies and mitochondria. No intact OS material was found. Therefore, even at this young age there was no evidence of rod OS in animals lacking functional rhodopsin genes. Immunohistochemical analysis of rhodopsin in 8-week old animals from all three genotypes showed positive staining in the wild-type and the heterozygote but no immunoreactivity in the mutant. Evidence of photoreceptor disorganisation was seen in the heterozygote. Finally, dark-adapted (rod) ERG responses from 10 and 13 week old animals were similar to wild-types and heterozygotes. ERGs were absent however in the homozygous mutants. The light-adapted (cone) ERG responses were slightly reduced in the homozygous mutants only.

Subsequently, different groups generated alternative mouse models with reduced or absent of rhodopsin expression (Lem *et al.*, 1999; Toda *et al.*, 1999; Frederick *et al.*, 2001; Liang *et al.*, 2004) and confirmed the early photoreceptor degeneration described by Humphries *et al.* (1997). Additionally, Sung *et al.* (1994) studied a naturally occurring stop codon mutation that removes the last five amino acids of rhodopsin (Q334ter). These authors observed an abnormal accumulation of mutant rhodopsin in the plasma membrane of photoreceptor cells, indicating that the C-terminus of rhodopsin is required for transportation to or retention in the outer segments.

Most of the work mentioned above focused on the effects of decreased or absent rhodopsin expression on photoreceptor structure or survival. Tan *et al.* (2001) however demonstrated that over-expression of wild-type rhodopsin can also lead to photoreceptor degeneration. A two-fold increase in opsin expression was accompanied by a 33% increase in 11-*cis* retinal levels and resulted in a reduction of the ERG a-wave amplitudes, which were indistinguishable from the background. Even a 23% increase in opsin levels was sufficient to induce degeneration similar to the various retinal degeneration mouse models.

Work on many different rhodopsin mutant models has showed that most mutations confer similar phenotypes, characterised by photoreceptor degeneration that is completed within a few months of age. In a review discussing the molecular genetics of RP, Humphries *et al.* (1992) raised the question as to how mutations in rhodopsin cause RP. Does phototransduction have any direct relevance to the manifestation of RP? The fact that rhodopsin functions as a light-absorbing protein might be coincidental. Another possibility is that some mutant rhodopsin molecules may not be efficiently transported from the ER after translation, compromising the function and structure of photoreceptor cells. If the mutant proteins do get transferred to the outer segment disks, this may destabilise the disks. It is therefore still not clear what molecular mechanism underlies the RP phenotype when rhodopsin is mutated.

1.2.2.1.4. Peripherin 2: the retinal degeneration slow mutation (*Prph2*^{rds})

The slowly progressing retinal degeneration associated with a spontaneous mutation in the peripherin 2 gene (*Prph2*^{rds}) was first reported in the inbred mouse strain 020/A by van Nie *et al.* (1978) and soon after the same group mapped the gene to mouse chromosome 17 (Demant *et al.*, 1979). It was over a decade before a candidate gene was identified (Travis *et al.,* 1989) and another 6 years before the exact nature of the mutation, which prevented the translation of the gene, was revealed (Ma *et al.*, 1995). The first evidence as to the nature of the *Prph2* gene came from two papers published in 1991. Firstly, Travis *et al.* (1991) showed that Prph2 is a 39 kDa, 346 amino acid, photoreceptor-specific integral membrane component of OS discs, which is responsible for the *rds* mutation. Subsequently, Connell *et al.* (1991) found that there was a 92.5% identity at the protein level between a known bovine protein called peripherin and the candidate Rds protein identified by Travis *et al.* (1991). Not much was known about the function of peripherin at the time, apart from the fact that it is found in rod photoreceptor cells along the rim region of the OS discs.

During the decade between mapping the gene to chromosome 17 and identifying its genetic basis, there was extensive phenotypic analysis of the mutant mice. In a wild-type mouse, the retina takes three weeks to fully develop (Young, 1984). The photoreceptor cells of 7-day-old retinas have an IS, but no OS. The latter starts to form at P10 and its development and elongation are completed by P21. In the homozygous mutant *rds* retina while P7 retinas are identical to wild-type (Sanyal *et al.,* 1984), there is a subsequent failure to develop OS. Loss of photoreceptor cells begins from as early as 2 weeks of age and thereafter, the ONL, OPL and photoreceptor layers begin to reduce in thickness (Sanyal *et al.,* 1980, 1984). Photoreceptor degeneration is more rapid up to the age of 2-3 months (Sanyal *et al.,* 1980; Nir *et al.,* 1990) but the loss is distributed over many months (Cohen, 1983; Sanyal *et al.,* 1980). The inner retinal layers and the RPE remain unaffected until after loss of visual cells, when structural changes begin to involve the entire retina (Sanyal *et al.,* 1980). With the gradual decline of the photoreceptors in older animals, the IS appear to be reduced

in length and contained fewer mitochondria and other organelles (Jansen & Sanyal, 1984).

The expression of some other photoreceptor proteins is also altered in the mutants. Prph2 is normally detected predominantly in the OS layer of rod-dominant bovine and mouse photoreceptors, but in the homozygous mutant it is absent and in the heterozygous mutant there is ectopic labelling in the IS (Molday *et al.,* 1994). Opsin mRNA and protein levels are also significantly lower in homozygous mutants (Schalken *et al.*, 1985), due to reduction in the synthesis of opsin (Nir *et al.*, 1990). At the onset of degeneration, some of the photoreceptor cells show positive opsin expression (Nir *et al.,* 1990; Jansen *et al.,* 1987), which in older retina is localised to elongated membranes emanating from a few ciliary tips (Nir *et al.,* 1990).

Biochemical analysis performed in *rds/rds* mutants revealed that cGMP levels are decreased in the mutant (Sanyal *et al.,* 1984; Sanyal, 1984), whereas cAMP PDE activity is higher (Sanyal, 1984). This is in agreement with the observation that cAMP is less concentrated in the photoreceptor outer segments, whereas cGMP is preferentially concentrated in OS (Orr *et al.,* 1976).

In terms of understanding the molecular basis underlying the retinal degeneration in the *rds/rds* mutants there have been a number of suggestions. The morphological observation that the formation of the disks, an essential step in the development of the OS, is blocked from the first week of retinal development in the *rds/rds* retina (Jansen & Sanyal 1984), while the degeneration takes a year to be completed, demands an explanation. Travis *et al.,* (1991) suggested that photoreceptor degeneration might be happening because of three different possibilities. Firstly, photoreceptor cells degenerate because of prolonged oxygen toxicity. Steinberg (1987) showed that pO_2 is 120 mmHg at the level of the OS as a result of the high density of choroidal capillaries in the area, and drops to 30 mmHg at the level of the IS, due to their high metabolic activity. Lack of OS would therefore impose a high pO_2 on the IS. Secondly, failure to form OS may lead to metabolic changes that, in turn, might cause degeneration. Finally, degeneration could be explained by a loss of trophic factors, provided by other retinal cells, like RPE or Muller cells that are required by OS. Previously Nir *et al.,* (1990) suggested that mutated *Prph2* compromises a key metabolic process and the defect of disc morphogenesis is only one of its downstream consequences.

It seems however that a structural, rather than biochemical, role is attributable to Prph2. Travis *et al.,* (1991) proposed that the Prph2 protein stabilises discs through either homophilic or heterophilic interactions with itself or with another disc membrane protein, now known to be the rod outer segment membrane protein 1 (Rom1) (Bascom *et al.*, 1992; Molday, 1994) This is compatible with the postulate that lack of Prph2 would not prevent membrane biogenesis, but would block the subsequent folding of membranes into discs, which is in fact the case.

In conclusion, the retinal location of Prph2 and the phenotype associated with the *rds* mutation both suggest that this membrane protein may play a role in the assembly, morphogenesis and maintenance of the disk rim structure (Connell *et al.,* 1991; Molday, 1994).

1.3. The link between apoptosis, reactive oxygen species and RP

In the first part of the Introduction (**section 1.1.2**.) the generation of ROS in mitochondria was discussed, as well as their damaging effects on DNA, protein and lipids. Cellular defence mechanisms exist which protect against oxidative stress, either at the stage of its generation or later, when it attacks cellular molecules. In the second part of the Introduction (**section 1.2.1**.) a description of the mouse eye was given, and its anatomy and function were discussed. Attention was focused on photoreceptor cells since mutations in photoreceptor-specific genes have been implicated in apoptotic cell death during RP-type retinal degeneration.

The main question in this project is concerned with whether there is a link between oxidative stress and retinal degeneration. If the answer is positive, what is the role of oxidative stress in the disease phenotype? A number of points support the assertion that there is a link between the two.

1.3.1. The susceptibility of the retina

The retina is particularly sensitive to oxidative damage (**Figure 10**) (Winkler *et al.,* 1999). Firstly, it is constantly exposed to different wavelengths of light, some of which can cause injury to photoreceptor cells (Noell *et al.,* 1966). Secondly,

there is a high concentration of polyunsaturated fatty acids (PUFAs) in the outer segments (op den Kamp, 1979; Stone *et al.,* 1979), which can participate in oxidative chain reactions that result in the disruption of retinal structure. Thirdly, there is a high oxygen tension in the outer retina originating from the choroidal blood flow (Rodieck, 1973). Towards the tip of the outer segments the oxygen partial pressure is about 120 mm Hg, and it drops to about 30 mm Hg towards the photoreceptor inner segment (Steinberg, 1987). Fourthly, rod photoreceptors have one of the highest rates of energy utilisation of any cell in the body. The metabolic rate, as this is reflected by oxygen consumption, has been reported to be much higher in the retina than in most other tissues (Rodieck, 1973). For example, in the human retina, the total rate of oxygen consumption has been calculated to be 23 ml/ 100g of retina/ minute (Rodieck, 1973), which is about 7 times higher than that reported for the brain (Kety & Schmidt, 1948). The increased Na^+K^+ ATPase activity supporting the 'dark current', the high rate of cGMP turnover and neurotransmission, each require large amounts of energy in the retina, which is generated mainly by oxidative metabolism (Ames *et al.,* 1992). Finally, in the IS of photoreceptors there is a high density of mitochondria and high concentration of oxidative enzymes. Using electron microscopy, it was demonstrated that the apical portion of rod IS has dense aggregates of mitochondria (Sjostrand, 1953). Lowry *et al.* (1956) showed that, in the IS of rabbit and monkey retinas, there was increased activity of the mitochondrial enzymes malate dehydrogenase (MDH) and glutamic-aspartic transaminase. Lastly, high cytochrome *c* oxidase (COX) and succinate dehydrogenase (SDH) activities have been found in photoreceptor IS, using different staining methods (Wislocki & Sidman, 1954; Andrews *et al.,* 1999). For all these reasons, the retina is particularly sensitive to metabolic stress, including oxidative stress.

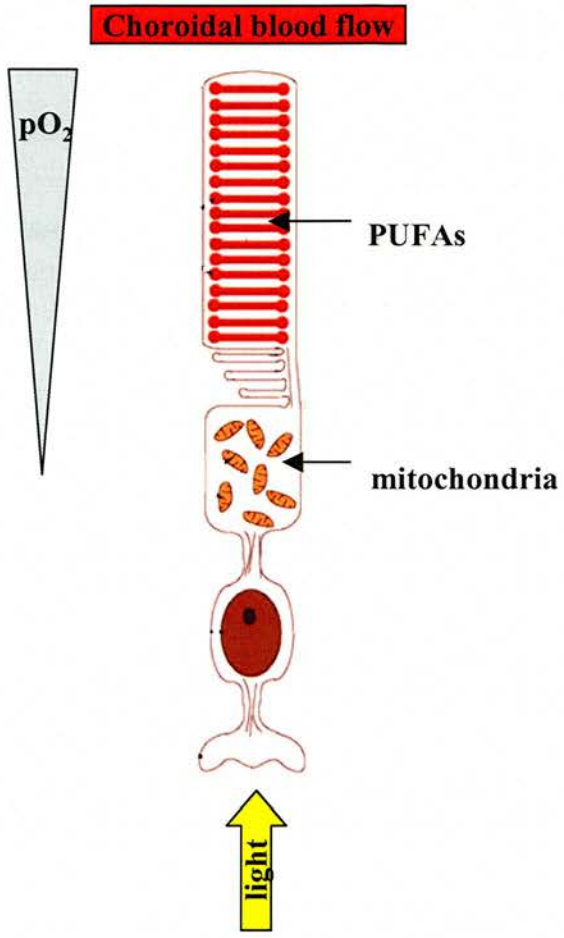

Figure 10: The susceptibility of the retina

The factors that make the retina particularly susceptible to damage from oxidative stress are shown. The retina is constantly exposed to visible light, there is a high concentration of polyunsaturated fatty acids (PUFAs) in the outer segments, there is high oxygen tension imposed on the cell due to their close proximity to the choroidal blood flow, and there is a high density of mitochondria in the inner segment.

1.3.2. Mechanisms of cell death

Programmed cell death (PCD) is an essential event that takes place during both development and disease. It is initiated by specific signals and requires both *de novo* and controlled gene expression. PCD serves to remove unwanted cells from a multicellular organism (Schwartz *et al.,* 1993). There are different mechanisms by which it can occur, namely apoptosis and autophagy, each of which has distinctive morphological, biochemical and physiological characteristics. In autophagy, a cell destroys itself by digesting its own constituents. It is characterised by the formation of large autophagosomes, autolysosomes, autophagic vacuoles, myelin whorls, multivesicular bodies and engulfment of entire organelles (Bursch, 2000; Larsen & Sulzer, 2002). Its genetic regulation is not well understood. Morphologically, apoptosis is characterised by the circularisation of the cell, nuclear and chromatin condensation, DNA fragmentation, cytoplasmic vacuolisation, disruption of the nuclear envelope and formation of vesicles (apoptotic bodies) destined for degradation and phagocytosis by neighbouring cells such as macrophages (Kerr *et al.,* 1987; Bursch, 2000; Larsen & Sulzer, 2002). In addition to these two types of PCD, cell death can also occur via necrosis, which is an unprogrammed type of cell death and is the outcome of severe disruption of cellular processes (Allan *et al.,* 1987). Necrosis is characterised by mitochondrial swelling, rupture of internal and plasma membranes, chromatin aggregation, nucleus invagination, organelle lysis and eventually total disintegration of organised structures (Allan *et al.,* 1987; Hall *et al.,* 1997).

The terms PCD and apoptosis are often used interchangeably, since the latter is the best studied type of cell death. It has been repeatedly demonstrated that apoptosis is triggered by various stimuli, including cellular stress, loss of housekeeping functions and/or developmental signals. Once triggered, apoptosis can be executed through different pathways, which involve members of a family of cysteine proteases called caspases. Apoptosis can occur via three different pathways; either via death receptors, involving caspase 8, or mediated by ER stress and involving caspase 12, or by the intrinsic or mitochondrial pathway,

mediated by mitochondria (Rao *et al.*, 2004). The latter pathway is of particular interest to this project as it involves the mitochondrion, the organelle that is not only the major source of oxidative stress in the cell, but also the major source of cellular energy, therefore controlling both the life and death of a cell.

The molecular events underlying this 'intrinsic' pathway of apoptosis have been extensively studied (**Figure 11**) (Blackstone & Green, 1999; Green & Kroemer, 2004; Spierings *et al.*, 2005; Heath-Engel & Shore, 2006). It is defined by the process of mitochondrial outer membrane permeabilisation (MOMP). The latter is both executed and regulated by members of the B-cell leukemia/lymphoma 2 (BCL-2) protein family, which interact with the MOM and with each other to activate or inhibit the release of apoptosis-promoting proteins from the mitochondrial IMS. MOMP can happen either with or without the involvement of the MIM (Green *et al.*, 2004). In the former case, the non-selective mitochondrial permeability transition pore (MPTP) is formed by constituents of both the MIM and the MOM. It leads to loss of the membrane potential ($\Delta\psi_m$) and swelling of the mitochondrial matrix. This swelling can disrupt the MOM and lead to MOMP (Green & Reed, 1998). If the MIM is not involved, then members of the BCL-2 family, such as Bax and Bak, can act directly on the MOM and cause MOMP. Upon MOMP, there is cytosolic release of proteins, like cytochrome *c*, HSP10, Smac, Omi, endonuclease G, and apoptosis inducing factor (AIF), that are normally residing in the IMS. Once released, cytochrome *c* interacts with apoptotic peptidase activating factor 1 (APAF1), changes its conformation and the two oligomerise to form part of the apoptosome. The latter activates caspase 9 by causing it to dimerise, which in turn activates the downstream 'executor' caspases 3 and 7, by cleaving the corresponding procaspases (**Figure 11**).

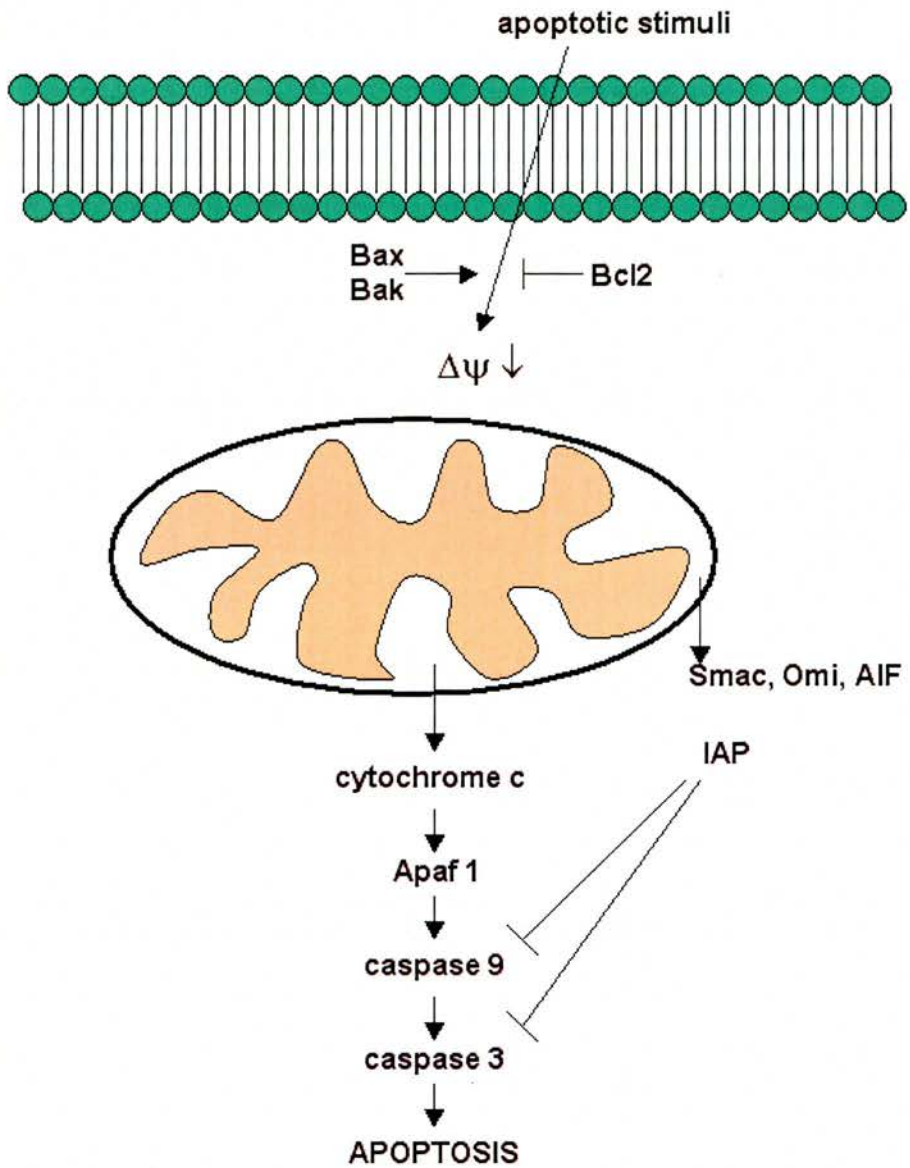

Figure 11: The intrinsic pathway of apoptosis.

Upon stimulation of MOMP, cytochrome *c* is released from the mitochondrial IMS into the cytosol, where it interacts with Apaf1 and activates caspase 9. The latter then activates the executor caspase 3. The initiation of apoptosis by MOMP is inhibited by Bcl2 but promoted by both Bak and Bax. Together with cytochrome *c*, smac (DIABLO) is also released and blocks the pro-apoptotic action of IAF (Modified image from Mak *et al. Arthritis Res* 2002 **4**(Suppl 3): S243).

Inhibitory and activating interactions between anti- and pro-apoptotic proteins orchestrate apoptosis. Inhibitor of apoptosis proteins (IAPs) bind and ubiquitinate caspases for proteasomal degradation. IAPs are themselves blocked by IAP inhibitors, like second mitochondria-derived activator of caspases (Smac). AIF translocates from the IMS to the nucleus via the cytosol to promote DNA condensation (Cande *et al,* 2002). Also, the protein Omi is released from the IMS into the cytosol, where it promotes apoptosis by blocking inhibitors (Wolf & Green, 2002).

In some types of apoptosis, the morphology, intra-organellar organisation and intracellular location of mitochondria change, prior to cytochrome *c* release. Mitochondrial morphology is determined by fusion and fission events and can range from multiple spherical organelles to branched, tubular structures (Bereiter-Hahn *et al.,* 1994; Bleazard *et al.,* 1999). Skulachev *et al.* (2004, 2006) showed that during apoptosis there is massive 'thread-grain' transition from extended to small round-shaped mitochondria. These move from the periphery of the cell towards the nucleus, possibly to enable released proteins, such as endonuclease G, to enter the nucleus for the execution of final apoptotic events.

The fission of mitochondria and MOMP are both required but are not sufficient for subsequent release of cytochrome *c* (Heath-Engel & Shore, 2006). They have to be accompanied by remodelling of cristae, infoldings of the MIM, where about 85% of cytochrome *c* is stored. This remodeling depends on Ca^{2+} released from the ER (Germain *et al.*, 2002) and involves both fusion of individual cristae and opening of the junctions between them and the IMS (Scorrano *et al.,* 2002).

It is also noteworthy that although caspases are believed to be the principal proteins orchestrating and carrying out apoptosis (Samali *et al.,* 1999; Slee *et al.,* 1999a, 1999b; Wolf & Green, 1999), a caspase-independent apoptosis pathway also exists (Borner & Monney, 1999). This was discovered when apoptotic phenotypes were still evident despite inhibition of caspases using Z-VAD.fmk (McCarthy *et al.,* 1997). As Borner and Monney (1999) discuss however, the non-specificity of these inhibitors and/or the possible existence of as yet unidentified caspases does not rule out the involvement of caspases in every apoptotic pathway. However, in degenerating photoreceptor cells both during development (Donovan *et al.,* 2001) and in the *rd/rd* mouse model for RP (Donovan & Cotter,

2002) a decreased level of APAF1 and a lack of release of cytochrome *c* from mitochondria, indicate failure to form an apoptosome which would subsequently activate caspases, consistent with an alternative apoptotic pathway.

1.3.3. Apoptosis and reactive oxygen species

The involvement of mitochondria in apoptosis, and the fact that it is the major source of oxidative stress in the cell, implicate ROS in this type of cell death. Additionally, the dual nature of cytochrome *c*, as both an electron carrier in the ETC and a pro-apoptotic substance released during apoptosis, supports the link between oxidative stress and apoptosis. Indeed, the involvement of ROS and cellular REDOX state in apoptosis has been the focus of a number of reviews (e.g. Blackstone & Green, 1999), which suggest that ROS can be both a triggering factor for apoptosis and a downstream consequence of it. Buttke & Sandstrom (1994) point out that many chemical or physical treatments, like ionisation or UV irradiation, are capable of inducing apoptosis and also evoke oxidative stress. Increase of ROS, for example by exposure to low doses of H_2O_2 (Barbouti *et al.* 2002) or depletion of antioxidants (Matsui *et al.*, 2003), has also been shown to result in apoptosis in various cell types.

An antioxidant role for BCL-2 has also been proposed in the context of cell death. *In vitro* work by Hockenbery *et al.* (1993), investigating the generation of ROS during apoptosis, showed that cell death induced by H_2O_2 treatment or interleukin 3-deprivation was blocked by BCL-2 or was repressed by GPX4 but not by SOD2. Also, the antioxidant N-acetyl cysteine, which increases GSH, was also shown to partially inhibit apoptosis. These results point towards a prominent role for ROS in cell death and an antioxidant role for BCL-2 after $O_2^{-\bullet}$ and H_2O_2 production. BCL-2 has also been shown to block cell death induced by gamma-irradiation, which produces hydroxyl radicals by direct radiolytic attack on water (Blok & Loman, 1986; Sentman *et al.,* 1991). Finally, Zhong *et al.* (1993) reported that BCL-2 can inhibit the death of a neural cell line due to a range of stimuli, including membrane peroxidation and free radical-induced damage caused by menadione. It has been suggested that BCL-2 acts either as a direct radical scavenging protein, or as a metal-binding protein (Kane *et al.,* 1993).

Jacobson and Raff (1995) argued however that protection against PCD by BCL-2 is independent of its ability to inhibit the effects of ROS. Although antioxidants have been shown to block certain ROS-dependent signal transduction pathways that induce PCD, they do not block the effector phase of PCD. These authors therefore concluded that ROS are not an essential part of PCD, but can be generated as a consequence of it.

Nevertheless, genetic evidence for a role of ROS in cell death is suggested by familial amyotrophic lateral sclerosis, since mutations in the antioxidant enzyme *SOD1* argue strongly for ROS-mediated loss of motor neurons (Rosen *et al.*, 1993).

1.3.4. Apoptosis and retinal degeneration

The cell death pathway by which photoreceptor cells degenerate in response to different stimuli has been addressed in a number of papers (Travis, 1998; Pierce, 2001). It is apparent that there is not a single type of cell death associated with a particular trigger for photoreceptor degeneration. The fact that markers for apoptosis, autophagy and/or necrosis have been seen within a single model of photoreceptor degeneration implies an overlap between them. It is known that photoreceptor cell death in normal developing retina peaks at P7 and occurs mainly by apoptosis (Young, 1984; Chang *et al.*, 1993; Portera-Caillau *et al.*, 1994; Donovan & Cotter, 2002). Morphological signs of autophagy are observed in the destruction of photoreceptor outer segments by the RPE (Reme *et al.*, 1999), although this is best described as heterophagy. Autophagy has also been implicated in developmental retinal cell death (Guimaraes *et al.*, 2003). Photoreceptor degeneration induced by light damage has been shown to occur by apoptosis (Donovan *et al.*, 2001; Donovan & Cotter, 2002; Hao *et al.* 2002; Lohr *et al.*, 2006), necrosis (Moriya *et al.*, 1986; Zhang *et al.*, 2005; Lohr *et al.*, 2006) and/or autophagy (Reme *et al.*, 1999; Lohr *et al.*, 2006). *In vitro* work on chemically-insulted cultured retinal neurons, by Ca^{2+} overload or ceramide synthesis inhibition, demonstrated apoptotic death of these cells (He *et al.*, 2000; Germain *et al.*, 2006). Finally, photoreceptor degeneration in a rat model for ischemia-reperfusion was also shown to occur through apoptosis (Katai & Yoshimura, 1999).

RP is a diverse group of hereditary disorders and consequently our interest lies in the mechanisms by which photoreceptor cells die in response to different genetic mutations, rather than as part of the tissue development or in response to external insults. Photoreceptor degeneration in the *rd1/rd1* mouse model occurs by apoptosis, as this has been repeatedly shown to include intra-nucleosomal DNA fragmentation (Chang *et al.,* 1993; Lolley *et al.,* 1994; Portera-Cailliau *et al.,* 1994). Nevertheless, signs of autophagy and necrosis have also been observed in degenerating *rd1/rd1* retinas (Lohr *et al.,* 2006). In the *rds* mouse model for RP, which fails to produce a protein necessary for efficient OS formation, photoreceptors have been shown to die by apoptosis (Chang *et al.,* 1993; Portera-Cailliau *et al.,* 1994; Lohr *et al.,* 2006), although signs of neuro-inflammation, usually associated with necrosis (Allan *et al.,* 1987), have also been observed (Lohr *et al.,* 2006). Finally, in the rhodopsin knockout mouse model, photoreceptor degeneration occurs by apoptosis (Chang *et al.,* 1993; Portera-Cailliau *et al.,* 1994) and there has been no evidence of alternative types of cell death.

1.3.5. Reactive oxygen species and retinal degeneration

Evidence for a link between apoptosis and oxidative stress, as well as between apoptosis and retinal degeneration has been presented. Is there evidence for an involvement of oxidative stress in retinal degenerations?

Working *in vitro*, Sanvicens *et al.* (2004) investigated the role of oxidative stress in photoreceptor degeneration, by treating the photoreceptor-related cell line 661W with the nitric oxide donor sodium nitroprusside. ROS production did increase in mitochondria and this in turn triggered the apoptosis of these cells, in a manner requiring both calpains and caspases.

Photoreceptor degeneration in BALB/C mice following exposure to excessive levels of white light was accompanied by increased intracellular Ca^{2+} levels, generation of $O_2^{-\bullet}$ and mitochondrial depolarisation (Donovan *et al.,* 2001), all of which are signs of oxidative stress. Additionally, degeneration in this model was successfully prevented by treatment with a nitric oxide synthase inhibitor, indicating a role for nitric oxide in light damage.

A direct involvement of oxygen toxicity in photoreceptor degeneration was suggested by a study by Yamada *et al.* (2001). The authors exposed wild-type mice to 75% O_2 for one or two weeks. No effects were observed at the first time-point, but the thickness of the ONL was significantly reduced after a 2-week exposure, showing that hyperoxia can lead to photoreceptor cell death. However, these concentrations of oxygen are unlikely to occur *in vivo* during retinal degeneration.

The involvement of oxidative stress in the *rd1/rd1* and *rds/rds* mouse retinal degeneration mutants has been suggested by Lohr *et al.* (2006). These authors compared the relative expression of ceruloplasmin and clusterin during these retinal degenerations. In the *rd/rd1* mutant, these markers of oxidative stress were constitutively over-expressed, and in the *rds/rds* mutant they were also elevated to varying degrees throughout the period studied.

Very little work has been done on investigating the effect of decreased *Sod2* expression in retinal diseases. Sandbach *et al.* (2001) analysed the ocular pathology of Sod2-deficient mice. They studied *Sod2*$^{-/-}$ mice at P10 and P20, since their survival time was extended by the use of the Sod-mimetic, MnTBAP. In 10-day-old mice, only the photoreceptor layer in the central retina was thinner when compared to controls of the same age. In 20-day-old animals, both the INL and the photoreceptor layers were thinner, while the RPE was the same as in wild-type. The total retinal thickness was reduced compared to controls of the same age. While the total retinal thickness in wild-type mice increased significantly between P10 and P20, this was not the case for Sod2-deficient mice. The optic nerve was smaller in the 20-day-old Sod2-deficient animals, but the extra-ocular muscles appeared to be normal. In summary, mice showing homozygous Sod2 deficiency, a major antioxidant enzyme, showed a retinal degeneration phenotype. This implies that oxidative stress can cause photoreceptor degeneration. Thus far there has been no published work analysing the retinal phenotype of *Sod2* heterozygous mice.

1.4. Hypothesis

The rationale behind this project was stimulated by the publication of two papers. The first one is a review on the mechanisms of cell death in inherited retinal degenerations by Travis (1998). The author first discusses the genetic heterogeneity of RP, since mutations in 40 genes have been found to lead to nonsyndromic RP, 30 of which have been identified (**Table 1**). These genes influence many different aspects of photoreceptor and RPE function. Additionally, mutations in genes whose expression is not confined to the retina can cause photoreceptor degeneration as a secondary phenotype (e.g. tissue inhibitor of metalloproteinase 3, TIMP3) (Fariss *et al.*, 1998). According to Travis (1998), this heterogeneity reflects the increased vulnerability of photoreceptor cells, which, as discussed above, can be attributed to light exposure, high oxygen tension imposed by the choroidal blood flow, high polyunsaturated lipid content and the high metabolic rate of these cells. Irrespective of the genetic trigger and the subsequent structural or metabolic changes leading to photoreceptor degeneration, Travis (1998) suggested that the predominant mode of cell death in all inherited retinal degenerations is apoptosis.

This proposal has to be reconciled with a paper that was published a few years later by Clarke *et al.* (2001). These authors observed that in some models of photoreceptor degeneration, the probability of cell death does not increase with time and, instead of exhibiting sigmoidal kinetics, is consistent with exponential kinetics (**Figure 12**). The model was called the 'one-hit model' and supports a constant or decreasing probability of cell death with time, which is random and independent of the death of any other cell. It contradicts the widely accepted 'cumulative damage' hypothesis, according to which neurons gradually accumulate damage until a threshold is reached, after which the homeostasis of the cell is disrupted and cell death occurs (Cassarino & Bennett, 1999).

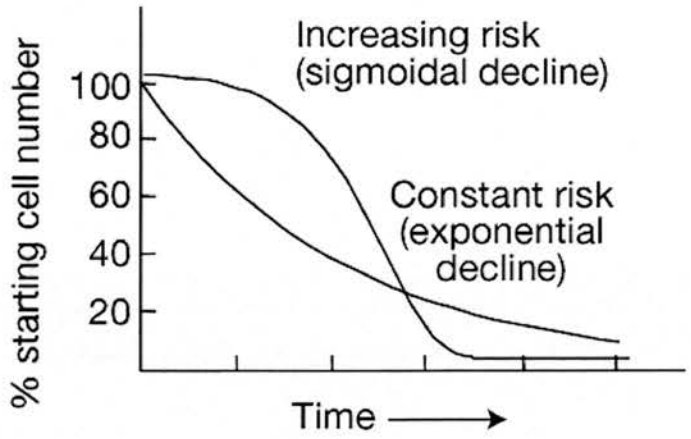

Figure 12: Schematic representation of the kinetics of cell loss

Constant and increasing risk of neuronal death manifest as an exponential or sigmoidal decline in cell number, respectively. [Image from Clarke *et al.*, 2001]

Clarke *et al.* (2001) suggest that this 'one-hit' model can be explained in terms of a mutant steady state (MSS). Mutant neurons show an abnormal MSS, but function normally and are at a constant, not increasing, risk of death during the course of the degeneration. Alterations in the expression/function of a few mutant-response genes/proteins are proposed to result in the crossing of the threshold that leads to apoptosis.

The concept of a MSS was taken further by Wright *et al.* (2004) and the importance of oxidative stress as an underlying factor in retinal degeneration was proposed. The authors examined the allometric relationships between rates of neurodegeneration resulting from equivalent mutations in a diverse group of genes from five mammalian species (mouse, rat, dog, pig and human) with different maximum lifespan potentials (LSP). The rates of retina and brain neurodegenerations varied by up to two orders of magnitude and were strongly correlated with LSP and rates of mitochondrial ROS production. Cell death in these disorders is known to occur via the intrinsic apoptotic pathway and hence the dual role of mitochondria, as the mediator of this pathway and as the major source of ROS, suggests that these two functions are linked. Wright *et al.* (2004)

therefore proposed that redox status is a principal factor that sets the probability of cell death in response to a diverse range of cellular stressors (**Figure 13**).

This influence is probably exerted at the level of MOMP, as the pro- and anti-apoptotic protein-lipid interactions in the mitochondrial membrane regulate the commitment to apoptosis. The mitochondrion therefore acts as a stress sensor where different types of stress integrate and determine the probability of apoptosis. By changing the steady state level of oxidative stress within mitochondria, rates of apoptosis would change accordingly, irrespective of the nature of the mutation causing degeneration.

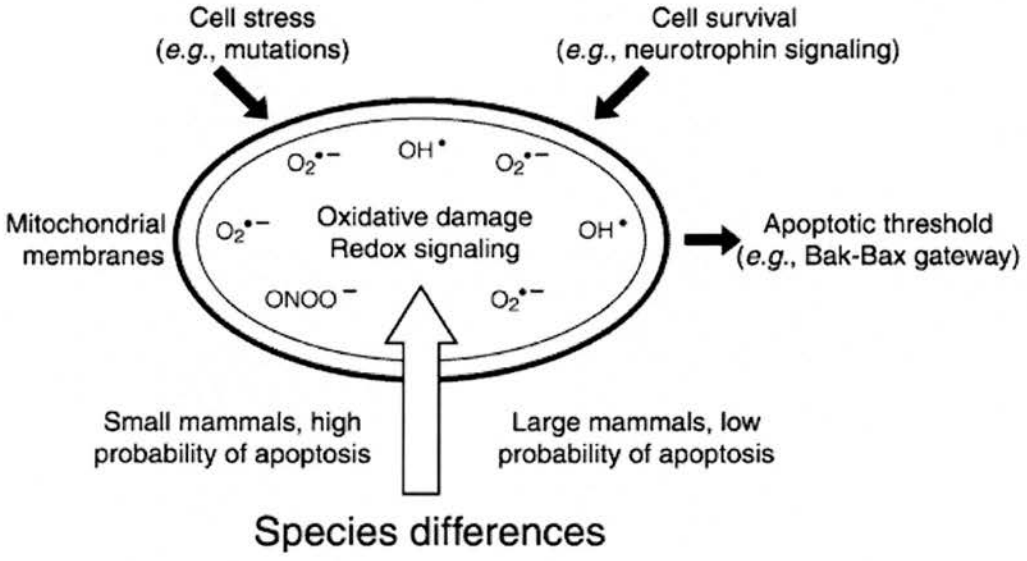

Figure 13: Species differences in rates of neurodegeneration on the mitochondrial regulation of apoptosis

Species- and cell type-specific differences in steady state ROS production are suggested to influence mitochondrial regulation of apoptosis and apoptotic thresholds. The precise mechanism is unclear but may involve altering ROS-mediated signalling pathways and/or influencing the degree of oxidative damage to mitochondrial components of the apoptotic machinery. [Image from Wright *et al.*, 2004]

The proposed model by Wright *et al.* (2004) can be applied to RP. As shown in **Table 1**, mutations in 40 genes have been implicated in photoreceptor degeneration. These mutations are in a wide range of functionally different genes and pathways which impose distinct types of stress to the cells. For example, mutated RHO impairs visual transduction and may cause ER stress (Galy *et al.*, 2005), whereas mutated peripherin 2 compromises the formation of OS. Each of these mutations affects the apoptotic threshold of cells via different routes and could influence MOMP, a critical step in the intrinsic apoptotic pathway. Apoptotic thresholds are also influenced by ROS production, which is directly implicated in some neurodegenerative diseases, like Alzheimer's disease and Parkinson's disease. The differences in degeneration rates between species and their correlation with ROS production (Wright *et al.*, 2004), as well as cell differences in ROS production and oxygen consumption (Hogan *et al.,* 1971), further suggest that ROS affect apoptotic thresholds. Oxidative stress does not need to be directly implicated in a disease phenotype for constitutive ROS production to affect apoptotic thresholds. Indeed, in some neurodegenerative diseases, like the retinal degenerations caused by splicing factor mutations (Hutton *et al.*, 1998) there is no evidence for increased oxidative stress. Growth factor withdrawal can influence MOMP and cell death without a direct effect on oxidative stress (Leveillard *et al.*, 2004). However, when the disease does cause increased oxidative stress, this, combined with the species- and cell type-specific steady-state ROS production, can further influence the probability of apoptosis. As a result, modifying ROS production by altering their proposed influence on the apoptotic machinery should affect the probability of cell death, regardless of whether oxidative stress is directly implicated in the disease. Photoreceptors are vulnerable cells because they are already exposed to high oxidative stress (Travis, 1998). They are therefore presumed to have an increased steady state ROS production, which may increase the probability of apoptosis occurring compared with other tissues. An additional insult in the form of any of the mutations known to cause RP would therefore result in crossing of the apoptotic threshold and cell death. This vulnerability could explain the extreme genetic heterogeneity observed in RP.

1.5. The current project

This project investigates the importance of oxidative stress in photoreceptor degeneration. The hypothesis under test is that oxidative stress either directly or indirectly influences the probability of apoptosis in photoreceptor degeneration. Alteration of the cell's oxidative state should therefore change the rate of photoreceptor degeneration. Decreased expression of the *Sod2* gene should increase the rate of cell loss, whereas increased antioxidant defence should slow it down. Firstly, the mouse mutants retinal degeneration 1 (*rd1/rd1*), atypical retinal degeneration 1 (*atrd1/atrd1*), rhodopsin knockout ($Rho^{-/-}$) and peripherin/retinal degeneration slow (*rds/rds*) were investigated for evidence of oxidative damage, by analysis of oxidative stress markers. The mutants were also crossed to a superoxide dismutase 2 heterozygous mouse ($Sod2^{+/-}$), which has decreased mitochondrial antioxidant activity, to examine the effect on disease progression. Finally, mutants were treated with the mitochondrially-targeted antioxidant MitoQ, following a preliminary study assessing its toxicity by oral administration. The rates of photoreceptor degeneration were estimated and the cellular REDOX status of each mutant was assessed in order to elucidate the role of oxidative stress in photoreceptor degeneration.

CHAPTER 2

MATERIALS AND METHODS

2.1. Animals

Different mouse mutants of *Mus musculus* were used in this project. All procedures were carried out according to the Home Office's guidelines. Mice were fed *ad libitum* and kept under standard lighting with a 12 hr light:dark cycle. *Sod2*$^{+/-}$ mice were provided by Dr. C.J. Epstein (University of California, San Francisco) and were on a C57BL/6J background. *Prph2*$^{rds/rds}$ mice were provided by Dr. Robin Ali (UCL, London) and were on a CBA background. *Rho*$^{-/-}$ mice, on a C57BL/6 background, were made available by Dr. Peter Humphries (Trinity College, Dublin). The *Pde6b*$^{rd1/rd1}$ and *Pde6b*$^{atrd1/atrd1}$ mice, both on a C3H background, were provided by Prof. Ian Jackson (MRC HGU, Edinburgh). Each retinal degeneration mutant was crossed to *Sod2*$^{+/-}$ heterozygous mice to produce double mutants.

2.2. Tissue collection

i. Ear-clips collected from the animals were used for DNA extraction and genotyping.

ii. Following the culling of the animal by cervical dislocation, the eyes were removed using L-shaped forceps and placed immediately in tubes on ice.

iii. For retina extraction and subsequent protein isolation, the eyes were incubated in ice-cold PBS. Under a light microscope, at a magnification of x20, the posterior part of the eye was immobilised with L-shaped forceps, and using a metallic scalpel, a sagittal incision was made on the front of the eye at the centre. Using fine forceps, pressure was then imposed on the back, at the area of the optic nerve head, to push first the lens out, followed by the retina. Occasionally the RPE was attached to the retina, which was removed with forceps.

iv. For tissue sectioning the eyes were incubated either in ice-cold phosphate buffered saline (PBS) or ice-cold 4% paraformaldehyde (PFA).

2.3. Molecular genetic techniques

2.3.1. Animal genotyping

Animals were genotyped initially by Polymerase Chain Reaction (PCR) using extracted DNA, followed, if required, by sequence analysis or restriction enzyme digests.

2.3.2. DNA extraction

DNA was extracted from ear-clips taken from the animals. The clips were incubated in 100 µl 25mM NaOH/0.2M EDTA and heated for 20 min at 95°C using a PCR block. The incubation buffer was neutralised by addition of 100 µl of 40 mM Tris-HCl. The samples were finally mixed by vortexing and stored at 4°C. This results in DNA in a buffer containing 20mM Tris-HCl / 0.1mM EDTA at ~pH 8.1 with ~25mM Na^+ ions which is suitable for storing DNA.

2.3.3. Polymerase chain reaction

2.3.3.1. Primer design

The web resource Primer 3 (Rozen and Skaletsky, 2000) was used to aid design of oligonucleotide primers, supplied as lyophilised pellets by MWG Biotech or Sigma. Stocks were adjusted to 100 pmol/µl with dH_2O, mixed by inverting overnight (o/n) at 4°C and stored at -20°C. 10 pmol/µl dilutions were prepared, aliquoted and stored at -20°C for use in reactions.

2.3.3.2. PCR conditions

PCR was used to amplify the genomic regions of interest. All PCRs were carried out in the following mixture:

Reagent	Stock concentration	Volume (µl)	Final Concentration
dNTPs*	2 mM	2.5	0.2 mM
Buffer*	x 10	2.5	x 1
$MgCl_2$*	50 mM	0.75	1.5 mM
Taq Platinum*	5 units/µl	0.2	0.04 units
Primers (each)	10 µM	2.5	1 µM
DNA		1	
dH_2O		13.05	
FINAL VOLUME		25	

* Reagents supplied by Invitrogen

The primers and PCR conditions, for genotyping each mutant, are shown in the table below.

	PCR conditions		Primer info	
Template	**Annealing T °C**	**Fragment size**	**Direction**	**Primer sequence 5'>>3'**
Sod2$^{+/-}$	56	wild-type 501 bp	forward (shared)	CGAGGGGCATCTAGTGGAGAA
		mutant 400 bp	reverse (wild-type)	TTAGGGCTCAGGTTTGTCCAGAA
			reverse (mutant)	CACACATCGGGAAAATGGTTT
Pde6b^{rd1}	60	277 bp	forward	ACCTGAGCTCACAGAAAGGC
			reverse	GCTTCTAGCTGGGCAAAGTG
Pde6b^{atrd1}	53	224 bp	forward	TTGAAGATGCAGTGCCACAT
			reverse	CAGCCCAGAGGAGAAACAAC
Rho$^{-/-}$	61	wild-type 394 bp	forward (shared)	TTCAAGCCCAAGCTTTCGCG
		mutant 139 bp	reverse (wild-type)	AGGTTAGAGCTGGAGGACTG
			reverse (mutant)	TAAGACTGATTGGACCATTC
Prph2^{rds}	57	wild-type 350 bp	forward (shared)	TCAAAGAGCCAGACGAGAAGT
		mutant 250 bp	reverse (wild-type)	CCCGTTCTTCACAGACCAGG
			reverse (mutant)	TGGGCTGTATATGAATGAAAATC

2.3.3.3. Electrophoresis

To estimate the size of DNA fragments that were amplified by PCR, the products were separated by agarose gel electrophoresis. Agarose gels ('Hi Pure' Low, BioGene) of the appropriate percentage (usually 2%) were prepared in 0.5x TBE buffer (20x stock: 216 g Tris base, 110 g boric acid, 18.6 g EDTA, make to 1 litre with dH_2O) with 0.2 mg/ml ethidium bromide. The PCR samples were incubated in 1x agarose gel DNA loading buffer (Stock 6x: 25 µg bromophenol blue, 25 µg xylene cyanol, 3 ml glycerol, 6.95 ml H_2O), loaded in a gel immersed in 0.5xTBE buffer and run at 150 V for about one hour. The bands were visualised using a UV transilluminator (Syngene). The size marker used routinely was bacteriophage lambda DNA digested with *HindIII* (DNA Marker X, Roche).

2.3.4. Purification of DNA gel bands

Fragments that were separated on agarose gels and required further manipulation for analysis were excised and purified using the gel extraction kit by Qiagen, according to the manufacturers' instructions.

The *rd1/rd1* and a*trd1/atrd1* samples were purified in this way prior to restriction digests and sequencing, respectively.

2.3.5. Restriction enzyme digests

Restriction enzymes were supplied by Boehringer Mannheim or by New England Biolabs. The amount of each enzyme added was 5% or less of the final reaction volume, using the appropriate 10x buffer diluted to 1x concentration with dH_2O. Digests were left at 37°C for several hours or o/n before the digested fragments were separated by electrophoresis on an agarose gel.

The *rd1/rd1* PCR products were digested with *DdeI* and *SnaBI*. The *rd1* mutation in exon 7 of the *Pde6b* gene converts a *SnaBI* restriction site (TAC/GTA; wild-type) to a *DdeI* site (C/TNAG; mutant).

2.3.6. Sequence analysis

Sequence analysis was required for genotyping the *atrd1/atrd1* mutants. Following amplification of the desired genomic fragment by PCR, extraction of the band from the agarose gel and purification using the Qiagen kit as described above, the DNA sequence was analysed using the following protocol set up in a 96-well plate.

Sequencing reaction:

Extracted DNA	1 µl
Primer	1 µl
Big Dye Terminator version III	4 µl
2 mM $MgCl_2$	4 µl
dH_2O	10 µl

Sequencing program:

96 °C	5 min	
96 °C	30 sec	⎫
55 °C	15 sec	⎬ x 35 cycles
60 °C	4 min	⎭
12 °C	forever	

DNA precipitation:

Following sequencing, 5 µl of 125 mM EDTA and 60 µl of 100% alcohol were added to each well and the mix was allowed to stand for at least 15 min at room temperature (RT). The plate was sealed and centrifuged at 3,500 rpm for 30 min at RT. The seal was then removed and the plate was turned up-side-down and re-centrifuged at 1,000 g for 1 min to remove the supernatant (s/n). The pellet was washed with 100 µl of 70% alcohol and the plate was centrifuged at 3,600 rpm for 10 min at RT, before removing the s/n as before. Finally the plate was allowed to fully dry at RT for at least 15 min.

Sequencing products were separated using an ABI 3100 by HGU technical staff. Sequencing traces were analysed using Sequencher software.

2.4. Histological and histochemical methods

2.4.1. Preparation of frozen sections

2.4.1.1. Freezing of mouse eyes

Immediately after excision from the animal, the eyes were incubated in ice-cold PBS and further processed as soon as possible. Working in a fume-hood, the eyes were snap-frozen in melting iso-pentane and then incubated in OCT™ embedding compound (Raymond Lamb) in appropriate small plastic vials (Agar Scientific). The latter containing the frozen eyes, were then immersed in liquid nitrogen until fully frozen, and placed into a -70 °C freezer for long-term storage.

2.4.1.2. Sectioning of frozen mouse eyes

A Leica CM 3050S cryostat was used for cutting semi-thin frozen sections of mouse eyes. The chamber and blade temperatures varied from -18 °C to -24 °C, and the thickness of the sections ranged from 2 to 10 μm. Once cut, the sections were transferred to glass slides, air-dried for one hour and either used immediately or stored in slide mailers (Agar Scientific) at -20°C.

2.4.2. Preparation of paraffin-embedded sections

2.4.2.1. Paraffin-embedding of mouse eyes

Immediately after excision from the animal, the eyes were incubated in 4% PFA for 15-20 hours at 4°C. They were then dehydrated by 30-minute incubations in 30%, 50% and 70% alcohol, prior to a series of 40-minute incubations in 70%, 85%, 95% and 2x100% alcohol, 2x in xylene and finally 4x in wax. These incubations were done using the semi-automated Tissue-Tek® VIP™ tissue processor (Miles Scientific). At the end of the program, the eyes were transferred into moulds with molten wax, and following orientation using a pair of forceps, the wax was allowed to set on ice.

2.4.2.2. Sectioning of paraffin-embedded mouse eyes

The wax block, with the specimen embedded in it, was trimmed to the desired size and the edges angled to improve the capture of sections. The wax-embedded tissue was sectioned at 5-10 μm on a microtome (Leica MZ6) and strips of sections were floated out in a 47 °C water bath. With the aid of fine paintbrushes, the sections were transferred to slides (Superfrost® Plus, BDH) and the slides incubated at 65°C o/n to allow sections to dry.

2.4.2.3. De-waxing

To remove the wax from wax-embedded tissue sections, slides were incubated 3x in xylene for 10 min each, followed by three 10-minute incubations in 100% alcohol and single 10-minute incubations in 90%, 70%, 50%, 30% alcohol and finally running tap water.

2.4.3. Haematoxylin and Eosin (H&E) procedure

Tissue cryosections were air-dried for 15 min at RT, fixed for 10 minutes in formal calcium solution (3.6% (v/v) formaldehyde, 1.1% (w/v) calcium chloride) (Baker 1958) and then washed in dH_2O.

Paraffin sections were de-waxed and washed in dH_2O.

For both types of section, sequential incubations in haematoxylin (5 min), acid/alcohol (10 sec), lithium carbonate (10 sec) and eosin (5 min) were interrupted by 1-min-washes in running tap water. Finally, dehydration through alcohols (3 x 5 min in 100% alcohol), clearing (3 x 5 min in xylene) and mounting in distrine plastizer xylenlene (DPX) completed the staining procedure. The slides were analysed by bright field microscopy.

2.4.4. Outer nuclear layer (ONL) analysis

Following the de-waxing of paraffin-embedded eye sections that included the optic nerve head (ONH), the sections were stained with H&E as described above. Using a bright field microscope and the IPLab program, images were taken at a x40 or x60 magnification at the middle of the distance between the ONH and the edge of the retina at each side. The number of rows of nuclei in the outer nuclear layer (ONL) and the inner nuclear layer (INL) were counted and the data transferred into Microsoft Excel files for analysis.

2.4.5. Dual COX/SDH histochemistry

Individual reactions for cytochrome *c* oxidase (COX) (Old & Johnson, 1989) and succinate dehydrogenase (SDH) (Old & Johnson, 1989) were combined in order to detect cells with no histochemically demonstrable COX activity.

The COX reaction medium was prepared by combining 200 µl cytochrome *c* stock solution (500 µM cytochrome *c* in 0.2 M phosphate buffer pH 7.0) and 800 µl 3,3'-diaminobenzidine tetrahydrochloride (DAB) stock solution (5 mM DAB in 0.2 M phosphate buffer pH 7.0).

The SDH reaction medium was prepared by combining 100 µl sodium succinate stock solution (1.3 M sodium succinate), 10 µl sodium azide stock

solution (100 mM sodium azide) and 800 µl NitroBlue Tetrazolium (NBT) stock solution (1.875 mM NBT). All stock solutions were prepared in 0.2 M phosphate buffer pH 7.0.

2µm-thick cryosections were air-dried for an hour at RT. The sections were first incubated in the COX buffer at 37°C for 50 minutes. They were then washed 3 x 5 min in PBS before being incubated in the SDH buffer at 37°C for 45 minutes. Sections were washed 3 x 5min in PBS (pH 7.4) and dehydrated in a graded alcohol series (30, 50, 70, 90, 100%). They were then incubated for an additional 10 minutes in 100% alcohol to remove all residual purple SDH stain. Finally the sections were cleared in clearing agent (Histoclear; National Diagnostics) and mounted in DPX (R.A. Lamb, Eastbourne, UK).

2.4.6. Terminal deoxynucleotidyl transferase-mediated dUTP Nick End Labelling (TUNEL)

The commercial TUNEL kit, DeadEnd™ Fluorometric TUNEL System, supplied by Promega, was applied on paraffin-embedded tissue sections of 5-10 µm thickness and the manufacturer's instructions followed. The sections were de-paraffinised by immersion in fresh xylene in a Coplin jar for 2 x 5min and incubated in 100% alcohol for the same amount of time. They were then re-hydrated by incubation in a series of alcohols (100%, 90%, 70%, 50%) for 3 min in each, washed in 0.85% NaCl for 5min, followed by a 5-minute wash in PBS, fixing in 4% methanol-free formaldehyde (MFF; 75 ml PBS, 25 ml 16% methanol-free formaldehyde solution, pH 7.4) solution in PBS for 15min, and permeabilising by treatment with proteinase K (20 µg/ml) for 8-10 min. Two 5-minute washes in PBS were interrupted by an additional fixation step in 4% MFF solution for 5 min, before the sections were covered with equilibration buffer for 10-15 min. All the incubations up to this point were done at RT. They were then treated with recombinant terminal deoxynucleotidyl transferase (rTdT) Incubation Buffer, including rTdT enzyme, labelled nucleotides and equilibration buffer, and incubated at 37 °C for 1 hour in the dark. The reaction was terminated by immersion of the slides in 2x saline-sodium citrate (SSC; 87.7 g NaCl, 44.1 g sodium citrate, 500 ml dH_2O, pH 7.2) for 15 min at RT, followed by three 5-minute washes in PBS and another three in dH_2O. Finally, the slides were

mounted in Vectashield (Vector laboratories) with DAPI and analysed under a fluorescence microscope.

For this protocol the proposed positive controls were sections treated with DNase I (10 u/ml) for 10 min at RT, prior to incubation in the reaction mix. The negative control was a section treated with the reaction mix lacking the rTdT enzyme.

2.4.7. Immunohistochemistry

De-waxed sections were circled with a wax pen and washed with PBS before incubation in blocking agent (PBS with 1% BSA) for at least 2 hours at RT. Sections were the incubated o/n with primary antibody in blocking agent at 4 °C, followed by 2 hours of 20 min PBS washes. Sections incubated with a fluorescently labelled secondary antibody in blocking agent for 2 hours at RT, followed by 2 hours of 20 min PBS washes. Slides were mounted with Vectashield mounting medium. Slides could be stored at 4 °C for several weeks.

2.4.8. Antigen retrieval

Since antigens are often affected by the processing of wax sections, for effective staining with antibodies, an antigen retrieval step was used. De-waxed sections were incubated in 0.01 M tri-Sodium citrate and 0.01 M citric acid pH 6.0 (41 ml 0.1 M tri-sodium citrate, 9 ml citric acid, 450 ml dH_2O) and boiled in a microwave at full power for 20 minutes. They were then allowed to cool down to RT and were briefly washed in PBS before any further use.

2.4.9. Antibodies used for immunohistochemistry

Antigen	Host	Immunogen	Supplier	Catalogue #
4-(iodobutyl)triphenyl-phosphonium methanesulfonate (IBTP)	Rabbit	IBTP	Antipodean Pharmaceuticals	
4-Hydroxynonenal (HNE)	Rabbit	Free HNE (E)-4-hydroxynonenal	Alexis Biochemicals	210-767-R100
8-oxoGuanine (8-oxoG)	Mouse		QED Biosciences	12501

Caspase 3 (active form) (CASP3)	Rabbit		BD Biosciences	559565
Cu/ZnSOD (SOD1)	Sheep	Cu/ZnSOD from human erythrocytes	Calbiochem	574597
Malondialdehyde (MDA)	Rabbit		Alpha Diagnostics	MDA11-S
MnSOD (SOD2)	Sheep	MnSOD from human liver	Calbiochem	574596
Nitrotyrosine (Ntyr)	Rabbit		Calbiochem	487924
Phosphodiesterase 6 β-subunit (Pde6b)	Rabbit	Synthetic peptide: HQYFG(K/R)KLSPEN VAGAC, corresponding to amino acids 20-36 of mouse and cow Pde6b.	Abcam	Ab5663
PolyADP ribose polymerase (PARP)	Rabbit	Peptide derived from the p85 fragment of PARP.	Promega	SOD-110

2.5. Protein procedures

2.5.1. Protein extraction and quantification

The tissue was homogenised on ice, using a Dounce homogeniser, in a buffer containing 1520 µl PBS, 400 µl 2% Triton-X 100 and 80µl of protease inhibitors. Following centrifugation for 5 minutes at 100 g, the supernatant of the sample was retained.

The protein concentration of the preparation was measured using the Coomassie-Blue-based Bradford spectrophotometric assay (Pierce). Standard curves were prepared using BSA in appropriate incubation buffers.

2.5.2. Western Blotting

Two different methods were followed for separating proteins, using either 'home-made' or pre-cast one-dimensional gels.

2.5.2.1. Protein separation using Laemmli one-dimensional gels

Denaturing (SDS) polyacrylamide gel electrophoresis (PAGE) gels were prepared in a Hoefer SE 600 Vertical Slab Unit. The appropriate percentage of resolving gel was made (Sambrook *et al.*, 1989) and poured to allow approximately 1 cm below the comb for the stacking gel. It was then overlaid with 1 ml isobutanol saturated with H_2O, at a 1:1 ratio, while setting. Isobutanol was then washed away and the stacking gel was poured on top of the resolving gel and allowed to set. Usually a 10% resolving gel was used, the formulation of which is given in the table below.

	Stacking Gel	**Resolving Gel**
1.5 M Tris-HCl buffer pH 8.8	0	5 ml
1 M Tris-HCl buffer pH 6.8	2.4 ml	0
2% Bis-acrylamide	975 µl	2.68 ml
40% Acrylamide	1.8 ml	4.86 ml
20 % Sodium Dodecyl Sulfate (SDS)	188 µl	200 µl
10% Ammonium Persulfate (APS)	189 µl	200 µl
Tetramethylethylenediamine (TEMED)	37.5 µl	20 µl
dH_2O	13.35 ml	7.16 ml

Protein samples, with 1x loading SDS-buffer (6x stock: 3.5 ml 1 M Tris-HCl pH 6.8, 3 ml glycerol, 1 g SDS, 0.93 g DTT, 1.2 mg bromophenol blue, made up to 10 ml with dH_2O), were denatured by heating at 70 °C for 20 minutes in a PCR block and immediately returned to ice, prior to separation on the gel. A Broad Range Protein Marker (BioRad) was used. The gels were run in 1x SDS running buffer (5x stock: 15.1 g Tris-base, 72 g glycine, 25 ml 25% SDS, make up to 1 litre with water) at 50mV o/n or until the dye front reached the bottom of the gel.

2.5.2.2. Protein separation using pre-cast NuPAGE Novex Bis-Tris Gels (Invitrogen)

Protein samples were incubated with 2.5 µl 4x NuPAGE LDS Sample Buffer, 1 µl 10x NuPAGE Reducing Agent and dH_2O to a total volume of 10 µl. They were then denatured at 70 °C for 10 min, prior to being loaded on 4-12% NuPAGE Novex Bis-Tris Gels, immersed in 1x SDS running buffer, prepared by adding 40 ml 20x NuPAGE MOPS SDS Running Buffer to 760 ml of dH_2O. The SeeBlue

Plus 2 prestained standard marker (Invitrogen) was used and the samples were run for 45 min at 200 V constant voltage.

2.5.2.3. Semi-dry transfer of proteins to membranes

Depending on the protein separation protocol, different methods were used for the transfer of proteins onto membranes.

Following protein separation using Laemmli gels, proteins were transferred to a Hybond-P membrane (Amersham Biosciences) using a semi-dry transfer device (BioRad). The membrane was firstly pre-soaked in methanol, then transferred in dH_2O and finally transferred into transfer buffer (3.03 g Tris-base, 14.4 g glycine, 200 ml methanol, made up to 1 L with dH_2O). Six pieces of filter paper, the same size as the membrane, were also immersed in transfer buffer. On the lower negative electrode of the transfer device, 3 pieces of filter paper, the membrane, the gel with the separated proteins and finally another 3 pieces of filter paper were layered in order. Air bubbles were removed by rolling a plastic roller over the construct. Proteins were transferred at (1.5 x area) mA/cm^2 or higher, at a maximum of 25 V for 1-2 hrs.

2.5.2.4. Wet transfer of proteins to membranes

Following protein separation using the device supplied by Invitrogen, proteins were transferred onto Hybond-P membrane according to the manufacturer's instructions. A Hybond-P membrane and 2 pieces of Whatman filter paper, cut to the size of the gel, and blotting pads provided by the manufacturer were soaked in transfer buffer. On the transfer device, starting from the cathode, 2 blotting pads, a filter paper, the gel, the transfer membrane, another filter paper and finally 2 blotting pads were layered in order. Transfer of the protein was performed using 30 V constant voltage for 1 hour.

2.5.2.5. Ponceau staining

To ensure that the membrane transfer was successful, to allow the identification of unstained markers and to verify equal loading of protein samples, the membrane was stained with Ponceau S solution (Sigma) for several minutes and de-stained in dH_2O.

2.5.2.6. Immunodetection of proteins

2.5.2.7. Antibodies used in Western blots

Membranes were blocked for 30 min at RT or o/n at 4 °C in 5% non-fat dried milk in Tris buffered saline with Tween (TBST: 10 ml 1M Tris-base pH 7.5, 30 ml 5M NaCl, 1 ml Tween 20, made up to 1 litre with H_2O) on a rotary shaker, followed by three 5-minute washes in TBST. Membranes were incubated in primary antibody diluted in 5% milk in TBST in a sealed bag on a rotator for 1 hour at RT, followed by three 5-minute washes in TBST. The membrane was then treated with horseradish peroxidase (HRP)-conjugated secondary antibody in the same way, followed by three more washes in TBST.

Detection of the secondary antibody was carried out with Enhanced Chemiluminesence (ECL) Western blotting detection reagents (Amersham Biosciences), according to the manufacturer's instructions. Following draining of excess wash buffer, the membrane with the protein side up, was covered with detection reagent (equal volumes of detection solutions 1 and 2). Incubation lasted for 1 minute. Excess detection reagent was drained off and the membrane was placed in an X-ray film exposure cassette. A sheet of Kodak X-Omat AR imaging film was placed on top of the membrane and, following sufficient time for exposure, a phosphorimager X-ray machine (Konica Minolta) was used for development of the film.

2.5.2.8. Antibodies used for Western Blottings

Antigen	Host	Immunogen	Supplier	Catalogue
4-(iodobutyl)triphenyl-phosphonium methanesulfonate (IBTP)	Rabbit	IBTP	Antipodean Pharmaceuticals	N/A
Cu/ZnSOD (SOD1)	Sheep	Cu/ZnSOD from human erythrocytes	Calbiochem	574597
MnSOD (SOD2)	Rabbit	Human MnSOD	Stressgen	SOD-110

2.6. Biochemical procedures

2.6.1. Enzyme assays

2.6.1.1. Preparation of mitochondrial fractions from mouse tissues

The method described by Taylor & Turnbull (1997) was applied. The tissue was collected on ice, washed in isolation medium (120 mM KCl, 20 mM HEPES, 5 mM $MgCl_2$, 1 mM EGTA pH 7.2, 5 mg/ml BSA) for removal of any blood, drained on a filter paper and weighed in plastic Eppendorf tubes. Using a Dounce homogeniser, the tissue was homogenised on ice in 5x weight/volume isolation medium and the homogenate centrifuged at 600 g for 10 min at 4 °C. The s/n was collected and re-centrifuged under the same conditions. The second s/n was used for enzyme measurements.

The specific amount of protein used for each assay was not possible to measure due to the increased amount of BSA in the preparation medium. A typical volume of 1 to 10 µl of homogenate, corresponding to 0.2 to 2 mg of tissue, was used for each assay, and the appropriate calculations were performed for activity measurements in µmol/min/g tissue.

2.6.1.2. Spectrophotometry

All spectrophotometric assays were done using a dual-beam, temperature-controlled Cary 300 UV-Vis spectrophotometer (Varian). Data was analysed using Cary WinUV software (Varian).

2.6.1.3. Citrate Synthase assay (Taylor & Turnbull, 1997)

2.6.1.3.1. Reagents

Assay medium: 100 mM Tris-HCl, pH 8.0

5 mM acetyl-coenzyme A (CoA)

10 mM 5,5'-dithiobis-2-nitrobenzoic acid (DTNB)

50 mM oxaloacetate (freshly prepared by incubation of 0.033 g oxalacetic acid in 250 µl $KHCO_3$)

10% Triton-X 100 (w/v)

2.6.1.3.2. Protocol

Citrate synthase activity was measured following the formation of 5-thio-2-nitrobenzoate ion (NBT) at 412 nm (E_{412} = 13.6/cm/mM). One ml assay medium was supplemented with 50 µM acetyl-CoA, 100 µM DTNB, mitochondrial preparation and 0.1% (w/v) Triton-X 100. Addition of 250 µM oxaloacetate started the enzymatic synthesis of citrate, during which the reduced coenzyme A (CoA-SH) released from acetyl-CoA reacted with DTNB to yield NBT. The reaction was measured for 2 min at 30 °C.

2.6.1.4. Complex I (NADH: ubiquinone oxidoreductase) assay (Taylor & Turnbull, 1997)

2.6.1.4.1. Reagents

Assay medium: 25 mM potassium phosphate, pH 7.2; 5 mM $MgCl_2$; 3 mM KCN;

2.5 mg/ml BSA

13 mM NADH

65 mM ubiquinone-1 in ethanol

1 mg/ml antimycin A in ethanol

1 mg/ml rotenone in ethanol

2.6.1.4.2. Protocol

The activity of complex I was measured by following the decrease in absorbance due to the oxidation of NADH at 340 nm with 425 nm as the reference wavelength (E_{340} = 6.22/cm/mM).

Mitochondrial fractions were diluted in the hypotonic assay medium and rapidly freeze-thawed three times in liquid nitrogen. 0.13 mM NADH, 65 mM Ubiquinone-1 and 2 μg/ml antimycin A were added to the assay medium and the absorbance change was recorded for 1 min to establish the baseline of the reaction. Following addition of mitochondrial preparations, NADH:ubiquinone oxidoreductase activity was measured for 4-5 minutes (Slope I) prior to addition of 3 μg/ml rotenone, after which the activity was measured for an additional 3-4 minutes (Slope II). Complex I activity was calculated as the rotenone-sensitive NADH:oxidoreductase activity, as indicated by the difference between Slope I and Slope II.

2.6.2. Reduced glutathione (GSH) measurements (Tietze, 1969)

2.6.2.1. Sample preparation

As soon as the tissue was collected from the animal, it was washed in ice-cold 0.9% NaCl solution to remove any blood and was weighed. Using a Dounce homogeniser, it was then homogenised on ice in 5 x weight/volume ice-cold 3% perchloric acid. The homogenised tissue was centrifuged at 9,000 g for 10 minutes at 4 °C and the supernatant was retained for glutathione measurement.

2.6.2.2. GSH assay

The reaction mix included the reagents listed below at the concentrations and volumes noted.

Reaction mixture	Stock concentration	Working concentration	Optimised final concentration	Optimised volume in 1 ml-reaction
Phosphate-EDTA buffer	O.1M sodium phosphate/0.005 M EDTA buffer pH 7.5	as stock	as stock	450 µl
DTNB	2.7 mM	1.12 µM	0.06 µM	500 µl
Glutathione reductase	as bought			20 µl
NADPH	4.8 µM	as stock	0.12 µM	25 µl

GSH concentration was measured by the production of NBT. The assay started with the above reagents and the background absorption was measured for a few seconds. A known amount of the GSH standard or the tissue sample was added and the production of NBT monitored spectrophotometrically at 412 nm at 25 °C for 5 minutes.

2.6.2.3. GSH standard curves

The concentration of glutathione was determined by comparison with a standard curve generated by using appropriate concentrations of purified reduced glutathione. The volumes of the reagents used for the standard curve are given in the table below.

GSH (µM)	0	0.01	0.02	0.05	0.1	0.2	0.5	1	1.5	2
all volumes in µl			.							
BUFFER	0.455	0.455	0.454	0.453	0.450	0.445	0.430	0.405	0.380	0.355
DTNB 0.06 µM	0.500	0.500	0.500	0.500	0.500	0.500	0.500	0.500	0.500	0.500
GR (1:50)	0.020	0.020	0.020	0.020	0.020	0.020	0.020	0.020	0.020	0.020
NADPH 0.12 µM	0.025	0.025	0.025	0.025	0.025	0.025	0.025	0.025	0.025	0.025
STANDARD GSH	0.000	0.001	0.001	0.003	0.005	0.010	0.025	0.050	0.075	0.100

2.7. Administration of substances to mice and related assays

2.7.1. MitoQ experiments

2.7.1.1. Administration of MitoQ

MS010 (MitoQ) was supplied by Antipodean Pharmaceuticals (New Zealand). It is a yellow powder, which is stored at 4 °C in the dark. It was administered to the animals orally through the drinking water at a concentration of 500 μM unless otherwise specified. The water bottles were covered with tin foil to keep the solution in the dark. Fresh dilutions were made and administered every three days.

2.7.2. IBTP experiments

2.7.2.1. *In vivo* administration of IBTP

4-iodobutyl-triphenylphosphonium (IBTP) was supplied by Antipodean Pharmaceuticals (New Zealand) as a lyophilised powder and was stored in the dark at 4°C. It was administered to animals orally through the drinking water at a concentration of 500 μM and fresh dilutions were made and administered every three days. The water bottles were covered with tin foil.

2.7.2.2. *In vitro* use of IBTP

2.7.2.3. Preparation of mitochondrial fractions

Mitochondria from different mouse tissues were prepared by homogenisation in STE medium (250 mM sucrose, 5 mM Tris-HCl, 1 mM EGTA, pH 7.4) followed by centrifugation at 2,400 rpm for 10 minutes at 4 °C. Protein concentration was determined as described in Section **2.5.1**.

2.7.2.4. Energisation of mitochondrial fractions and IBTP treatment

Mitochondrial fractions were energised by incubation in KCl buffer (110 mM KCl, 10 mM Hepes, 1 mM EGTA, pH 7.2) containing 10 mM succinate and 8 μg /ml rotenone for 5 minutes at RT. Addition of 5 μM IBTP and subsequent

incubation at 30 °C for 15 minutes, was followed by repeated washing steps after centrifugation at 600 g and re-suspension in STE medium. The samples were finally suspended in a small volume of STE and their protein concentrations measured as described above.

2.7.2.5. Detection of IBTP

Following its use both *in vivo* and *in vitro*, IBTP was detected immunologically on Western blots. Control (non-treated) and treated samples of known concentration were loaded on denaturing SDS PAGE gels and separated electrophoretically using the protocols described in sections **2.5.5.2** and **2.5.2.4** were followed. The primary antibody provided by Antipodean Pharmaceuticals (New Zealand), was raised in rabbit and typically used at a dilution of 1:2,000.

2.7.3. ^{3}H-MitoQ experiments

2.7.3.1. Administration of ^{3}H-MitoQ

Tritium-labelled MitoQ (0.743 mCi/ml) was provided by Antipodean Pharmaceuticals (New Zealand) in a liquid form and stored in the dark at –20 °C. It was administered to wild-type animals orally, through their drinking water, for a period of 10 days. 0.0743 μCi of ^{3}H-MitoQ was added to 500 μM dilutions of unlabelled MitoQ and, to minimise handling and contamination with radioactivity, the total volume required for the 10-day experiment was prepared at the start of the assay and then stored in the dark at 4 °C.

2.7.3.2. Preparation of samples for scintillation counting

Following the culling of the ^{3}H-MitoQ administered animal, the tissues of interest (heart, brain, liver and eyes) were quickly collected and placed in pre-weighed Eppendorf tubes. The latter were weighed again to determine the weight of the tissues. The tissue samples were then homogenised, using a Dounce homogeniser, in ice-cold STE. The homogenates of known concentration (weight/ml) were stored at -20 °C until assayed in a scintillation counter.

2.7.3.3. Scintillation counting

The tritium content of the samples was measured in liquid scintillant (BDH) using a LS 6500 Multi-Purpose scintillation counter (Beckman Counter^{TM}). In 5 ml scintillation vials (LabLogic) samples of known protein content were mixed with an equal volume of the scintillation fluid. The quenching program was set for 5 minutes.

2.8. Equipment, consumables and reagents

2.8.1. Equipment

EQUIPMENT	Type/Model	Supplier
Balance		Metter
Bench-top microcentrifugation	Biofuge fresco	Heraeus
Cassettes for film development		Amersham
Coplin jars		Agar Scientific
Cryostat	CM 3050 S	Leica
Laemli one-dimensional gels-device		Anachem
L-shaped forceps		Merlin Medical
Microscope for tissue dissection	Leica MZ6	Leica
Microtome	Reichert-Jung 2030 Biocut	Leica
Microwave		Proline Microchef
Oven (37 incubations)	HERACell 240	Thermo Electron Corporation
Paraffin section mounting bath		Electrothermal
PCR machines	PTC-225	MJ Research
pH meter		Fisher Scientific
Phosphorimager X-ray	SRX-101A	Konica Minolta
Rotary shaker		Thermo Electron Corporation
Scintillation counter	LS 6500 Multi-Purpose	Beckman Counter TM
Silica quartz cuvettes		Ultrospec
Software programs	Microsoft Excel	Microsoft
	Sequencher	Gene Codes Corporation
	IPLab program	Scanalytics
	Cary WinUV	Varian
Spectrophotometers		
	6505 UV/Vis Spec	Jenway

	Cary 300 UV-Vis s	Varian
Transblot semi-dry transfer device		Biorad
UV illuminator	Gene Genius	Syngene
		UVP Inc
VIP machine	Tissue-Tek®	Mikes Scientific
Vortexing		Whirlmixer
Water purification system		Millipore

2.8.2. Consumables

CONSUMABLES	Type/model	Supplier
Automatic pipette		Jencons
Bijoux		Sterilin
Cassettes for VIP		Tespa or Surgipath
Eppendorf pipettes (P2-P1000)		Pipetman Gilson
Falcon tubes (15-50 ml)		Cellstar
Film		Kodak
Filter paper		Schleicher & Schuell Microscience
Hybond-P membrane		Amerxham Biosciences
Invitrogen gels		Invitrogen
PAP pen		Miles Scientific
Parrafin	Tissue Tek III	Sakura
PCR tubes (0.5or 1.5 ml)		Eppendorf
Scalpel		Swann-Morton
Scintillation vials		LabLogic
Slide coverslips		VWR International
Slide mailers		Agar Scientific
Slides	Microscope slides	H.V. Skan Ltd
	Superfrost slides	BDH
Small plastic vials		Agar Scientific

2.8.3. Reagents

2.8.3.1. Molecular reagents

Reagents	Supplier
Big Dye VIII	ABI PRISM
Bromophenol blue	BDH

Buffer for PCR	Invitrogen
DdeI	Roche
DNTP's	Invitrogen
Ethylenediaminetetraacetic acid	BDH AnalaR
Ethidium bromide	Sigma
Glycerol	Sigma
Magnesium Chloride	Invitrogen
Sodium Hydroxide	Sigma
SnaBI	New England Biolabs
Platinum *Taq* polymerase	Invitrogen
Tris/Borate/EDTA	from Technical Services
Tris-HCl	Sigma
Xylene cyanol	Sigma
DNA Ladder	Promega

2.8.3.2. Histology reagents

Reagents	Supplier
Alcohol (Ethanol)	Fisher Chemicals
Calcium Chloride	Sigma
Citric acid	Sigma
Cytochrome *c*	Sigma
DAB	Sigma
Dnase I	Roche
DPX	BDH Gurr®
Eosin	Surgipath
Formaldehyde	Riedel-de Haen
Haematoxylin	Raymond A. Lamb
Histoclear	Raymond A. Lamb
Iso-pentane	BDH GPR
Liquid nitrogen	from Technical Services
Lithium carbonate	Sigma
NaCl	BDH AnalaR
NitroBlue tetrazolium (NBT)	Sigma
OCT	Raymond Lamb
Phosphate buffered saline	from Technical Services
Paraformaldehyde	BDH
Proteinase K	Promega
Sodium azide	Sigma
Sodium succinate	Sigma

Tri-sodium citrate	Fisher Chemicals
Vectashield	Vector
Xylene	Fisher Chemicals

2.8.3.3. Protein reagents

Reagents	Supplier
Acrylamide solution	BioRad
Ammonium persulfate (APS)	Sigma
Bis-acrylamide	BIoRad
Bovine Serum Albumin	Sigma
Bromophenol blue	BDH
Coomassie Blue	Pierce
Glycerol	BDH GPR
Glycine	Sigma
Isobutanol	Sigma
Methanol	Fisher
Milk powder	Safeway
Phosphate buffered saline	from Technical Services
Ponceau S solution	Sigma
Protease inhibitors	Roche
Sodium Dodecyl Sulfate (SDS)	Fisher Scientific
Sodium Chloride	BDH AnalaR
TEMED	Invitrogen
Tris-base	Sigma
Tris-HCl	Sigma
Triton-X100	Sigma
Tween 20	Sigma

2.8.3.4. Biochemical reagents

Reagents	Supplier
Acetyl-Coenzyme A	Sigma
Antimycin A	Sigma
Bovine serum albumin (BSA)	Sigma
Dithionitrobenzoic acid	Sigma
Ethyleneglycoltetraacetic acid	BDH AnalaR
Glutathione Reductase	Fluka
Hepes	Sigma
Magnesium Chloride	BDH
Nicotinamide adenine dinucleotide (reduced)	Roche
Oxaloacetic acid	Sigma

Perchloric acid	Aldrich
Potassium Chloride	Sigma
Potassium Cyanide	Aldrich
Reduced GSH standard	Aldrich
Rotenone	Sigma
FluoranSafe XE Scintillation Fluid	BDH
Sucrose	Sigma
Tris-HCl	Sigma
Triton-X100	Sigma
Ubiquinone-1	Sigma

CHAPTER 3

MEASURING OXIDATIVE STRESS AND PHOTORECEPTOR DEGENERATION

3.1 Introduction

In this chapter the selection and optimisation of methods for the detection and analysis of both retinal degeneration and oxidative stress in mouse retinal degeneration mutants are discussed.

There are a number of methods available for following the progression of retinal degenerative diseases. In humans, RP can be detected and studied by functional assays, such as electroretinography (ERG), where the ability of the photoreceptors to respond to light is assessed. When working with animal models, the use of ERGs is technically difficult and requires specialised equipment, so that it is most suitable for confirming structural changes at later stages of a project. However, the ready availability of murine tissue samples allows the use of whole mouse eyes for a straightforward experimental approach to monitor rates of degeneration. The organisation of the retina into layers, each comprised of distinct cell types, allows the counting of the number of cells present in the tissue and the collection of information on its structural and functional integrity.

As discussed in the Introduction, the main cellular mechanism of photoreceptor degeneration in inherited retinal degenerations, such as RP, is apoptosis. Methods have been developed for studying apoptosis at the morphological, molecular, biochemical and genetic levels. In this project, the level of apoptosis in mouse retinal degeneration mutants was assessed by terminal deoxynucleotidyl transferase dUTP nick end labelling (TUNEL) assays, by a modified Annexin V assay and by immunohistochemistry for the apoptosis-associated proteins poly (ADP-ribose) polymerase (PARP) and caspase 3.

Oxidative stress can be quantified either directly, by measuring the production of free radicals, or indirectly, by measuring the extent of their damaging effects. Although the direct measurement approach would be more accurate, the short half-life of free radicals and their fast reactivity with target molecules compromises this approach. Therefore, the level of oxidative stress in this project was indirectly quantified via its damaging effects on macromolecules, and methods for measuring oxidative damage at the DNA, protein and lipid level were used. DNA damage was detected immunohistochemically for the DNA lesion 7,8-dihydro-8-oxoguanine (8-oxoG) and indirectly by the cytochemical assay cytochrome c oxidase/ succinate dehydrogenase (COX/SDH). Oxidative

damage at the protein level was quantified both by immunohistochemistry for nitrotyrosine (Ntyr), the major product obtained by the nitration of tyrosine by peroxynitrite, and by spectrophotometric assays measuring the specific activities of oxidative stress-sensitive enzymes. Finally, the level of lipid peroxidation in the mutant samples was monitored by immunohistochemical assays for the two major natural products of lipid peroxidation, namely 4-hydroxynonenal (HNE) and malondialdehyde (MDA).

The methods of choice are introduced and briefly discussed below. The optimised protocols of the methods that were eventually selected for measuring oxidative stress and photoreceptor degeneration are outlined in detail in Chapter 2.

3.1.1 Measuring photoreceptor degeneration by outer nuclear layer analysis

Outer nuclear layer (ONL) analysis is an unbiased method for following photoreceptor degeneration. The basis of this method is purely observational. The loss of nuclei in the ONL is a reflection of the degeneration of the corresponding photoreceptor cells. As the phenotype of RP is predominantly characterised by the loss of photoreceptor cells, the disease does not affect the survival of inner nuclear layer (INL) cells. The thickness of the latter is therefore not affected, making it a good internal control for measuring photoreceptor degeneration in retinal degeneration mutants.

Retinal degeneration has often been analysed by ONL thickness analysis. Sarra *et al.* (2001), investigated the beneficial effects of gene replacement therapy on OS formation and photoreceptor function of the *rds* mouse and measured the ONL thickness on semi-thin paraffin-embedded mouse eye sections, cut in the horizontal plane. Only sections including the optic nerve head (ONH) were included in their analysis, which was based on measuring the area covered by the ONL in section fragments at set distances from the ONH. Frederick *et al.* (2001) studied the mechanisms leading to photoreceptor degeneration in mouse models of autosomal dominant RP and also followed the progression of photoreceptor degeneration by counting the number of rows of nuclei present in the ONL.

3.1.2 Measuring apoptosis

3.1.2.1 Terminal deoxynucleotidyl transferase dUTP nick end labelling (TUNEL) assay

The terminal deoxynucleotidyl transferase dUTP nick end labelling (TUNEL) assay is commonly used for detection of apoptotic cells. Using chromatin cleavage, the most characteristic feature of apoptotic cell death, as a marker, Gavrieli *et al.* (1992) developed this method for *in situ* labelling of DNA breaks. The specificity of the assay is based on the binding of terminal deoxynucleotidyl transferase (TdT) to the 3' OH end of DNA, and the subsequent incorporation of biotinylated deoxyuridine at these sites, resulting in the synthesis of polydeoxynucleotide polymers. Avidin-peroxidation is used to amplify the signal and the samples are analysed by conventional light microscopy.

3.1.2.2 Annexin V assay

Apoptotic cell death is often accompanied by changes in the structure of the cell's plasma membrane (PM). The latter is highly asymmetric in its phospholipid composition, with predominantly phosphatidylcholine and sphingomyelin on the external leaflet, and phosphatidylethanolamine and phosphatidylserine (PS) on the inner leaflet (Op den Kamp, 1979). Soon after the onset of apoptosis, PS is translocated by flippases from the inner to the outer leaflet of the PM, which functions as a tag for specific recognition by macrophages and subsequent phagocytosis of the dying cells (Fadok *et al.*, 2003). PS also becomes accessible to the negatively charged phospholipid binding protein, annexin V, which specifically binds PS in the presence of Ca^{2+} (Bevers *et al.*, 1999).

3.1.2.3 Poly(ADP-ribose) polymerase (PARP) assay

The role of poly(ADP-ribose) polymerase (PARP) in apoptosis has been extensively investigated (Uchida *et al.*, 2001; Smulson *et al.* 1998; Diefenbach & Burkle, 2005). PARP-1 acts as an endogenous detection system for DNA breaks. Once activated, PARP-1 produces ADP-ribose polymers, causing the depletion of intracellular NAD^+ and a fall in ATP levels. NAD^+, which requires ATP for its production, serves as a precursor for NADP and regulates vital cellular processes.

It is therefore proposed that cellular NADP depletion, following over-activation of PARP-1, can lead to cell death if the energetic requirements for its re-synthesis are not met. In early apoptotic cells, a transient PARP-1 stimulation leads to poly(ADP ribose) accumulation. To prevent excessive NAD^+ consumption and to ensure that there is sufficient energy for execution of apoptosis, PARP1 is inactivated by caspase-3 cleavage. Two fragments are generated: a 24-kDa fragment, which stays in the nucleus, retains its DNA-binding activity and inhibits the uncleaved nuclear PARP1, and an 89-kDa fragment that is transferred to the cytoplasm at a late stage of apoptosis.

Commercially available antibodies that specifically detect the 85kDa (apparent molecular weight) fragment of the caspase-cleaved PARP, but do not detect the intact molecule, are available. Their specificity for the cleaved from of PARP makes them good markers for apoptosis induced by a variety of environmental stimuli, including free radicals and oxidising molecules.

3.1.2.4 Caspase 3 assay

It has been extensively documented that apoptosis is orchestrated by caspases, which are proteins that are present in the cells as inactive precursors and require proteolytic processing for activation. Once activated, caspases can themselves proteolyse downstream caspases and generate a cascade of reactions that results in the cleavage of key structural components, as well as of proteins critical for cell survival (Wolf *et al.*, 1999). Caspase-3, a key executioner of apoptosis, is synthesised as a 32-kDa pro-enzyme and requires cleavage to its 17-20 kDa active subunit. Its expression has been shown to be increased after IR injury both at the gene and at the protein levels (Katai & Yoshimura, 1999). Additionally, caspase 3 activation has been reported during photoreceptor degeneration in transgenic rats with the S334ter mutation in the rhodopsin gene. The specificity of caspase 3 activation in apoptosis makes it an ideal marker for detection of apoptotic cells in mutant retinas

3.1.3 Measuring oxidative damage

3.1.3.1 Measuring oxidative damage at the DNA level

3.1.3.1.1 7, 8-dihydro-8-oxoguanine assay

DNA is prone to oxidative damage and a number of different DNA lesions, in both nuclear and mitochondrial DNA, have been reported following exposure to different reactive agents, including UV light, ionising radiation and ROS. DNA lesions can be generated in the form of base modifications or DNA strand breaks. The most important, stable and well-studied product of oxidative DNA damage is 7,8-dihydro-8-oxoguanine (8-oxoG). If not repaired, this results in mutagenesis due to G:C to T:A transversions during DNA synthesis (Shibutani *et al.*, 1991).

3.1.3.1.2 Cytochrome oxidase/Succinate dehydrogenase (COX/SDH) assay

Of particular interest in this project is the integrity of the mitochondrially-encoded ETC subunits of cytochrome *c* oxidase (COX), which is the fourth complex of the ETC that transfers electrons from the reduced cytochrome *c* to molecular oxygen and at the same time pumps protons from the matrix into the IMS of mitochondria. Of its 14 subunits, only three are encoded by mtDNA, the remaining being nuclear encoded (Nijtmans *et al.*, 2004). In contrast to COX, succinate dehydrogenase (SDH), the second complex of the ETC, is only nuclear encoded. This difference between the two complexes has been used for the generation of reliable cytochemical methods to visualise the activities of these complexes and to make inferences about damage to mtDNA. It is therefore assumed that a compromised COX activity in the presence of intact SDH activity, reflects damage to mtDNA. Due to the close proximity of mtDNA to the main source of oxidative stress in the cell, it is further postulated that compromised COX activity is indicative of oxidatively damaged mtDNA.

The COX/SDH assay assesses the functional integrity of these two enzymes. The failure of a cell to be stained brown for COX activity can indicate that mitochondrially encoded COX subunits fail to assemble in the multi-subunit enzyme. This type of COX-negative cell would then be easily detected by its blue SDH-positive staining.

3.1.3.2 Measuring oxidative damage at the lipid level

3.1.3.2.1 Hydroxynonenal and malondialdehyde assays

Additional potential targets of free radicals include cellular lipids. In this context, the rod outer segment membranes of the retina are highly enriched in long chain polyunsaturated fatty acids (PUFAs), making them highly susceptible to lipid peroxidation.

Lipid peroxidation (LP) is a process that starts with the interaction between free radicals and lipids and involves hydrogen abstraction from fatty acids (Meagher & Fitzgerald, 2000; Yang *et al.*, 2002). PUFAs are susceptible to LP because of their double bonds that allow easy hydrogen abstraction by ROS. The lipid peroxides that are formed are unstable compounds and tend to rapidly degrade into a variety of products, such as short-chain aldehydes, which are in turn capable of covalent attachment to proteins by forming adducts with amino acid residues. Such aldehydes are relatively stable and are therefore able to diffuse out of the cell and attack distant targets. Malondialdehyde (MDA) and 4-Hydroxynonenal (HNE) are the major LP products formed and commercially available antibodies, capable of identifying these protein adducts are often used for measuring levels of LP.

3.1.3.3 Measuring oxidative damage at the protein level

3.1.3.3.1 Nitrotyrosine assay

Protein tyrosine nitration is an additional marker for oxidative stress (reviewed by Ischiropoulos, 2003). It is a covalent modification of proteins that results from the addition of a nitro group onto one of the two equivalent ortho carbons of the aromatic ring of tyrosine residues. The source of nitrogen is nitric oxide (NO), which can react with superoxide anions and form peroxynitrite that is in turn capable of nitrating tyrosine residues in proteins and form nitrotyrosines (NTyr) (McBride *et al.*, 1999). The latter can be identified by commercially available antibodies, which are often used to measure this form of protein modification.

3.1.3.3.2 Enzyme assays

Increased levels of oxidative stress may result in reduction of the activity of enzymes whose chemical and physical structures make them sensitive to such an inactivation. For example, an enzyme with iron-sulfur (Fe-S) clusters is particularly prone to inactivation because superoxide anions can react with the iron to form hydroxyl radicals (Fenton reaction), which disturb its structure and activity. Additionally, the close proximity of an enzyme to the source of free radicals can also influence the degree of its oxidative damage.

3.1.3.3.2.1 Citrate synthase assay

Citrate synthase (CS) catalyses the first reaction of the citric acid cycle (Krebs cycle), which is the condensation of acetyl coenzyme A with oxaloacetate (OAA) to form citrate and co-enzyme A (CoA-SH). It is localised in the mitochondrial matrix, but is nuclear encoded, synthesised on cytoplasmic ribosomes and subsequently transported into the mitochondrial matrix (Remington, 1992). CS is commonly used as a quantitative enzyme marker for the presence of mitochondria and, since it has no iron-containing prosthetic groups or Fe-S centers, it is not prone to inactivation by free radicals. The activity of CS can be measured spectrophotometrically in mitochondrial fractions prepared from tissue homogenates, following the method of Shepherd and Garland (1969). The assay medium contains Tris-HCl buffer at pH 8.0, which has been shown to be the optimal pH for citrate synthase activity. This is supplemented with acetyl-coenzyme A, 5,5′-dithiobis (2-nitrobenzoic acid) (DTNB), mitochondrial protein and Triton-X100. The latter is a detergent that is required for the disruption of mitochondrial membranes to ensure the complete release of total measurable CS activity. As shown in **Figure 14**, the background absorption is measured for 10 to 20 seconds, before addition of excess OAA initiates the formation of citrate. The CoA-SH released from acetyl CoA during the enzymatic synthesis of citrate reacts with DTNB to yield 5-thio-2-nitrobenzoate ions, whose formation is monitored at 412 nm (E_{412} = 13.6/cm/mM) for about one minute.

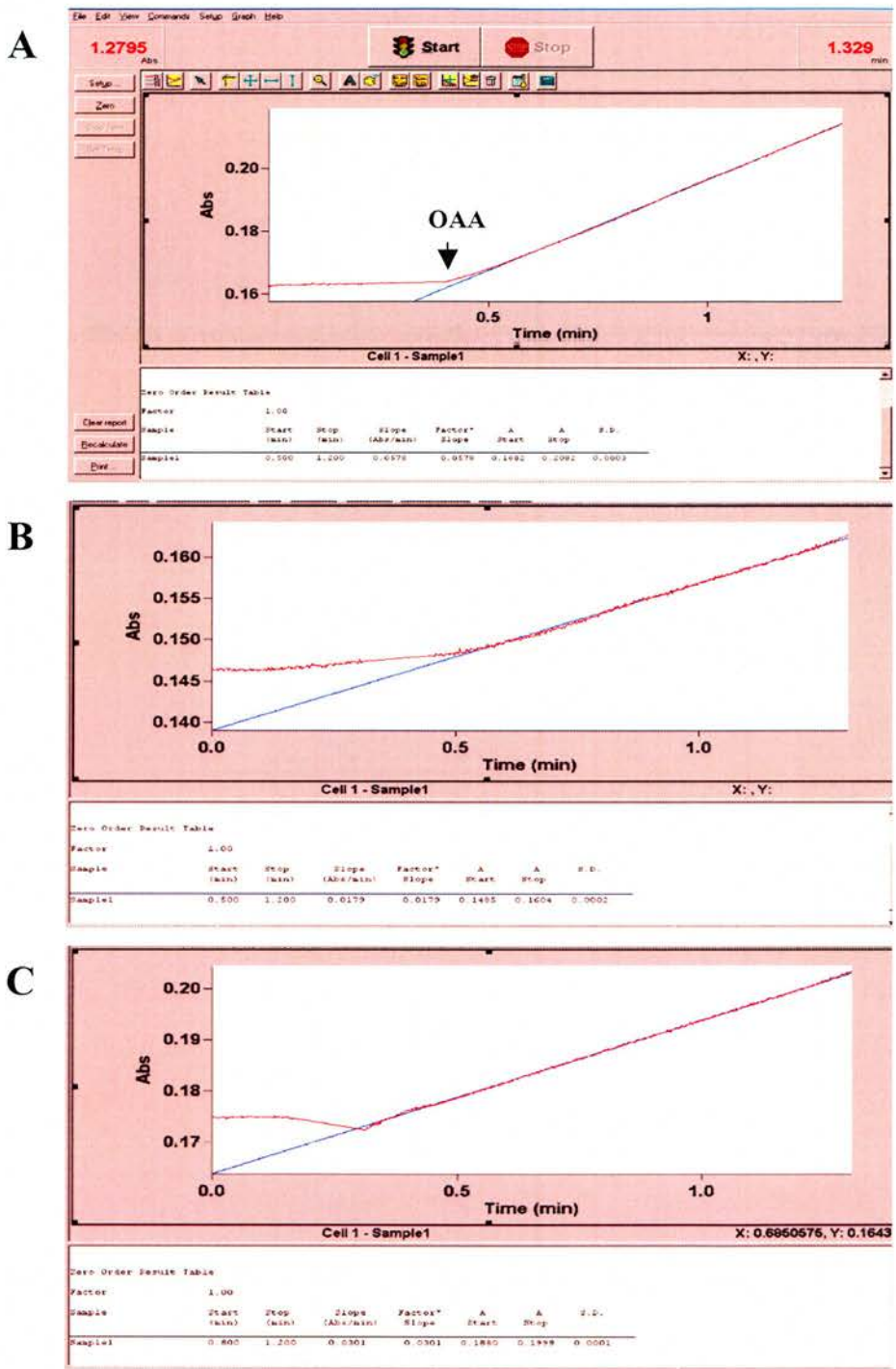

Figure 14: The citrate synthase assay

(**A**) The activity of citrate synthase is measured spectrophotometrically for about 1.5 minutes at 412 nm. The background absorption is measured for about 30 seconds, before addition of oxaloacetate (OAA) results in formation of citrate. (**B**) Typical citrate synthase rate from a wild-type mouse retinal sample (**C**) Typical citrate synthase rate from a mutant mouse retinal sample.

3.1.3.3.2.2 Complex I assay

Complex I (CI), also known as NADH:ubiquinone oxidoreductase, is the first and largest complex of the ETC. It removes two electrons from NADH and transfers them to ubiquinone and at the same time pumps four protons out of the matrix, contributing to the generation of the proton gradient. CI is a complex of 46 subunits, which include 8 Fe-S clusters (Brink *et al.*, 1987; Nijtman *et al.*, 2004). As mentioned above, Fe-S clusters are prone to react with superoxide anions (Fenton reaction) to produce hydroxyl radicals that compromise CI acivity.

Prior to assaying CI, the mitochondrial fractions prepared from tissue samples need to be rapidly freeze-thawed three times in liquid nitrogen to ensure complete release of total measurable CI activity. The assay medium includes potassium phosphate at pH 7.2, $MgCl_2$, KCN and BSA, as the latter increases rotenone sensitivity in human skeletal muscle mitochondrial fractions. The medium is hypotonic to further ensure measurement of maximum CI activity. At the start of the assay, the reaction mix also includes the electron donor NADH, the electron acceptor ubiquinone-1 and the complex III inhibitor, antimycin A. As shown in **Figure 15**, the specific activity of CI is measured by following the decrease in absorbance due to the oxidation of NADH at 340 nm with 425 nm as the reference wavelength (E_{340} = 6.22/cm/mM, Ragan *et al.*, 1988). Total NADH:ubiquinone oxidoreductase activity is measured for 4-5 minutes (Rate 1) before addition of rotenone, after which the assay is continued for a further 4-5 minutes (Rate 2). CI activity is calculated as the rotenone-sensitive NADH:ubiquinone oxidoreductase activity by the substraction of the two rates, prior and after rotenone addition (Rate 1- Rate 2). The difference between the two rates reflects not only the activity of CI but also the purity of the sample, as contamination with other cellular compartments can increase the measurable levels of non-CI enzymes with rotenone-insensitive NADH:ubiquinone oxidoreductase activity.

A

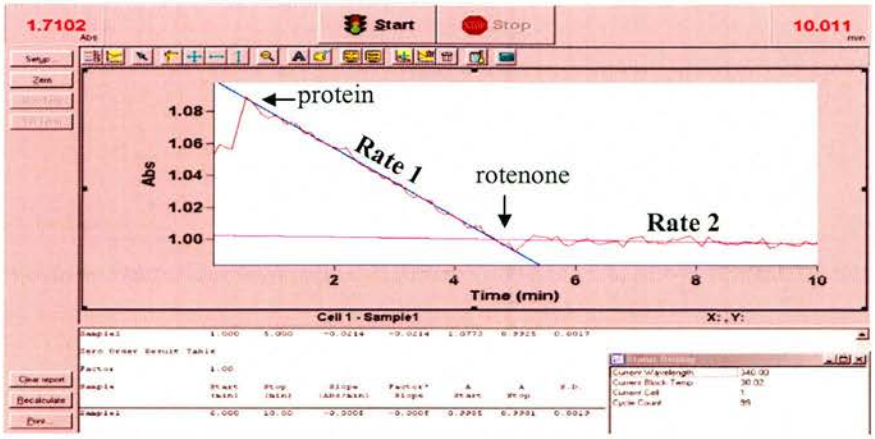

B

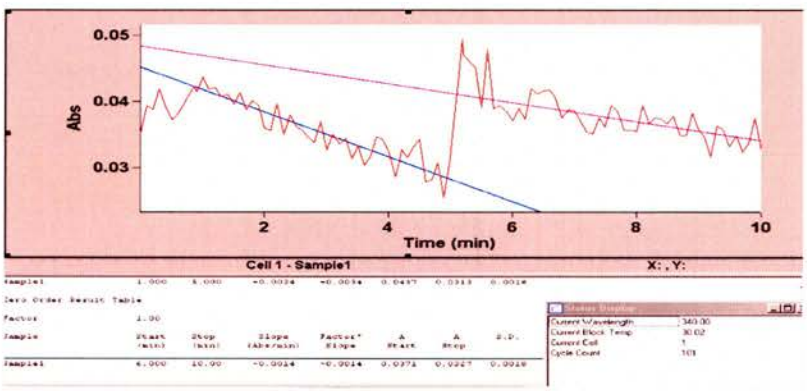

C

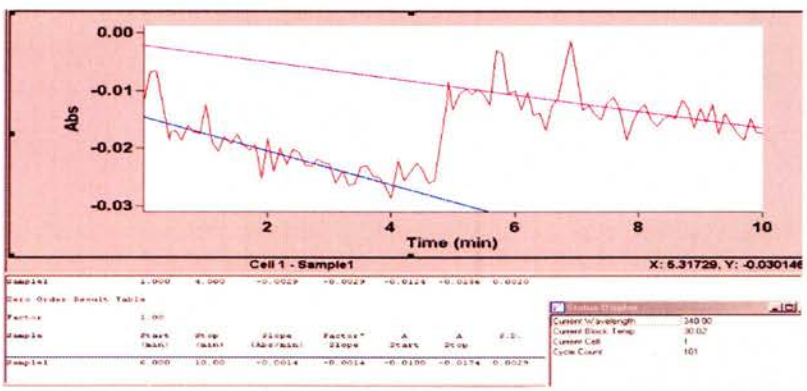

Figure 15: The complex I assay

(**A**) The activity of complex I is measured spectrophotometrically for 10 minutes at 340 nm with 425 nm as reference. The background absorption is measured for a few seconds before addition of mitochondrial protein. Total NADH:ubiquinone oxidoreductase activity is measured for 4-5 minutes (Rate 1). After addition of rotenone the rate is measured for another 5-6 minutes (Rate 2). Complex I activity is calculated as the rotenone-sensitive NADH:ubiquinone oxidoreductase, by the difference between the two rates (Rate 1-Rate 2) (**B**) Typical complex I rate from a wild-type retinal sample (**C**) Typical complex I rate from a mutant retinal sample.

3.1.3.4 Measuring oxidative status

3.1.3.4.1 Reduced glutathione measurements

Glutathione is one of the most abundant soluble antioxidants in the brain (Mytilineou et al., 2002). It is a tripeptide containing cysteine, glycine and glutamate which serves to detoxify hydrogen peroxide to water and oxygen, together with the enzymes glutathione peroxidase (GPX) and glutathione reductase (GR). Its active group is the cysteine thiol (-SH) (Pastore *et al.*, 2003), which helps maintain the cysteinyl-thiol groups of proteins in the reduced state (Mytilineou *et al.*, 2002).

Although the reduced glutathione (GSH) levels can be readily measured, accurate measurement of oxidised glutathione (GSSG) is considered a challenge, because of the much lower GSSG levels present within cells, the limited retina availability, and the absence of a convenient chemical signature, which would allow its robust measurement. The reduced form of glutathione can be measured using a modified version of an assay first outlined by Tietze (Tietze, 1969) which is based on the following chemical reactions

$$GSH + DTNB \rightarrow NBT + GS\text{-}NBT \text{ (Ellman reaction)}$$
$$GS\text{-}NBT + GSH \rightarrow NBT + GSSG$$
$$GSSG + NADPH + H^+ \rightarrow 2\ GSH + NADP^+$$

$$DTNB + NADPH + H^+ \rightarrow 2\ NBT + NADP^+$$

The sulfhydryl group of GSH reacts with 5,5′-dithiobis (2-nitrobenzoic acid) (DTNB) and produces nitroblue tetrazolium (NBT), which is yellow. GS-NBT is concomitantly produced, and is then reduced by glutathione reductase (GR) to recycle the GSH and produce more NBT. GR also reduces GSSG to GSH, which reacts with DTNB. In these reactions, the rate of NBT production is directly proportional to this recycling reaction, which is in turn proportional to the concentration of GSH in the sample. The chromophoric product NBT absorbs at 412 nm and the colour formation is monitored for 5 min at 25°C.

3.2 Results and optimisations

3.2.1 Positive controls

To be able to select and optimise methods for measuring apoptosis and oxidative stress, samples known to include apoptotic cells and/or oxidative modifications were selected and used as positive controls in subsequent experiments.
Three types of positive control were used.

1. Samples from mouse lines known to develop retinal degeneration.

Tissue samples from two mouse retinal degeneration mutant lines were used. Atypical retinal degeneration (*Pde6b* $^{atrd1\text{-}3}$) mutants, that were generated by *N*-ethyl-*N*-nitrosourea (ENU) mutagenesis, have mutations in the rod cGMP phosphodiesterase beta subunit (*Pde6b*) gene and have been shown to lose all the retinal photoreceptor cells within a few weeks of age (Thaung *et al.*, 2002; Hart *et al.*, 2005). Similarly, the retinal degeneration 1 (*Pde6b* $^{rd1/rd1}$) mutants are also mutated in the *pde6b* gene and develop photoreceptor degeneration which is complete by the third week of the animal's age.

2. Cell cultures in which apoptosis was induced.

The efficiency of apoptotic detection methods was also assessed in HeLa cell cultures that were treated with various concentrations (0.5μM–5 mM) of hydrogen peroxide (H2O2). The latter is known to induce apoptosis mediated by oxidative damage (Barbouti *et al*, 2002).

3. Brain sections from a mouse model for multiple sclerosis

Matyszak *et al.* (1995) generated a mouse model for multiple sclerosis, a chronic demyelinating disease in which infectious agents have been implicated in the pathogenesis. The animals were intra-cranially injected with heat-killed Bacillus Calmette-Guerin (BCG), which resulted in an acute inflammatory response and formation of cerebral white matter and apoptotic lesions. A limited number of frozen brain sections from these mice were available and were used for assessing the efficiency of apoptosis- and oxidative stress-specific antibodies.

3.2.2 Outer Nuclear Layer (ONL) analysis

In this project, two approaches were initially investigated for following photoreceptor degeneration in the mutants. Although they were both based on the principle of measuring the thickness of the ONL, they differed in the staining

method of the sections and the subsequent approach to analysis. In deciding which type of sections (frozen or paraffin-embedded) was more appropriate for comparative histopathology, it was clear that the aim was the preservation of histological structure. Both paraffin-embedded and frozen sections of wild-type mouse eye were prepared and stained with haematoxylin and eosin (H&E). As shown in **Figure 16**, the histological structure was intact in the pre-fixed paraffin-embedded section, while in the frozen section, although the retinal layers are still detectable, the histological structure was not usually as well preserved. It was therefore decided to proceed with investigating methods of analyzing ONL thickness by working on paraffin-embedded mouse eye sections.

The first approach (**Figure 17**) involved staining of the sections with 4′, 6-diamidino-2-phenyl-indol (DAPI), the most common DNA-specific dye that is excited by ultraviolet (UV) light and stains the nuclei bright blue. Although DAPI staining is very specific, even a moderate increase in the concentration of the dye can result in an image of such brightness that detection of individual nuclei in retinal layers is compromised. For this reason it was decided that, on DAPI-stained sections, the approach mentioned above by Sarra *et al.* (2001) would be used and the area covered by nuclei, rather than their exact number, would be measured. Following de-paraffinisation, the sections were immediately mounted in Vectashield with DAPI staining and analyzed by fluorescent microscopy. Images were taken at a magnification of x40 and transferred to the IPLab program for analysis. Each image was segmented and rotated in such a way that the retinal layers were parallel to the horizontal plane. A rectangular area of set width and height such that it fully included both the ONL and INL was selected at the centre of the image and the areas occupied by the ONL and INL were measured in pixels. The data were entered in Microsoft Excel worksheets for further data analysis.

The second approach (**Figure 18**) involved H&E staining of the eye section. Images at x63 magnification were captured by bright-field microscopy and, as before, were analysed using the IPLab program. Each image was rotated so that the retinal layers were parallel to the horizontal plane, and the number of rows of nuclei in each layer was counted. The data was collected and analysed in Microsoft Excel spreadsheets.

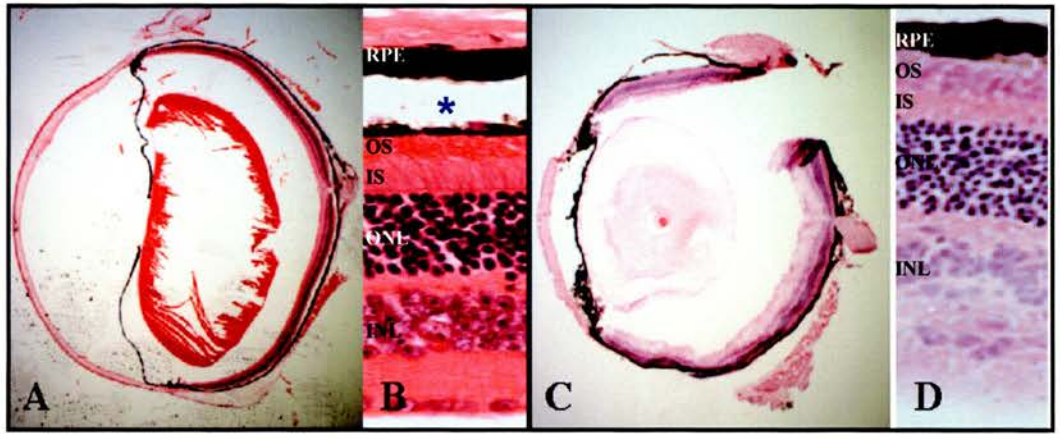

Figure 16: Tissue Histology

The histology of both paraffin-embedded (**A, B**) and frozen (**C, D**) mouse eye sections was assessed by haematoxylin and eosin staining. Images from 5 mm thick sections are shown at magnifications x20 (**A, C**) and x100 (**B, D**). Note the detachement of the RPE in the fixed retina (blue star).

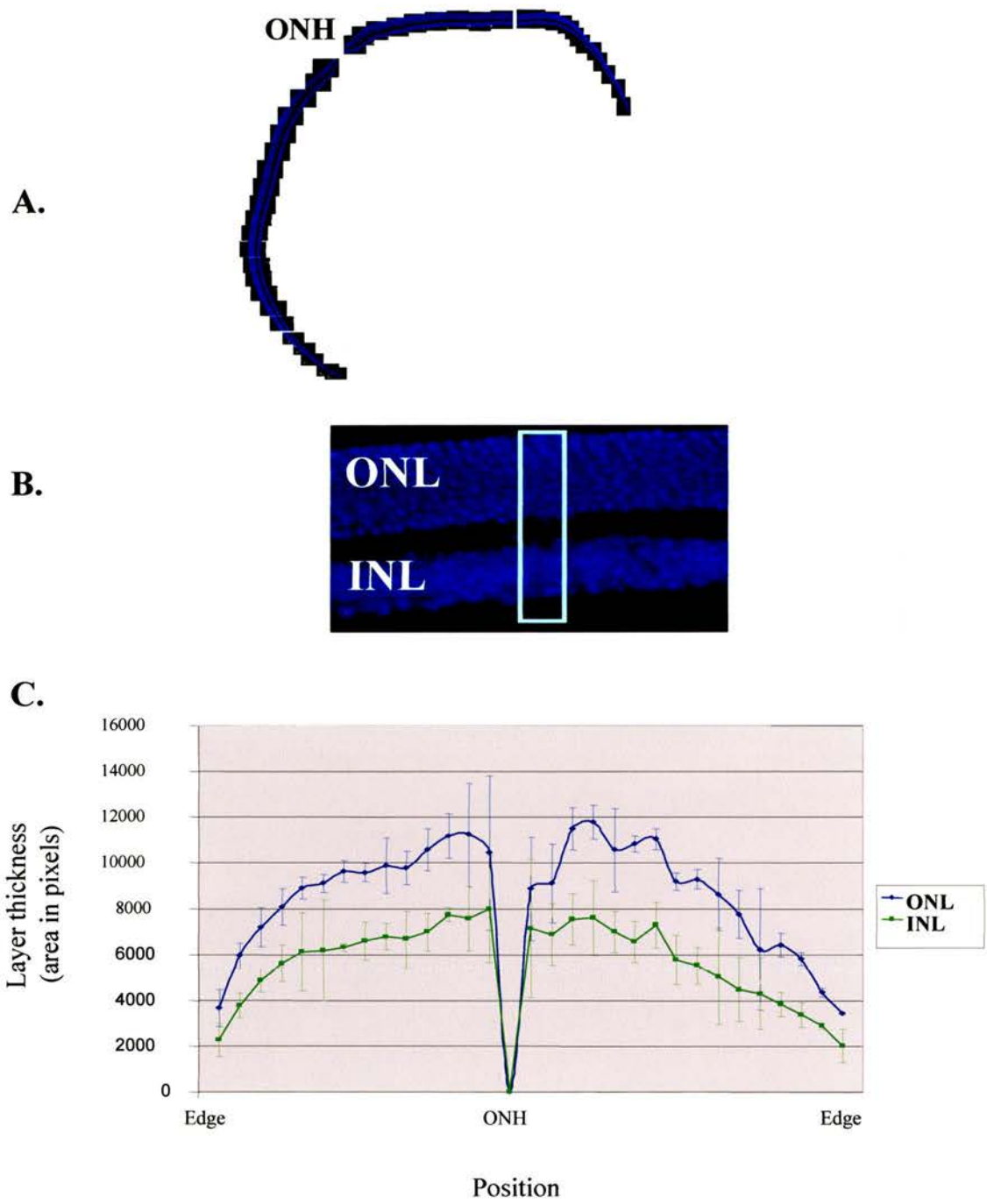

Figure 17: Outer nuclear layer analysis by DAPI staining

ONL analysis was performed on mouse eye sections stained with DAPI. (**A**) Serial images of a whole section were taken at a magnification of x63. (**B**) On each of the images captured, the thickness of the ONL was measured in terms of its area (pixels) (**C**) Sections from 3 animals were analyzed and the results are presented graphically. The error bars are standard deviations. (ONH: optic nerve head)

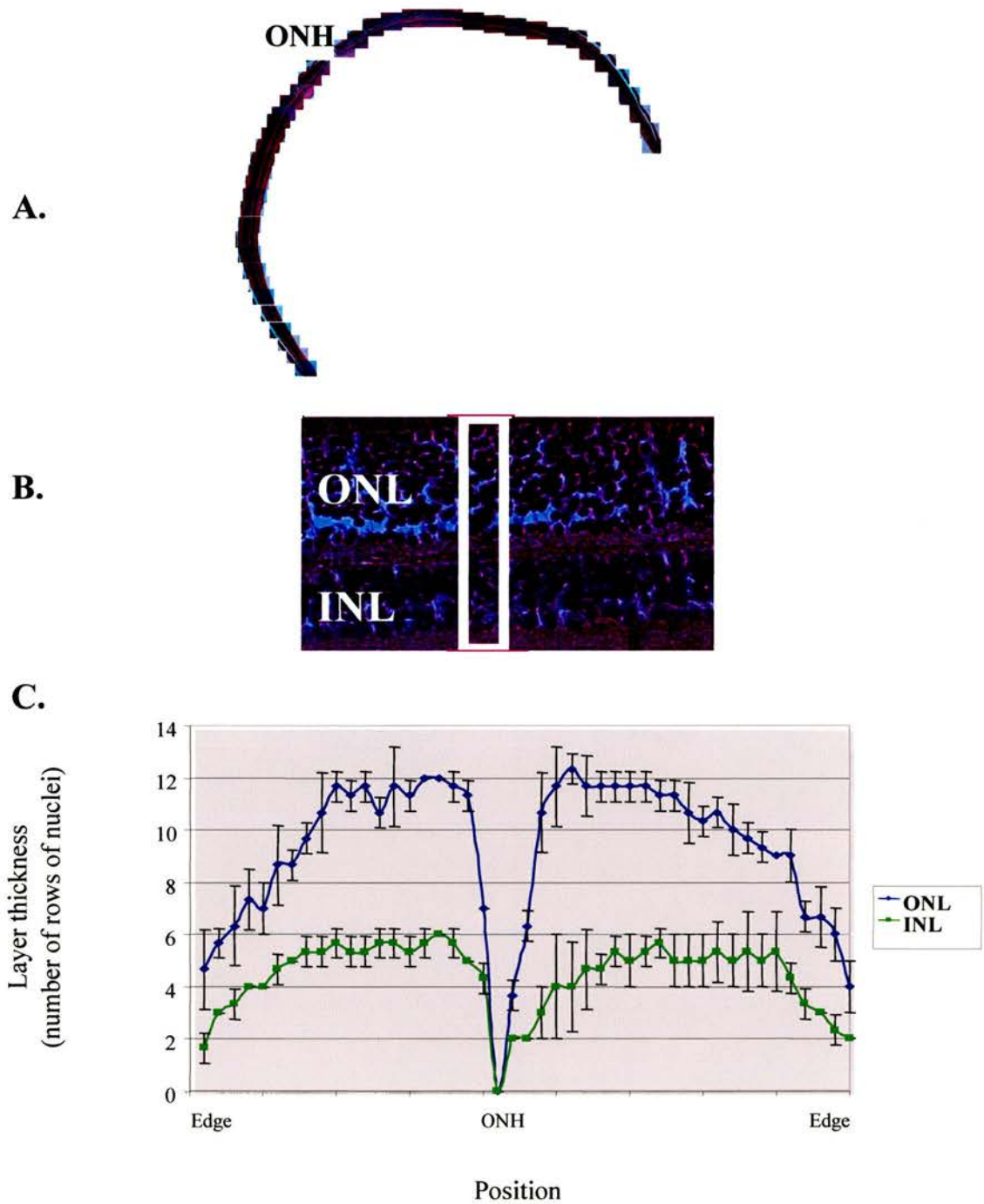

Figure 18: Outer nuclear layer analysis by H&E staining

ONL analysis was performed on mouse eye sections stained with H&E. (**A**) Serial images of a whole section were taken at a magnification of x63. (**B**) On each of the images captured, the thickness of the ONL was measured in terms of number of rows of nuclei (**C**) Sections from 3 animals were analyzed and the results are presented graphically. The error bars are standard deviations. (ONH: optic nerve head)

Using both methods, ONL thickness analysis was first performed on wild-type retinas. For each method, three eye sections corresponding to three different wild-type animals were stained and serial images covering the whole of the retina (from one edge to the other) were taken. To ensure a fair comparison between sections, all the sections used were sagittal (horizontal plane) and included part of the optic nerve head (ONH). Also, to overcome the problem of different retinal lengths, the sections under comparison were aligned at the ONH. The ONL and INL thicknesses were measured and the data was analysed.

The results are shown in **Figures 17 and 18**. As shown, the thickness pattern of the retina revealed by the two methods was very similar. The ONL and INL were of equal thickness at one edge of the retina, but the ONL became gradually thicker towards the ONH, peaking halfway through that distance, and then staying constant, until interrupted by the ONH. On the other side of the ONH, the retina was almost a mirror image of the opposite side of the ONH, with the ONL and the INL becoming increasingly equal in thickness towards the edge of the retina.

The inter-sample variation of ONL thickness analysis was also assessed. For this, the selected protocol was applied on samples from 5 male and 5 female C57Bl/6 mice aged 8 weeks. The results of the analysis, shown in **Figure 19**, reveal that different samples had very similar nuclear layer thickness patterns irrespective of sex.

3.2.3 Terminal deixynucleotidyl transferase dUTP nick end labelling (TUNEL) assay

In this project, the efficiency of the DeadEnd Fluorometric TUNEL System (Promega) to detect apoptotic photoreceptor cells in mouse retina sections was assessed. It is a modified TUNEL assay in which the levels of fragmented DNA in apoptotic cells can be measured. The terminal deoxynucleotidyl transferase recombinant enzyme (rTdT) catalytically incorporates fluorescein-12-dUTP at 3'-OH DNA ends and the fluorescein-12-dUTP-labelled DNA can then be visualised directly by fluorescence microscopy.

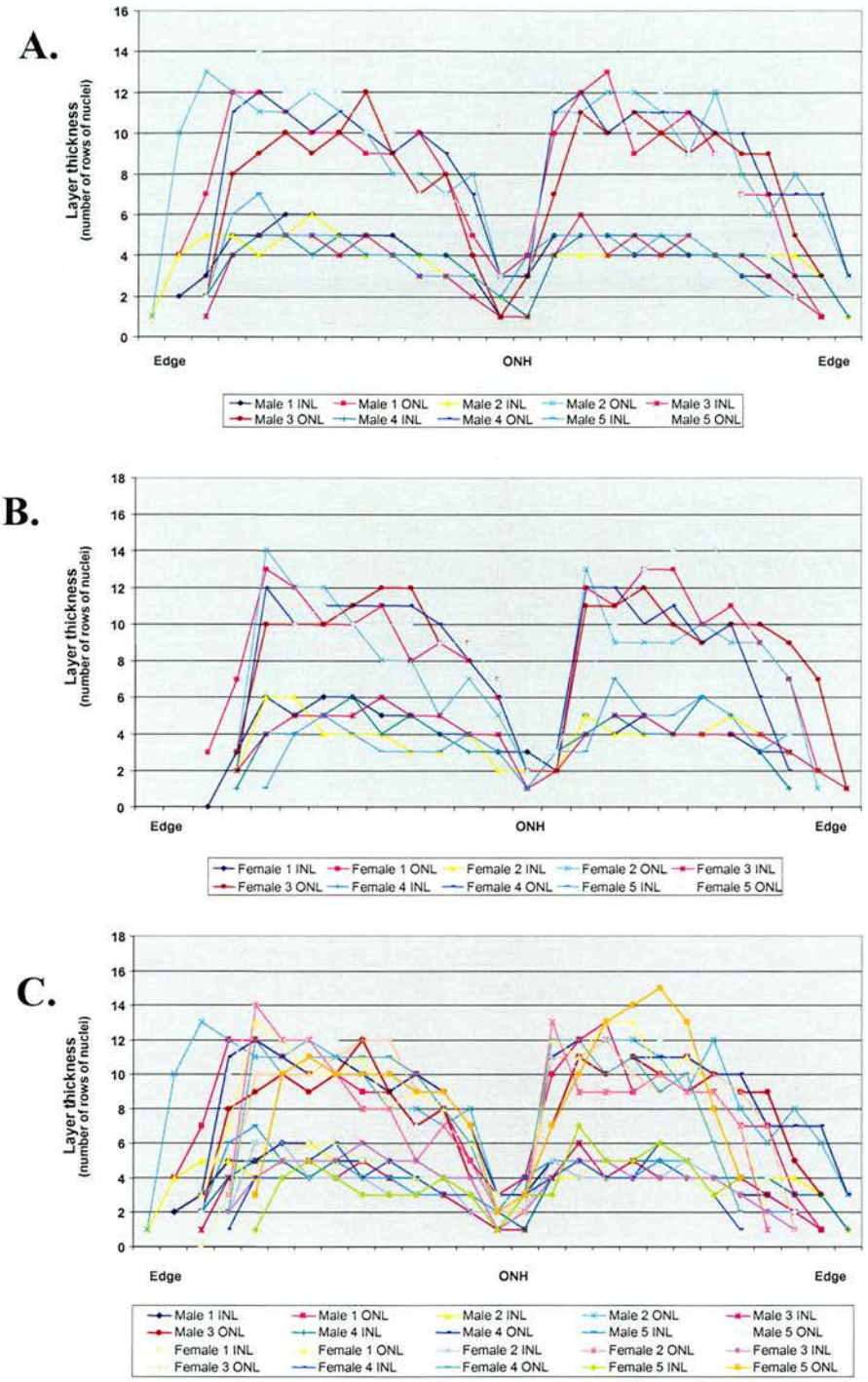

Figure 19: Outer nuclear layer analysis on male and female mouse eyes

Outer nuclear layer analysis was performed on mouse eye sections from 5 male (**A**) and 5 female (**B**) mouse samples. These 'spidergrams' show the thickness patterns of the outer nuclear (ONL) and the inner nuclear layers (INL) of the retina. Combined data (**C**) show no differences between male and female samples.

As shown in **Figure 20**, the application of this assay for the detection of apoptotic cells on paraffin-embedded mouse eye sections was successful. The positive control section was treated with *DnaseI* so that all cell nuclei present in the tissue section were labelled as TUNEL positive. The negative control section was treated with *DnaseI* in the same way as the positive control, but the reaction mix lacked the rTdT enzyme, preventing incorporation of fluorescein-12-dUTP. As expected, no cell nuclei were positively labelled in these samples. Apoptotic cells were successfully detected in mouse eye sections from the *atrd* mutants, while the wild-type sample was clear of any labelling. Additionally, application of the assay on frozen brain sections of the BCG multiple sclerosis model successfully showed TUNEL positive cells

3.2.4 Annexin V assay

Two commercially available annexin V assays (Sigma and US Biological) were applied to both paraffin-embedded and frozen mouse eye sections from *atrd* mutant mice. In addition, their efficiency was assessed on cultured HeLa cells treated with various concentrations of H_2O_2. No Annexin V-positive cells were detected in any of the positive controls.

3.2.5 Poly(ADP-ribose) polymerase (PARP) assay

A commercially available antibody (Promega) was used for detection of the large fragment of the caspase-cleaved PARP-1. Immunocytochemistry and immunohistochemistry were performed on H_2O_2-treated, at various concentrations, HeLa cells and on eye sections from *atrd* mice, respectively. In neither experiment were any apoptotic cells detected by this antibody.

3.2.6 Caspase 3 assay

A commercially available anti-caspase-3 antibody (BD Biosciences) was used for the detection of apoptotic cells. Immunocytochemistry and immunohistochemistry were performed on H_2O_2-treated HeLa cells and on homozygous *atrd* mutant mouse eye sections, respectively. In neither of the two positive control samples were any apoptotic cells successfully detected.

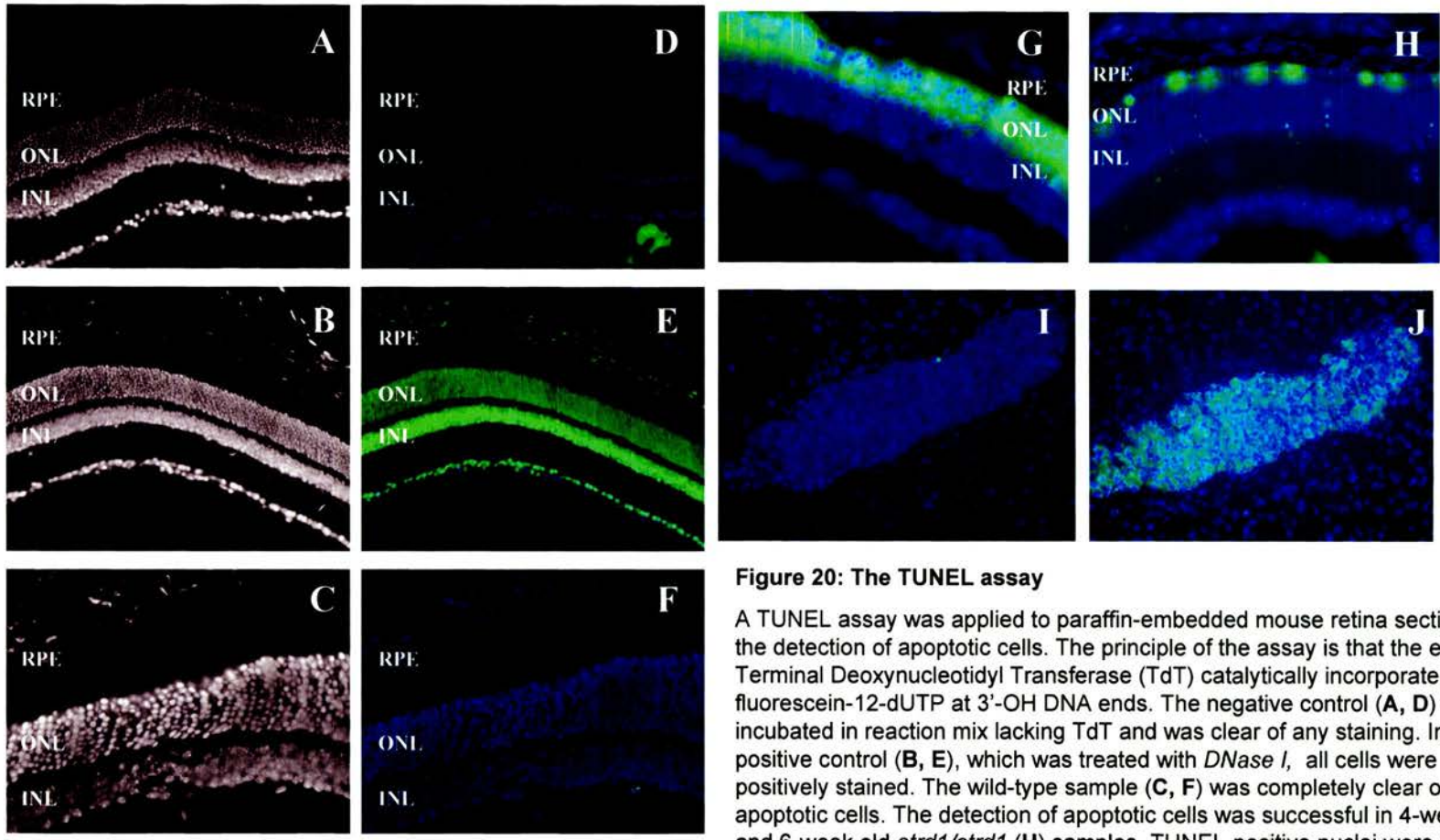

Figure 20: The TUNEL assay

A TUNEL assay was applied to paraffin-embedded mouse retina sections for the detection of apoptotic cells. The principle of the assay is that the enzyme Terminal Deoxynucleotidyl Transferase (TdT) catalytically incorporates fluorescein-12-dUTP at 3'-OH DNA ends. The negative control (**A, D**) was incubated in reaction mix lacking TdT and was clear of any staining. In the positive control (**B, E**), which was treated with *DNase I,* all cells were positively stained. The wild-type sample (**C, F**) was completely clear of apoptotic cells. The detection of apoptotic cells was successful in 4-week (**G**) and 6-week old *atrd1/atrd1* (**H**) samples. TUNEL-positive nuclei were also detected on frozen brain sections of the BCG multiple sclerosis model (**J**), but not on the negative control (**I**).

3.2.7 7, 8-dihydro-8-oxoguanine assay

A commercially available anti-8-oxoG antibody (QED Biosciences) and the Fab166 antibody generated by phage display technology by Soultanakis *et al.* (2001) were used for the detection of oxidative damage at the DNA level. The conventional protocol for immunohistochemistry was applied to both frozen and paraffin sections from *atrd* mouse eyes. Additionally, the antibody was used for detection of apoptotic cultured HeLa cells following H_2O_2 treatment at various concentrations. None of the antibodies showed efficient staining of 8-oxoG lesions in any of the controls.

3.2.8 COX/SDH assay

In this project, the COX/SDH assay was applied to frozen sections of *atrd1* mouse eyes (**Figure 21**). The thickness and histology of the sections was first optimised for detection of individually stained photoreceptor cells. Although the efficiency of both COX and SDH staining was confirmed in COX-deficient colonic crypts and by individual application to eye sections, no COX-deficient photoreceptors were detected in the mutant samples. Modification to the protocol, including reversal of the order of staining and different incubation times, failed to detect COX-negative cells. This could imply species- or tissue-specific differences in the presence of COX-negative cells.

3.2.9 Hydroxynonenal and malondialdehyde assays

Commercially available antibodies to MDA (Alpha Diagnostics) and HNE (Alexis Biochemicals) were used in this project to detect and quantify LP in retinal degeneration mutants. They were initially applied to both paraffin and frozen eye sections from *atrd1/atrd1* mice, by following the conventional protocol for immunohistochemistry. In addition, the efficiency of the antibodies to detect LP adducts was assessed in cultured HeLa cells following H_2O_2 treatment at various concentrations. No positive staining using either antibody was seen on

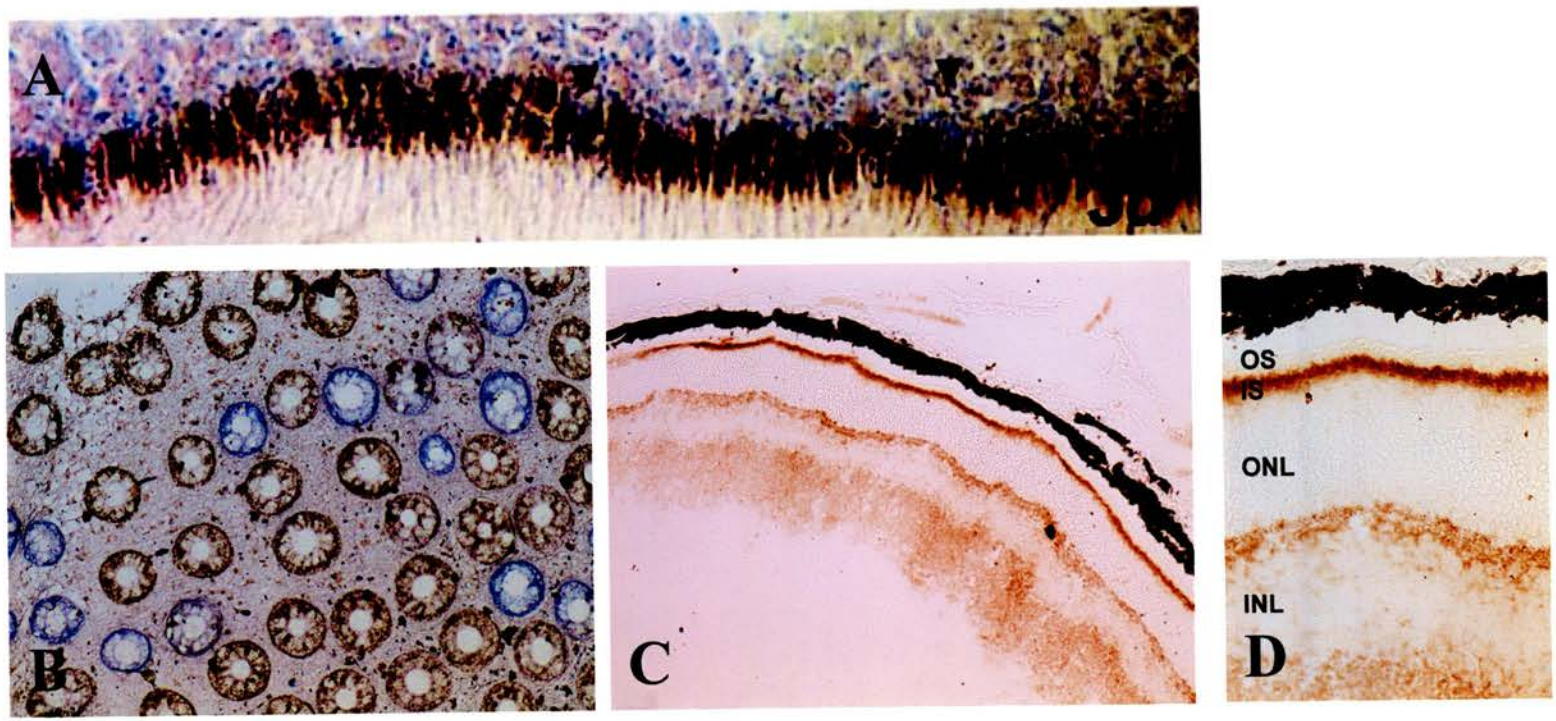

Figure 21 : The COX/SDH assay

(**A**) COX-deficient photoreceptors (*arrowheads)* were detected in the perifovea of an 84-year-old donor (Barron *et al.*, 2001). (**B**) COX-deficient crypts were detected in human colon tissue from a colorectal cancer patient. (**C,D**) The assay was applied to eye sections from 1-week old *atrd1/atrd1* mutants. There is increased staining for COX in the IS of the photoreceptor cells but no COX-deficient photoreceptor cells were detected at a x20 or x60 magnification.

retinal sections from the retinal degeneration mutants. Similarly, application of the antibodies to cultured HeLa cells subjected to H_2O_2 treatment at various concentrations failed to detect any signs of LP.

3.2.10 Nitrotyrosine assay

A commercially available antibody against NTyr (Calbiochem) was used in an attempt to detect and quantify the degree of protein tyrosine nitration in the retinas of retinal degeneration mutants. The antibody was applied at a range of different concentrations to both paraffin and frozen eye sections of *atrd1/atrd1* mice, on frozen brain sections from the BCG model and on HeLa cells treated with H_2O_2 at different concentrations. No staining was seen in any of the positive controls and the levels of protein nitration in retinal degeneration mutants could not be measured.

3.2.11 Citrate synthase assay

As shown in **Figure 22** and **Table 2**, all the constituents of the reaction mix for the spectrophotometric assay of CS were optimised to ensure maximum measurable activity. The spectrophotometric assay for CS was optimised using wild-type mouse liver samples. Retinal samples from wild-type and mutant mice were also assayed to ensure that the assay conditions were optimal for this tissue. Typical examples of the graphical results from wild-type and mutant retinas are shown in **Figure 14**, where they are seen to be practically identical. The optimised concentrations of the different assay constituents are given in the Materials & Methods section. The assay was robust when applied to different mouse tissues.

3.2.12 Complex I assay

As shown in **Figure 23** and **Table 3**, all the reagents included in the spectrophotometric assay for CI were optimised to ensure maximum measurable activity. This was done mainly on mouse liver samples, and the finalised concentrations of all the reagents included in the assay are given in the Material & Methods section. The CI assay worked robustly in mouse retinal samples (**Figure 15**).

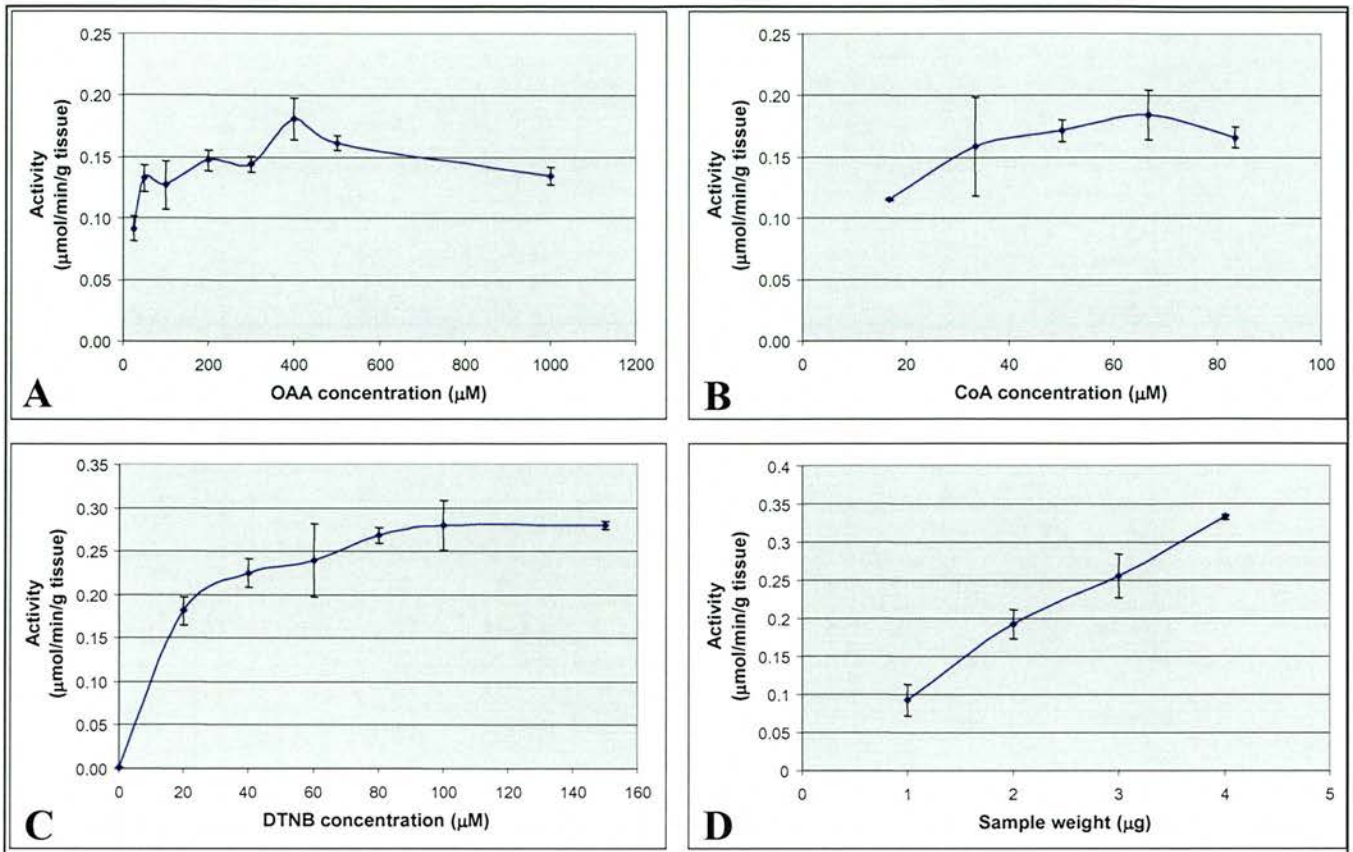

Figure 22: Optimisation of the citrate synthase assay

The constituents of the reaction mix for the spectrophotometric assay for citrate synthase were optimized to ensure maximum measurable activity. Using mitochondrial preparations from wild-type mouse liver samples, the activity of citrate synthase was measured with increasing concentrations of (**A**) oxaloacetate, (**B**) acetyl CoA and (**C**) DTNB. The measured activities are given in Table 2. (**D**) Using the optimised concentrations, the linear relationship between activity and amount of sample used was confirmed.

OAA (µM)	activity	sd	CoA (µM)	activity	sd	DTNB (µM)	activity	sd	sample weight (µg)	activity	sd
25	0.0915	0.0013	**16.7**	0.1154	0.0001	**0**	0.0011	0.0001	**1**	0.0926	0.0028
50	0.1327	0.0015	**33.3**	0.1585	0.0054	**20**	0.1813	0.0022	**2**	0.1923	0.0026
100	0.1272	0.0027	**50.0**	0.1717	0.0012	**40**	0.2246	0.0022	**3**	0.2555	0.0039
200	0.1471	0.0011	**66.7**	0.1842	0.0028	**60**	0.2393	0.0057	**4**	0.3327	0.0004
300	0.1441	0.0008	**83.3**	0.1662	0.0011	**80**	0.2680	0.0012			
400	0.1809	0.0023				**100**	0.2798	0.0039			
500	0.1614	0.0008				**150**	0.2790	0.0006			
1000	0.1346	0.0010									

Table 2 : Optimisation of the citrate synthase assay

The activity of citrate synthase was measured in mouse liver samples with increasing concentrations of the reagents included in the spectrophotometric assay. Highlighted in red are the optimised concentrations of the reagents.

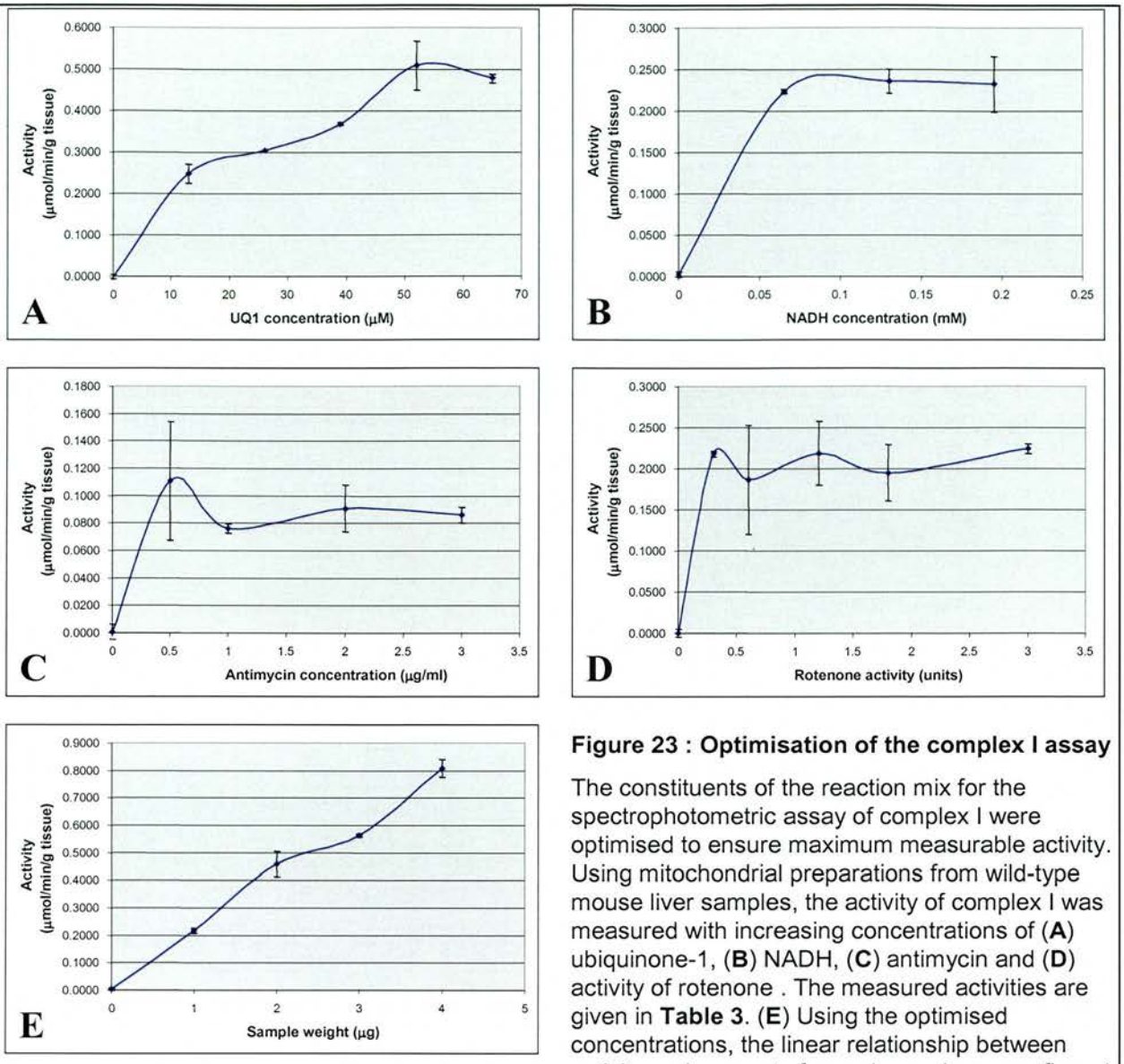

Figure 23 : Optimisation of the complex I assay

The constituents of the reaction mix for the spectrophotometric assay of complex I were optimised to ensure maximum measurable activity. Using mitochondrial preparations from wild-type mouse liver samples, the activity of complex I was measured with increasing concentrations of (**A**) ubiquinone-1, (**B**) NADH, (**C**) antimycin and (**D**) activity of rotenone . The measured activities are given in **Table 3**. (**E**) Using the optimised concentrations, the linear relationship between activity and amount of sample used was confirmed.

UQ1 µM	Activity	sd	NADH mM	Activity	sd	Rotenone µg/ml	Activity	sd	Antimycin µg/ml	Activity	sd	Sample weight µg	Activity	sd
0	-0.0016	0.0045	0	0.0023	0.0035	0	-1.4E-17	4.5E-03	0	0.0008	0.0057	1	0.00233	0.0035
13	0.2476	0.0227	0.065	0.2235	0.0023	0.3	2.2E-01	3.4E-03	0.5	0.1109	0.0432	2	0.21624	0.0080
26	0.3039	0.0000	0.13	0.2355	0.0148	0.6	1.9E-01	6.6E-02	1	0.0764	0.0034	3	0.459	0.0466
39	0.3682	0.0023	0.195	0.2323	0.0330	1.2	2.2E-01	3.9E-02	2	0.0908	0.0171	4	0.5627	0.0068
52	0.5088	0.0580				1.8	1.9E-01	3.4E-02	3	0.0860	0.0057	5	0.80707	0.0318
65	0.4783	0.0102				3	2.2E-01	5.7E-03						

Table 3: Optimisation of the complex I assay

The activity of complex I was measured spectrophotometrically in mouse liver samples with increasing concentrations of the reagents included in the assay. Highlighted in red are the optimised concentrations of the reagents.

3.2.13 Strain Comparison

As mentioned in the Introduction, a number of investigators have highlighted the importance of the genetic background on the viability of *Sod*$^{-/-}$ null mice. Mice on a C57Bl/6, DBA or CD1 background survive for up to 1, 8 or 10 days, respectively (Li *et al.*, 1995; Huang *et al.*, 2001). It was necessary therefore to ensure that the markers of oxidative stress used in this project were not significantly different between the different genetic backgrounds on which the retinal degeneration mutants were present. Additionally, a comparison was made between male and female samples.

In this context, the activities of citrate synthase and complex I were measured in tissues collected from 5 male and 5 female animals on a Balb/c, CBA, CD1, C57Bl/6 or DBA backgrounds. The results, shown in **Figure 24**, revealed that, for these enzymes, there was no difference between the genetic backgrounds or the genders.

3.2.14 Reduced glutathione (GSH) measurements

The concentrations of all reagents used in GSH measurement were optimised using mouse liver samples and the results are shown in **Figure 25** and **Table 4**. Before a new series of assays was performed, a standard curve was prepared based on a minimum of four different concentrations of purified GSH (**Table 5**). A typical GSH standard curve is presented in **Figure 26.**

It is worth noting that the original protocol suggested the addition of triethanolamine (TE) to the samples, at a final concentration of 5%, prior to measuring contents. TE is an organic compound that is often used as a buffer, and since the samples for GSH measurements were prepared in perchloric acid, the pH would need to be adjusted to neutrality. As shown however in **Figure 27A**, addition of 5% TE to the GSH standard samples, used in setting up the standard curve, completely inhibited the measurements and the linearity of the standard curve was lost. It was therefore decided to further investigate this by assessing how TE exerted its apparent inhibitory effect on GSH measurements. For this, mouse brain and liver samples were used, as well as a standard concentration of 5

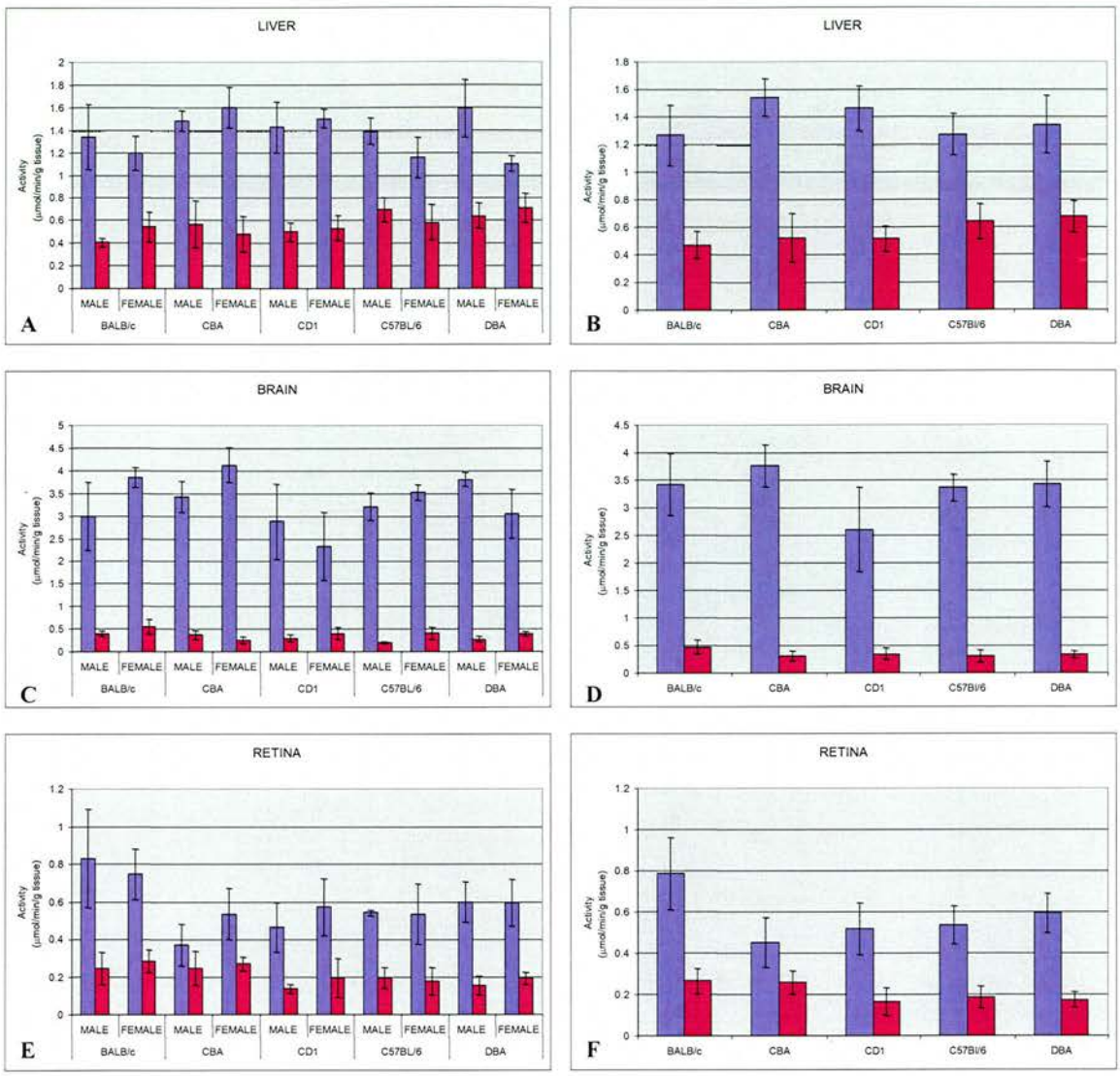

Figure 24: Strain comparison for citrate synthase and complex I enzyme activities

The activities of citrate synthase (blue columns) and complex I (maroon columns) were measured in (**A**, **B**) liver, (**C**, **D**) brain and (**E**, **F**) retina samples from wild-type Balb/c, CBA, CD1, C57Bl/6 and DBA mouse strains. For each strain a comparison was done between male and female samples (**A**, **C**, **E**) [n=5]. Samples from both sexes were pooled for a comparison between the strains (**B**, **D**, **F**). There was no effect of either sex or mouse strain on the activities of these two enzymes ($p>0.05$).

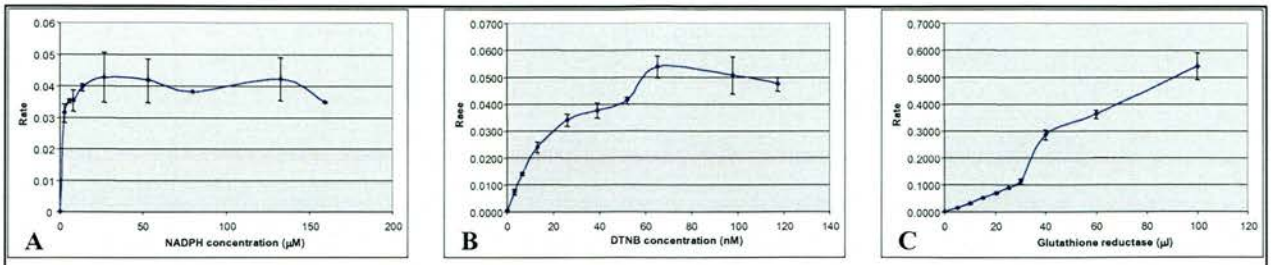

Figure 25: Optimisation of the reduced glutathione (GSH) concentration protocol

The different ingredients of the reaction mix used in the protocol for measuring reduced GSH content were optimised. (**A**) Optimisation of NADPH (**B**) Optimisation of DTNB (**C**) Optimisation of GR. The measured activities are given in **Table 4**.

DTNB nM	Rate	sd	NADPH µM	Rate	sd	GR µl	Mean	sd
0	0.0003	0.0003	0	0.00005	7E-05	0	0.0001	0.0001
3	0.0074	0.0010	0.0024	0.0314	0.003	5	0.0140	0.0003
6	0.0142	0.0005	0.0048	0.0352	6E-04	10	0.0303	0.0015
12	0.0240	0.0021	0.0072	0.03525	0.003	15	0.0506	0.0011
24	0.0339	0.0021	**0.012**	0.0396	0.001	**20**	0.0678	0.0013
36	0.0377	0.0028	0.024	0.04265	0.008	25	0.0879	0.0018
48	0.0413	0.0012	0.048	0.04165	0.007	30	0.1129	0.0101
60	0.0489	0.0028	0.072	0.0381	0	40	0.2863	0.0181
90	0.0448	0.0013	0.12	0.04215	0.007	60	0.3617	0.0159
112	0.0475	0.0025	0.144	0.03485	2E-04	100	0.5403	0.0502

Table 4: Optimisation of the reduced glutathione measurement protocol

The protocol for measuring the reduced glutathione concentration in samples was optimised for all the different ingredients included in the reaction mix. Highlighted in red are the optimal concentrations.

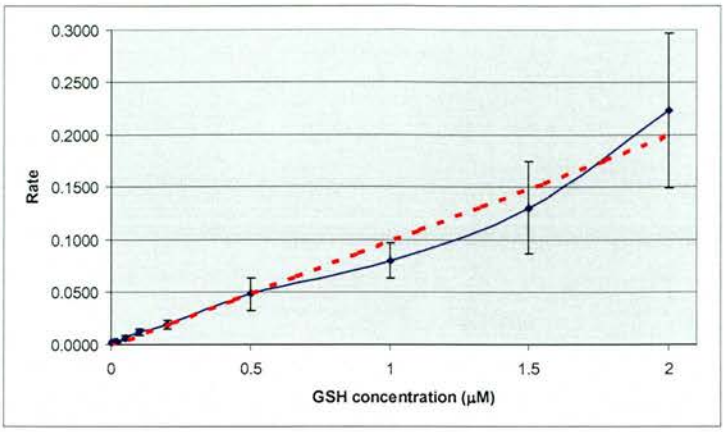

Figure 26: The reduced glutathione (GSH) standard curve

The concentration of glutathione was determined by comparison to a standard curve generated by using appropriate concentrations of purified reduced glutathione

GSH (μM)	0	0.01	0.02	0.05	0.1	0.2	0.5	1	1.5	2
all volumes in μl										
BUFFER	0.455	0.455	0.454	0.453	0.450	0.445	0.430	0.405	0.380	0.355
DTNB (0.06μM)	0.500	0.500	0.500	0.500	0.500	0.500	0.500	0.500	0.500	0.500
GR	0.020	0.020	0.020	0.020	0.020	0.020	0.020	0.020	0.020	0.020
NADPH (0.12 μM)	0.025	0.025	0.025	0.025	0.025	0.025	0.025	0.025	0.025	0.025
STANDARD	0.000	0.001	0.001	0.003	0.005	0.010	0.025	0.050	0.075	0.100
Mean Rate	0.0021	0.0029	0.0026	0.0066	0.0117	0.0189	0.0485	0.0799	0.1308	0.2230
St.Dev.	0.0000	0.0006	0.0006	0.0022	0.0031	0.0039	0.0156	0.0166	0.0436	0.0739

Table 5: Volumes for the reduced glutathione standard curve

Using the optimised concentrations of the reagents included in the protocol for GSH measurements, a standard curve was set up using the given volumes of the reagents.

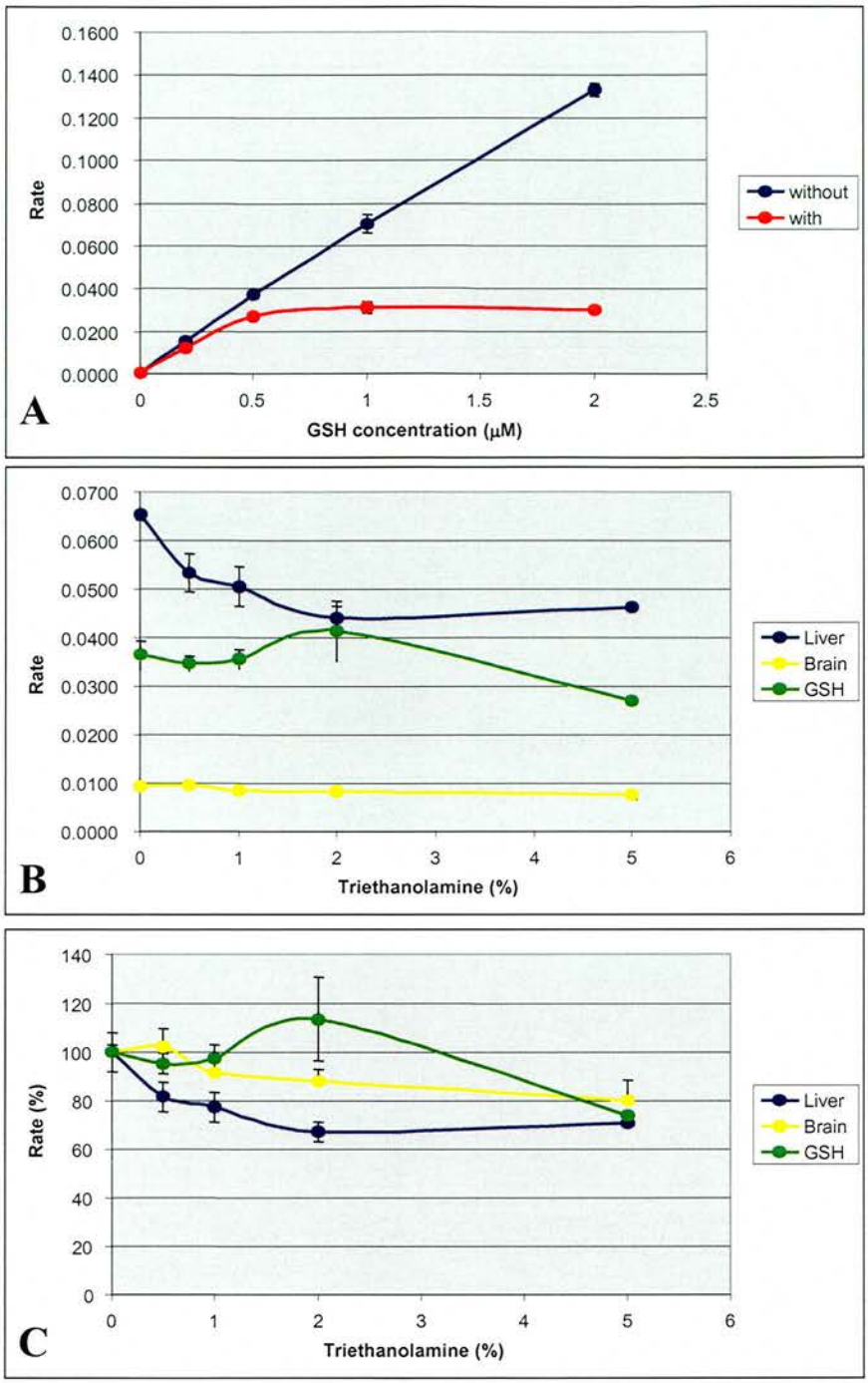

Figure 27: The inhibitory effect of triethanolamine on reduced glutathione measurements

(**A**) Addition of 5% triethanolamine (TE) in the reaction mix for measurements of GSH, as suggested by the original protocol by Tietze (1969), had an inhibitory effect on the measurements of purified GSH. (**B**) The rates obtained from mouse liver, mouse brain and purified GSH samples with increasing percentages of TE were measured. (**C**) The inhibitory effect of TE on the above samples was also expressed in percentages.

μM of purified GSH. As shown in **Figures 27B** and **C**, measurements of the GSH standard sample changed with increasing TE concentration, and at 5%, the measured GSH level had decreased by a significant 30% (p=0.04). TE treatment did not affect the GSH measurements in mouse brain samples however. In the liver samples, addition of TE even at a low 1% final concentration significantly decreased by 20% the measured GSH concentration (p=0.04). The inhibitory effect of TE in this sample increased progressively with TE concentration, so it was omitted from the final reaction mixture.

The optimised concentrations of the reagents used in the GSH measurement protocol are given in the Materials & Methods section. The protocol was also applied to different mouse tissues, including liver, brain, heart and retina. The results given by the different tissues and genotypes were found to show good reproducibility.

In summary, the protocol for GSH measurements worked robustly in all mouse tissues assayed, including the retina.

3.3 Summary and Conclusions

The aim of this project was to investigate the role of oxidative stress in photoreceptor degeneration and, in this chapter, methods for measuring these parameters were evaluated.

3.3.1 Apoptotic assays

The rates of photoreceptor degeneration were measured by ONL analysis and TUNEL assays. Two methods for measuring the thickness of the nuclear layers were compared and were shown to produce very similar results. The ONL and INL in both DAPI- and H&E-stained sections showed similar thickness patterns, measured in pixels and number of rows of nuclei, respectively. However, it was decided to perform ONL analysis on H&E-stained sections only. Reasons for this decision included the ease of tissue staining and analysis, as well as the preservation of the stained samples for a long period of time. Additionally, a comparison between male and female retinal samples demonstrated that the retinal layers in males and in females do not show any significant difference in

thickness, and hence, no further sex distinction should be made when selecting samples for analysis.

Although the ONL analysis as a method for measuring the rate of photoreceptor degeneration is based on measuring the number of living cells in the retina, TUNEL assays are used for detecting dying cells. The TUNEL assay has been previously used for the detection of apoptotic cells on eye sections. Arroyo *et al.* (2005) detected increased numbers of apoptotic photoreceptor cells in frozen human eye sections from patients with primary or recurrent retinal detachments. Also, Doonan *et al.* (2003), while investigating the involvement of caspases in apoptosis, applied the TUNEL assay on samples from the *rd1/rd1* mouse and from an *N*-methyl-*N*-nitrosourea-treated Balb/c mouse and successfully detected apoptotic photoreceptor cells. In this project, a commercially available kit by Promega was used and proved to be an efficient means of detecting apoptotic cells in paraffin-embedded mouse eye sections.

However, as discussed by Stadelman & Lassmann (2000), in contrast to other methods, the TUNEL assay is not specific to apoptosis and can also detect necrotic cells. For example, it has been demonstrated that in human atherosclerotic plaques nonapoptotic nuclei can be labelled by the TUNEL technique (Koeck *et al.*, 1998). Therefore, it has been recommended that this assay be applied in conjunction with other methods, more specific to apoptosis.

For this reason methods specific to apoptosis were also used. The annexin V method has the advantage of being highly specific to apoptosis (Martin *et al.*, 1995). However, for the purpose of this project, a potential disadvantage of the assay is that it was initially developed for the detection and quantification of apoptosis in living cells after separation by flow cytometry. Hence, the assay needed to be appropriately modified for application to tissue sections. No published work has been reported in which the annexin V assay has been applied to tissue sections, and, as a result, the failure of the assay to work was to some extent predictable.

The cleaved form of PARP is also used as a marker for apoptotic cells. Poly (ADP-ribosyl)ation is a post-translational modification of a series of proteins involved in DNA repair, transcription and apoptotic cell death. This modification occurs in every nucleated cell of mammals, plants and lower eukaryotes, but is not present in yeast cells (Lindahl *et al.*, 1995). The reaction is regulated by the

joint action of PARP and of Poly (ADP-ribose) glycohydrolase (PARG) (Scovassi & Diederich, 2004; Burkle *et al.*, 2005; Diefenbach & Burkle, 2005). In the presence of DNA strand breaks, PARP-1 is activated and binds to the substrate nicotinamide adenine dinucleotide (NAD^+). The latter is cleaved into nicotinamide and an adenosine diphosphate (ADP)-ribosyl moiety, which is then transferred to glutamate or aspartate residues in target proteins. Additional ADP-ribosyl transfer cycles result in the formation of negatively-charged polymers on the proteins, whose function is consequently compromised. Target proteins of PARP include DNA polymerase α and β and various histones. The formation of NAD^+ polymers is transient as they are rapidly removed by PARG for NAD^+ re-cycling. Therefore, the orchestrated action of PARP and PARG determines cellular NAD^+ levels.

An antibody against PARP has been previously used for detecting apoptotic photoreceptor cells. Miller et al. (2006) used the mouse 661W photoreceptor cell line as a neuronal model of CI-1010 ((R)-alpha-[[(2-bromoethyl)-amino]methyl]-2-nitro-1H-imidazole-1-ethanol monohydrobromide)-mediated retinal degeneration and demonstrated a link between onset of apoptosis and PARP cleavage. Additionally, Li *et al.* (2002) were able to detect apoptotic ganglion cells in retinal sections from p53-deficient mice that were injected with NMDA. In this project however, the antibody against the cleaved form of PARP that was used failed to detect apoptotic cells. Possible explanations are the inefficiency of the antibody and/or the absence of apoptotic cells with cleaved PARP. The latter explanation is the least likely, given that the assay was applied to positive controls of two types, *atrd1/atrd1* retinal sections and H_2O_2 treated cells. Given, therefore that the antibody used was not appropriate, additional methods specific to apoptosis were used.

The involvement of caspase 3 in apoptosis is also well documented, and therefore an antibody specific to this protein was applied to apoptotic positive controls. It should be noted however that the involvement of caspases in certain types of photoreceptor degeneration has been controversial, as although they were initially thought to play a central role in the mechanism, it was later shown that certain apoptotic characteristics can occur in the absence of caspase activity (Borner & Monney, 1999). In mouse retinal degeneration models of light damage

used by Donovan *et al.* (2002) to demonstrate caspase-independent apoptosis, caspase-3 levels were markedly reduced in the mature retina and did not increase following light exposure. Therefore, these authors supported the view that it does not play a role in the apoptosis of photoreceptors in the light damage model. In this context, lack of caspase-3-positive cells in the *atrd1/atrd1* eye sections could be explained by a lack of involvement of the protein in photoreceptor degeneration in this model. The fact that the antibody also failed to work on cultured cells however points to its inefficiency in detecting apoptotic cells with the protocol used.

In this project however, and under the conditions specified in the Methods & Materials section, none of these three apoptosis-specific antibodies were able to successfully detect dying photoreceptor cells in the positive control samples. It was therefore decided not to pursue their optimisation for detection of apoptotic photoreceptor cells in the retinal degeneration mutants analysed in this project.

3.3.2 DNA damage

Attempts to measure oxidative damage at the DNA, lipid and protein level were also carried out using different methods. Firstly, an antibody against the most common oxidative DNA lesion 8-oxoG was used. Increased amounts of 8-oxoG have been found in mtDNA isolated from brain tissue from Alzheimer's patients (Nunomura *et al.*, 1999). Also, Soultanakis *et al.* (2001) studied oxidative DNA damage in rat alveolar type II epithelial cells (RLE) and TK6 (a human B lymphoblastoid cell line) cells treated with various concentrations of H_2O_2 to induce oxidative damage. By coupling staining for Fab166 with the mitochondrial marker MitoTracker, the authors were able to demonstrate mtDNA damage in cells. Finally, Cortina *et al.* (2005) showed increased levels of 8-oxoG in photoreceptor synaptic terminals, following bright light treatment in rats. In the current project however, the antibody against 8-oxoG failed to stain any cells in the positive controls. As in the case of the antibody against the cleaved form of PARP, the most likely explanation for this result involves the inefficiency of the antibody, under the experimental conditions used, to detect DNA oxidative damage, rather than the lack of DNA damage in the samples that were assayed.

Secondly, the COX/SDH assay was applied to positive control samples in an attempt to quantify mtDNA damage. Mitochondria have their own genome (mtDNA) and its mutation rate has been shown to be at least 10-fold higher than that of nuclear DNA (Brown *et al.*, 1979). This can be attributed to limited mtDNA repair, absence of protective histones on mtDNA and its close proximity to the free-radical generating ETC. Mutations in mtDNA have been repeatedly shown to be the cause of various human diseases, including Leber's hereditary optic neuropathy (LHON) (Chinnery & Turnbull, 2000). A retinal degeneration phenotype is also often observed with mtDNA mutations. Retina is a good candidate therefore for detecting mtDNA mutations, as it is a tissue that is highly metabolically active and is primarily composed of postmitotic non-proliferative neurons. The retina is also exposed to wavelengths of light that have been shown to damage mtDNA (Wallace, 2005). It is therefore conceivable that mutations in mtDNA impair the function of the encoded genes to a greater extent in mutants with retinal degeneration than in wild-type retinas.

The COX/SDH method is commonly used for the detection and analysis of mtDNA mutations in a variety of tissues, but most extensively in human muscle and colon. Limited work has been done on COX/SDH assay in retina. In 1999, Andrews *et al.* cytochemically studied COX and SDH staining in the human retina and RPE. Their observations were very interesting, revealing high COX and SDH activity in unmyelinated parts of retinal ganglion cell axons, the OPL, the IS of photoreceptor cells and the RPE. There was essentially no or very low reactivity in the OS of photoreceptor cells and in the INL respectively. In a subsequent study, Barron *et al.* (2001) investigated the occurrence of somatic mtDNA mutations in the macula during aging. The COX/SDH assay was applied to section of human eyes donated from aged humans (**Figure 21**). The observation of a much higher rate of mutated mtDNA in the central than the peripheral retina, and its correlation with the presence of COX-negative photoreceptors, confirmed the reliability of the assay for detection of mtDNA damage. These authors provided the following explanation for their results. Damaged COX impairs the function of the ETC and causes further biochemical/metabolic defects, influencing the production of ATP and the integrity of ATP-dependent cellular processes. One such process is the ATP-binding cassette transporter, which is responsible for transferring retinoids

between the neural retina and the RPE. Inhibition of this transporter has been shown to lead to lipofuscin accumulation in the RPE, generation of free radicals and RPE cell death. The latter effect could lead to death of the associated photoreceptor cells. Finally, the COX/SDH staining method has been successfully used to detect COX-negative colonic crypts from patients with colorectal cancer (Greaves *et al.*, 2006).

In this project, although the efficiency of the assay was confirmed by the detection of COX-deficient crypts on colon sections from cancer patients, no COX-negative photoreceptor cells were detected in any of the mouse retina samples assayed. This result can be explained either by the lack of this type of cell in the samples or by species and age differences between the samples analysed by Barron *et al.* (2001) and the present study. It was therefore concluded that in this project the COX/SDH assay would not be used further as an indication of oxidative stress in the mutants of interest.

3.3.3 Lipid damage

Oxidative damage to lipids was attempted to be measured by the levels of MDA and HNE. MDA is mainly formed by the peroxidation of PUFAs with at least two methylene-interrupted double bonds (Del Rio *et al.*, 2005). When present at low basal concentrations (<1 μM), MDA has low chemical reactivity and often acts as a signalling molecule (Petersen & Doorn, 2005). Increased MDA levels however result in its interaction with cellular molecules and formation of adducts with nucleic acid bases and protein residues. These adducts have been associated with a number of disease phenotypes, including amyotrophic lateral sclerosis and Parkinson's disease. MDA is therefore often used as a biological marker for progression of neurodegenerative diseases (Dib *et al.*, 2002).

HNE, which was discovered in 1980 by Benedetti *et al.* (1980), is an αβ-unsaturated acyl aldehyde that can covalently modify cellular target proteins, thereby affecting their structure and/or function (Bennaars-Eiden *et al.*, 2002; Petersen & Doorn, 2004). Like MDA, HNE has been shown to act as a signalling molecule at low concentrations, and even at higher concentrations, it was initially considered a second messenger for free radicals (Awasthi *et al.*, 2003; Yang *et al.*, 2003). Now however, the cytotoxic nature of HNE is well established and is

attributed to its ability to initiate LP, disturb cellular Ca^{2+} homeostasis, deplete GSH and cause apoptosis. Altered levels of HNE have been implicated in a number of neurodegenerative diseases, like Alzheimer's disease and atherosclerosis (Zarkovic, 2003a; Zarkovic, 2003b). HNE is therefore commonly used as marker for oxidative stress and LP.

The levels of these two markers of lipid peroxidation in retinal degeneration mouse mutants have not been previously reported. However, failure to efficiently detect signs of LP in the positive controls, using antibodies either to MDA or to HNE, resulted in the decision not to use these antibodies as markers for LP in this project

3.3.4 Protein damage

Oxidative damage to proteins was assessed by both immunohistochemistry for nitrotyrosine and by enzyme assays.

Although the signalling role of NO at low, basal concentrations has been well established (Bishop & Anderson, 2005), at higher nanomolar concentrations it can reversibly inhibit the mitochondrial respiratory chain at either complex I and/or complex IV (Brown, 2001; Brown *et al.*, 2004). At these concentrations NO can also cause nitration of other proteins. At higher (mM) concentrations NO and its derivatives are capable of irreversibly inhibiting respiration, which eventually leads to cell death (Brown, 2001). Protein nitration appears to be a mechanism whose specificity is dictated by the proximity of proteins to the site of generation of nitrating agents, by the abundance of candidate protein targets and of tyrosine residues within them, as well as by the secondary and tertiary structure of the proteins (Ischiropoulos, 2003; Gow *et al.*, 2004). Consequently, a substantial number of mitochondrial proteins are nitrated *in vivo*, covering all essential metabolic and antioxidant pathways (Aulak *et al.*, 2001; Aulak *et al.*, 2004; Koeck *et al.*, 2005). An increasing amount of evidence associates elevated nitrotyrosine levels with disease phenotypes, leading to the former's role as a biomarker of oxidative stress attributed to production of nitrating species (Halliwell, 1997). Tyrosine nitration has been documented in retinal proteins of diabetic mice (Du *et al.*, 2002), aged rats (Louie *et al.*, 2002), rats exposed to damaging light (Miyagi *et al.*, 2002) and in different models of ischemic

proliferative retinopathy (e.g., diabetes mellitus, retinopathy of prematurity, retinal vein occlusion) (Sennlaub *et al.*, 2002). Here, an antibody against nitrotyrosine was applied to mutant retinal sections, however with no success. A possible explanation is the lack of efficiency of the specific antibody used in detecting this type of protein modification.

Spectrophotometric assays for oxidative-stress sensitive and insensitive enzymes were also optimised in this project. Since the main source of oxidative stress is the mitochondrion, enzymes participating in mitochondrial functions are likely candidates of such an insult. Reduced mitochondrial enzyme activities have previously been reported in a number of human neurodegenerative diseases, like Alzheimer's and Parkinson's disease (Gibson *et al.*, 1998; Schapira, 1999; Krasnianski *et al.*, 2005). In this study the mitochondrial enzymes citrate synthase and complex I were used as oxidative stress-insensitive and –sensitive activities respectively, and both were successfully assayed and optimised for use in the study.

3.3.5 GSH measurements

The method for measuring the concentrations of reduced glutathione (GSH) was optimised. Glutathione is a ubiquitous molecule that is produced in all mammalian organs and tissues, although its concentration varies markedly between tissues. The liver has the highest glutathione concentration, whereas this is lower in the plasma and urine (Pastore *et al.*, 2003). GSH is synthesised in the cytosol, where more than 85% of the cellular content is present at a millimolar concentration (Pastore *et al.*, 2003). Mitochondria lack the glutathione synthetic machinery and therefore rely on this antioxidant's uptake from the cytosol for the maintenance of the mitochondrial pool, whose importance is evident by its close proximity to the main intracellular source of oxidants.

In cells, total GSH can be free or bound to proteins. When free, it is mainly in its reduced form (GSH), which can be converted to the oxidative form (GSSG) by GPX, which is normally 'recycled' back to GSH by GR. The relative amounts of these two forms of glutathione are an indication of the oxidative state of the cells. In the resting state, when the reduced form of glutathione predominates over the oxidised one, the ratio GSH/GSSG exceeds 100, whereas,

under oxidative stress, this is reduced to 1-10 (Pastore *et al.*, 2003). In addition to changes in the relative amounts of the two forms of glutathione, the level of total glutathione in the cell also decreases under oxidative stress. Different mechanisms have been suggested for this, including insufficient supply of glutathione precursors (Dringen, 2000) and production of nitric oxide, cytokines or other oxidants (Mytilineou *et al.*, 1999). The expression levels and activities of the enzymes responsible for synthesising glutathione have been shown to remain unchanged, ruling out the possibility that glutathione depletion can be attributed to failure of synthesis. Increased expression of gamma-glutamyltranspeptidase might reflect compromised glutathione re-synthesis. A rapid depletion of intracellular glutathione has been demonstrated in an *in vitro* model of photoreceptor apoptosis, accompanying an early and sustained increase of ROS production (Carmody *et al.*, 1999).

In this project, the protocol for measuring reduced GSH levels in mouse tissue samples was optimised efficiently and was therefore used in order to measure the GSH concentration in the retinal degeneration mutants.

3.3.6 Conclusion

To summarise, although various methods were attempted for measuring photoreceptor degeneration and oxidative stress, only some were efficiently optimised for application to the retinal degeneration samples. In the following chapters, photoreceptor degeneration will be assessed by ONL analysis and TUNEL assays. Oxidative damage will be assessed by spectrophotometric enzyme assays for CI and CS and by measuring the concentrations of reduced glutathione.

CHAPTER 4

PHENOTYPIC ANALYSIS OF MOUSE RETINAL DEGENERATION MUTANTS

4.1. Introduction

In this chapter, a phenotypic analysis of four mouse models of RP, representing mutations in three genes implicated in the disease, was carried out to provide a baseline for comparison with later experiments, in which oxidative stress pathways are manipulated in various ways. We used the *retinal degeneration 1* (*rd1*) mouse and the recently generated *atypical retinal degeneration 1* (*atrd1*) mouse. They both have mutated forms of the *pde6β* gene, whose product, the β subunit of cyclic 3' 5' guanosine monophosphate phosphodiesterase 6 (cGMP PDE6β), is involved in the process of rod phototransduction. The r*d1/rd1* mutant has a naturally occurring transversion in the 7th exon of the gene (Beck *et al.*, 2000), whereas the *atrd1/atrd1* mutant has a missense mutation (T1860A) in exon 15 of the same gene, which converts a histidine residue to a glutamine at codon 620 (Thaung *et al.*, 2002). The extensively studied *Rho*$^{-/-}$ and *rds/rds* mice were also analysed in this project. The rhodopsin knockout mouse was generated by Humphries *et al.* (1997) by targeted homologous recombination and disruption of the rhodopsin gene which is also in the visual transduction cascade, in which it initiates the whole process of signal transduction. The *rds/rds (Prph2* $^{rds/rds}$*)* mouse results from a spontaneous mutation in the peripherin 2 (*Prph2*) gene, in which a 9.2-Kb insetion into exon 2 results in premature truncation of the protein (Ma *et al.*, 1995). Peripherin 2 has a structural role in the formation of rod outer segments. Details on the known specific pathologies of each of these models were given in the Introduction (**part 1.2.2.1**.).

The rates of degeneration in the above mutants were estimated both by outer nuclear layer (ONL) analysis and by TUNEL assays for detection of apoptotic photoreceptor cells. The expression level and localisation of the proteins rhodopsin and phosphodiesterase 6 were also assessed by immunohistochemistry on paraffin eye sections. For each mouse mutant, the activities of the mitochondrial enzymes citrate synthase and complex I were measured spectrophotometrically in four different tissues, including the retina. Finally, the reduced glutathione (GSH) concentration was measured in the same tissues collected from all of the mutants. The aim of this chapter was to phenotypically

analyse the retinal degeneration mutants, and to elucidate the role of oxidative stress in the manifestation of the disease phenotype.

4.2. Results

4.2.1. Rates of photoreceptor degeneration in retinal degeneration mutants

The rate of photoreceptor degeneration was measured in all four mutants by both ONL and TUNEL analysis. Paraffin sections were stained with H&E and the thickness of the ONL was compared to that of the INL, which does not degenerate. The thickness of the two nuclear layers was measured by the number of rows of nuclei. Age-matched wild-type animals were used as controls for each mutant.

The *rd1/rd1* mutants were analysed at set one-week periods up to the age of one month (**Figure 28**). At P7, the mutant was indistinguishable from the wild-type. Although the ONL in the wild-type and the mutant were identical, comprising 13 (s.d. 0.00) and 12.7 (s.d. 0.58) rows of nuclei respectively, there were no IS or OS yet developed in either. At 2 weeks of age, photoreceptor degeneration was markedly evident in the *rd1/rd1* mutants. Although in the wild-type samples the ONL remained at a thickness of 12.7 (s.d. 0.58) rows of nuclei, in the mutant the same layer was reduced to 2.3 (s.d. 0.58) rows. From this time-point onwards there was a significant difference between the ONL measurements in the mutant and wild-type samples ($p<0.001$; $n=5$). The degeneration in the mutant was complete by the third postnatal week. At no time-point was the thickness of the INL significantly different between the mutant and wild-type samples (p-values not significant).

In agreement with the ONL analyses, the TUNEL analyses for detection of apoptotic cells in *rd1/rd1* samples showed progressive degeneration of photoreceptor cells with age (**Figure 28**). At P7, both the wild-type and the mutant samples had a low percentage of apoptotic cells in the ONL with values at 3.3 % (s.d. 5.6) and 7% (s.d. 2.7), respectively, that were not significantly different from each other. At all later time-points, the percentage of TUNEL-positive cells in the wild-type was zero, but was significantly increased in the mutant samples (all $p<0.05$, $n=5$). A decrease observed in the percentage of

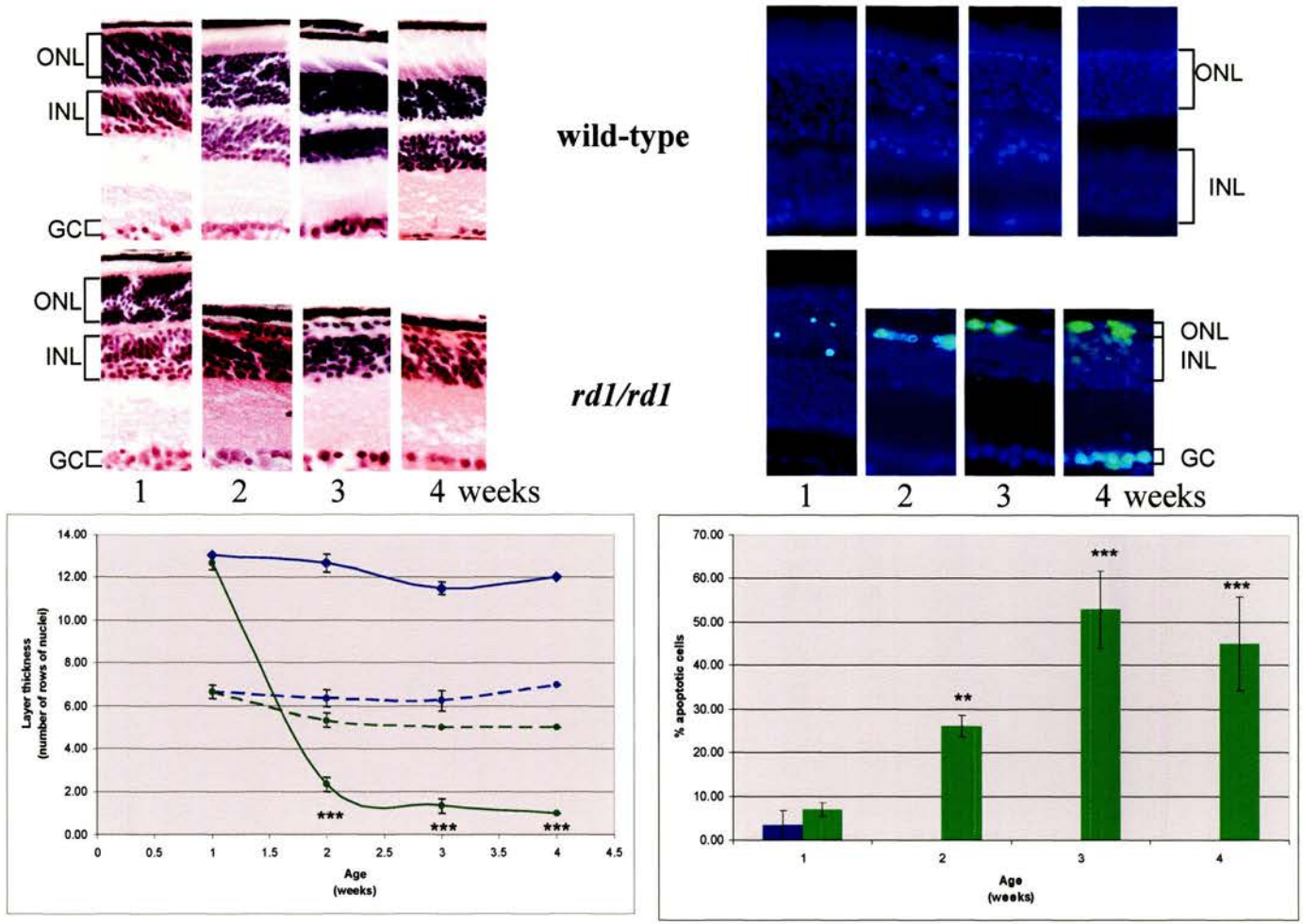

Figure 28: Photoreceptor degeneration in *rd1/rd1* mutants

ONL analysis (left panel) and TUNEL assays (right panel) were performed on paraffin-embedded eye sections from *rd1/rd1* mutants. A comparison was made between wild-type (blue) and *rd1/rd1* mutants (green). ONL analysis (ONL: solid lines, INL: dotted lines) revealed that in *rd1/rd1* mutants photoreceptor degeneration is complete by 3 weeks of age. Also, an increasing number of apoptotic cells was detected with age between 1 and 3 weeks.(** p<0.01, *** p<0.001) (ONL: outer nuclear layer; INL: inner nuclear layer; GC: ganglion cells)

TUNEL-positive cells at the last time-point, at 4 weeks of age, was not significantly different to the previous one at 3 weeks ($p>0.05$; $n=5$). It is also worth noting that in some of the oldest *rd1/rd1* samples, but in none of the wild-type, there were some nuclei in the INL, as well as some ganglion cells, that showed positive TUNEL staining.

The *atrd1/atrd1* mutant showed photoreceptor degeneration that was complete at 6 weeks of age (**Figure 29**). At the first time-point of analysis, at 2 postnatal weeks of age, the wild-type and the mutant samples had an identical mean ONL thickness at 12 rows of nuclei. Thereafter however, there was a change in the thickness of this layer in the mutant with increasing age, which was significantly reduced compared with wild-type at all time-points (all $p < 0.05$; $n=5$). The thickness of the INL remained relatively constant with time and was not significantly different between wild-type and mutant genotypes. At the last time-point, at 6 weeks of age, the thickness of the INL in the mutant was significantly lower than that of the wild-type ($p=0.02$; $n=5$), probably reflecting the extension of the disease phenotype (cell death) to other retinal layers.

TUNEL analysis on *atrd1/atrd1* samples showed comparable results to the ONL analysis (**Figure 29**). Firstly, even in the wild-type samples there was a small number of apoptotic cells within the first three weeks of age. However there was an increased number of apoptotic cells detected in the *atrd1/atrd1* mutants at the same time-points, but these were not significantly different from wild-type ($p>0.05$; $n=5$). This can be probably attributed to the large variation seen in the detection of TUNEL-positive cells in the controls. At 4 weeks of age however, the difference between the two genotypes was significant ($p<0.001$; $n=5$) with the mutant having more than 20% of its photoreceptor cells stained positive for TUNEL. This percentage decreased to about 10% at 6 weeks of age and remained significantly different from wild-type.

ONL analysis was also performed on samples of the $Rho^{-/-}$ mutant (**Figure 30**) at 1-month intervals, as it is known from published data that it takes about 3 months for degeneration to be complete in this mutant. Indeed, it was confirmed that the thickness of the ONL was noticeably reduced to about one-third of the normal by the second month of age and further decreased to a single row of photoreceptor nuclei by 3 months of age ($p<0.001$; $n=4$). It remained at this thickness when analysed at 6 months of age. The INL in mutant samples

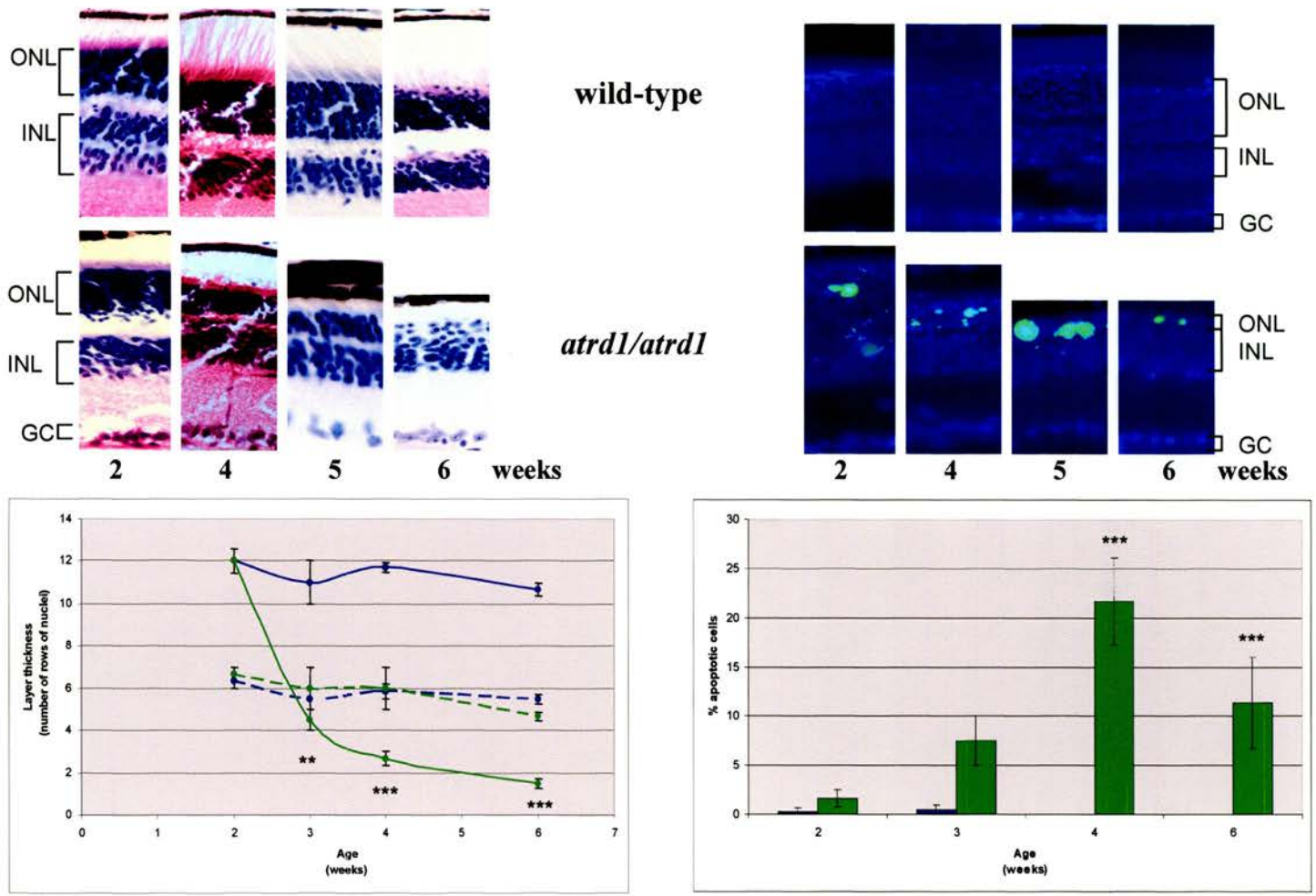

Figure 29: Photoreceptor degeneration in *atrd1/atrd1* mutants

ONL analysis (left panel) and TUNEL assays (right panel) were performed on paraffin-embedded eye sections from at*rd1/atrd1* mutants. A comparison was made between wild-type (blue) and at*rd1/atrd1* mutants (green). ONL analysis (ONL: solid lines, INL: dotted lines) revealed that in at*rd1/atrd1* mutants photoreceptor degeneration is complete by 6 weeks of age. An increasing number of apoptotic cells was detected up to the age of 4 weeks, but decreased sharply in the following time point of analysis .(** p<0.01, *** p<0.001) (ONL: outer nuclear layer; INL: inner nuclear layer; GC: ganglion cells)

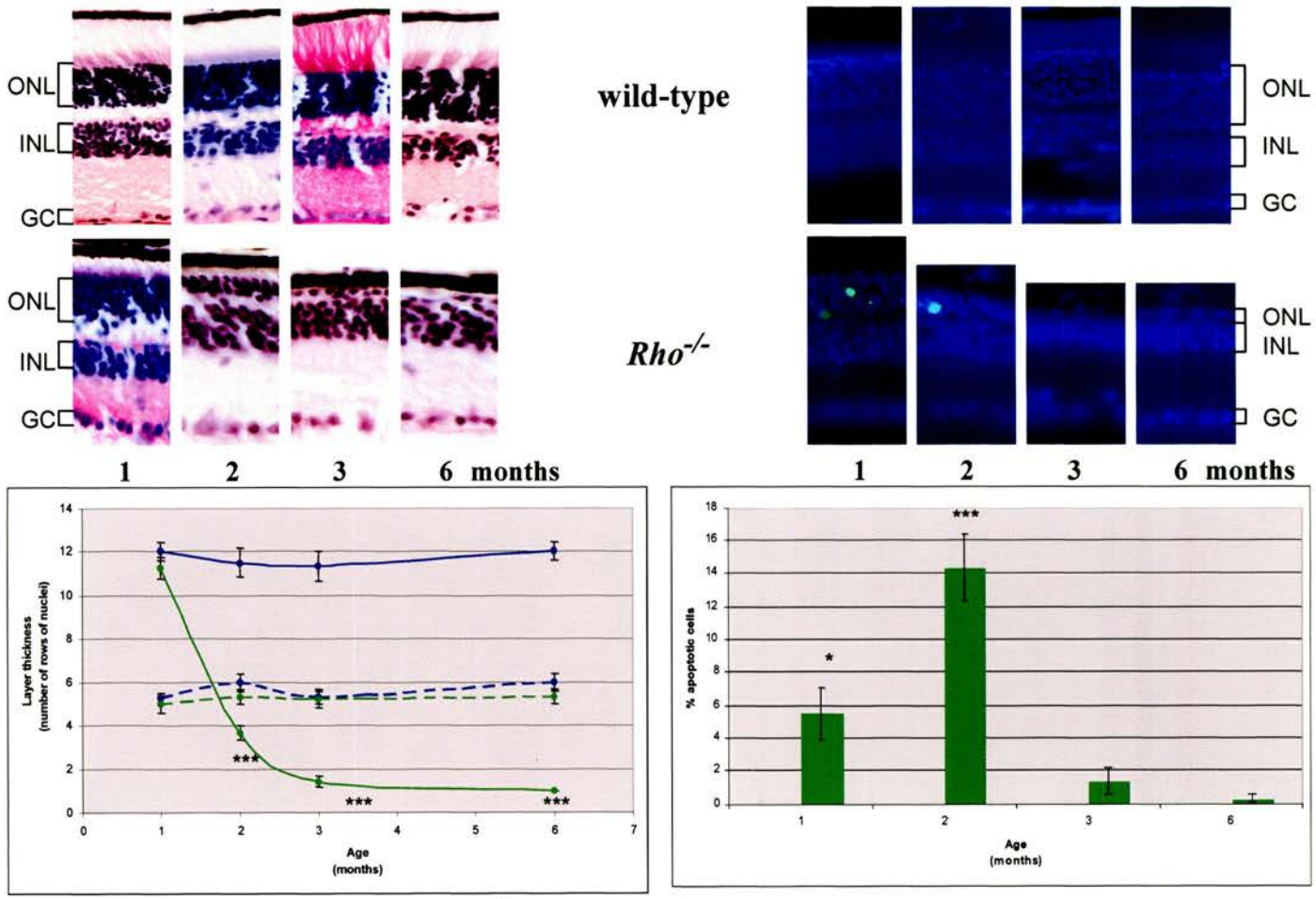

Figure 30: Photoreceptor degeneration in *Rho*$^{-/-}$ mutants

ONL analysis (left panel) and TUNEL assays (right panel) were performed on paraffin-embedded eye sections from *Rho*$^{-/-}$ mutants. A comparison was made between wild-type (blue) and *Rho*$^{-/-}$ mutants (green). ONL analysis (ONL: solid lines, INL: dotted lines) revealed that in *Rho*$^{-/-}$ mutants photoreceptor degeneration is complete by 3 months of age. An increasing number of apoptotic cells was detected up to the age of 2 months, but decreased sharply in the subsequent time point of analysis. .(* $p<0.05$, *** $p<0.001$) (ONL: outer nuclear layer; INL: inner nuclear layer; GC: ganglion cells)

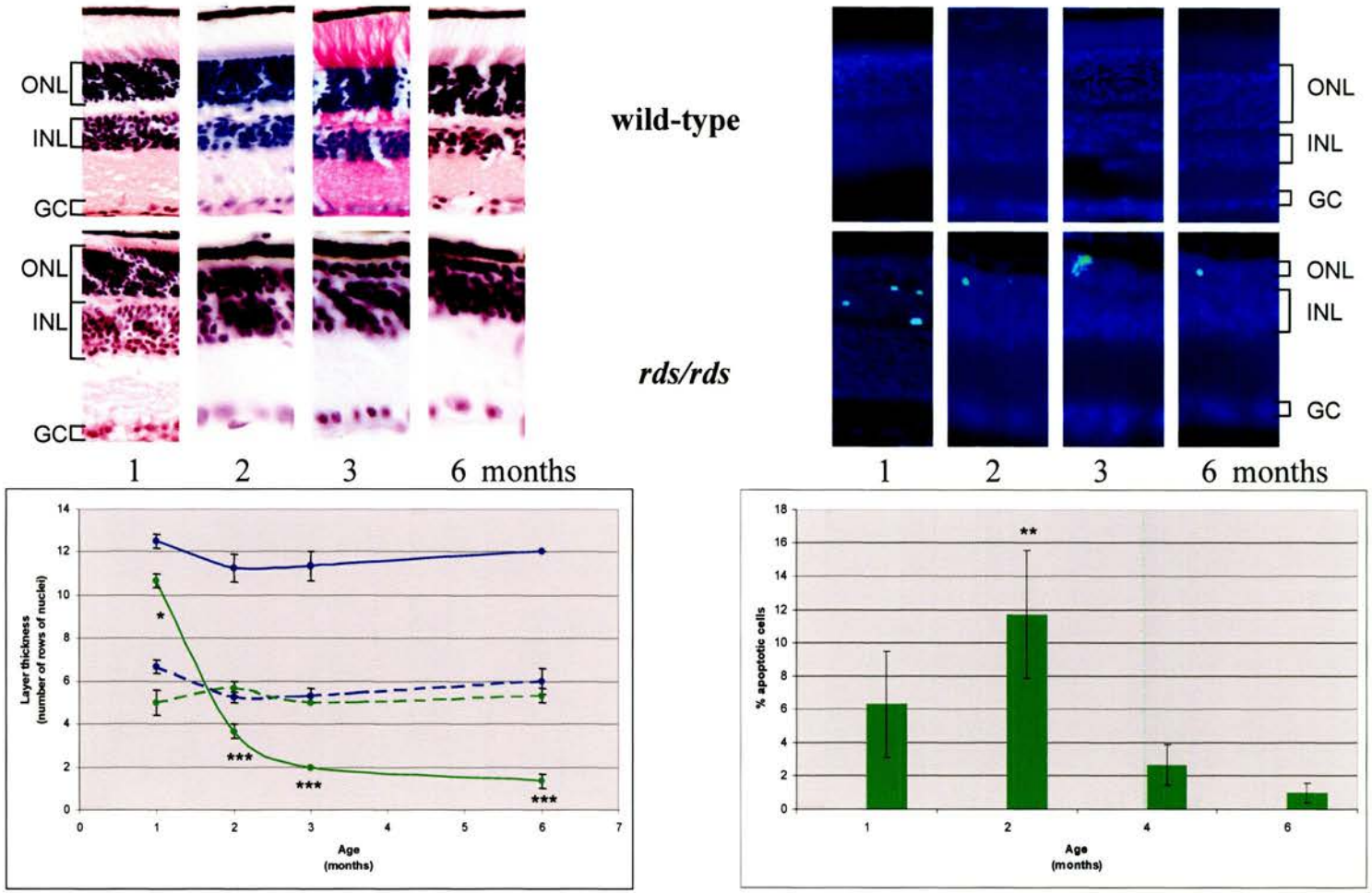

Figure 31: Photoreceptor degeneration in *rds/rds* mutants

ONL analysis (left panel) and TUNEL assays (right panel) were performed on paraffin-embedded eye sections from *rds/rds* mutants. A comparison was made between wild-type (blue) and *rds/rds* mutants (green). ONL analysis (ONL: solid lines, INL: dotted lines) revealed that in *rds/rds* mutants photoreceptor degeneration is complete by 3-4 months of age. An increasing number of apoptotic cells was detected up to the age of 2 months, but decreased sharply in the subsequent time point of analysis. .(* $p<0.05$, ** $p<0.01$, *** $p<0.001$) (ONL: outer nuclear layer; INL: inner nuclear layer; GC: ganglion cells)

was constant at about 5-6 rows of nuclei throughout the analysis and was never significantly different from control samples ($p>0.05$; n=4).

TUNEL analysis on *Rho*$^{-/-}$ samples was done at the same time-points as the ONL analysis (**Figure 30**). At no point did the wild-type samples show any signs of TUNEL-positive cells. In the mutants, there was an increased percentage of apoptotic cells detected within the first two months of retinal degeneration ($p=0.002$; n=4). Thereafter however, the percentage of cells that stained positively for TUNEL was not significantly different from control samples ($p>0.05$; n=4).

The final mutant to be analysed for photoreceptor degeneration was *rds/rds* (**Figure 31**). In contrast to the other mutants analysed above, this was the only one that had a significantly thinner ONL at the first time-point of the analysis (1 month), when compared to the wild-type ($p=0.01$; n=3). Initially, the decrease in ONL thickness in the mutant progressed rapidly, falling to about one-third of wild-type by the second month of age, and more slowly afterwards, until complete at 3-4 months of age. The INL in both genotypes remained at a stable thickness at each time-point.

The results from TUNEL analysis on *rds/rds* sections agreed well with those collected by ONL analysis of the same samples (**Figure 31**). There was an increasing number of apoptotic cells detected in the mutant at 1 month of age, but this was not significantly different from wild-type controls of the same age ($p>0.05$; n=3). Lack of significance was again due to the large variation seen between mutant samples analysed. At 2 months of age, in the mutant more than 10% of the ONL photoreceptor cells were TUNEL-positive, compared to none in wild-type ($p=0.03$; n=3). However both the percentage of detectable apoptotic cells and the significance were significantly reduced at subsequent time-points.

4.2.2. Photoreceptor markers in the retinal degeneration mutants

4.2.2.1. Immunohistochemical detection of rhodopsin

The expression level and localisation of rhodopsin (**Figure 32**) was assessed in retina sections from the four mutants. The efficiency of the anti-rhodopsin antibody was confirmed on adult wild-type sections, where it localises to the OS of rod photoreceptor cells.

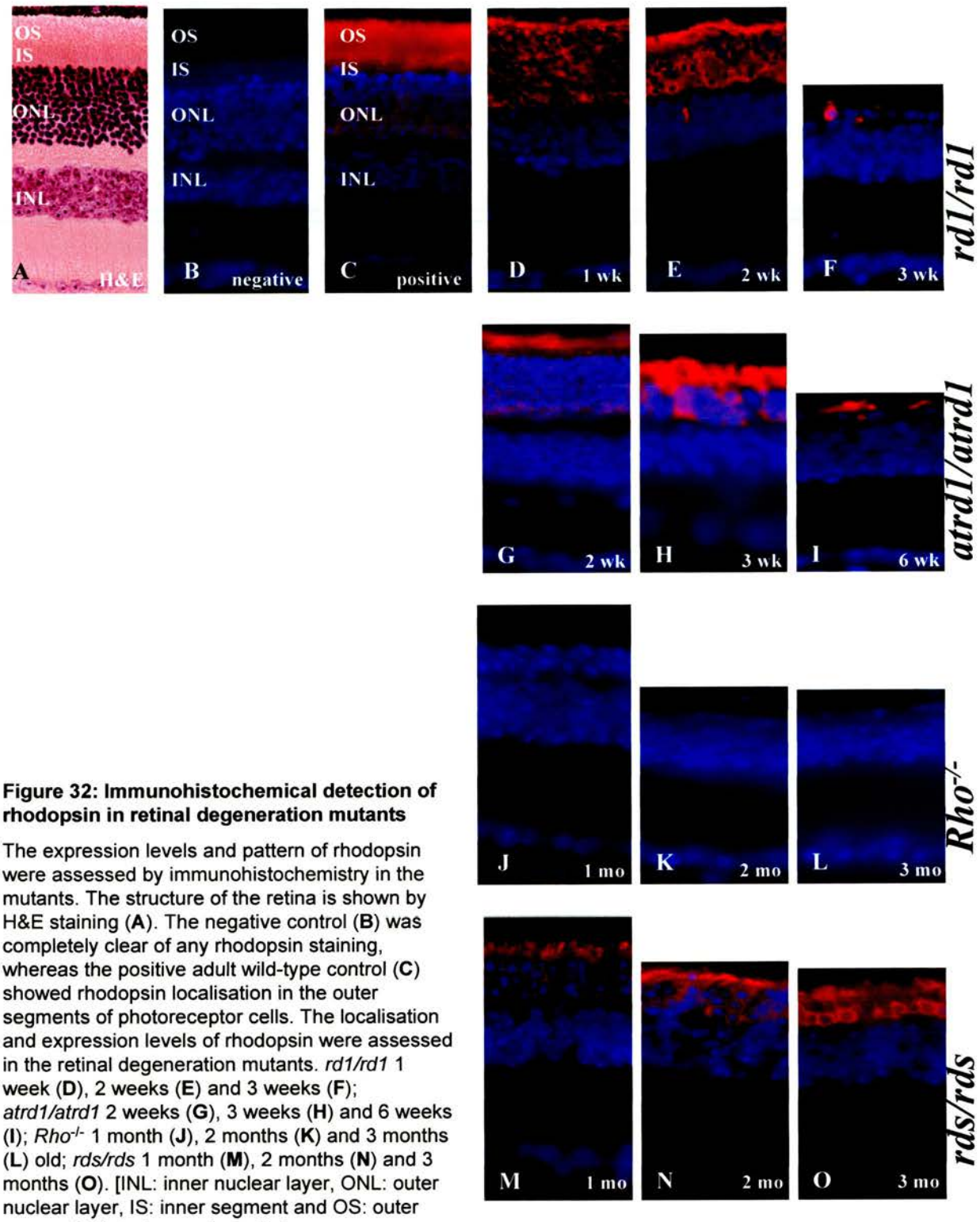

Figure 32: Immunohistochemical detection of rhodopsin in retinal degeneration mutants

The expression levels and pattern of rhodopsin were assessed by immunohistochemistry in the mutants. The structure of the retina is shown by H&E staining (**A**). The negative control (**B**) was completely clear of any rhodopsin staining, whereas the positive adult wild-type control (**C**) showed rhodopsin localisation in the outer segments of photoreceptor cells. The localisation and expression levels of rhodopsin were assessed in the retinal degeneration mutants. *rd1/rd1* 1 week (**D**), 2 weeks (**E**) and 3 weeks (**F**); *atrd1/atrd1* 2 weeks (**G**), 3 weeks (**H**) and 6 weeks (**I**); *Rho*$^{-/-}$ 1 month (**J**), 2 months (**K**) and 3 months (**L**) old; *rds/rds* 1 month (**M**), 2 months (**N**) and 3 months (**O**). [INL: inner nuclear layer, ONL: outer nuclear layer, IS: inner segment and OS: outer segment of photoreceptor cells]

In the 1-week old *rd1/rd1* mouse retina, when the OS and IS of photoreceptor cells have not yet formed, rhodopsin expression was localised at the ONL. One week later, when degeneration was already evident, the protein remained in the same layer, which was nevertheless reduced in thickness by that time. With the completion of photoreceptor degeneration, at 3 weeks of age, rhodopsin expression had disappeared.

In a 2-week old *atrd1/atrd1* mutant, rhodopsin seemed to be localised in the shortened OS of the photoreceptor cells. As in the case of the *rd1/rd1* mutant, with completion of the degeneration, rhodopsin expression in the *atrd1/atrd1* mutant was abolished.

Rhodopsin expression in the $Rho^{-/-}$ mutant was completely absent, consistent with the genotype of this rhodopsin null mouse.

Finally, in the *rds/rds* mutant, which fails to form any OS, rhodopsin was localised initially at the tips of the IS, in the area from where OS would normally protrude. As degeneration progressed, rhodopsin expression was evident in the ONL only, localising at the plasma membrane surrounding the remaining nuclei of the ONL.

4.2.2.2. Immunohistochemical detection of rod cGMP phosphodiesterase 6b

The efficiency of the anti-Pde6b antibody was confirmed on wild-type adult sections where it localised at the OS of photoreceptor cells (**Figure 33**). Faint staining was also seen in the inner plexiform layer.

The *rd1/rd1* mutant, before any evidence of degeneration at 1 week of age, the protein was localised where OS would potentially form. However, as soon as degeneration was evident at 2-3 weeks, Pde6b showed a non-specific pattern of expression spreading in all retinal layers. Faint localisation in the IPL was the only positive sign of this protein's expression at later stages.

A very similar pattern of Pde6β localisation was seen in the *atrd1/atrd1* mouse, which is also mutated in the *Pde6b* gene, but whose mutation lies in a different exon of this gene. It was initially found expressed apically of the ONL, but as soon as degeneration was markedly evident, the protein was localised in the IPL.

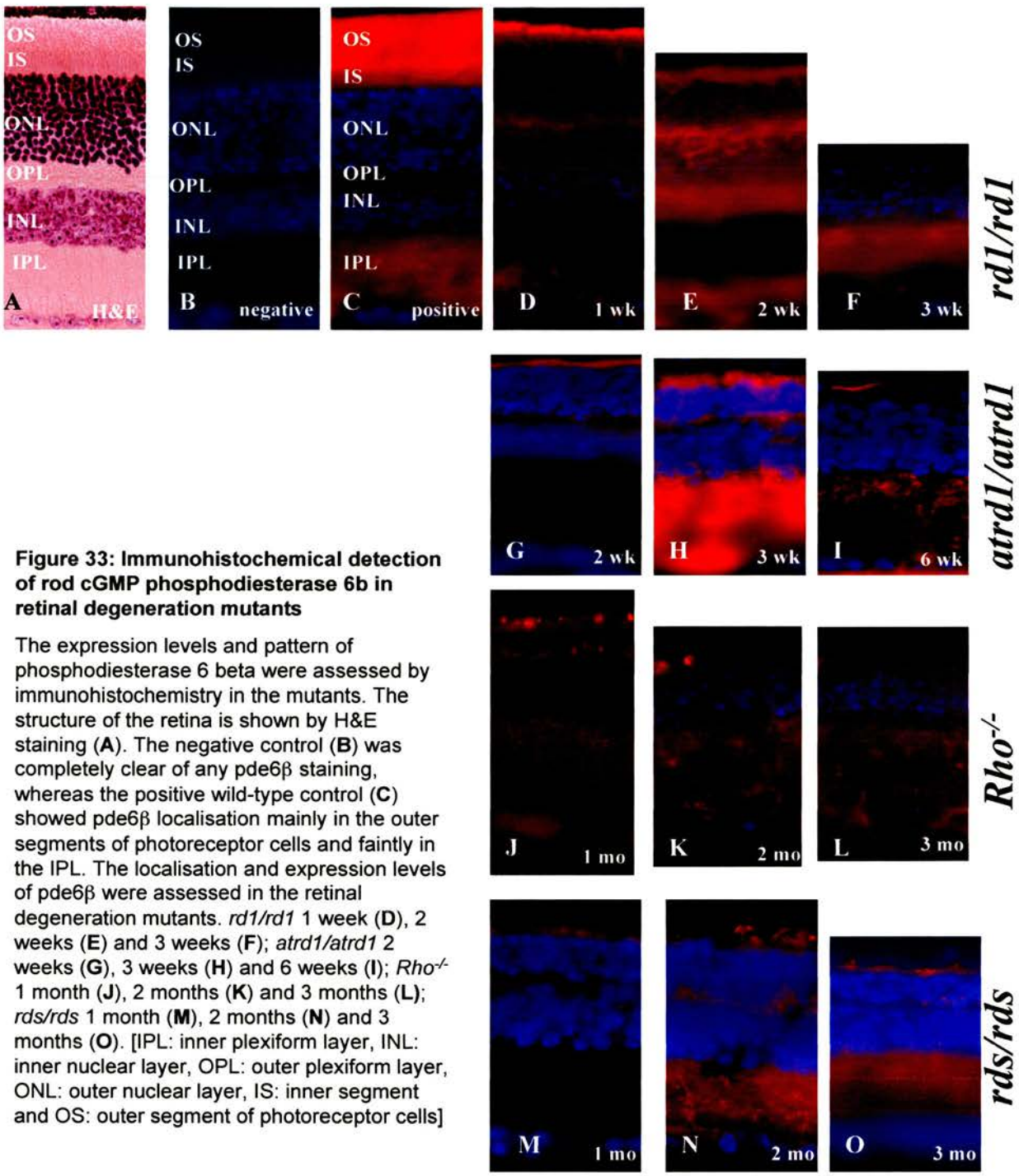

Figure 33: Immunohistochemical detection of rod cGMP phosphodiesterase 6b in retinal degeneration mutants

The expression levels and pattern of phosphodiesterase 6 beta were assessed by immunohistochemistry in the mutants. The structure of the retina is shown by H&E staining (**A**). The negative control (**B**) was completely clear of any pde6β staining, whereas the positive wild-type control (**C**) showed pde6β localisation mainly in the outer segments of photoreceptor cells and faintly in the IPL. The localisation and expression levels of pde6β were assessed in the retinal degeneration mutants. *rd1/rd1* 1 week (**D**), 2 weeks (**E**) and 3 weeks (**F**); *atrd1/atrd1* 2 weeks (**G**), 3 weeks (**H**) and 6 weeks (**I**); *Rho*$^{-/-}$ 1 month (**J**), 2 months (**K**) and 3 months (**L**); *rds/rds* 1 month (**M**), 2 months (**N**) and 3 months (**O**). [IPL: inner plexiform layer, INL: inner nuclear layer, OPL: outer plexiform layer, ONL: outer nuclear layer, IS: inner segment and OS: outer segment of photoreceptor cells]

In the *Rho*$^{-/-}$ mutant, Pde6b staining was low from an early age, and was effectively absent by completion of photoreceptor degeneration.

Finally, in the *rds/rds* mutant retina, which fails to form outer segments, Pde6β was again expressed at a very low level and was found mainly in the IPL

4.2.3. Complex I and citrate synthase enzyme activities in wild-type and retinal degeneration mutants

The specific activities of the mitochondrial enzymes citrate synthase (CS) and complex I (CI) were measured spectrophotometrically. Liver, brain, heart and retina samples were collected from each of the retinal degeneration mutants and assayed as described in the Materials & Methods (**section 2.6.1**.). The samples collection was performed before progressed photoreceptor degeneration, to ensure presence of the cells of interest. Therefore, the 'fast' strains (rd1/rd1 and atrd1/atrd1) were assayed at 1 week of age, whereas the 'medium' strains were assayed at 1 month of age. They were compared to wild-type samples. (**Table 6, Figure 34**).

In the wild-type liver, the activity of CS was 1.6949 μmol/min/g tissue and none of the mutants showed citrate synthase activity significantly different from the wild-type in this tissue (all $p>0.05$; n=3-5). The CI activity in the wild-type liver was significantly lower than that of CS at 0.5969 μmol/min/g tissue ($p=0.0073$; n=4). The activity of CI in the liver samples from all the mutants remained at levels similar to wild-type (all $p>0.05$; n=3-5).

In brain samples, the results were comparable to those obtained in liver samples, in terms of unchanged enzyme activities in the mutants compared to the wild-type control. In brain samples, however, the specific activity of CS was consistently higher than in liver samples, within the range of 4-6 μmol/min/g tissue. The specific activity of CI in the same brain samples was lower than in the liver, ranging from 0.24 to 0.38 μmol /min/g tissue. As in the case of the liver, none of the enzymes showed decreased activity in any of the mutants compared to the wild-type (all $p>0.05$; n=3-5).

The specific activity of CS in the heart samples was considerably higher than in liver or brain, ranging from 14 to 27 μmol/min/g tissue. The results

LIVER							
		Citrate Synthase			Complex I		
Strain	**n**	**activity**	**se**	**p_w-value**	**activity**	**se**	**p_w-value**
Wild type	4	1.6949	0.1893		0.5969	0.2011	
rd1/rd1	4	2.4467	0.4353	0.1644	0.4743	0.0779	0.5904
atrd1/atrd1	5	1.7838	0.4554	0.8744	0.4807	0.0564	0.5559
Rho$^{-/-}$	4	2.3787	0.3408	0.1300	0.3215	0.1168	0.2812
rds/rds	3	2.3260	0.3538	0.1499	0.4796	0.1843	0.6964
BRAIN							
		Citrate Synthase			Complex I		
Strain	**n**	**activity**	**se**	**p_w-value**	**activity**	**se**	**p_w-value**
Wild type	5	3.7515	0.7808		0.2444	0.0518	
rd1/rd1	4	5.3456	0.4538	0.1446	0.3236	0.0522	0.3235
atrd1/atrd1	4	4.3842	0.9078	0.6118	0.3758	0.0211	0.0704
Rho$^{-/-}$	3	4.0025	0.2766	0.8208	0.3001	0.0613	0.5236
rds/rds	3	6.0147	0.6241	0.0935	0.3430	0.0513	0.2564
HEART							
		Citrate Synthase			Complex I		
Strain	**n**	**activity**	**se**	**p_w-value**	**activity**	**se**	**p_w-value**
Wild type	4	13.9632	2.3818		1.8227	0.3594	
rd1/rd1	3	27.5270	6.5664	0.0794	1.3934	0.0998	0.3672
atrd1/atrd1	3	18.0613	5.9593	0.5063	1.3424	0.3161	0.3815
Rho$^{-/-}$	3	15.4951	5.4382	0.7862	2.5000	0.0325	0.1728
rds/rds	3	14.3333	3.2423	0.9283	3.2235	0.8895	0.1631
RETINA							
		Citrate Synthase			Complex I		
Strain	**n**	**activity**	**se**	**p_w-value**	**activity**	**se**	**p_w-value**
Wild type	6	1.1066	0.1144		0.7248	0.1651	
rd1/rd1	6	1.0074	0.2115	0.6885	0.1541	0.0370	**0.0071**
atrd1/atrd1	4	1.3502	0.3817	0.4865	0.1969	0.0630	**0.0377**
Rho$^{-/-}$	6	0.8719	0.0632	0.1028	0.1058	0.0087	**0.0038**
rds/rds	3	0.8983	0.1653	0.3309	0.0991	0.0107	**0.0361**

Table 6: Enzyme activities in wild-type and retinal degeneration mutants

Citrate synthase and complex I activities (μmol/min/g tissue) were measured in liver, brain, heart and retina from wild-type and retinal degeneration mutants (*rd1/rd1, atrd1/atrd1, Rho*$^{-/-}$ and *rds/rds*). The standard errors (se) and statistical significance compared with wild-type (p_w-value) are shown. Statistical significant values p_w <0.05 are highlighted in red.

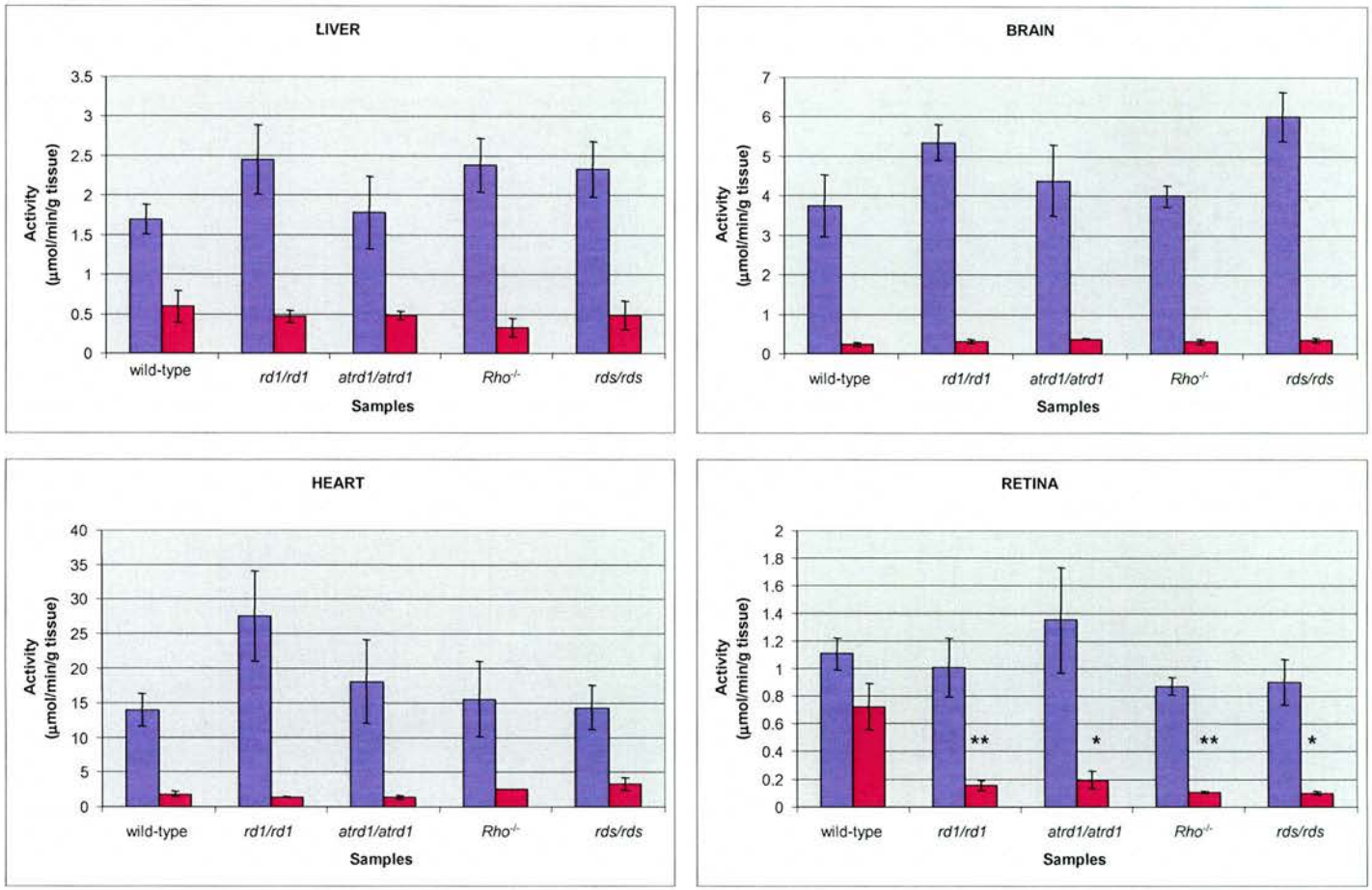

Figure 34: Enzyme activities of citrate synthase and complex I in mouse tissues from wild-type and retinal degeneration mutants

The activities of citrate synthase (blue columns) and complex I (maroon columns) were measured spectrophotometrically in the liver, brain, heart and retina of wild-type and retinal degeneration mutants. In all four mutants, the activity of citrate synthase remained at wild-type levels. Complex I activity remained similar to wild-type levels in the liver, brain and heart samples of all the mutants. It was however significantly decreased in the retinas of all four retinal degeneration mutants (all $p<0.05$), reflecting oxidative damage in this tissue.(* $p<0.05$, ** $p<0.01$ compared with wild-type)

showed no significant difference in activity between controls and mutants. The activity of CI in heart samples was higher than that measured in other tissues, ranging from 1.3 to 3.2 μmol/min/g tissue. No significant differences were recorded in CI activity of heart between control and mutant samples ($p>0.05$; n=3-4).

The CS activity measured in the wild-type retina was similar to that in the liver, at 1.1 μmol/min/g tissue. In the mutants, it ranged from 0.9 to 1.4 μmol/min/g tissue, and was similar to the control ($p>0.05$; n=3-6). In the wild-type retina, the specific activity of CI was similar to that in liver, at 0.7 μmol/min/g tissue. It was however significantly reduced in the retinas from all four mutants (all $p<0.05$; n=3-6).

4.2.4. Reduced glutathione (GSH) measurements in wild-type and retinal degeneration mutants

Reduced glutathione (GSH) concentrations were measured in the liver, brain, heart and retina of wild-type animals and retinal degeneration mutants (**Table 7**, **Figure 35**). In the wild-type liver the GSH measured was 4.2 μmol/g protein. GSH concentrations were not significantly different from wild-type in liver samples from all four mutants, ranging from 3.6 to 5.2 μmol/g protein (all $p>0.05$; n=3). The GSH concentration in the wild-type brain samples was much lower than liver, at about 1 μmol/g protein. In the *rd1/rd1*, *atrd1/atrd1* and *Rho*$^{-/-}$ mutants, the GSH concentration remained the same as wild-type, within a range of 1.2 to 1.4 μmol/g protein (all $p>0.05$; n=3). In the brain samples of *rds/rds* mutants GSH levels were significantly greater than wild-type, at 2.1 μmol/g protein ($p=0.04$; n=3). The GSH content was even lower in the wild-type heart, compared to both liver and brain samples of the same genotype. In wild-type heart the GSH concentration was 0.7 μmol/g protein. GSH concentrations were significantly reduced in the *rd1/rd1* and *atrd1/atrd1* mutants ($p=0.044$ and $p=0.048$, respectively; n=3), but not in the *Rho*$^{-/-}$ or *rds/rds* mutants ($p>0.05$; n=3). Finally, the GSH concentration of wild-type retina samples was the lowest of all four tissues analysed, at 0.08 μmol/g protein. This was significantly reduced to about half of this value in the retinas

LIVER				
Genotype	**n**	**concentration**	**se**	**p_w-value**
Wild type	3	4.2027	0.1542	
rd1/rd1	3	3.8625	0.7369	0.7752
atrd1/atrd1	3	3.5817	0.1700	0.2250
Rho$^{-/-}$	3	5.1527	0.1507	0.0758
rds/rds	3	4.2940	0.0485	0.8157
BRAIN				
Genotype	**n**	**concentration**	**se**	**p_w-value**
Wild type	3	0.9631	0.1082	
rd1/rd1	3	1.3998	0.0433	0.1586
atrd1/atrd1	3	1.3015	0.0751	0.3598
Rho$^{-/-}$	3	1.1672	0.0314	0.4683
rds/rds	3	2.1092	0.2360	**0.0437**
HEART				
Genotype	**n**	**concentration**	**se**	**p_w-value**
Wild type	3	0.6642	0.0619	
rd1/rd1	3	0.2579	0.0274	**0.0440**
atrd1/atrd1	3	0.3288	0.0273	**0.0480**
Rho$^{-/-}$	3	0.4714	0.0718	0.3324
rds/rds	3	0.9538	0.1623	0.3439
RETINA				
Genotype	**n**	**concentration**	**se**	**p_w-value**
Wild type	3	0.0841	0.0052	
rd1/rd1	3	0.0430	0.0029	**0.0253**
atrd1/atrd1	3	0.0747	0.0125	0.6852
Rho$^{-/-}$	3	0.0411	0.0023	**0.0235**
rds/rds	3	0.0778	0.0046	0.6741

Table 7: Reduced glutathione (GSH) concentrations in wild-type and retinal degeneration mutants

Reduced glutathione concentrations (μmol/g protein) were measured in liver, brain, heart and retina from wild-type and retinal degeneration mutants (*rd1/rd1, atrd1/atrd1, Rho*$^{-/-}$ and *rds/rds*). The standard errors (se) and statistical significance compared with wild-type (p_w-value) are shown. Statistical significant values (p_w<0.05) are highlighted in red.

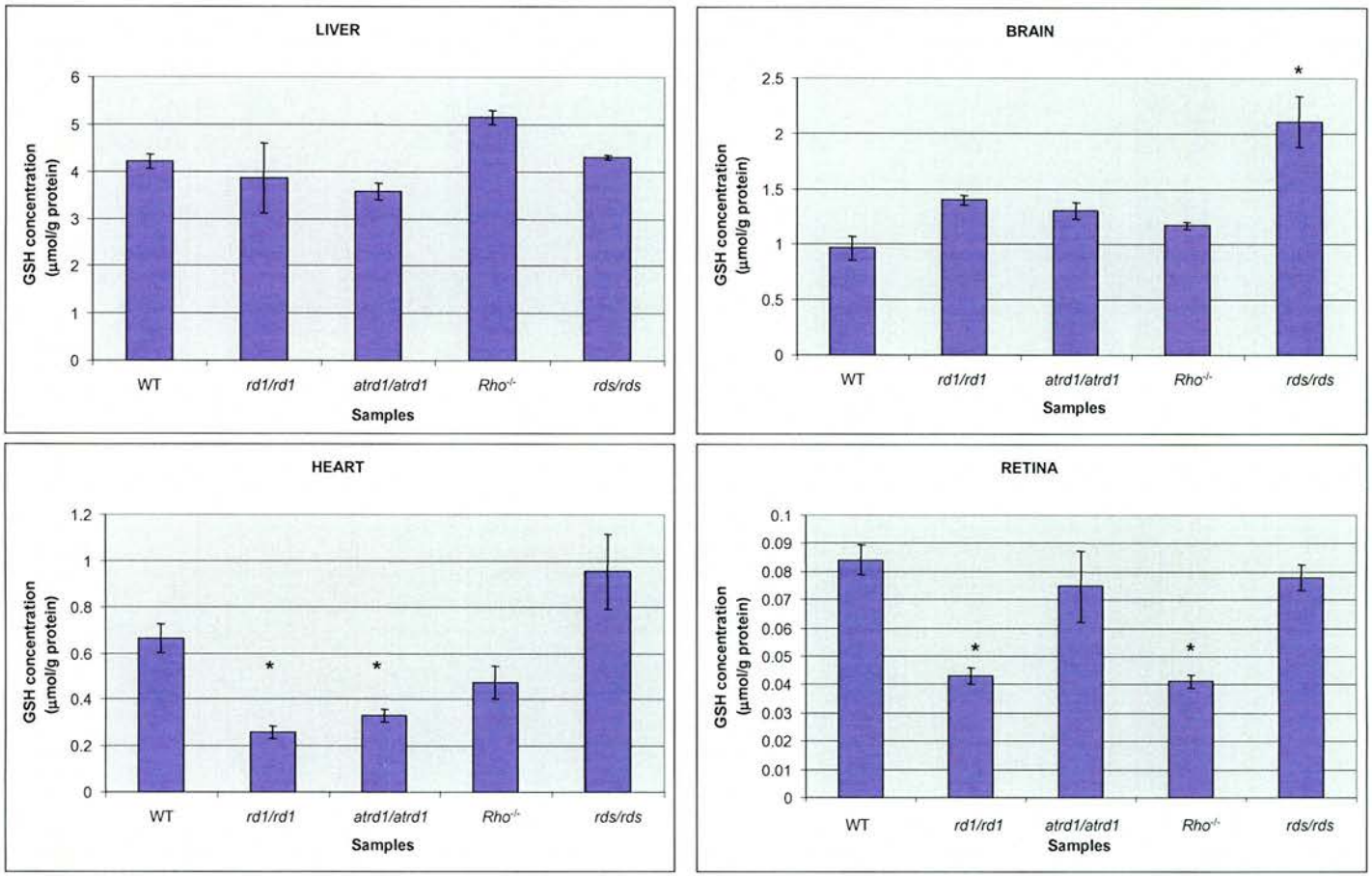

Figure 35: Reduced glutathione (GSH) concentrations in mouse tissues from wild-type and retinal degeneration mutants

GSH concentrations were measured in the liver, brain, heart and retina of wild-type and retinal degeneration (*rd1/rd1*, *atrd1/atrd1*, *Rho*$^{-/-}$, *rds/rds*) mutants.(* $p<0.05$)

of *rd1/rd1* (p=0.03; n=3) and the *Rho*$^{-/-}$ (p=0.02; n=3) mutants, but remained at wild-type concentrations in the *atrd1/atrd1* and *rds/rds* mutants.

4.3. Summary and Conclusions

In this chapter the rates of photoreceptor degeneration in four different retinal degeneration mutants were investigated. Photoreceptor degeneration in the *rd1/rd1*, *atrd1/atrd1*, *Rho*$^{-/-}$ and *rds/rds* mutants was estimated to be complete by 3 weeks, 6 weeks, 3 months and 3 months of age respectively. These results are compatible with previous reports (Portera-Cailliau *et al.*, 1994; Humphries *et al.*, 1997; Hart *et al.*, 2005; Lohr *et al.*, 2006). The results from TUNEL assays for the detection of apoptotic photoreceptor cells were also in good agreement with previously published data. In the *rd1/rd1* mutant, the number of TUNEL-positive cells has been reported to be low until P12 and then to peak at P14 (Portera-Cailliau *et al.*, 2004; Lohr *et al.*, 2006). In our analysis, the peak of apoptosis was delayed to P21, although there was a highly significant increase in apoptotic cells at about P14 and P28. The detection of apoptotic cells in *Rho*$^{-/-}$ mutants has been shown to peak at P24 (Hobson *et al.*, 2000), which was a week later than observed in this study. Finally, although positive TUNEL staining in *rds/rds* mutants has been shown to peak at P18 and P60 (Portera-Cailliau *et al.*, 1994; Lohr *et al.*, 2006), only a single peak at P14 was detected here. There have been no published reports on the detection of apoptotic cells in the *atrd1/atrd1* mutant, which peaks later (4 weeks) than in *rd1/rd1* (3 weeks), consistent with the slower rate of ONL loss. The discrepancies in TUNEL staining between published data and the data collected in this project could be explained by the fact that the time-points of analysis in this project were not very frequent. The authors in some published reports monitored photoreceptor degeneration daily, whereas in this project, sample collection for analysis was performed at weekly or monthly intervals. Also, it is worth noting that the genetic backgrounds of the mutants analyzed in the published reports are the same to the ones analyzed in this project. Therefore, the discrepancies cannot be attributed to genetic background differences.

In this analysis, the percentage of TUNEL-positive cells present in the mutant retinas depended on the rate at which the retina degenerates. In a 3-week old *rd1/rd1* mutant retina, more than 50% of the remaining photoreceptor cells

were apoptotic. The maximum detected percentage of apoptotic cells in the *atrd1/atrd1* mutant was 20% at 4 weeks of age. Finally, in the case of both the *Rho*$^{-/-}$ and *rds/rds* mutants, the highest percentage of TUNEL-positive cells was just above 10%. This apparent inverse relationship between the number of apoptotic cells and the rate of degeneration raises an issue of timing. It is not known how long it takes between DNA cleavage –which is detected by the TUNEL assay- and disappearance of the apoptotic photoreceptor cell from the retina. In the fast degenerating mutants, namely *rd1/rd1* and *atrd1/atrd1*, samples were assayed weekly, whereas this was done on a monthly basis for the *Rho*$^{-/-}$ and *rds/rds* mutants. Consequently, this could imply that, by the time apoptosis was assayed in these mutants, many apoptotic photoreceptor cells may have disappeared. However, in the case of the faster mutants, the tight time-points of analysis may have allowed the detection of more apoptotic cells than the 'slower' mutants.

Another interesting observation in the TUNEL assay results was the detection of apoptotic cells in additional retinal layers. Although the disease phenotype of RP is known to primarily involve the degeneration of photoreceptor cells, positive TUNEL staining was also observed in the ganglion cell layer of 4-week-old *rd1/rd1* samples. This agrees with previous reports demonstrating that, during photoreceptor degeneration, other cell types may make chemical adjustments as a result of the loss of photoreceptor cells. Consequently, in advanced stages of the disease, structural changes may involve all retinal cell types (Sanyal *et al.,* 1980).

The expression patterns of rhodopsin and rod cGMP phosphodiesterase have previously been analysed in some of the mutants studied in this project. Rhodopsin plays an important role in phototransduction and is often used as a marker for photoreceptor OS. Therefore it was expected that altered rhodopsin expression would be present in the retinal degeneration mutants in which the photoreceptors degenerate. Although immunohistochemical detection of rhodopsin was not performed on 1 or 2-week old wild-type retinas, it is known that rhodopsin is expressed in the tissue at P5 (Tartelin *et al.*, 2003). In a wild-type retina, at P7, rhodopsin is localised at an irregular array of membraneous structures, at P11, although it is present over the entire retina surface, it is considerably increased in outer segment disks and by P14, rhodopsin is

uniformely expressed at OS (Jansen *et al.*, 1987). As expected, rhodopsin expression was completely abolished in the *Rho*$^{-/-}$ mutant, but some was evident in the remaining mutants. At the first time-point of analysis at 1 week of age, before the formation of OS, rhodopsin expression in *rd1/rd1* mutants was localised at the ONL. It is not surprising that the protein was localised there because the OS, where it would normally localise, were not formed yet. At 2 weeks however, when photoreceptor OS should have started to be formed and degeneration in this mutant was evident, rhodopsin remained at the ONL. At the final time-point of analysis, rhodopsin expression was abolished in the *rd1/rd1* mutant, consistent with completion of degeneration. In the *atrd1/atrd1* mutant, at the first time-point of analysis at 2 weeks of age, rhodopsin was mainly localised at the OS, which were not fully differentiated. At 3 weeks, rhodopsin was found solely in the ONL, possibly due to the degeneration of photoreceptor cells. As it would have been expected due to progressed degeneration, rhodopsin expression was almost absent in the 6-week-old *atrd1/atrd1* mutant. Finally, in the *rds/rds* mutant, which fails to form OS, the rhodopsin localisation observed was consistent with previous work by Jansen *et al.* (1987) and later by Nir *et al.* (1990). Jansen et al. (1987) reported that in the *rds/rds* mutant, before the onset of degeneration, rhodopsin expression was evident in the ciliary protrusions, as in the wild-type retina. At the onset of degeneration, however, some photoreceptor cells had small membrane-bound vesicles that were rhodopsin-positive. Similarly, Nir *et al.* (1990) initially detected rhodopsin in vesicular membrane profiles and membrane whorls that appeared at the distal tip of the cilium, probably reflecting failure to form OS. In older retinas, the same authors detected the hishest labelling density for rhodopsin along the plasma membrane that surrounds nuclei.

The expression of Pde6b was also immunohistochemically detected in retinal degeneration mutants (**Figure 33**). The suitability of the antibody used was assessed on adult wild-type samples, in which Pde6b was localised mainly at the photoreceptor OS and faintly at the OPL and IPL. Although the localisation of Pde6b was not assessed on age-matched wild-type controls, it was not surprising that in the *rd1/rd1* mutants it was localised in the area where photoreceptor OS would potentially form. As soon as photoreceptor degeneration was evident however, Pde6β expression in the *rd1/rd1* mutant was more prominent in inner

retinal layers (like IPL and OPL) and was abolished upon completion of the degeneration. At the first (2 weeks) and last (6 weeks) time-points of analysis of the *atrd1/atrd1* mutant, Pde6b expression was very faint and unspecific, consistent with the genotype of this mutant. In **Figure 33H**, the increased expression of Pde6b observed in the IPL was probably an experimental artefact. This cannot be interpreted as mislocalisation of the protein because, firstly, at the previous and subsequent time-points its expression was comparatively low, and, secondly, mislocalisation should be confined in photoreceptor cells, in which Pde6b is normally localised, and not in a different type of cells where it is not expressed. In the *Rho*$^{-/-}$ mutant, the expression of Pde6b was very faint compared to the adult wild-type and, as expected, remained at this low level as degeneration progressed. Finally, in the 1-month-old *rds/rds* mutant, Pde6b expression was faint compared to the adult wild-type and localised where OS would potentially form. In subsequent time-points however, expression was more prominent in inner retinal layers. Although, even in the wild-type retina there was faint Pde6b expression at the IPL, the increased signal observed at the IPL of 2 and 3-month-old *rds/rds* mutant was considered an artefact, rather than mislocalisation.

The four retinal degeneration mutants studied in this project were also analysed for signs of oxidative damage. The specific activity of the oxidative stress-sensitive complex I (CI) was spectrophotometrically measured in liver, brain, heart and retina samples, using the activity of the oxidative stress-insensitive citrate synthase (CS) as an internal control.

Indeed, the CS activity was at wild-type levels in all the samples, irrespective of genotype. The activity of CI remained at normal levels in all the liver, brain and heart samples, but was significantly reduced in the retina samples collected from each retinal degeneration mutant. These results indicate that there is increased oxidative damage in the retinas of these mutants as a consequence of the specific mutations. Signs of oxidative stress have been previously reported in the *rd1/rd1* and *rds/rds* mutants by Lohr *et al.* (2006), who found increased expression of the oxidative stress markers ceruloplasmin and clusterin, accompanying the degeneration. However, thist is the first time that oxidative damage has been reported in the *atrd1/atrd1* and *Rho*$^{-/-}$ mutants, since a decrease in the specific activity of CI is a marker of oxidative stress.

The oxidative status of different tissues was also assessed by measuring the concentration of GSH, which serves as an indicator of oxidative stress. In wild-type liver, brain, heart and retina, the GSH concentrations were 4.2, 1, 0.6 and 0.1 μmol/g protein. The GSH concentration in the mouse retina has not been previously reported, but information on liver, brain and heart is available. For example, van Remmen *et al.* (1999) reported that the GSH concentration in wild-type liver, brain and heart are at a 12:1.5:1 ratio, which is in line with the findings of this project. In the retinal degeneration mutants, the GSH concentrations remained at wild-type levels in most samples. They were however significantly increased in *rds/rds* brain ($p=0.04$; $n=3$), decreased in *rd1/rd1* and *atrd1/atrd1* heart (both $p=0.04$; $n=3$), and decreased in *rd1/rd1* ($p=0.3$; $n=3$) and $Rho^{-/-}$ retina ($p=0.02$; $n=3$) samples. It is not clear why differences were detected in tissues other than the retina, since the mutated genes in these mice are specifically expressed in the retina and the degeneration is confined to this tissue. The decreased GSH concentrations however in the *rd1/rd1* and $Rho^{-/-}$ retinas may also indicate increased oxidative stress in retina.

Various papers have reported the involvement of oxidative stress in neurodegenerative diseases, including some involving a retinal phenotype. In a paper by Travis *et al.* (1991), the authors suggest that a possible mechanism explaining photoreceptor degeneration in the *rds/rds* mutant is the increased oxygen tension to which the cells are imposed, due to the lack of OS. If increased oxygen availability in the cell increases the production of its harmful ROS by-products, then this could explain the observed results. Outer segments do not develop in any of the retinal degeneration mutants analyzed in this chapter, and this could therefore provide a unifying explanation for the observed results.

Other explanations are possible, such as calcium overload in the *Pde6b* mutants. As discussed by Hussain *et al.* (1992), the compromised activity of Pde6b in *rd1/rd1* and *atrd1/atrd1* mutants results in increased concentration of free cGMP in the photoreceptor OS, greater dark current and consequently increased intracellular Ca^{2+} concentration. An increase in Ca^{2+} intracellular levels has been shown to act as a trigger for cell death (Olshevskaya *et al.*, 2004) and high outer segment Ca^{2+} concentration has also been implicated as a causal factor in apoptosis in other retinal degenerations (Yuan *et al.*, 2003, Fain 2006).

Additionally, Ca^{2+} can affect the activity of cGMP phosphodiesterase and rhodopsin and potentially influence the sensitivity of rod photoreceptor cells (Hussain *et al.*, 1992).

Finally, photoreceptor degeneration in *Rho*$^{-/-}$ mutants is possibly attributed to both the functional and structural role of rhodopsin in the retina. Liang *et al.* (2004) set out to understand how the lower expression of rhodopsin affects the structure and physiology of photoreceptor cells in *Rho*$^{+/-}$ heterozygotes and reported lower Rho density, OS of decreased size and accelerated electrophysiological responses in these mutants. These authors proposed that the electrophysiological differences between wild-type and *Rho*$^{+/-}$ heterozygotes were due to changes in the volume of the OS and concomitant changes in cation homeostasis, including that of calcium. The smaller volume of OS would accelerate the cellular fluxes of Ca^{2+}, and as in the case of the *Pde6b* mutants, Ca^{2+} overload could account for photoreceptor degeneration in *Rho* mutants, both homozygous and heterozygous. Another possibility, also suggested by Liang *et al.* (2004) is the altered expression of critical genes involved in ion homeostasis. Therefore, photoreceptor degenertion in *Rho*$^{-/-}$ mutants could be attributed to a combination of structural changes, altered cation exchanges and gene expression levels.

In summary, retinal degeneration was complete within a few weeks or months, in all the mouse mutants analysed in this chapter. Although they were each mutated in functionally different genes, signs of oxidative damage to the retina were detected in each mutant. However, these results do not necessarily imply that oxidative stress is a primary factor in these retinal degenerations. Although oxidative stress has been shown to be a primary cause of cell death in other neurodegenerative disorders like Alzheimer's and Parkinson's (Ninomura *et al.*, 1999; Kim *et al.* 2002), its presence in the retinal degeneration mutants analysed here might be independent to the photoreceptor degeneration observed. Additional work including analysis with more markers of oxidative stress, to elucidate the exact nature of oxidative stress in mutated retinas, and experimental modification of the levels of oxidative stress to alter rates of degeneration, would be beneficial.

CHAPTER 5

PHENOTYPIC ANALYSIS OF RETINAL DEGENERATION MUTANTS CROSSED TO SOD*2* HETEROZYGOTES

5.1. Introduction

In this chapter, the role of oxidative stress in photoreceptor degeneration is investigated by genetically modifying the levels of Sod2 in the retinal degeneration mutants. The *rd1/rd1*, *atrd1/atrd1* and *Rho*$^{-/-}$ mutants were crossed to *Sod2*$^{+/-}$ heterozygous mice and double mutants were generated. The genotypes of the animals analysed were *rd1/rd1 Sod2*$^{+/-}$, *atrd1/atrd1 Sod2*$^{+/-}$ and *Rho*$^{-/-}$ *Sod2*$^{+/-}$. The *rds/rds* mutant was not crossed to the *Sod2* mutant as the *Prph2* locus is closely linked to *Sod2* (~10 cM) on mouse chromosome 17. In this chapter, the genotype of *Sod2*$^{+/-}$ mutants was initially confirmed and their retinal phenotype was analysed, by both ONL and TUNEL analysis. The rates of retinal degeneration in the double mutants were measured by the same methods and comparisons were made with age-matched wild-type and single retinal degeneration mutants. In addition, the effect of decreased *Sod2* expression on the activities of citrate synthase (CS) and complex I (CI), as well as on retinal reduced glutathione (GSH) concentrations, were assessed in liver, brain, heart and retina samples from the mutants.

5.2. Results

5.2.1. Confirming the genotype of *Sod2*$^{+/-}$ mutants

Different methods were used to confirm the decreased levels of Sod2 enzyme in the *Sod2*$^{+/-}$ mice. Western blots were performed on protein samples prepared from retinas of mutant and wild-type animals (**Figure 36A-D**). Although the level of Sod1, the cytosolic isoform of superoxide dismutase, remained the same in the two genotypes, the level of Sod2 was markedly decreased in the heterozygote, consistent with the expected 50% reduction in *Sod2*$^{+/-}$ mutants.

Additionally, immunohistochemistry for Sod1 and Sod2 was performed on frozen eye sections from wild-type and mutant animals (**Figure 36E-I**). Sod1 was most strongly expressed in the OS of photoreceptor cells and its level remained the same in the two genotypes. Sod2, however, was strongly expressed in the IS of photoreceptor cells, as well as in the IPL and OPL. Sod2 expression was decreased in the heterozygous *Sod2*$^{+/-}$ samples, when compared to the wild-type controls.

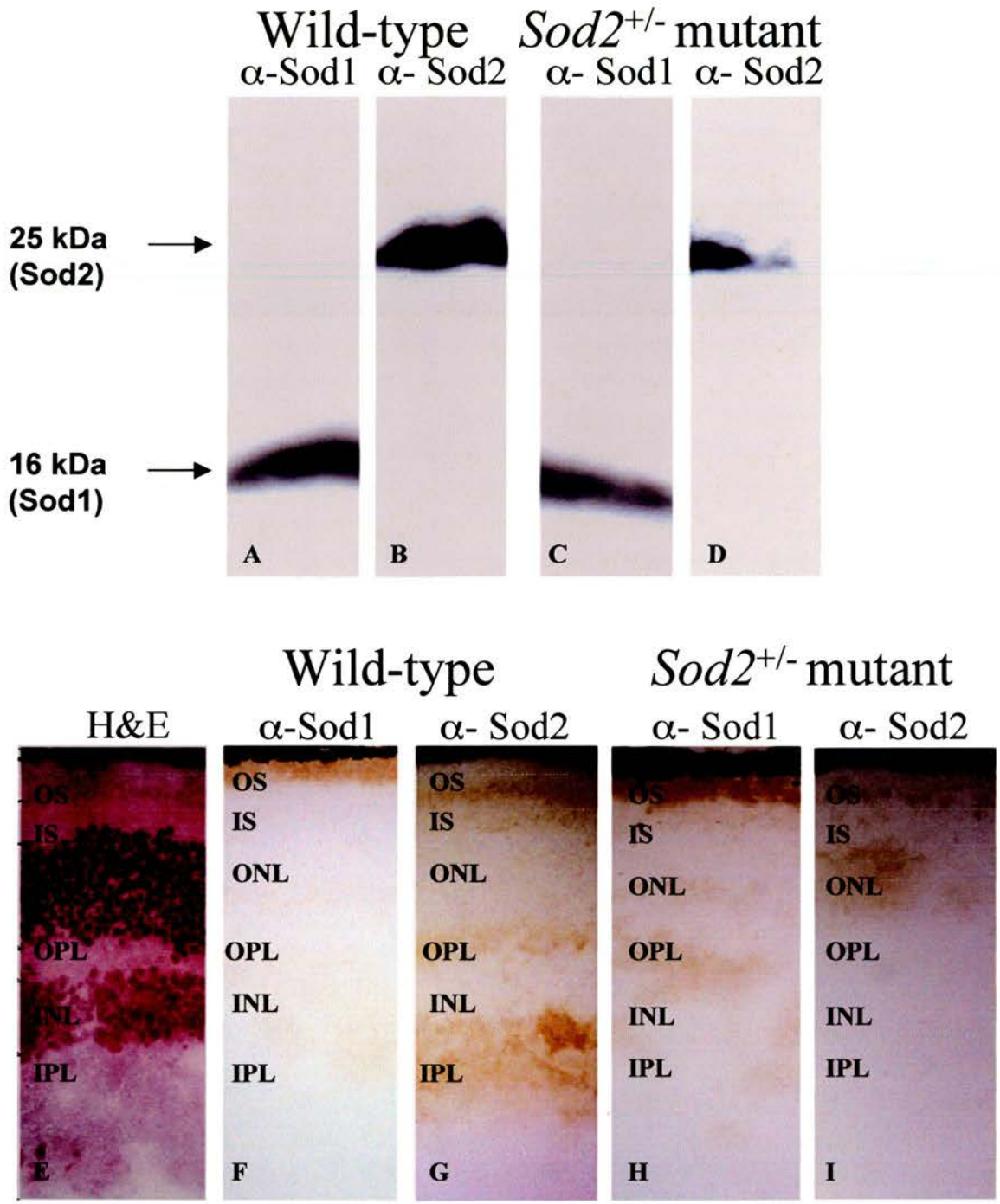

Figure 36: Confirming the genotype of *Sod2*$^{+/-}$ heterozygous mice

The decreased Sod2 content of *Sod2*$^{+/-}$ mutant retinas was confirmed by using anti-Sod1 (α-Sod1) and anti Sod2 (α-Sod2) antibodies separately in Western blotting (**A-D**) and by immunohistochemistry (**E-I**). The level of Sod1 was the same in the wild-type (**A**) and *Sod2*$^{+/-}$ mutant (**C**) whereas that of Sod2 was decreased in the mutant (**D**) in comparison to the wild-type (**B**). However, lack of a loading control in this experiment demands confirmation of the result. Immunohistochemistry for Sod1 and Sod2 on frozen eye sections from wild-type (Sod1, **F**; Sod2, **G**) and mutant (Sod1, **H**; Sod2, **I**) mice also confirmed decreased levels of Sod2 in the heterozygous sample [IPL: inner plexiform layer, INL: inner nuclear layer, OPL: outer plexiform layer, ONL: outer nuclear layer, IS: inner segment and OS: outer segment of photoreceptor cells]

5.2.2. Phenotypic analysis of *Sod2*$^{+/-}$ mouse eyes

5.2.2.1. Photoreceptor degeneration analysis

ONL analysis and TUNEL analysis were performed on paraffin-embedded sections of eyes from *Sod2*$^{+/-}$ mice to assess the degree of retinal degeneration in these mutants. Samples were collected at set time intervals of two months until one year of age.

No retinal degeneration was evident in the *Sod2*$^{+/-}$ mutant by ONL analysis (**Figure 37A**). The mean thickness of the ONL across all time-points remained unchanged in the mutants, as did that of the INL, at 11.07 (s.d. 0.64) and 5.54 (s.d. 0.52) nuclei thick, respectively (**Figure 37B**). The corresponding values for the wild-type animals were 11.11 (s.d. 0.76) for the ONL and 5.63 (s.d. 0.4) for the INL. No degeneration of either nuclear layer was noted in either genotype up to one year of age (**Figure 37C**), as the thickness of both the ONL and INL was not significantly different between the first and last time-points of the analysis.

TUNEL analysis was performed for the detection of apoptotic cells in the retina of *Sod2*$^{+/-}$ animals. In agreement with the results from the ONL analysis, no TUNEL-positive cells were detected at any age (**Figure 38**), confirming the lack of a retinal degeneration phenotype in *Sod2*$^{+/-}$ animals up to one year of age.

5.2.2.2. Markers for photoreceptor cells

Paraffin-embedded eye sections from *Sod2*$^{+/-}$ mice were subjected to immunohistochemistry using different markers of photoreceptor cells. The staining patterns for rhodopsin and rod cGMP phosphodiesterase (Pde6b) were assessed in the *Sod2*$^{+/-}$ mutants and compared to wild-type samples of the same age (**Figure 39**). Rhodopsin was successfully localised in the OS of rod photoreceptor cells and was unaltered by the age or genotype of the samples analysed. Similarly, the antibody against Pde6b stained the same retinal layers in both the wild-type and mutant samples, namely the OS of rod photoreceptor cells and the two plexiform layers.

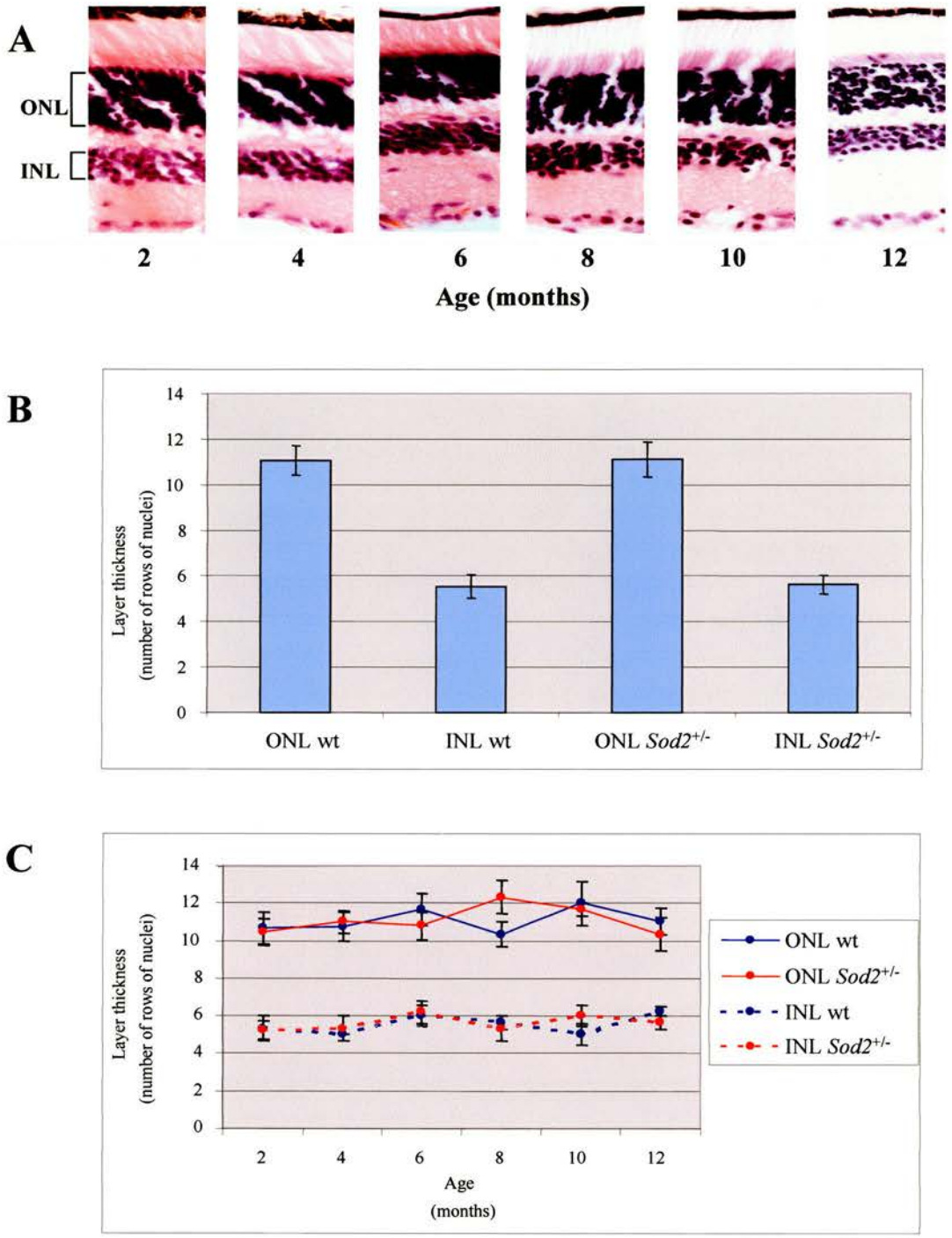

Figure 37: Outer nuclear layer (ONL) analysis of *Sod2*$^{+/}$ heterozygous mice

Paraffin-embedded eye sections from *Sod2*$^{+/-}$ mutants were stained with H&E for histology evaluation and ONL analysis. Samples were collected every two months for one year. (**A**) The histology of the *Sod2*$^{+/-}$ eyes remained very good throughout the first year. (**B**) The mean thickness of the outer and inner nuclear layers across all time-points remained unchanged, irrespective of genotype. (**C**) ONL analysis showed no degeneration of photoreceptor cells with time.

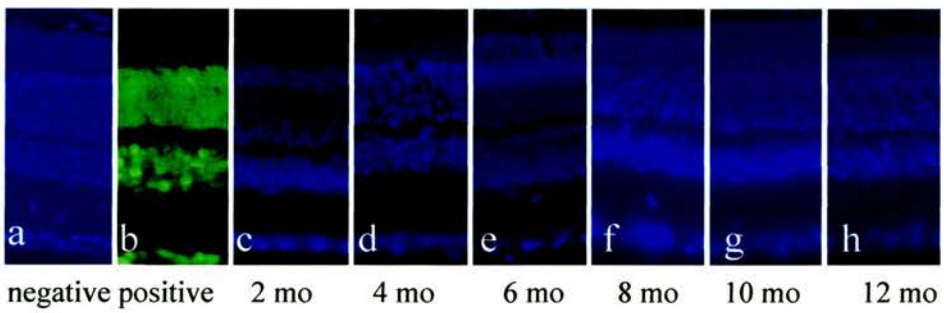

Figure 38: TUNEL analysis of *Sod2*$^{+/-}$ mutants

TUNEL assays on paraffin-embedded eye sections from *Sod2*$^{+/-}$ mutant mice. No TUNEL-positive apoptotic cells were detected in the negative control (a) but all nuclei were TUNEL-positivie in the positive control (b). No apoptotic photoreceptor cells were detected in the Sod2+/- heterozygote samples (**c**, 2; **d**, 4; **e**, 6; f, 8; **g**, 10; **h**, 12 months old)

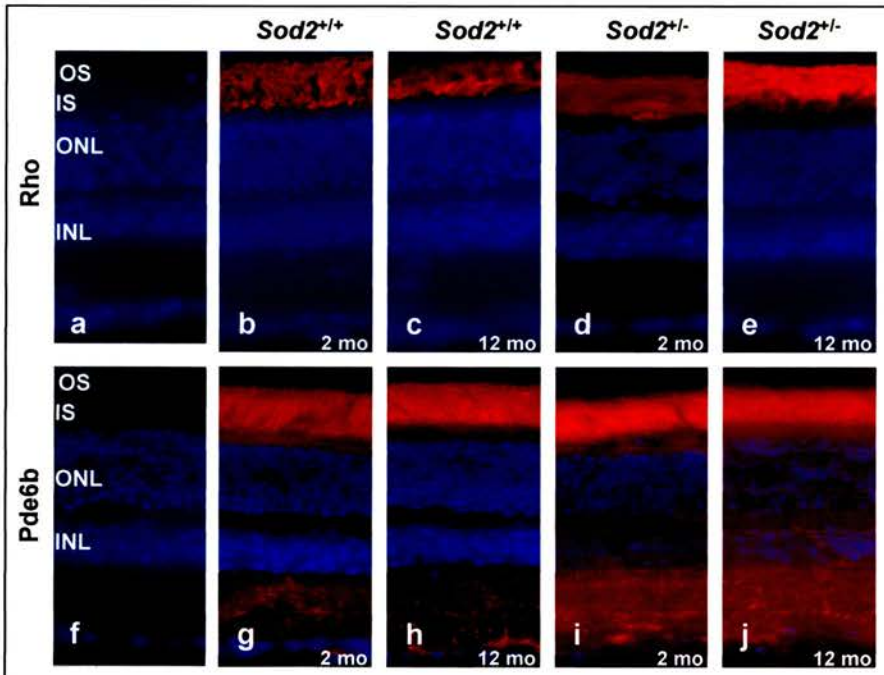

Figure 39: Photoreceptor markers in *Sod2*$^{+/-}$ mutants

Immunohistochemistry for rhodopsin (Rho) (**a-e**) and rod cGMP phosphodiesterase 6 β subunit (Pde6b) (**f-j**) on paraffin-embedded eye sections from wild-type (**b, c, g, h**) and *Sod2*$^{+/-}$ heterozygous (**d, e, i, j**) mice. Samples were collected at 2 (**b, d, g, i**) or 12 (**c, e, h, j**) months of age. The negative controls for the antibodies are shown (**a, f**).

5.2.3. Effect of the *Sod2*$^{+/-}$ genetic background on degeneration rates of retinal degeneration mutants

As previously shown, in the *rd1/rd1* mutants, retinal degeneration is completed by 3 weeks of age. ONL analysis showed that there was no significant difference in the rate of photoreceptor degeneration between the single *rd1/rd1* and double *rd1/rd1 Sod2*$^{+/-}$ mutants, in both of which cell loss was completed by postnatal week 3 (**Figure 40**). At no time-point of the analysis was there a significant difference in the thickness of either the ONL or the INL, between the two genotypically different mutants.

In agreement with the ONL analysis results, TUNEL assays showed an increasing number of apoptotic cells in the mutants compared to wild-type controls. The results were similar whether Sod2 was fully or partially expressed (**Figure 40**). At all time-points when samples were analyzed the percentage of TUNEL-positive cells was comparable between the two groups. The TUNEL staining previously observed in retinal layers in older *rd1/rd1* mutants, was also observed on a *Sod2*$^{+/-}$ background.

Similar to the *rd1/rd1* mutants, decreased levels of Sod2 in the *atrd1/atrd1* mutants had no effect on the rate of photoreceptor degeneration (**Figure 41**). All nuclei were lost from the ONL of double *atrd1/atrd1 Sod2*$^{+/-}$ mutants within 6 weeks of age. The ONL and INL thicknesses remained almost identical between the single and double mutants.

Similar to the ONL analysis, TUNEL-positive cells were increasingly detectable with time in the *atrd1/atrd1 Sod2*$^{+/-}$ double mutants (**Figure 41**). At no point in the analysis were the double mutants significantly different from the single retinal degeneration mutants, in terms of the percentage of TUNEL positive cells.

In *Rho*$^{-/-}$ mice, it takes significantly longer for photoreceptor degeneration to be completed, namely 3 months. Crossing these mutants to *Sod2*$^{+/-}$ mice and ONL analysis, revealed that the course of photoreceptor degeneration did not change in response to decreased Sod2 levels (**Figure 42**). All photoreceptor cells were lost by three months of age and the rate at which

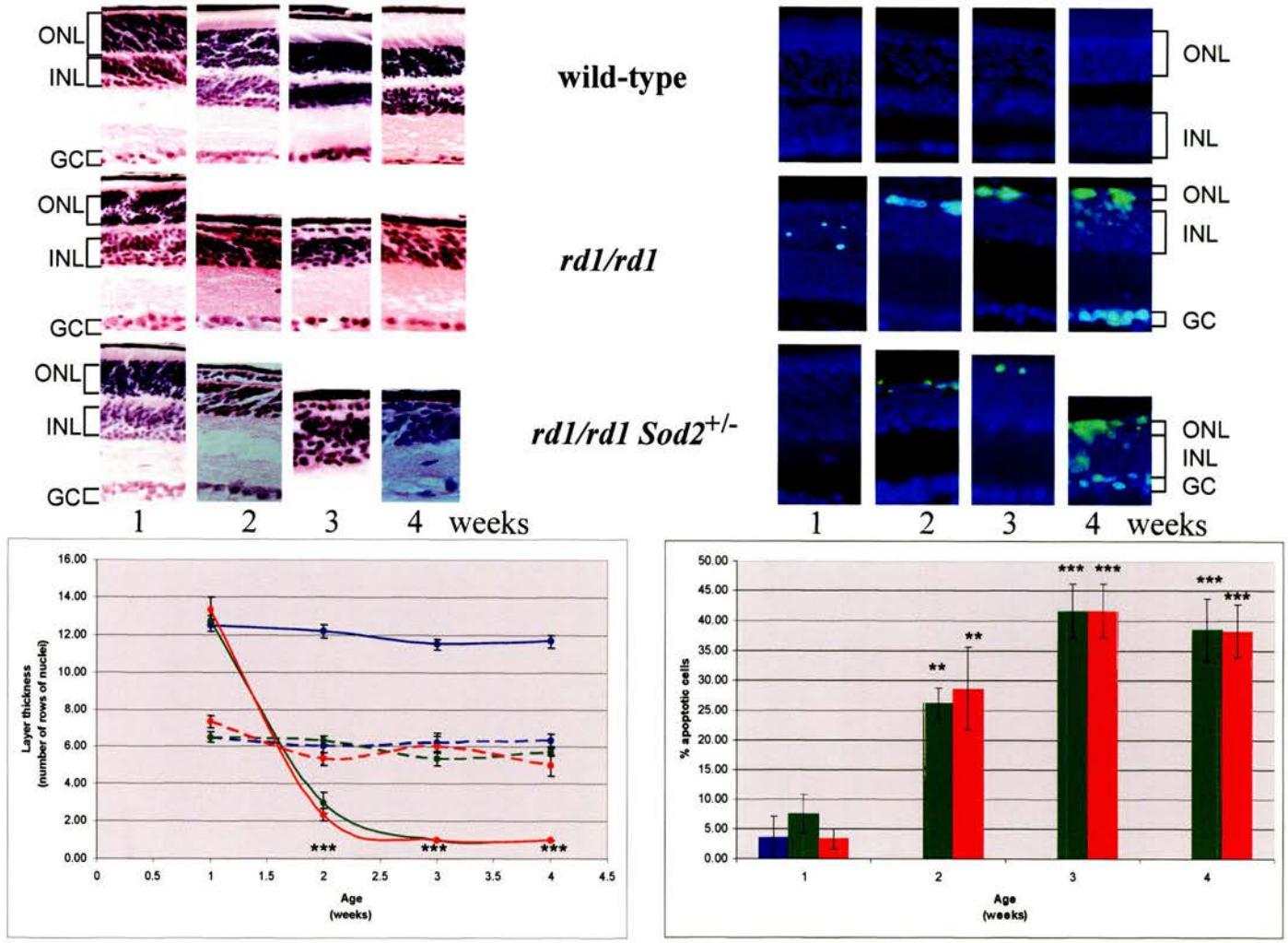

Figure 40: Photoreceptor degeneration in *rd1/rd1 Sod2*$^{+/-}$ double mutants

ONL analysis (left panel) and TUNEL assays (right panel) were performed on paraffin-embedded eye sections from *rd1/rd1 Sod2*$^{+/-}$ mutants. A comparison was made between wild-type (blue) and *rd1/rd1* mutants (green) and *rd1/rd1 Sod2*$^{+/-}$ double mutants (red). ONL analysis (ONL: solid lines, INL: dotted lines) revealed that in *rd1/rd1* mutants photoreceptor degeneration is complete by 3 weeks of age, irrespective of *Sod2* expression. The decreased Sod2 levels did not affect the number of apoptotic cells detected either.(* $p<0.05$, ** $p<0.01$, *** $p<0.001$ compared to wild-type) (ONL: outer nuclear layer; INL: inner nuclear layer; GC: ganglion cells)

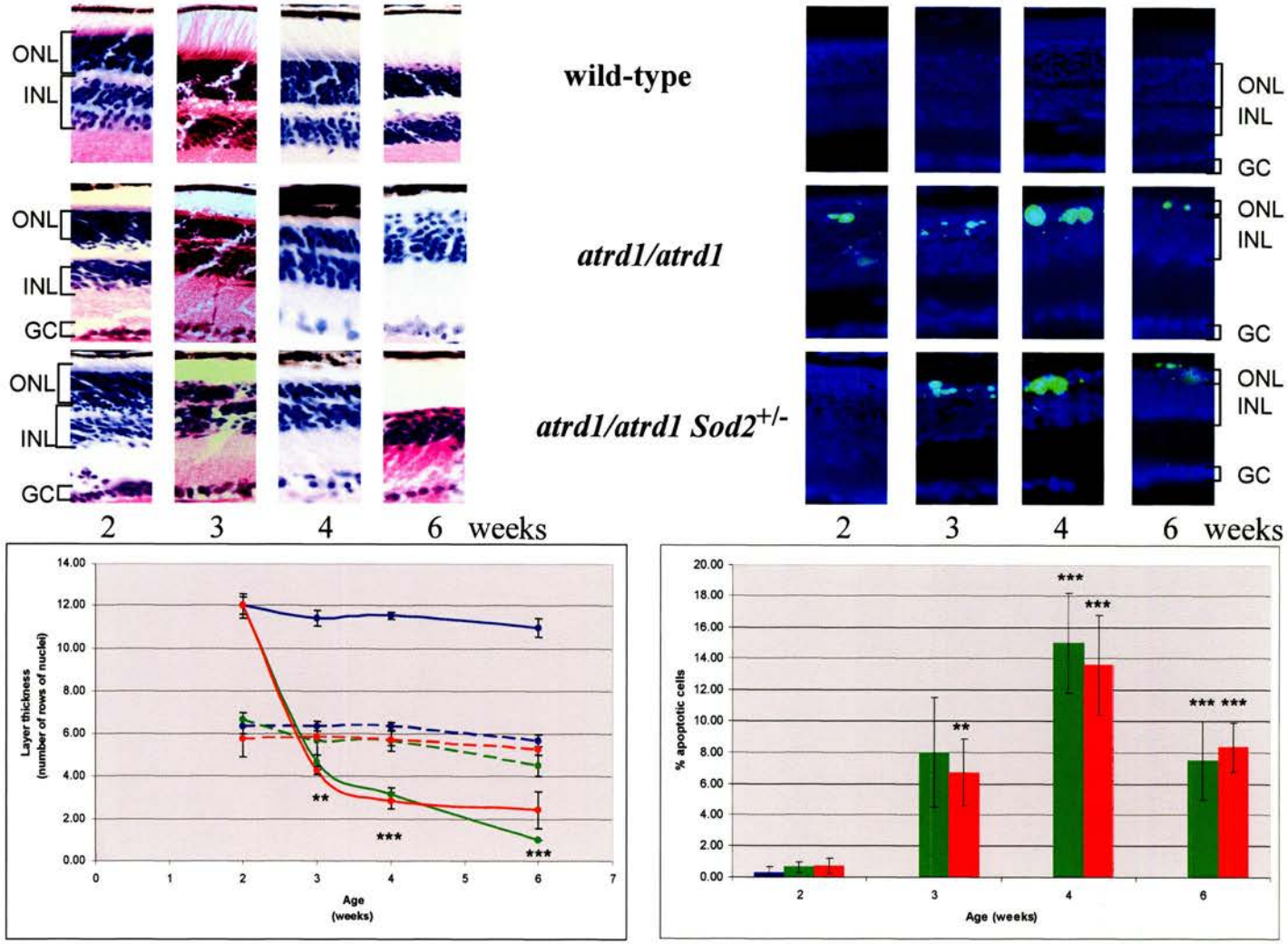

Figure 41: Photoreceptor degeneration in a*trd1/atrd1 Sod2*$^{+/-}$ double mutants

ONL analysis (left panel) and TUNEL assays (right panel) were performed on paraffin-embedded eye sections from a*trd1/atrd1 Sod2*$^{+/-}$ mutants. A comparison was made between wild-type (blue), a*trd1/atrd1* mutants (green) and a*trd1/atrd1 Sod2*+/- double mutants (red). ONL analysis (ONL: solid lines, INL: dotted lines) showed that in a*trd1/atrd1* mutants photoreceptor degeneration was complete by 6 weeks of age, irrespective of *Sod2* expression. The decreased Sod2 levels did not affect the number of apoptotic cells detected in single or double mutants. (* p<0.05, ** p<0.01, *** p<0.001 compared with wild-type) (ONL: outer nuclear layer; INL: inner nuclear layer; GC: ganglion cells)

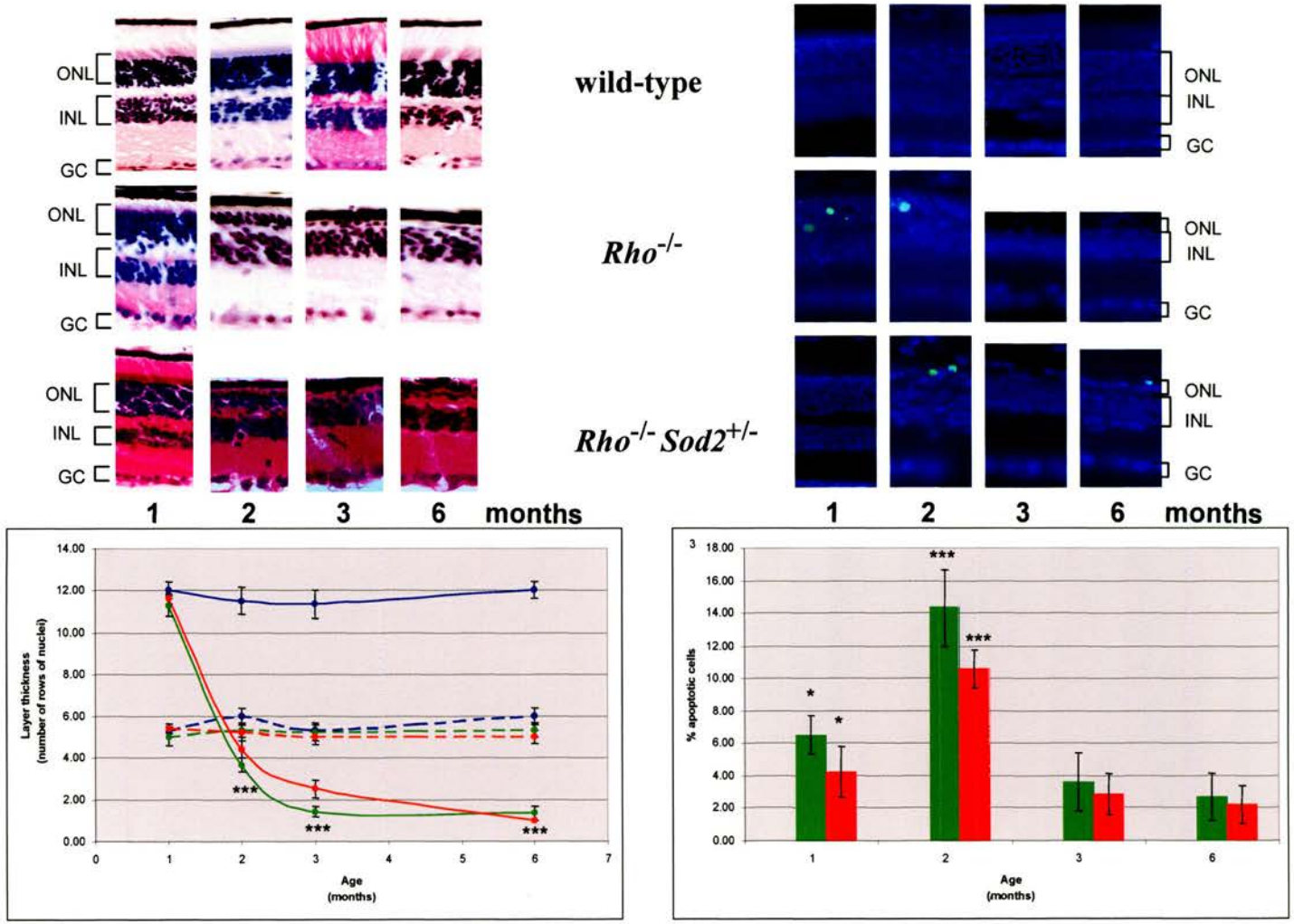

Figure 42: Photoreceptor degeneration in *Rho*$^{-/-}$ *Sod2*$^{+/-}$ double mutants

ONL analysis (left panel) and TUNEL assays (right panel) were performed on paraffin-embedded eye sections from *Rho*$^{-/-}$ *Sod2*$^{+/-}$ mutants. A comparison was made between wild-type (blue), *Rho*$^{-/-}$ mutants (green) and *Rho*$^{-/-}$ *Sod2+/-* double mutants (red). ONL analysis (ONL: solid lines, INL: dotted lines) revealed that in *Rho*$^{-/-}$ mutants photoreceptor degeneration is complete by 3 months of age, irrespective of *Sod2* expression. The decreased Sod2 levels did not affect the number of apoptotic cells detected in the single and double mutants. (* $p<0.05$, *** $p<0.001$ compared with wild-type) (ONL: outer nuclear layer; INL: inner nuclear layer; GC: ganglion cells)

this happened was also almost identical between the two genotypes. At no time-point was there a significant difference in the thickness of either the ONL or the INL between the single and double mutants.

The results from TUNEL assays performed on *Rho*$^{-/-}$ *Sod2*$^{+/-}$ double mutants, with half the wild-type Sod2, showed a similar pattern to that seen in the single *Rho*$^{-/-}$ mutant (**Figure 42**). Detection of TUNEL-positive cells peaked at the second month of age, after which the percentage of apoptotic cells remained at lower levels. Although fewer apoptotic cells were detected on a *Sod2*$^{+/-}$ background, this was not statistically significant.

5.2.4. The effect of decreased *Sod2* expression on the enzyme activities of retinal degeneration mutants

The specific activities of CS and of CI, representing oxidative stress-insensitive and –sensitive activities respectively, were measured in mitochondrial samples prepared from different tissues collected from mutant mice, and a comparison was made between single retinal degeneration mutants and those crossed to *Sod2*$^{+/-}$ mice. The specific activities of these two enzymes were measured in the liver, heart, brain and retina isolated from the animals, and mitochondrial fractions were prepared for spectrophotometric assays. Comparisons between the two *Sod2* genetic backgrounds (wild-type and heterozygous knock-out), were made and the numerical results of the analysis are given in **Table 8**. The results are also graphically presented in **Figure 43**.

There were two general observations from the numerical results obtained. Firstly, as expected, CS activity was always higher than that of CI in all the tissues, with the CI/CS ratio of wild-type animals ranging from 0.07 to 0.12. Secondly, the CI/CS ratio was highest in the retina when compared to the other tissues.

The CI enzyme activities in the *Sod2*$^{+/-}$ single mutant samples were uniformely affected by the decreased expression of *Sod2*. CS activity remained the same as wild-type in all tissues assayed (**Table 8**). In contrast, the specific activity of CI was reduced in liver ($p=0.05$; $n=5$), brain ($p=0.03$; $n=5$), heart ($p=0.04$; $n=5$) and retina ($p=0.05$; $n=3$) by approximately 50-80% in each tissue.

LIVER									
		Citrate Synthase				Complex I			
Genotype	n	activity	se	p_w-value	p_m-value	activity	se	p_w-value	p_m-value
Wild type	4	1.6949	0.1893			0.5969	0.2011		
Sod2$^{+/-}$	5	2.0647	0.2043	0.2358		0.1608	0.0454	**0.0496**	
rd1/rd1	4	2.4467	0.4353	0.1644		0.4743	0.0779	0.5904	
rd1/rd1 Sod2$^{+/-}$	5	2.275	0.2821	0.1516	0.7404	0.1495	0.0272	**0.0413**	**0.0035**
atrd1/atrd1	5	1.7838	0.4554	0.8744		0.4807	0.0564	0.5559	
atrd1/atrd1 Sod2$^{+/-}$	5	2.175	0.3255	0.2743	0.5045	0.1752	0.0201	**0.0498**	**0.0009**
Rho$^{-/-}$	4	2.3787	0.3408	0.13		0.3215	0.1168	0.2812	
Rho$^{-/-}$ *Sod2*$^{+/-}$	4	2.0165	0.3001	0.3995	0.4555	0.4522	0.1767	0.6083	0.5602
BRAIN									
		Citrate Synthase				Complex I			
Genotype	n	activity	se	p_w-value	p_m-value	activity	se	p_w-value	p_m-value
Wild type	4	3.7515	0.7808			0.2444	0.0518		
Sod2$^{+/-}$	5	3.875	0.5603	0.9175		0.0509	0.0116	**0.0323**	
rd1/rd1	4	5.3456	0.4538	0.1446		0.3236	0.0522	0.3235	
rd1/rd1 Sod2$^{+/-}$	5	3.8162	0.4261	0.9482	**0.0493**	0.2251	0.0442	0.792	0.2000
atrd1/atrd1	4	4.3842	0.9078	0.6118		0.3758	0.0211	0.0704	
atrd1/atrd1 Sod2$^{+/-}$	5	5.1783	0.5236	0.1958	0.4773	0.215	0.0571	0.7153	**0.0384**
Rho$^{-/-}$	3	4.0025	0.2766	0.8208		0.3001	0.0613	0.5236	
Rho$^{-/-}$ *Sod2*$^{+/-}$	4	3.9824	0.8009	0.8416	0.9858	0.217	0.0453	0.7016	0.3112
HEART									
		Citrate Synthase				Complex I			
Genotype	n	activity	se	p_w-value	p_m-value	activity	se	p_w-value	p_m-value
Wild type	4	13.9632	2.3818			1.8227	0.3594		
Sod2$^{+/-}$	5	15.8853	1.5219	0.5014		0.8714	0.1706	**0.037**	
rd1/rd1	3	27.527	6.5664	0.0794		1.3934	0.0998	0.3672	
rd1/rd1 Sod2$^{+/-}$	3	16.9338	2.2636	0.4217	0.2019	1.5166	0.293	0.5601	0.7108
atrd1/atrd1	3	18.0613	5.9593	0.5063		1.3424	0.3161	0.3815	
atrd1/atrd1 Sod2$^{+/-}$	3	15.3039	1.6449	0.6868	0.6787	1.5622	0.1226	0.5773	0.5523
Rho$^{-/-}$	3	15.4951	5.4382	0.7862		2.5	0.0325	0.1728	
Rho$^{-/-}$ *Sod2*$^{+/-}$	3	15.2696	1.1299	0.6787	0.9696	0.5895	0.1955	0.0424	**0.0006**
RETINA									
		Citrate Synthase				Complex I			
Genotype	n	activity	se	p_w-value	p_m-value	activity	se	p_w-value	p_m-value
Wild type	6	1.1066	0.1144			0.7248	0.1651		
Sod2$^{+/-}$	3	0.6581	0.2472	0.0955		0.1393	0.0618	**0.0482**	
rd1/rd1	6	1.0074	0.1148	0.6885		0.1541	0.0370	**0.0071**	
rd1/rd1 Sod2$^{+/-}$	3	0.8824	0.0337	0.2614	0.7065	0.0857	0.0326	**0.0337**	0.2793
atrd1/atrd1	4	1.3502	0.3817	0.4865		0.1969	0.0630	**0.0377**	
atrd1/atrd1 Sod2$^{+/-}$	5	0.932	0.1200	0.3387	0.3361	0.0402	0.0057	**0.0106**	**0.0479**
Rho$^{-/-}$	6	0.8719	0.0632	0.1028		0.1058	0.0087	**0.0038**	
Rho$^{-/-}$ *Sod2*$^{+/-}$	3	0.9706	0.1047	0.4768	0.4197	0.1206	0.0418	**0.0419**	0.6398

Table 8: Enzyme activities in wild type and retinal degeneration mutants crossed to *Sod2* heterozygotes

Citrate synthase and complex I activities (μmol/min/g tissue) were measured in liver, brain, heart and retina from wild type, retinal degeneration mutants (*rd1/rd1, atrd1/atrd1* and *Rho*$^{-/-}$) and retinal degeneration mutants crossed to *Sod2* heterozygotes (*rd1/rd1 Sod2*$^{+/-}$, *atrd1/atrd1 Sod2*$^{+/-}$, and *Rho*$^{-/-}$ *Sod2*$^{+/-}$) . The standard errors (se) and statistical significance compared with wild type (p_w-value) and with single retinal degeneration mutants (p_m-value) are shown. Statistical significant values (p_w or p_m<0.05) are highlighted in red.

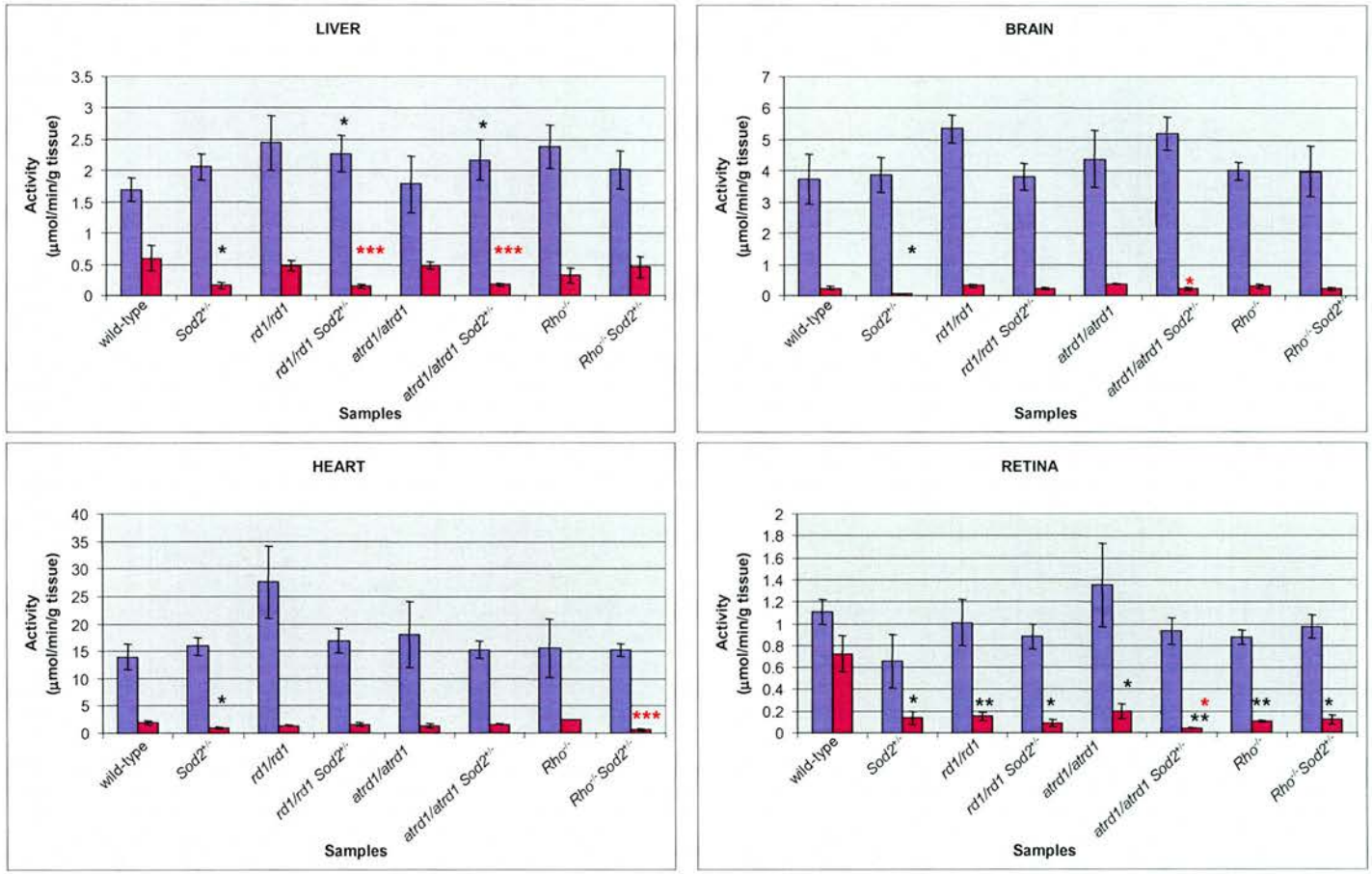

Figure 43: Enzyme activities of citrate synthase and complex I in mouse tissues from wild type and retinal degeneration mutants crossed to *Sod2*$^{+/-}$ heterozygotes

The activities of citrate synthase (blue columns) and complex I (maroon columns) were measured spectrophotometrically in the liver, brain, heart and retina of retinal degeneration double mutants obtained by crossing to *Sod2* heterozygous mice. The activity of citrate synthase remained at wild-type levels in all the tissues of all the mutants. The activity of complex I was significantly reduced in all the tissues of the *Sod2* heterozygous animals. It was also reduced in the liver, brain and heart of some of the retinal degeneration mutants with decreased *Sod2* expression. In the retina, decreased levels of Sod2 caused a further significant decrease in complex I activity only in the *atrd1/atrd1* mutant . All numerical results and p-values are given in Table 6.(* $p<0.05$, ** $p<0.01$, *** $p<0.001$ compared with wild-type (black) or with single retinal degeneration mutants (red))

Decreased Sod2 levels in the retinal degeneration double mutants did not have the same effect in reducing CI as in the *Sod2*$^{+/-}$ mutants in all tissues. Although the specific activity of CS in the double mutants remained at wild-type levels in all tissues, CI activity was significantly lower than the wild-type only in some. None of the brain or heart samples from the double mutants had significantly reduced CI activity, which was found only in the *rd1/rd1 Sod2*$^{+/-}$ ($p=0.04$; $n=5$) and at*rd1/atrd1 Sod2*$^{+/-}$ livers ($p=0.05$; $n=5$). However, the activity of CI was significantly decreased in all the retina samples from double mutants (all $p<0.05$; $n=3$-6).

What is of particular interest in this chapter is the effect that the decreased *Sod2* expression had on the retinal degeneration mutants. Therefore, comparisons between the single and the double mutants, rather than with wild-type (**Table 8**) were made. CS activity in double mutants remained unaffected by decreased Sod2 levels, apart from in the brain *rd1/rd1 Sod2*$^{+/-}$ sample, where CS activity was marginally increased ($p=0.05$; $n=5$). Compared with single retinal degeneration mutants, CI activity was reduced in the liver samples from the *rd1/rd1 Sod2*$^{+/-}$ ($p=0.004$; $n=5$) and at*rd1/atrd1 Sod2*$^{+/-}$ ($p=0.0009$; $n=5$) mutants, in the *atrd1/atrd1 Sod2*$^{+/-}$ brain samples ($p=0.04$; $n=5$), the *Rho*$^{-/-}$ heart samples ($p=0.0006$; $n=3$) and finally in the retina samples of *atrd1/atrd1 Sod2*$^{+/-}$ mutants ($p=0.05$; $n=5$).

5.2.5. Reduced glutathione concentrations in the retinal degeneration mutants crossed to *Sod2*$^{+/-}$ mice

GSH concentrations were measured in liver, brain, heart and retina samples from retinal degeneration mutants crossed to *Sod2*$^{+/-}$ mice (**Table 9**, **Figure 44**). Comparisons were made between these double mutants and the respective single retinal degeneration mutants, to elucidate the effect of the decreased Sod2 expression on GSH concentrations.

GSH concentrations were significantly decreased in the *Sod2*$^{+/-}$ mutants in the liver ($p=0.002$; $n=3$), brain ($p=0.05$; $n=3$) and retina ($p=0.004$; $n=3$) by 57, 70 and 72%, respectively. They were also decreased in the heart samples by approximately 25% but this was not statistically significant ($p=0.33$; $n=3$).

LIVER					
Genotype	**n**	**concentration**	**se**	**p_w-value**	**p_m-value**
Wild type	3	4.2027	0.1542		
Sod2$^{+/-}$	3	1.7984	0.1704	**0.0020**	
rd1/rd1	3	3.8625	0.7369	0.7752	
rd1/rd1 Sod2$^{+/-}$	3	3.6429	0.2300	0.3088	0.8775
atrd1/atrd1	3	3.5817	0.1700	0.2250	
atrd1/atrd1 Sod2$^{+/-}$	3	3.8118	0.1111	0.3437	0.5916
Rho$^{-/-}$	3	5.1527	0.1507	0.0758	
Rho$^{-/-}$ *Sod2*$^{+/-}$	3	2.8714	0.2620	0.0527	**0.0121**
BRAIN					
Genotype	**n**	**concentration**	**se**	**p_w-value**	**p_m-value**
Wild type	3	0.9631	0.1082		
Sod2$^{+/-}$	3	0.2903	0.0342	**0.0495**	
rd1/rd1	3	1.3998	0.0433	0.1586	
rd1/rd1 Sod2$^{+/-}$	3	1.3087	0.2107	0.4255	0.8189
atrd1/atrd1	3	1.3015	0.0751	0.3598	
atrd1/atrd1 Sod2$^{+/-}$	3	1.5251	0.0369	0.0845	0.1046
Rho$^{-/-}$	3	1.1672	0.0314	0.4683	
Rho$^{-/-}$ *Sod2*$^{+/-}$	3	1.0280	0.0513	0.8174	0.2525
HEART					
Genotype	**n**	**concentration**	**se**	**p_w-value**	**p_m-value**
Wild type	3	0.6642	0.0619		
Sod2$^{+/-}$	3	0.5032	0.0451	0.3340	
rd1/rd1	3	0.2579	0.0274	**0.0440**	
rd1/rd1 Sod2$^{+/-}$	3	0.6515	0.0329	0.9376	**0.0060**
atrd1/atrd1	3	0.3288	0.0273	**0.0480**	
atrd1/atrd1 Sod2$^{+/-}$	3	0.4575	0.0393	0.2086	0.2274
Rho$^{-/-}$	3	0.4714	0.0718	0.3324	
Rho$^{-/-}$ *Sod2*$^{+/-}$	3	0.3786	0.0530	0.1449	0.6464
RETINA					
Genotype	**n**	**concentration**	**se**	**p_w-value**	**p_m-value**
Wild type	3	0.0841	0.0052		
Sod2$^{+/-}$	3	0.0236	0.0041	**0.0039**	
rd1/rd1	3	0,0430	0.0029	**0.0253**	
rd1/rd1 Sod2$^{+/-}$	3	0.0390	0.0037	**0.0202**	0.6456
atrd1/atrd1	3	0.0747	0.0125	0.6852	
atrd1/atrd1 Sod2$^{+/-}$	3	0.0465	0.0094	0.0955	0.3559
Rho$^{-/-}$	3	0.0411	0.0023	**0.0235**	
Rho$^{-/-}$ *Sod2*$^{+/-}$	3	0.0292	0.0026	**0.0032**	0.1466

Table 9: Reduced glutathione (GSH) concentrations in wild type and retinal degeneration mutants crossed to *Sod2* heterozygotes

Reduced glutathione concentrations (µmol/g protein) were measured in liver, brain, heart and retina from wild type, retinal degeneration mutants (*rd1/rd1, atrd1/atrd1* and *Rho*$^{-/-}$) and retinal degeneration mutants crossed to *Sod2* heterozygotes (*rd1/rd1 Sod2*$^{+/-}$, *atrd1/atrd1 Sod2*$^{+/-}$, and *Rho*$^{-/-}$ *Sod2*$^{+/-}$) . The standard errors (se) and statistical significance compared with wild type (p_w-value) and with single retinal degeneration mutants (p_m-value) are shown. Statistical significant values (p_w or p_m<0.05) are highlighted in red.

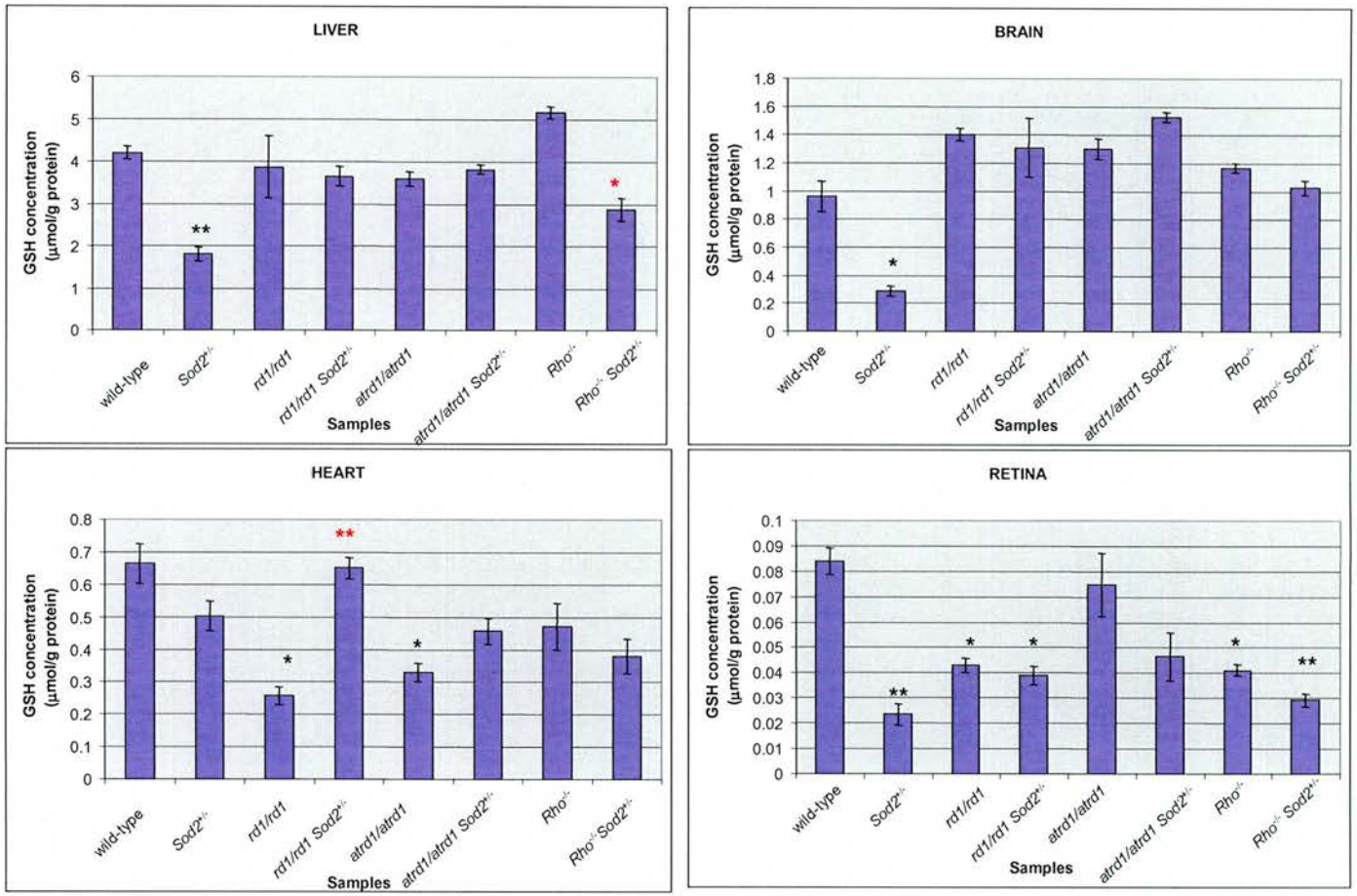

Figure 44: Reduced glutathione (GSH) concentrations in mouse tissues from wild-type and retinal degeneration mutants crossed to *Sod2*$^{+/-}$ heterozygotes

GSH concentrations were measured in the liver, brain, heart and retina of the retinal degeneration double mutants after crossing to *Sod2*$^{+/-}$ heterozygous mice. Compared to the single retinal degeneration mutants, decreased *Sod2* expression caused a significant decrease in the GSH content of the *Rho*$^{-/-}$ liver and the *rd1/rd1* heart samples. All other measurements remained at similar levels irrespective of Sod2 levels. (* $p<0.05$, ** $p<0.01$, *** $p<0.001$ compared with wild-type (black) or with single retinal degeneration mutants (red))

The decrease in the expression of *Sod2* in the retinal degeneration double mutants did not have an effect on the GSH concentrations compared with the single mutants in retina or brain samples. It did however cause a significant reduction of GSH concentrations in the *Rho*$^{-/-}$ liver (p=0.01; n=3) and *rd1/rd1* heart (p=0.006, n=3) samples.

5.3. Summary and conclusions

In this chapter, the influence of oxidative stress on photoreceptor degeneration was investigated by genetically decreasing the levels of the mitochondrial antioxidant enzyme Sod2 in retinal degeneration mutants. The progression of photoreceptor degeneration and the level of oxidative stress were assessed in *rd1/rd1 Sod2*$^{+/-}$, *atrd1/atrd1 Sod2*$^{+/-}$ and *Rho*$^{-/-}$ *Sod2*$^{+/-}$ mutants and comparisons were made with the single retinal degeneration mutants analyzed in the previous chapter.

Initially, the single *Sod2*$^{+/-}$ mutants were analysed. The decreased levels of Sod2 in retinal samples from the mutants were confirmed by both immunoblotting and immunohistochemistry. In the same samples, the levels of Sod1 were unchanged, confirming previous reports that there is no compensatory increase in the level of the cytosolic isoform of superoxide dismutase, in response to a decrease of the mitochondrial isoform (Williams *et al.*, 1998). In addition, the increase in oxidative state in the liver, brain, heart and retina of *Sod2*$^{+/-}$ mutants was confirmed by spectrophotometric enzyme assays and GSH measurements. As expected, the activity of citrate synthase (CS) remained at wild-type levels, while that of complex I (CI) was significantly reduced in all the *Sod2*$^{+/-}$ tissues assayed. Although the 50% reduction in CI activity measured in heart samples (p=0.037; n=5) is compatible with previous results by van Remmen *et al.* (2001), the 70% reduction in liver samples (p=0.049; n=5) was higher than the previously reported 30% decrease in the same tissue (van Remmen *et al.*, 1999). Brain and retina samples had the most pronounced reduction in CI activity, at 80% (brain: p=0.032; n=5, retina: p=0.048; n=3), but no published data are available for comparison. The previously reported reduction or lack of change in the GSH concentration of *Sod2*$^{+/-}$ livers and hearts, respectively (van Remmen *et al.*, 1999; 2001) were confirmed in our analysis. Additionally, the GSH level was

significantly reduced in brain and retina samples from *Sod2* heterozygous knockout mice (brain: p=0.049; n=3, retina: p=0.004; n=3). The increased oxidative status of the $Sod2^{+/-}$ mutants used in this project was therefore confirmed.

Having confirmed both the decreased level of Sod2 and its effects on oxidative damage to the mutant retina, $Sod2^{+/-}$ samples were further analysed for signs of photoreceptor degeneration. Sandbach *et al.* (2001) previously reported that MnTBAP-treated $Sod2^{-/-}$ null mice develop a retinal degeneration phenotype which, although it included thinning of some inner retinal layers, did not include photoreceptor degeneration. Here, $Sod2^{+/-}$ heterozygotes showed no signs of photoreceptor degeneration up to the age of one year, as neither the ONL became thinner with age, nor were any photoreceptor cells stained positively for TUNEL. It is doubtful whether in these mutants photoreceptors would degenerate after one year of age, as even in slowly degenerating mutants, like $Rom1^{-/-}$, the degeneration is evident within the first year (Clarke *et al.*, 2000). The unchanged expression of the OS photoreceptor markers rhodopsin and rod cGMP phosphodiesterase further supported the lack of an altered retinal phenotype in $Sod2^{+/-}$ mutants. In summary, the retinal phenotype of $Sod2^{+/-}$ mutants was limited to decreased CI activity, but did not show any evidence of photoreceptor degeneration.

In an attempt to assess the effect of decreased *Sod2* expression on the different retinal degeneration mutants, double mutants were generated. Decreased levels of Sod2 did not however influence the degeneration rates in any of the double mutants analyzed. In *rd1/rd1* $Sod2^{+/-}$, *atrd1/atrd1* $Sod2^{+/-}$ and $Rho^{-/-}$ $Sod2^{+/-}$ samples all photoreceptor cells were lost by the third week, sixth week and third month of age, respectively. These measurements were identical to those collected in the previous chapter when the single retinal degeneration mutants with wild-type levels of Sod2 were analysed.

The lack of an effect of decreased *Sod2* expression on rates of degeneration was not completely unexpected. In the homozygous *rd1* and the *atrd1* mutants, both of which have mutations in the *Pde6b* gene, photoreceptor degeneration is evident at two weeks of postnatal age, even before the differentiation of the photoreceptor cells is complete. This could therefore imply that the specific *Pde6b* mutations are of such severity that increased cellular

stress, in the form of genetically decreased levels of Sod2, cannot increase the rates of degeneration any further. In this context, the unaltered degeneration rate in the *Rho*$^{-/-}$ mutant was unexpected. The slower degeneration rate in *Rho*$^{-/-}$ retinas implies a less severe mutation, whose effect would, in theory, be more readily modified.

Nevertheless, biochemical analyses in the double mutants revealed some evidence of oxidative damage resulting from decreased *Sod2* expression. As expected, the activity of CS remained at wild-type levels in all the tissues assayed irrespective of genotype. Surprisingly, however, although decreased *Sod2* expression should have caused a decrease in the activity of CI in all the double mutant tissues, this was only the case in some, namely in the *rd1/rd1 Sod2*$^{+/-}$ and *atrd1/atrd1 Sod2*$^{+/-}$ livers and in all the double mutant retinas. What is particularly noteworthy is the comparison between the measurements obtained in the previous chapter, in single retinal degeneration mutants, and those collected in this chapter, in double mutants. Only in the case of the *atrd1/atrd1* mutant was retinal CI activity further reduced due to the *Sod2* heterozygote background ($p=0.048$; $n=5$). Finally, the GSH measurements in the retina of double retinal degeneration mutants remained unaffected by decreased Sod2 levels.

To summarise, the genetically decreased levels of Sod2 activity neither caused a retinal degeneration in mice nor did they change the rates of retinal degeneration or the number of detected apoptotic cells in mouse retinal degeneration models. The reduced activity of complex I in *rd1/rd1*, *atrd1/atrd1* and *Rho*$^{-/-}$ mutant retinas was only further decreased in the *atrd1/atrd1* mutant, as a result of the *Sod2* heterozygous genetic background.

CHAPTER 6

THE EFFECT OF MITOQ ON RETINAL DEGENERATION MUTANTS

6.1. Introduction

In this chapter, the redox state of the mouse retinal degeneration mutants *rd1/rd1*, *atrd1/atrd1*, *Rho*$^{-/-}$ and *rds/rds* was altered by administration of the mitochondrially-targeted antioxidant MitoQ. A preliminary study was performed on wild-type animals to investigate the toxicity of the drug, as well as its distribution in different tissues, and in particular in the retina. The degeneration rates of the photoreceptor cells were measured in the different mutants after administrating the antioxidant, by both ONL and TUNEL analyses. Finally, spectrophotometric assays assessing the activity of the mitochondrial enzymes citrate synthase (CS) and complex I (CI), and the reduced glutathione (GSH) concentrations of different tissues, were performed in MitoQ-treated and -untreated retinal degeneration mice.

6.2. Preliminary study: assessing the toxicity, uptake and distribution of MitoQ

6.2.1. Study set-up

A preliminary experiment was set up to assess the stability of MitoQ in drinking water as well as its effects on food and water consumption, health and breeding capacity of the mice that were administered this antioxidant.

The layout of the experiment is shown diagrammatically in **Figure 45**. Three cages (referred to as 'Adult'), each with 5 wild-type C57BL/6 male mice, were set up. The animals had free access to drinking water that was supplemented with 0 μM, 250 μM or 500 μM of MitoQ corresponding to control, low or high doses of the drug, respectively. At the start of this part of the study, which lasted for 3 months, the animals were 4 weeks old. The weight, food and water consumption of the animals were measured on a daily basis, and regular health checks were performed, based on coat condition, salivation, respiration and behaviour/movement. Three additional cages (referred to as 'Young'), corresponding to the same doses of the drug as above, were also set up, this time with breeding trios (one male x two females) in each cage, starting at the age of 6 weeks. The breeding trios and their litters were monitored daily

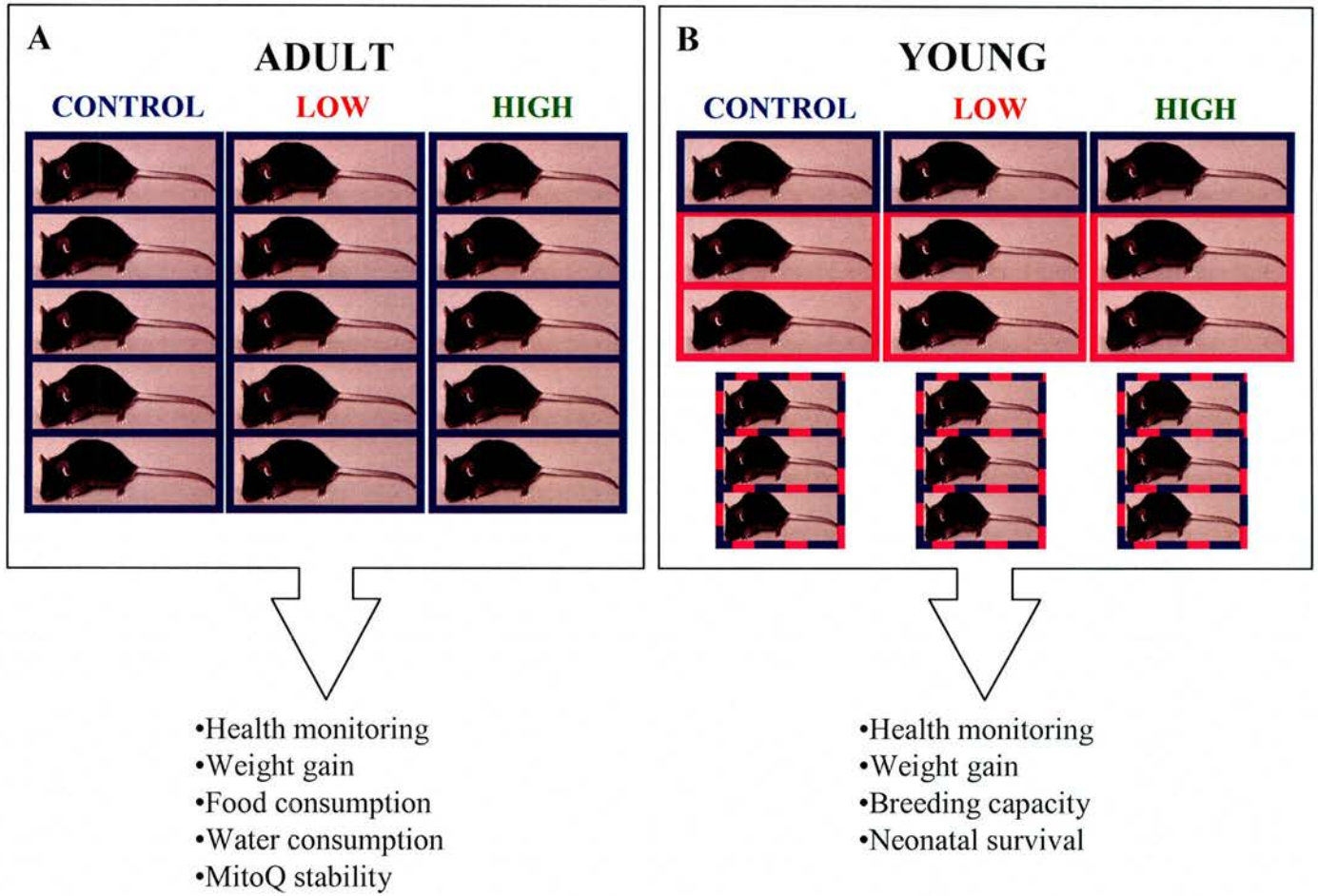

Figure 45: Preliminary study outline

A preliminary study was set up to assess the stability of MitoQ and its toxicity to mice. (**A**) 'Adult' experiment: Five 4-week old wild-type male C57Bl/6 mice were put in each of three cages and were administered plain drinking water (control) or drinking water supplemented with 250 μM MitoQ (low dose) or 500 μM MitoQ (high dose) for a period of 3 months. Data was collected to assess the effect of MitoQ on mouse health, weight gain and food and water consumption. (**B**) 'Young' experiment: Breeding trios (1 male x 2 female) were put in each of three cages and were administered plain drinking water (control) or drinking water supplemented with 250 μM MitoQ (low dose) or 500 μM MitoQ (high dose). The health of the trios and their litters was monitored daily for 3 months and data was collected for assessment of MitoQ effects on breeding capacity and neonatal survival (the gender of the mice in each cage is indicated by the colour of the picture box, blue: male, pink: female)

in the same way as the 'Adult' mice and the effects of MitoQ on both the breeding capacity of the mice and the survival of litters were assessed.

6.3. Results

6.3.1. Stability

MitoQ, which is a yellow powder, was stored at 4°C and kept in the dark. It was dissolved in water at the desired concentrations and administered to mice at room temperature. It was also protected from light, by covering water bottles with tin foil. The stability of MitoQ was assessed spectrophotometrically at 268 nm on a daily basis for a period of 3 weeks (**Figure 46A**). Starting from an initial absorbance measurement of 2.941 (s.d. 0.036) and 2.786 (s.d. 0.032) for the high and low doses, respectively, on day one, a significant decrease in absorbance was observed 4 days later. It was concluded that fresh solutions of MitoQ needed to be made up every three days.

6.3.2. Food consumption

The food consumption of the animals in the 'Adult' cages was measured by weighing the chow daily for a period of 4 weeks. Food consumption was increased with the age of mice, from about 3.2 g/animal/day at 4 weeks old to 4 g/animal/day at 8 weeks old in the MitoQ-untreated controls (**Figure 46C**). The food consumption was almost identical for the mice treated with no MitoQ, low or high dose. The mean food consumption during the period of the preliminary study was 3.5 ± 0.36, 3.49 ± 0.40 and 3.70 ± 0.48 g/animal/day for the control, low and high doses, respectively (**Figure 46D**).

6.3.3. Water consumption

The water consumption of the animals also increased slightly with age (**Figure 46E**). Animals administered plain water started with a water consumption of 4.9 ml/animal/day and by the end of the study they were consuming 5.1 ml/animal/day. Mice, administered with MitoQ started off with very low water consumption, at 1.1 and 1.7 ml/animal/day for the low and high dose,

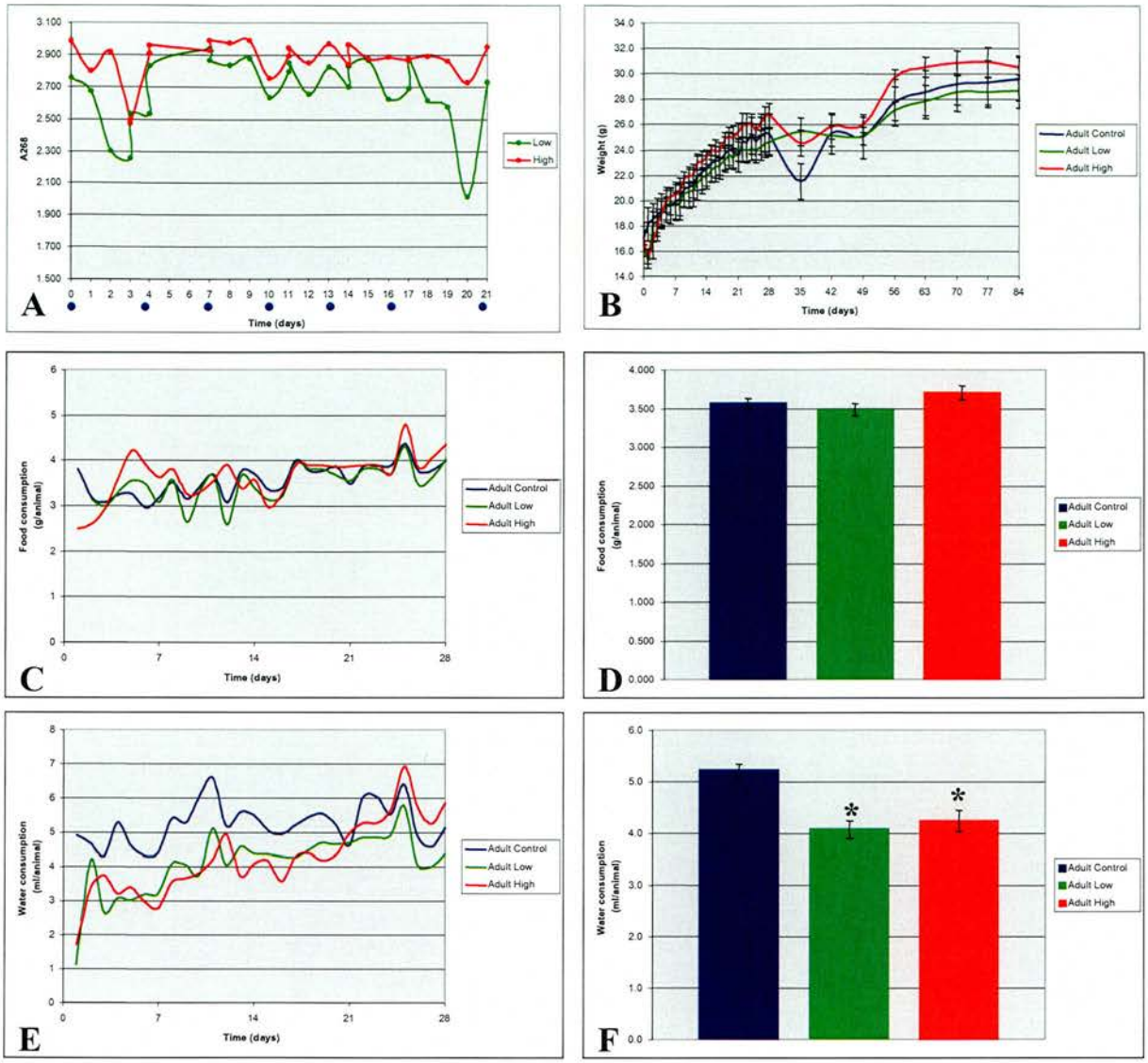

Figure 46: Preliminary study assessing the stability of MitoQ and the effects of its administration on weight gain, food consumption and water consumption.

Wild-type C57Bl/6 adult mice were administered plain water (control) or water supplemented with a low (250 μM) or high (500 μM) dose of MitoQ. (**A**) The stability of MitoQ was monitored daily by its absorbance at 268 nm for a period of 3 weeks. A significant drop in absorbance was recorded 4 days after preparation, although this was not consistent. Fresh MitoQ dilutions were subsequently prepared every three days. The weight gain (**B**) of adult male animals was monitored daily for a period of 4 weeks and weekly thereafter for an additional 2 months. No significant dose-related differences in weight gain were observed. The food (**C**, **D**) and water (**E**, **F**) consumption of the animals were measured daily for a period of 4 weeks. No significant differences were observed in food consumption. The water consumption of the animals on either dose of MitoQ was significantly reduced (indicated by *; $p=8.14 \times 10^{-7}$ (low dose) ; $p=1.33 \times 10^{-4}$ (high dose)) but this did not correlate with any side effects or weight loss which might compromise the animals' health.

respectively. This decrease in volume probably reflected the reluctance of the mice to consume drinking water with a new flavour. The consumption of water supplemented with the antioxidant increased and became more stable with time. However, comparing overall mean water consumption between controls (mean 5.2 ml/animal/day) and treated, there was a significant decrease in the latter, with p-values at 8×10^{-7} (mean 4.1 ml/animal/day) and 0.0001 (mean 4.2 ml/animal/day) for the low and high doses respectively (**Figure 46F**). It was decided however that this was not an alarming decrease in water consumption, since there were no health effects associated with this and the animals gained weight normally (see below).

6.3.4. Side effects

The health of the mice was monitored daily to assess any toxic effects that could be attributed to oral MitoQ administration. The coat condition, salivation, respiration, behaviour and movement of the animals showed no difference between the control and MitoQ-administered mice. No deaths were reported in the 'Adult' cages. However, one of the two females in the 'Young' cage on the high dose of MitoQ was culled 6 days into the experiment, following constant loss of weight, with abnormal behaviour and limited movement. The severity of this incident and its rapid manifestation, as well as the lack of similar cases, prevented us from attributing this death to the administration of the antioxidant drug.

6.3.5. Weight gain

Noticeable changes in weight can reflect metabolic or physiological problems. At the beginning of the study, the animals in both 'Adult' and 'Young' cages were at an age when developmental weight gain had not ceased. Their weights were measured daily for the first month and weekly thereafter until the end of the study at 3 months. Typically, mice of the C57BL/6 strain show a sharp increase in weight in the first few postnatal weeks of age, which then stabilises at around 20 and 25 grams for a female and a male mouse, respectively.

In the 'Adult' cages there were only male mice. At 4 weeks old, the mean weight of control mice was 16.9 ± 1.4 g which steadily increased to 29.6 ± 1.7 g by 4 months of age (**Figure 46B**). Mice administered a low or high dose of MitoQ

weighed 16.8 ± 0.7 g and 17.1 ± 0.6 g at the start of the study and 28.6 ± 1.3 g and 30.5 ± 0.9 g respectively at the end of it. None of these differences in weight gain were significantly different from each other ($p>0.05$). The fluctuations in weight, seen in the controls on week 5, did not correlate with a similar fluctuation in water and/or food consumption, and since weight gain soon stabilised, the incident was not considered significant.

The weight gain of the breeding trios in the 'Young' cages was also monitored daily (**Figure 47A-C**). The female pregnancies resulted in fluctuations in their weights, which increased steadily for 19-20 days and dropped sharply once the litters were delivered. Of the two females administered control water, only one produced litters during the time of the experiments. Also, as mentioned above, constant loss of weight by one of the females given the high dose of MitoQ, resulted in the decision to cull the mouse when its health was seriously compromised. The cause of death of this mouse remains unknown.

It was important for the study to ensure the well-being of the litters, and so their weight was also measured daily from the day of birth (P1) at least up to weaning, 21 days later (P21). The mice on the control, low and high MitoQ doses were born weighing 1.29 ± 0.1 g, 1.55 ± 0.3 g and 1.20 ± 0 g, respectively (**Figure 47D**). Litters on either dose of MitoQ showed both weights that were significantly different from the controls (Low dose: $p=0.005$, $n=33$; high dose: $p=0.001$, $n=19$), but in opposite directions. There was no correlation between pup-weight and MitoQ dose so this was not considered further. A sharp weight gain was observed in all three groups, with the weight measurements at P21 being 9.48 ± 0.6 g in controls, 11.6 ± 1.9 g in the low dose and 8.54 ± 1.21 g in the high dose-administered pups (**Figure 47E**). The weights of the treated mice were not significantly different from the controls.

6.3.6. Breeding capacity

To assess the effect of long-term oral MitoQ administration on the breeding capacity of mice, data was collected from the 'Young' cages. MitoQ was

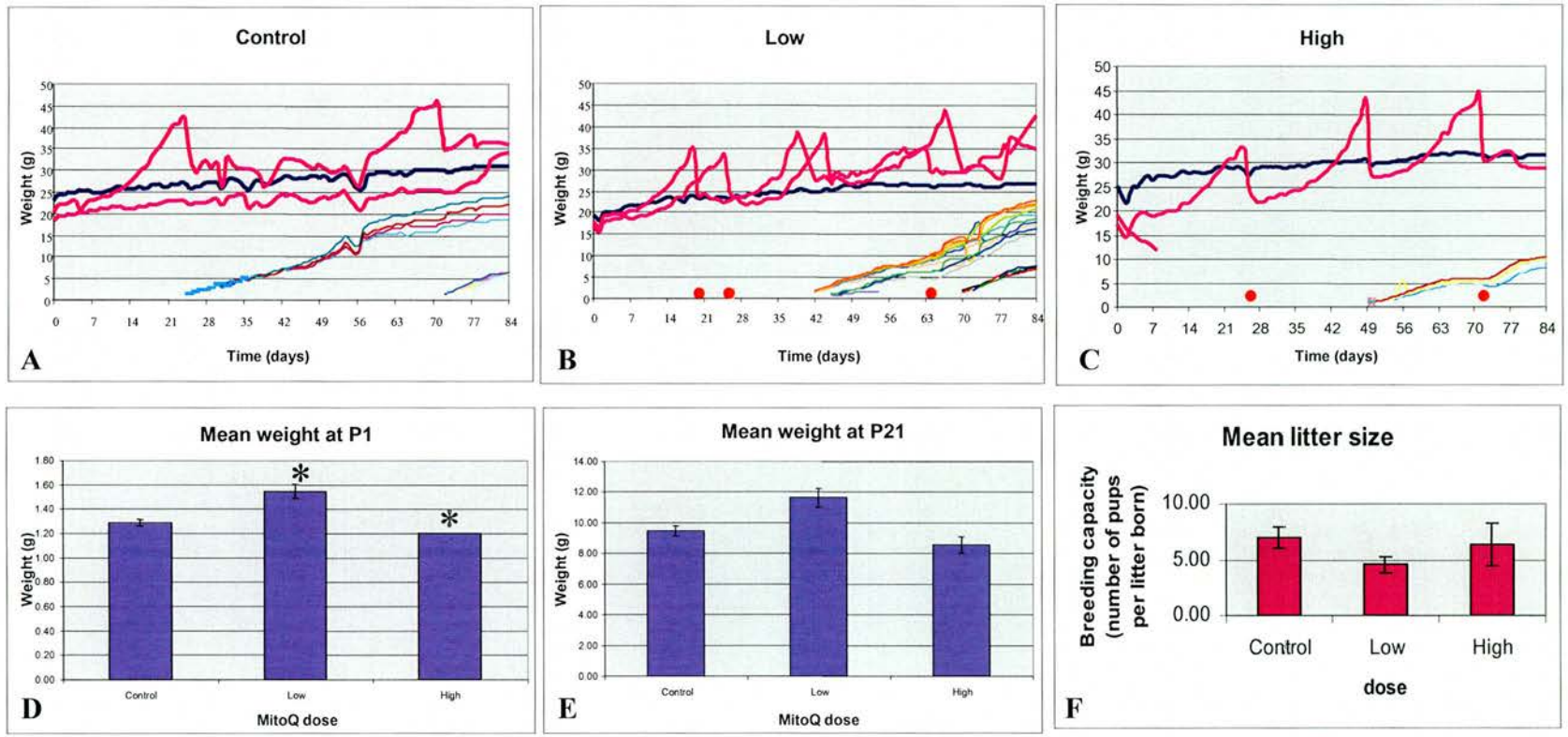

Figure 47: The effect of long-term MitoQ administration on the breeding capacity of wild-type mice and on neonatal survival

The weight gain of wild-type C57Bl/6 mice set up in mating trios was monitored daily for a period of 12 weeks (**A-C**). The animals were given either water alone or a low (250 μM) or high (500μM) MitoQ dose. The dark blue lines correspond to the weights of the males, while the pink ones to the females. The peaks observed in the females' weights indicate weight gain during pregnancy. The weights of their litters were also monitored daily at least until weaning at P21 (**A-C**). The red dots indicate litters that died on the day of birth. There were no significant differences in weight gain between the different groups of mice. Significant differences (∗) seen in the pups' weights at P1 (**D**) or P21 (**E**) did not correlate with MitoQ dose and were not considered alarming. There was no significant difference in litter size of mice administered different MitoQ doses.

administered to the animals from the day the breeding trios were set up. The reproductive performance of the mice was assessed by both the number and the size of the litters born. The trios administered water, low and high dose of MitoQ produced 2, 7 and 3 litters respectively, of which 0, 3 and 2 litters died within the first day after birth. The mean litter size was 7.0, 4.6 and 6.3 for the control, low and high MitoQ doses, respectively (**Figure 47F**). Although there was a significant difference in the number of litters produced by the breeding trios, their size was not significantly affected (Low dose: p=0.14; high dose: p=0.81).

6.3.7. Uptake of MitoQ

The uptake of MitoQ by mitochondria, cells and tissues was investigated by using either IBTP or tritium-labelled MitoQ (^{3}H-MitoQ).

The uptake of IBTP by tissue extraxts was firstly investigated. For this, wild-type heart, liver and retina homogenates were treated with IBTP, in the presence of energisation buffer, *prior* to fractionation into mitochondrial and cytosolic components. The uptake of IBTP by the different fractions was assessed by immunoblotting with an antibody directed against the triphenylphosphonium moiety of the IBTP molecule (**Figure 48**). The efficiency of the fractionation was assessed by blotting the membrane with an antibody against the mitochondrial isoform of Sod2. (**Figure 48B**). Mitochondria were successfully isolated from liver and retina samples, but some mitochondrial contamination was evident in the cytosolic fraction obtained from the heart. This was attributed to the evident difficulty when homogenising cardiac tissue, due to its high fibrous content. Blotting of the membrane with the anti–IBTP antibody, revealed the presence of IBTP solely in the cytosolic fractions of the tissues, and its absence from the mitochondrial ones (**Figure 48C**). It was concluded that, under these specific experimental conditions, IBTP was retained in the cytosol and not efficiently taken up by mitochondria.

The uptake of IBTP by isolated mitochondria was then assessed. For this, heart and liver mitochondrial preparations were treated with IBTP both in the presence and absence of energisation buffer (**Figure 49A, B**). Control

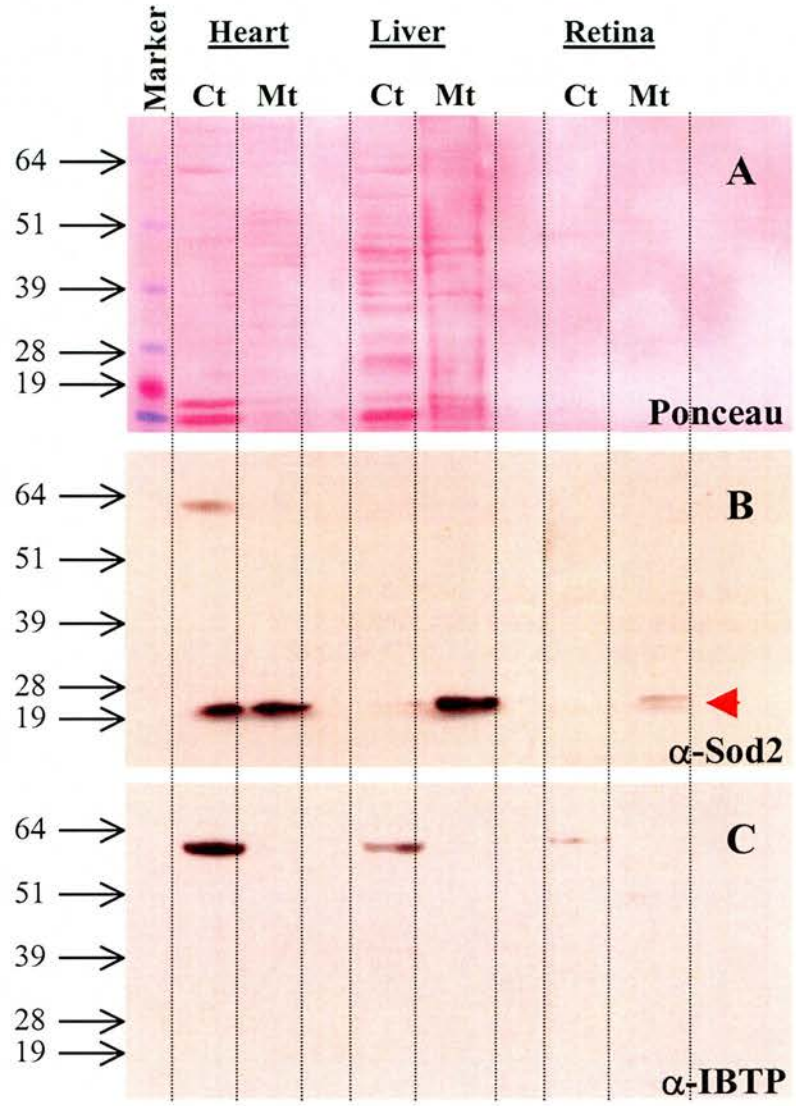

Figure 48: Reaction of IBTP with thiol proteins in cell fractions

Heart, liver and retina homogenates from wild-type animals were treated with IBTP prior to fractionation into cytosolic (Ct) and mitochondrial (Mt) fractions. Equal amount of protein were loaded in a denaturing gel, as confirmed by Ponceau staining (**A**). The efficiency of the fractionation was confirmed by blotting with an anti-Sod2 antibody which detects the mitochondria-specific 25 kDa Sod2 (red arrowhead) (**B**). The anti-IBTP antibody detected bands only in the cytoplasmic fractions of the tissues (**C**).

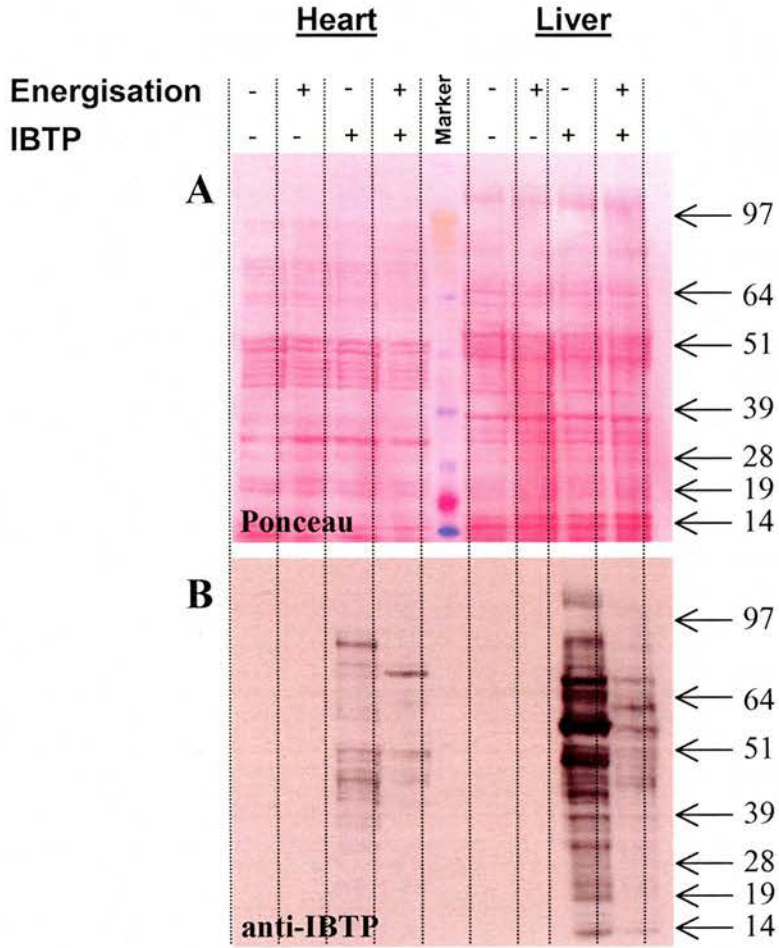

Figure 49: Reaction of IBTP with thiol proteins in isolated mitochondria

Heart and liver mitochondrial fractions from wild-type animals were energised or not prior to treatement or lack of treatment with IBTP and equal amounts of protein were loaded in a denaturing gel, as this was confirmed by Ponceau staining (**A**). No bands were detected by the antibody in the non-IBTP-treated samples, whereas bands were detected in the IBTP-treated samples, confirming the uptake of IBTP by isolated mitochondria. However, more bands were detected by anti-IBTP in the non-energised samples The arrows indicate protein sizes (kDa).

samples were not treated with IBTP. The results from the two tissues were comparable. No proteins were detected by anti–IBTP in samples that were not treated with IBTP, confirming the specificity of the in detecting IBTP-bound proteins. In the IBTP-treated samples however, an increased number of proteins were detected in the non-energised samples when compared to the energised samples. Although this result confirmed the uptake of IBTP by isolated mitochondria, it did not agree with the expectation that energisation should increase IBTP uptake by mitochondria.

Having verified the uptake of IBTP by isolated mitochondria, it was necessary to confirm that this was also the case upon oral administration of the compound to animals. IBTP was administered orally, at a concentration of 500 μM, to a pair of C57BL/6 wild-type mice for two weeks. At the end of the two weeks, the animals were culled and heart, brain, liver and retina samples were collected, and mitochondrial samples were prepared. In the case of the retina, only whole homogenates were used, rather than mitochondrial preparations, due to the limited availability of the tissue. The control samples included in the experiment were collected from mice not administered IBTP. The results from the immunoblotting experiment using the anti–IBTP antibody are shown in **Figure 50**. A band of about 190 kDa was detected in the heart mitochondrial sample treated with IBTP, but not in the control. Additional bands seen in IBTP-treated samples were considered non-specific, as they were also seen in the control samples that had not been treated with IBTP. It was concluded, firstly, that IBTP was taken up by heart mitochondria following oral administration of the compound, and secondly, that a comparison of control and IBTP-treated samples should be carried out before deciding which are specific bands reflecting the reaction of IBTP with thiol proteins in the mitochondrial fraction.

The efficiency of IBTP uptake by different tissues was further investigated, by its administration to *Sod2*$^{+/-}$ and *atrd1/atrd1* mutants. The former was chosen because it is defective in a major antioxidant enzyme, so that signs of oxidative stress should be evident in all tissues analyzed. The *atrd1/atrd1* mutants were examined because it is one of the retinal degeneration

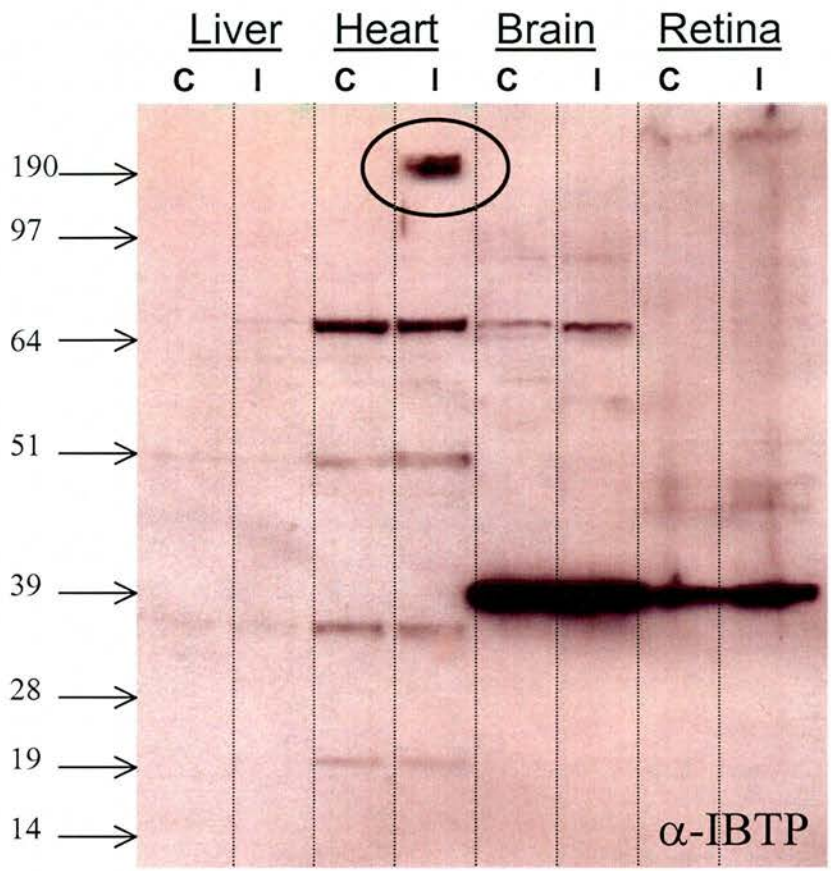

Figure 50 : Reaction of IBTP with thiol proteins in mitochondrial fractions of various wild-type mouse tissues

The uptake of IBTP was assessed *in vivo* using samples from wild-type animals. Liver, heart, brain and retina were collected from animals administered either control drinking water (C) or IBTP (I) for two weeks. Mitochondrial fractions were prepared from all the tissues, apart from retina, in which whole homogenates were used. These samples were then used for the immunoblotting experiment. There is only one band of about 190 kDa (circled) that is detected in the heart sample. This agrees with previous reports of good IBTP uptake by heart.

mutants that showed signs of oxidative damage, as reflected by decreased CI activity. For this part of the study, mutant mice were again administered IBTP. for 2 weeks at a concentration of 500 μM. At the start of the 2-week treatment, the *atrd1/atrd1* mice were 2 weeks old to ensure that retinal degeneration had not progressed and that photoreceptor cells would still be present by the end of the treatment. Although *Sod2*$^{+/-}$ mice show no retinal degeneration up to the age of one year, these mice were 2 months old at the start of the experiment to ensure the presence of potentially detectable oxidative protein modifications. As before, controls included mitochondrial samples prepared from age- and genotype-matched animals. Samples from wild-type animals were also included in this experiment. The results are shown in **Figure 51**. In the wild-type blot (**Figure 51A**) α-IBTP detected a protein at about 190 kDa in the IBTP-treated heart mitochondrial sample. A band of equal size, observed in the non-IBTP-treated sample, was substantially fainter. Non-specific bands were detected in control and IBTP-treated brain and retina samples. In the *Sod2*$^{+/-}$ immunoblot (**Figure 51B**) the antibody again detected a non-specific 40 kDa band in the heart, brain and retina samples, but not in the IBTP-treated sample. In the *atrd1/atrd1* blot (**Figure 51C**), a non-specific 40 kDa band was again detected, but no specific IBTP bands were present.

The control samples had not been treated with IBTP, and therefore the detection of any bands by α-IBTP are likely to be false-positives. However, as our purpose was to establish whether IBTP penetrates the tissues and accumulates in mitochondria following a two-week oral administration, an additional approach is to compare IBTP-treated wild-type and mutant samples. In this comparison (colour-coordinated in **Figure 52**), the presence of a band in the wild-type sample and its absence in the mutant samples would reflect the interaction of IBTP with the corresponding protein in the wild-type sample, but the lack of it in the mutant, due to oxidative protein modification. A strong band, at about 190 kDa, was again present in the wild-type heart mitochondrial sample, but absent in both the *Sod2*$^{+/-}$ and the *atrd1/atrd1* heart samples (Figure **52B**). In the retina blots (**Figure 52C**), there was an IBTP band of high molecular weight (~ 190 kDa) in the *Sod2*$^{+/-}$ blot only. The strong signal in the *atrd1/atrd1* blot at above 190 kDa was not considered genuine and possibly

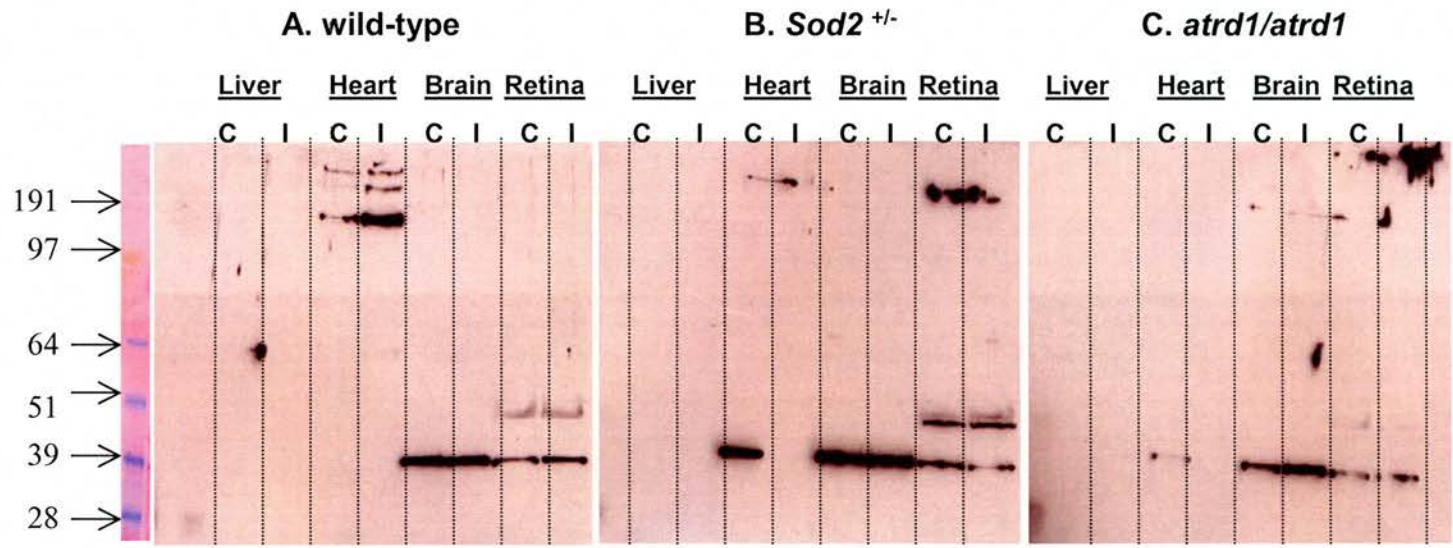

Figure 51: Reaction of IBTP with thiol proteins in mitochondrial fractions of various wild-type and mutant tissues

Liver, heart, brain and retina samples from (**A**) wild-type, (**B**) *Sod2*$^{+/-}$ mutant and (**C**) *atrd1/atd1* mutant animals were blotted with an antibody specific to IBTP. A comparison was made between samples collected from animals that were administered with pure water (C) and samples from IBTP-treated animals (I). The arrows on the left indicate protein sizes (kDa).

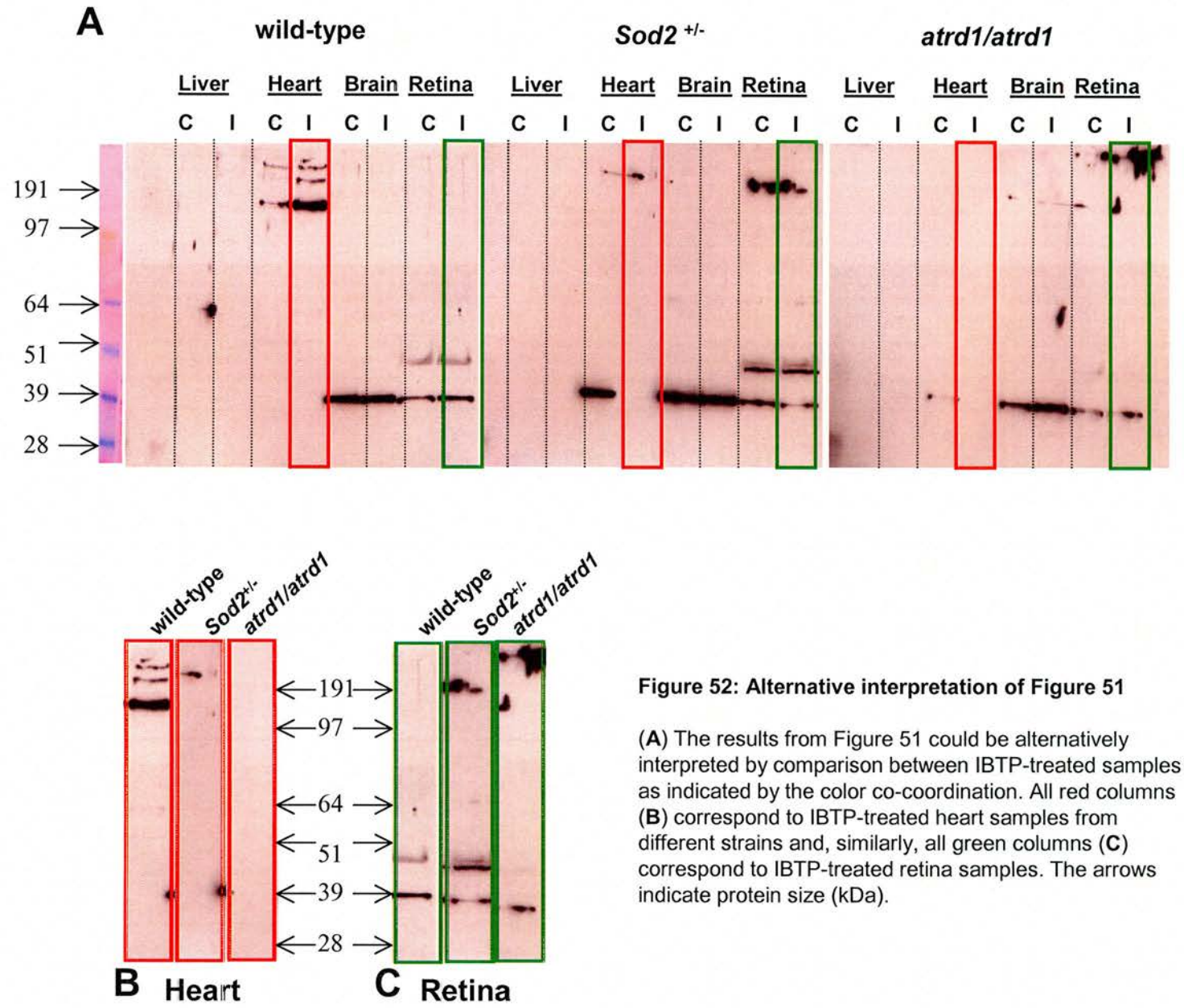

Figure 52: Alternative interpretation of Figure 51

(**A**) The results from Figure 51 could be alternatively interpreted by comparison between IBTP-treated samples as indicated by the color co-coordination. All red columns (**B**) correspond to IBTP-treated heart samples from different strains and, similarly, all green columns (**C**) correspond to IBTP-treated retina samples. The arrows indicate protein size (kDa).

corresponded to proteins retained at the top of the protein gel. Also, there were two bands in the wild-type retina sample, at 50 kDa and 40 kDa, which showed different intensities in the two mutants. In the *Sod2*$^{+/-}$ sample, the 50 kDa band is stronger while the 40 kDa band is of the same, if not less, intensity. In the *atrd/atrd11* sample the 50 kDa band had disappeared whereas the 40 kDa band was a lot fainter

To summarise the results from the use of IBTP *in vivo*, it has been shown, firstly that IBTP can successfully accumulate in mouse heart mitochondria following oral administration for 2 weeks at a concentration of 500 μM. Secondly, there was no convincing reduction in the number of specific bands detected by α-IBTP in the *Sod2*$^{+/-}$ and *atrd1/atrd1* samples compared with wild-type, which might have reflected increased oxidative damage in these mutants. Thirdly, although the specificity of the anti–IBTP antibody was confirmed on mitochondrial samples treated with the compound *after* fractionation (**Figure 49**), it appears to detect many non-specific bands in mitochondrial samples prepared after oral administrations of IBTP.

To obtain additional evidence for the uptake of MitoQ by retina, tritium-labelled MitoQ (^{3}H-MitoQ) was administered orally to wild-type C57BL/6 mice (n=3) for 2 weeks at a concentration of 500 μM. Tissue samples (heart, brain, liver, eye without retina, retina) were assayed in a scintillation counter and the uptake of ^{3}H-MitoQ was estimated on the basis of a standard curve. Control samples were collected from animals administered with pure drinking water. Uptake of ^{3}H-MitoQ was significant in all the tissues assayed (all $p<0.05$) (**Figure 53**). Measurements were highest in the heart and liver samples, at over 3 nmol/g wet weight. Uptake by the retina was about 1.3 nmol/g wet weight, while in the remainder of the eye, uptake was at just under 0.5 nmol/g wet weight. The experiment using ^{3}H-MitoQ therefore verified the uptake of the drug by heart, liver, brain and retina tissues.

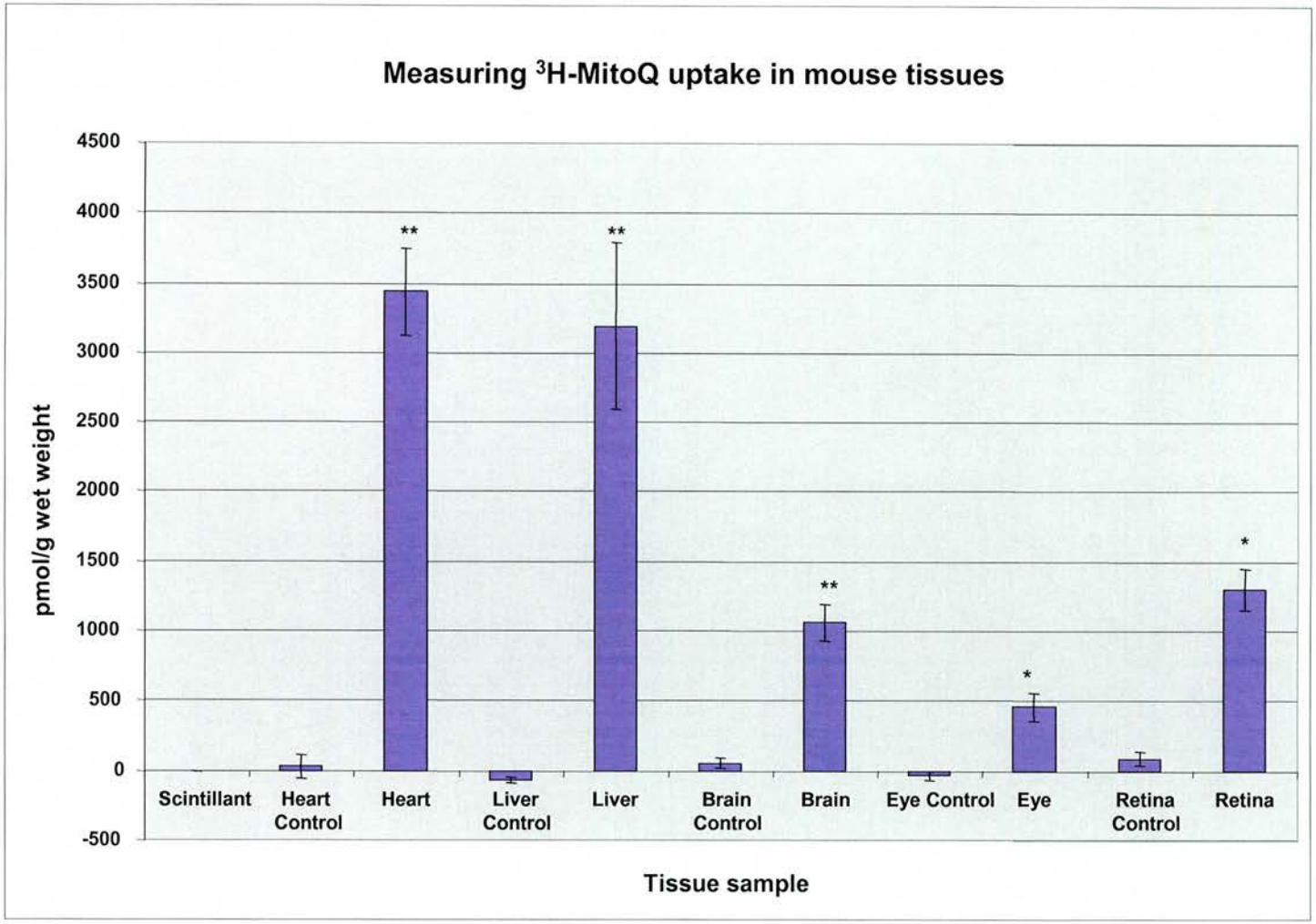

Figure 53: Uptake of orally-administered ^{3}H-MitoQ by different tissues.

The uptake of ^{3}H-MitoQ was assessed *in vivo*. Mice were administered 500 μM ^{3}H-MitoQ for two weeks and tissue contents were measured by scintillation counting. The control samples were collected from mice that were fed pure drinking water. The uptake was significant in all the tissues assayed (*: $p<0.05$; **: $p<0.01$; all n=3).

6.3.8. The effect of MitoQ administration on the retinal degeneration mutants

Having investigated the uptake of MitoQ by different tissues after oral administration, the aim of this chapter was to assess the effects of MitoQ administration on the rates of photoreceptor degeneration, mitochondrial enzyme activities and the reduced glutathione concentrations of the retinal degeneration mutants and wild-type controls.

6.3.8.1. Effects of MitoQ on the rates of photoreceptor degeneration

The rates of photoreceptor degeneration were measured by means of ONL analysis and TUNEL assays, as previously described. Firstly, the methods were applied on samples collected from 3-month-old wild-type animals (n=4) administered MitoQ at a low (250 μM) or high (500 μM) dose since conception. No photoreceptor degeneration was caused by MitoQ administration, as indicated by both an unchanged ONL thickness and the absence of TUNEL-positive apoptotic cells in these samples (**Figure 54**).

MitoQ administration had no effect on the rate of photoreceptor degeneration in the *rd1/rd1* mutant, as this was complete by the third week of life (**Figure 55**). An increasing number of apoptotic photoreceptor cells were detected by TUNEL assays with age and at no time-point were the percentages of TUNEL-positive cells significantly different between the untreated *rd1/rd1* mutants and those administered MitoQ (all $p>0.05$; n=5).

Similarly, long-term oral administration of MitoQ to *atrd1/atrd1* mutants had no effect on the rate of photoreceptor degeneration (**Figure 56**). In agreement with the ONL analysis results, TUNEL assays on MitoQ-treated mutant samples showed increasing percentages of apoptotic cells with age. At no time-point were these results significantly different from those obtained in mutant samples that were not treated with the antioxidant (all $p>0.05$; n=5).

In MitoQ-administered *Rho*$^{-/-}$ mutants, photoreceptor degeneration was complete by 3 months of age (**Figure 57**). The rate of degeneration was not significantly different between antioxidant-treated and untreated samples (all

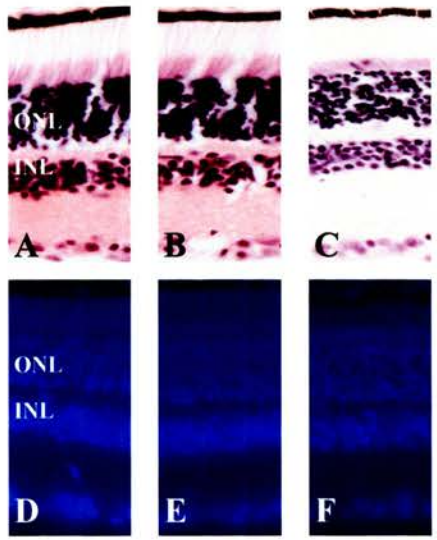

Figure 54: The effect of long-term MitoQ administration on photoreceptor survival in wild-type mice

ONL analysis (**A-C**) and TUNEL assays (**D-F**) were performed on eye sections from 3-month-old wild-type animals administered control drinking water (**A, D**) or water supplemented with a low (250 μM) (**B, E**) or high (500 μM) (**C, F**) dose of MitoQ. Neither analysis showed any indication of cell death attributed to the long term administration of the antioxidant drug.

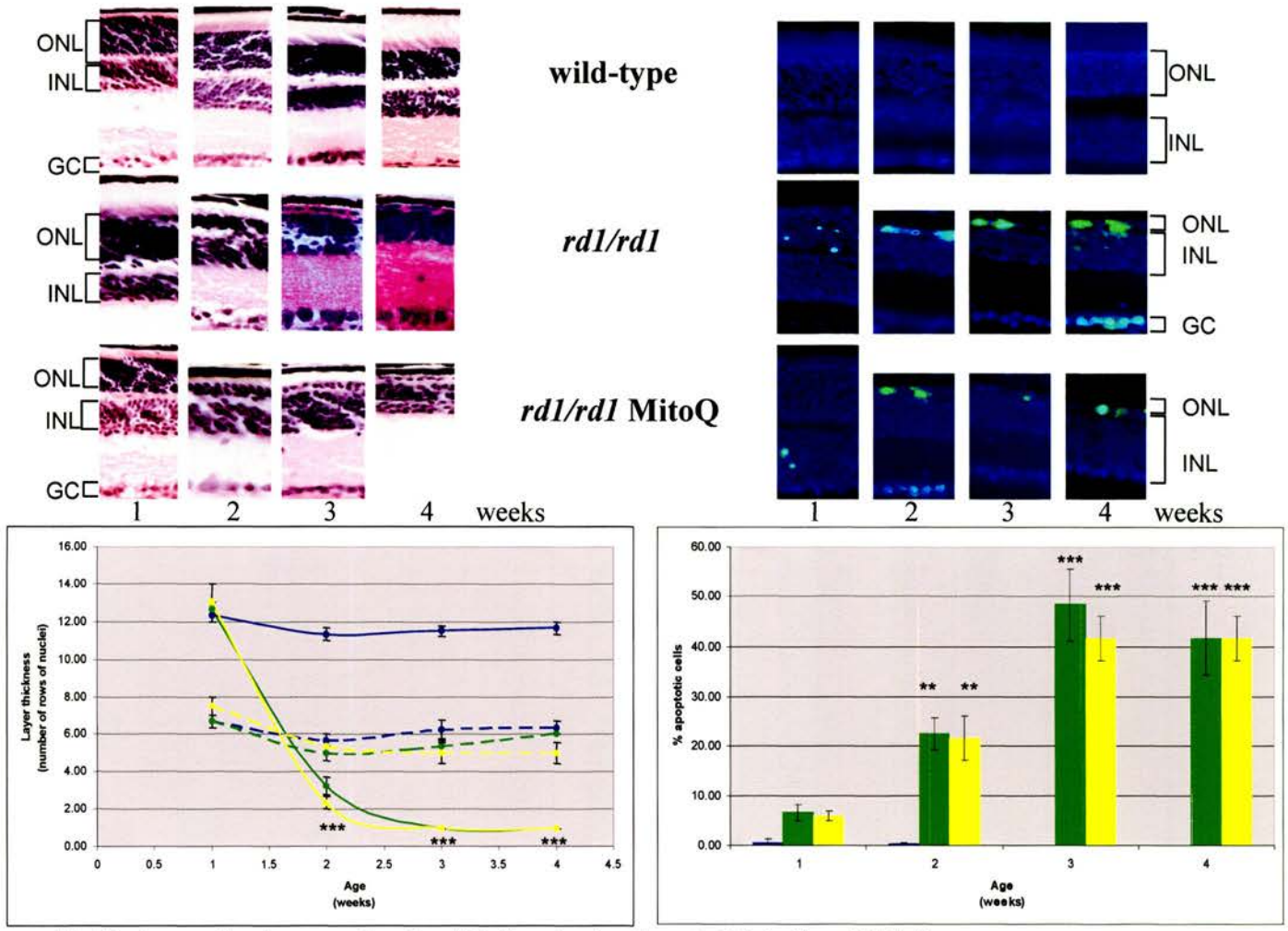

Figure 55: Photoreceptor degeneration in *rd1/rd1* mutants after administration of MitoQ

ONL analysis (left panel) and TUNEL assays (right panel) were performed on paraffin-embedded eye sections from *rd1/rd1* mutants administered MitoQ. A comparison was made between wild-type (blue) and *rd1/rd1* mutants (green) and *rd1/rd1* mutants administered MitoQ (yellow). ONL analysis (ONL: solid lines, INL: dotted lines) revealed that, irrespective of antioxidant treatment, photoreceptor degeneration in *rd1/rd1* mutants was complete by 3 weeks of age. MitoQ administration had no effect on the number of apoptotic cells detected by TUNEL assays. (** p<0.01, *** p<0.001 compared with wild-type) (ONL: outer nuclear layer; INL: inner nuclear layer; GC: ganglion cells)

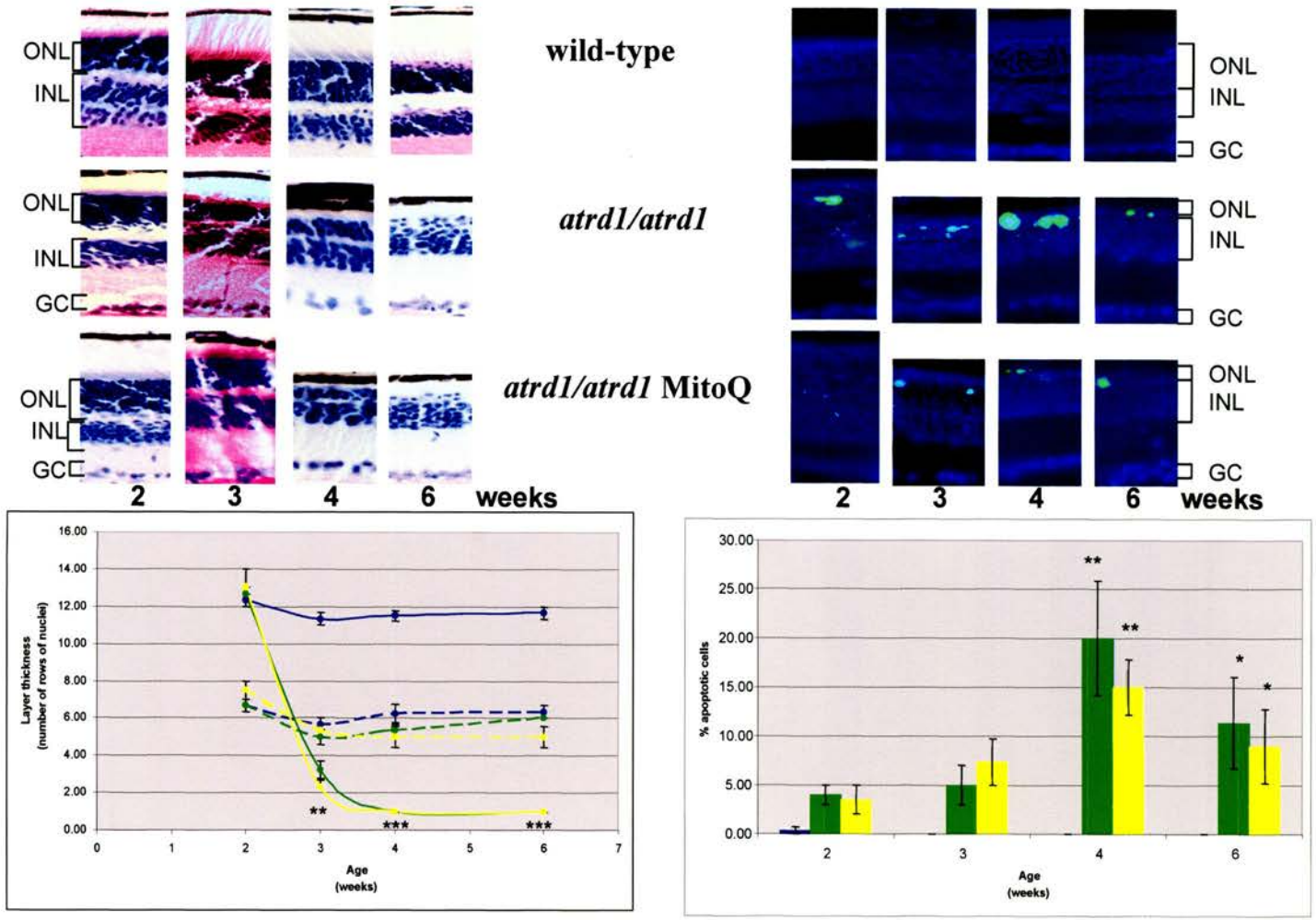

Figure 56: Photoreceptor degeneration in at*rd1/atrd1* mutants after administration of MitoQ

ONL analysis (left panel) and TUNEL assays (right panel) were performed on paraffin-embedded eye sections from at*rd1/atrd1* mutants administered MitoQ. A comparison was made between wild-type (blue) and at*rd1/atrd1* mutants (green) and at*rd1/atrd1* mutants administered MitoQ (yellow). ONL analysis (ONL: solid lines, INL: dotted lines) revealed that, irrespective of antioxidant treatment, photoreceptor degeneration in at*rd1/atrd1* mutants was complete by 6 weeks of age. MitoQ administration had no effect on the number of apoptotic cells detected by TUNEL assays.(* $p<0.05$, ** $p<0.01$, *** $p<0.001$ compared with wild-type (black)) (ONL: outer nuclear layer; INL: inner nuclear layer; GC: ganglion cells)

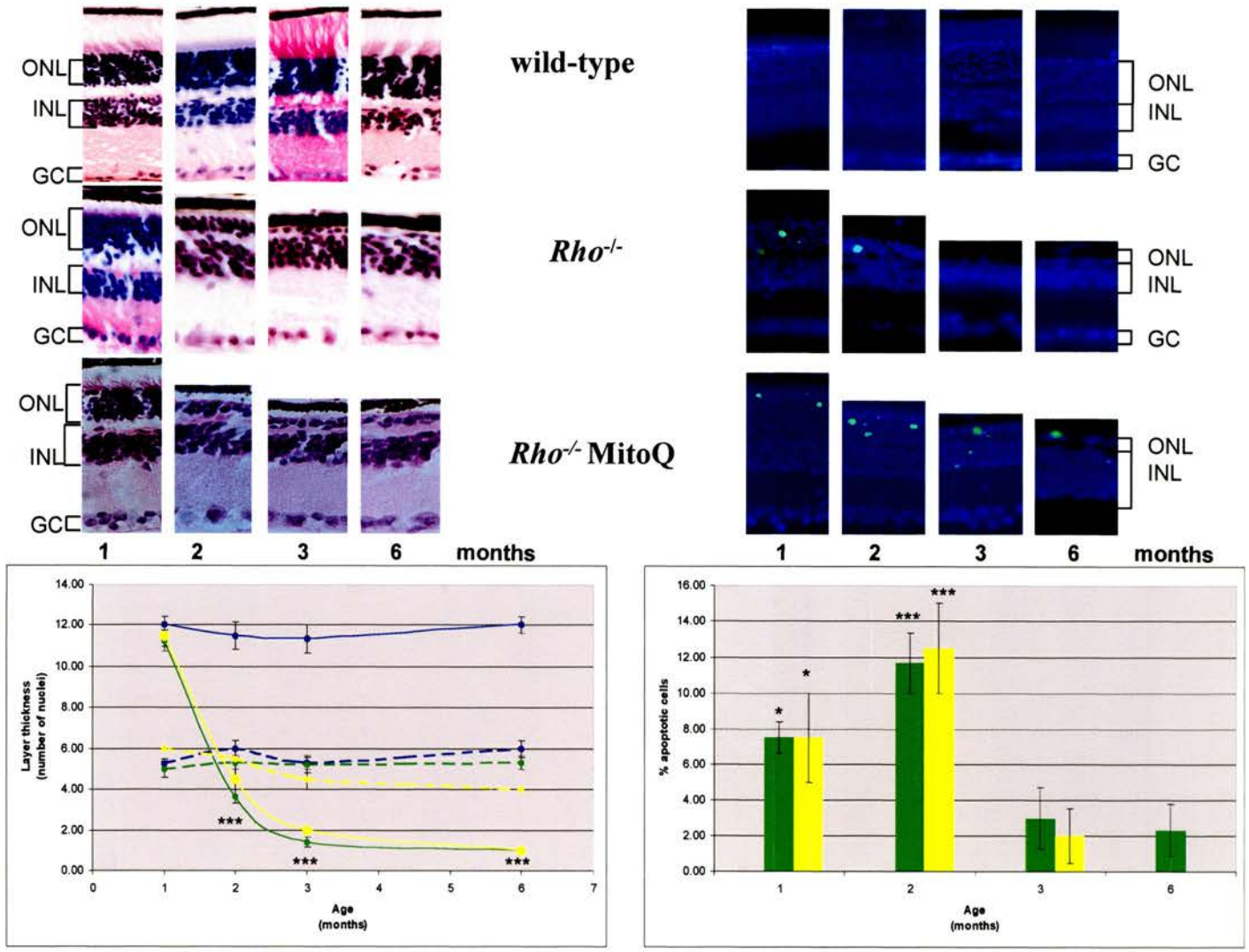

Figure 57: Photoreceptor degeneration in *Rho*$^{-/-}$ mutants after administration of MitoQ

ONL analysis (left panel) and TUNEL assays (right panel) were performed on paraffin-embedded eye sections from *Rho*$^{-/-}$ mutants administered MitoQ. A comparison was made between wild-type (blue) and *Rho*$^{-/-}$ mutants (green) and *Rho*$^{-/-}$ mutants administered MitoQ (yellow). ONL analysis (ONL: solid lines, INL: dotted lines) revealed that, irrespective of antioxidant treatment, photoreceptor degeneration in *Rho*$^{-/-}$ mutants was complete by 3 months of age. MitoQ administration had no effect on the number of apoptotic cells detected by TUNEL assays.(* p<0.05, ** p<0.01, *** p<0.001 compared with wild-type (black)) (ONL: outer nuclear layer; INL: inner nuclear layer; GC: ganglion cells)

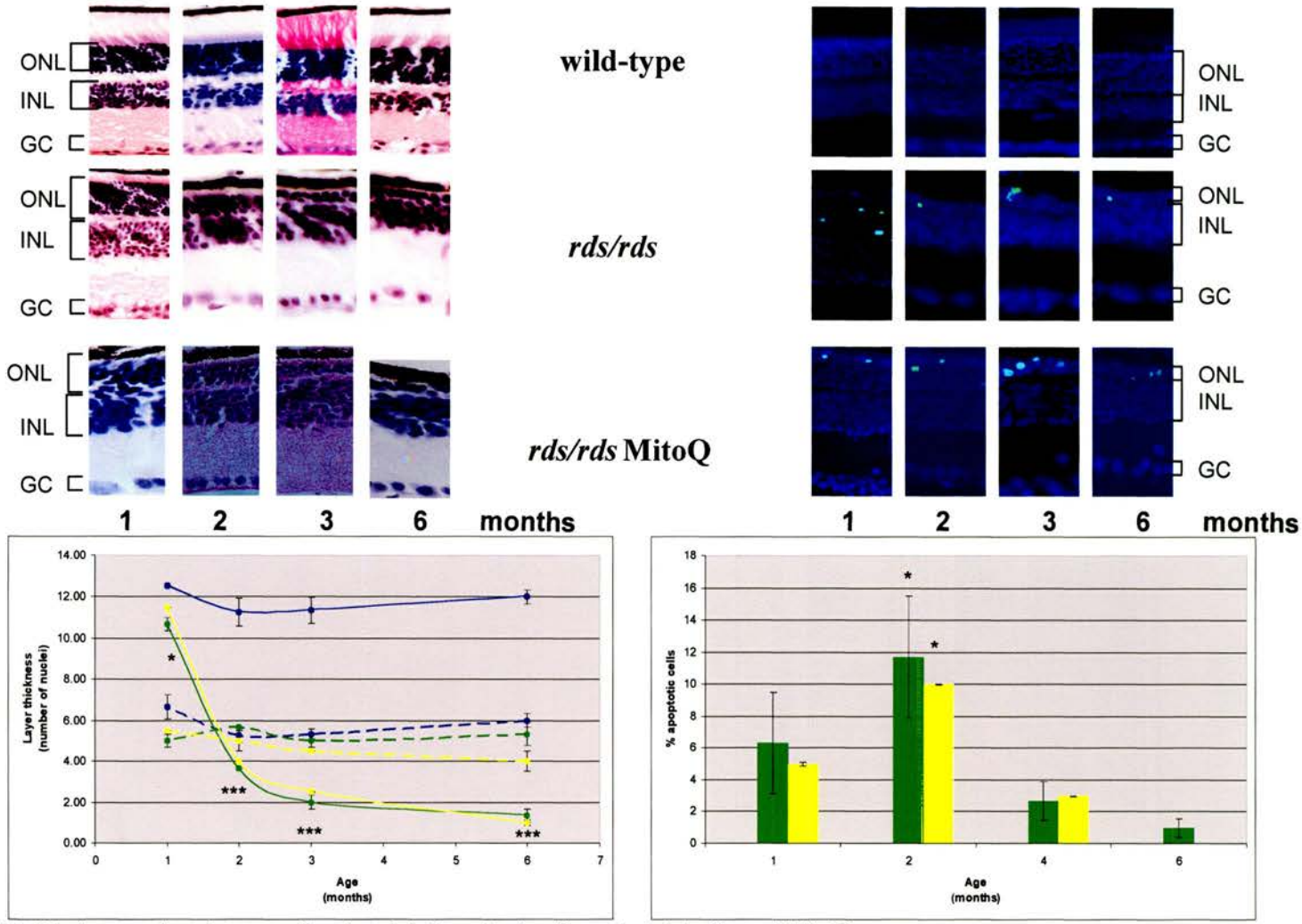

Figure 58: Photoreceptor degeneration in *rds/rds* mutants after administration of MitoQ

ONL analysis (left panel) and TUNEL assays (right panel) were performed on paraffin-embedded eye sections from *rds/rds* mutants administered MitoQ. A comparison was made between wild-type (blue) and *rds/rds* mutants (green) and *rds/rds* mutants administered MitoQ (yellow). ONL analysis (ONL: solid lines, INL: dotted lines) revealed that, irrespective of antioxidant treatment, photoreceptor degeneration in *rds/rds* mutants was complete by 3 months of age. MitoQ administration had no effect on the number of apoptotic cells detected by TUNEL assays. .(* $p<0.05$, ** $p<0.01$, *** $p<0.001$ compared with wild-type (black)) (ONL: outer nuclear layer; INL: inner nuclear layer; GC: ganglion cells)

p>0.05; n=5). The same conclusion was reached for the TUNEL assays, in which TUNEL-positive apoptotic cells were detected at an increasing percentage in the first two months of age and at lower percentages in the following months. MitoQ administration did not cause any significant changes in these measurements.

Finally, administration of the antioxidant to *rds/rds* mice again did not affect the rates of retinal degeneration in these mutants (**Figure 58**). According to the results from the ONL analysis, photoreceptor degeneration progressed at a similar rate in the *rds/rds* mutants, irrespective of treatment. In both treated and untreated samples, photoreceptor degeneration was complete by 6 months of age. The TUNEL assay results confirmed the above observation. There was a significant number of apoptotic cells detected in the *rds/rds* mutant retinas in the first two months of age, and the percentages were unaffected by MitoQ administration. At subsequent time-points of analysis, the percentage of TUNEL-positive cells in the retina dropped significantly and to the same extent in the presence or absence of MitoQ.

To summarise, all four retinal degeneration mutants were administered MitoQ until photoreceptor degeneration was complete. The results from both ONL analysis and TUNEL assays showed that MitoQ administration had no effect on the rates of photoreceptor degeneration in these mutants.

6.3.8.2. Effect of MitoQ administration on mitochondrial enzyme activities in retinal degeneration mutants

The specific activities of citrate synthase (CS) and complex I (CI) were measured in liver, brain, heart and retina mitochondrial samples collected from MitoQ-treated retinal degeneration mutant mice. A comparison was made between these results and those obtained from untreated mutant samples (**Table 10, Figure 59**).

Firstly, the specific activities of the enzymes were measured in wild-type samples collected from animals treated with MitoQ. In no tissue was the activity of either CS or CI either reduced or increased, when compared to samples from non-treated wild-type animals (all p>0.05; n=3-6).

LIVER									
		Citrate Synthase				Complex I			
Genotype	n	activity	se	p_w-value	p_m-value	activity	se	p_w-value	p_m-value
Wild type	4	1.6949	0.1893			0.5969	0.2011		
MitoQ	4	1.7739	0.6605	0.9122		0.6069	0.0869	0.9649	
rd1/rd1	4	2.4467	0.4353	0.1644		0.4743	0.0779	0.5904	
rd1/rd1 MitoQ	4	2.0165	0.5010	0.5700	0.5409	0.5105	0.1363	0.7342	0.8254
atrd1/atrd1	5	1.7838	0.4554	0.8744		0.4807	0.0564	0.5559	
atrd1/atrd1 MitoQ	3	2.3652	0.5033	0.2189	0.4441	0.4368	0.1903	0.6001	0.7903
Rho$^{-/-}$	4	2.3787	0.3408	0.1300		0.3215	0.1168	0.2812	
Rho$^{-/-}$ MitoQ	3	2.3346	0.0257	0.0877	0.9354	0.7838	0.2291	0.6042	0.1086
rds/rds	3	2.3260	0.3538	0.1499		0.4796	0.1843	0.6964	
rds/rds MitoQ	3	2.1103	0.1029	0.2265	0.6732	0.4140	0.1005	0.5844	0.8095
BRAIN									
		Citrate Synthase				Complex I			
Genotype	n	activity	se	p_w-value	p_m-value	activity	se	p_w-value	p_m-value
Wild type	5	3.7515	0.7808			0.2444	0.0518		
MitoQ	4	4.8915	0.7694	0.3401		0.2191	0.0529	0.7452	
rd1/rd1	4	5.3456	0.4538	0.1446		0.3236	0.0522	0.3235	
rd1/rd1 MitoQ	2	4.0993	0.0478	0.8008	0.1413	0.3175	0.0683	0.4714	0.9491
atrd1/atrd1	4	4.3842	0.9078	0.6118		0.3758	0.0211	0.0704	
atrd1/atrd1 MitoQ	2	7.0551	0.8787	0.0630	0.1422	0.4019	0.2170	0.3235	0.3291
Rho$^{-/-}$	3	4.0025	0.2766	0.8208		0.3001	0.0613	0.5236	
Rho$^{-/-}$ MitoQ	3	4.8652	0.7877	0.3852	0.3598	0.1876	0.0071	0.4437	0.1422
rds/rds	3	6.0147	0.6241	0.0935		0.3430	0.0513	0.2564	
rds/rds MitoQ	3	3.4975	0.7695	0.8372	0.0639	0.3751	0.0372	0.1287	0.6388
HEART									
		Citrate Synthase				Complex I			
Genotype	n	activity	se	p_w-value	p_m-value	activity	se	p_w-value	p_m-value
Wild type	4	13.9632	2.3818			1.8227	0.3594		
MitoQ	3	9.2230	1.5564	0.1873		1.1013	0.1562	0.1658	
rd1/rd1	3	17.3775	6.5664	0.0794		1.3934	0.0998	0.3672	
rd1/rd1 MitoQ	3	18.7647	4.8917	0.3783	0.3448	2.0418	0.4833	0.7242	0.2591
atrd1/atrd1	3	18.0613	5.9593	0.5063		1.3424	0.3161	0.3815	
atrd1/atrd1 MitoQ	3	20.1814	5.9117	0.3245	0.8130	1.7980	0.4311	0.9663	0.4421
Rho$^{-/-}$	3	15.4951	5.4382	0.7862		2.5000	0.0325	0.1728	
Rho$^{-/-}$ MitoQ	3	10.7623	1.0155	0.3264	0.4405	1.6640	0.4003	0.7811	0.1059
rds/rds	3	14.3333	3.2423	0.9283		3.2235	0.8895	0.1631	
rds/rds MitoQ	3	15.0110	1.3199	0.7890	0.8848	0.4140	0.1969	0.0633	0.0936
RETINA									
		Citrate Synthase				Complex I			
Genotype	n	activity	se	p_w-value	p_m-value	activity	se	p_w-value	p_m-value
Wild type	6	1.1066	0.1144			0.7248	0.1651		
MitoQ	6	1.0074	0.1905	0.6646		0.5118	0.0836	0.2765	
rd1/rd1	6	1.0074	0.2115	0.6885		0.1541	0.0370	**0.0071**	
rd1/rd1 MitoQ	6	0.8523	0.0855	0.1053	0.5122	0.0924	0.0244	**0.0035**	0.1951
atrd1/atrd1	4	1.3502	0.3817	0.4865		0.1969	0.0630	**0.0377**	
atrd1/atrd1 MitoQ	5	0.8228	0.1447	0.1529	0.2005	0.1817	0.0589	**0.0189**	0.8652
Rho$^{-/-}$	6	0.8719	0.0632	0.1028		0.1058	0.0087	**0.0038**	
Rho$^{-/-}$ MitoQ	5	1.0224	0.1219	0.6134	0.2467	0.1294	0.0585	**0.0115**	0.6273
rds/rds	3	0.8983	0.1653	0.3309		0.0991	0.0107	**0.0361**	
rds/rds MitoQ	3	1.2439	0.0808	0.4602	0.1336	0.2063	0.0256	**0.0242**	**0.0180**

Table 10: Enzyme activities in wild type and retinal degeneration mutants administered MitoQ
Citrate synthase and complex I activities (μmol/min/g tissue) were measured in liver, brain, heart and retina from wild type, retinal degeneration mutants (*rd1/rd1, atrd1/atrd1, Rho*$^{-/-}$ and *rds/rds*) and retinal degeneration mutants administered MitoQ (*rd1/rd1* MitoQ, *atrd1/atrd1* MitoQ, *Rho*$^{-/-}$ MitoQ and *rds/rds* MitoQ. The standard errors (se) and statistical significance compared with wild type (p_w-value) and with single retinal degeneration mutants (p_m-value) are shown. Statistical significant values (p_w or p_m<0.05) are highlighted in red.

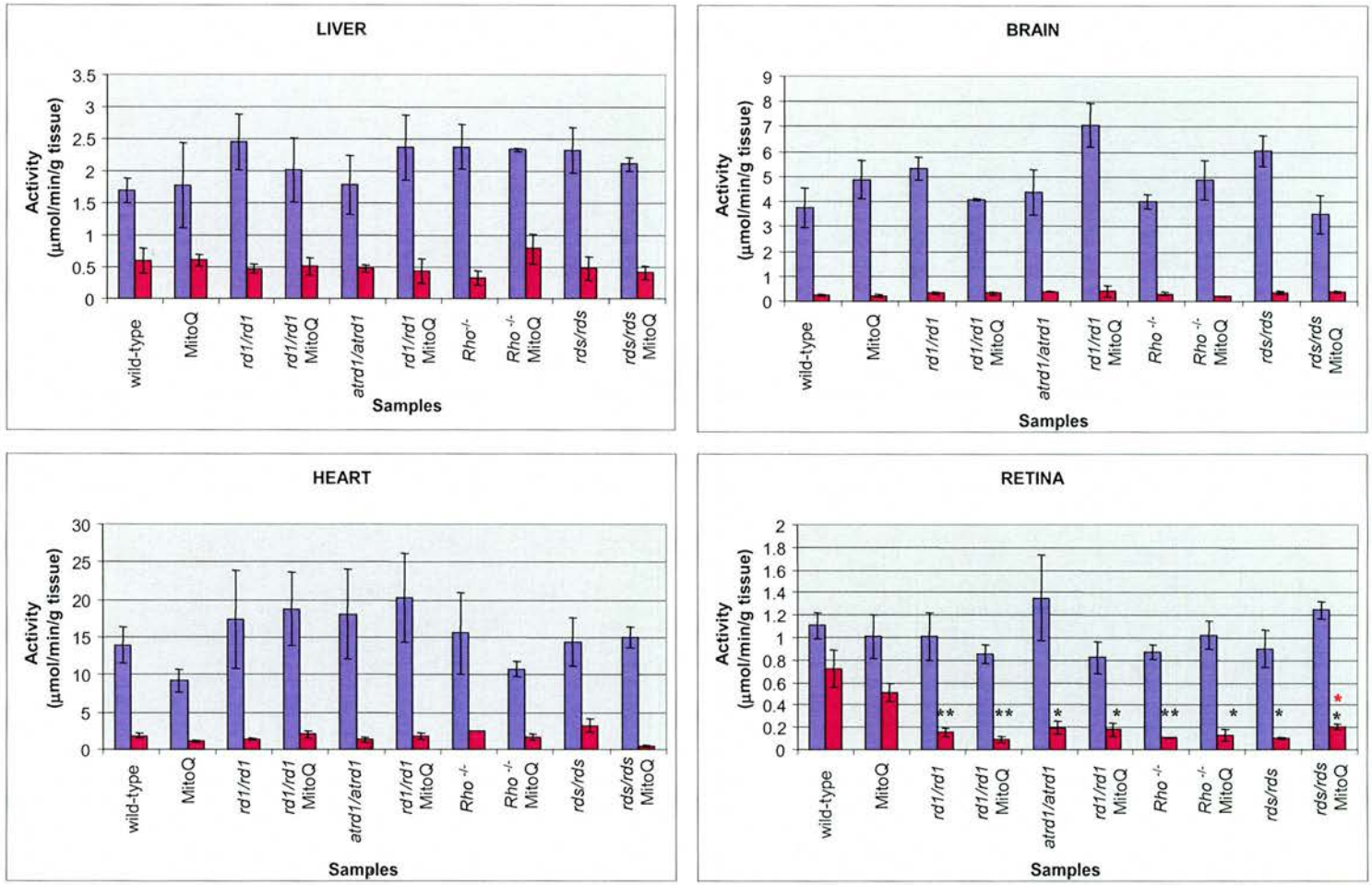

Figure 59: Enzyme activities in retinal degeneration mutants after administration of MitoQ

The activities of citrate synthase (blue columns) and complex I (maroon columns) were measured spectrophotometrically in the liver, brain, heart and retina of the retinal degeneration mutants treated with MitoQ. In all four mutants, treated with MitoQ or not, the activity of citrate synthase remained at wild-type levels. Complex I activity remained similar to wild-type levels in the liver, brain and heart samples of all the mutants, irrespective of treatment. It was significantly decreased, compared to the wild-type, in the retinas of all mutants given or not the antioxidant drug (all $p<0.05$, indicated by *). The latter partly restored the enzyme's activity in the retina of the *rds/rds* mutant ($p=0.018$, $n=3$). (* $p<0.05$, ** $p<0.01$, *** $p<0.001$ compared with wild-type (black) or with MitoQ-untreated retinal degeneration mutants (red))

Secondly, MitoQ administration had no effect on any of the CS or CI activities in liver, brain or heart samples, irrespective of genotype (all $p>0.05$; n=2-5). The same was the case for CS activities measured in retinal samples ($p>0.05$; n=3-6). All MitoQ-administered retinal degeneration mutants had significantly decreased CI activities in their retinas ($p<0.05$; n=3-6) when compared to wild-type. MitoQ administration did however significantly increase the activity of CI in the *rds/rds* mutants ($p=0.018$; n=3), although it was not restored to wild-type levels.

6.3.8.3. Effect of MitoQ administration on reduced glutathione measurements in retinal degeneration mutants

The GSH concentrations in the liver, brain, heart and retina of MitoQ-administered-retinal degeneration mutants were measured (**Table 11**, **Figure 60**).

Firstly, MitoQ administration had no significant effect on the GSH concentrations in any of the wild-type tissues assayed, or in any of the mutant liver samples (all $p>0.05$; all n=3). GSH concentrations in brain samples remained at wild-type levels in all of the mutants administered with the drug. A significant increase previously seen in the GSH concentration of *rds/rds* brain samples was not present in the mice treated with the antioxidant. Similar results were obtained for measurements in *rd1/rd1* and *atrd1/atrd1* heart samples. Upon MitoQ administration, the GSH concentration of $Rho^{-/-}$ heart samples was significantly increased from 0.47 (untreated) to 0.75 μmol/g protein (treated) ($p=0.027$; n=3). Finally, although antioxidant treatment increased the GSH concentration of $Rho^{-/-}$ mutant retinas from 0.041 μmol/g protein towards wild-type levels at 0.057 μmol/g protein, this was not statistically significant ($p=0.215$; n=3).

6.4. Summary and conclusions

In this chapter, the role of oxidative stress in photoreceptor degeneration was investigated by administering a mitochondrially targeted antioxidant to mouse models of RP. The retinal degeneration mutants *rd1/rd1*, *atrd1/atrd1*, $Rho^{-/-}$ and

LIVER					
Genotype	**n**	**concentration**	**se**	**p_w-value**	**p_m-value**
Wild type	3	4.2027	0.1542		
MitoQ	3	4.6227	0.3074	0.4986	
rd1/rd1	3	3.8625	0.7369	0.7752	
rd1/rd1 MitoQ	3	4.7126	0.1881	0.3138	0.5539
atrd1/atrd1	3	3.5817	0.1700	0.2250	
atrd1/atrd1 MitoQ	3	5.5596	0.4625	0.1355	0.0525
Rho$^{-/-}$	3	5.1527	0.1507	0.0758	
Rho$^{-/-}$ MitoQ	3	4.7995	0.8185	0.5197	0.7284
rds/rds	3	4.2940	0.0485	0.8157	
rds/rds MitoQ	3	4.3272	0.1667	0.7875	0.9175
BRAIN					
Genotype	**n**	**concentration**	**se**	**p_w-value**	**p_m-value**
Wild type	3	0.9631	0.1082		
MitoQ	3	1.3134	0.0461	0.2430	
rd1/rd1	3	1.3998	0.0433	0.1586	
rd1/rd1 MitoQ	3	1.4844	0.1013	0.1377	0.6804
atrd1/atrd1	3	1.3015	0.0751	0.3598	
atrd1/atrd1 MitoQ	3	1.6533	0.0786	0.0571	0.1502
Rho$^{-/-}$	3	1.1672	0.0314	0.4683	
Rho$^{-/-}$ MitoQ	3	1.4844	0.1068	0.1975	0.0968
rds/rds	3	2.1092	0.2360	**0.0437**	
rds/rds MitoQ	3	1.8954	0.1838	0.4004	0.1554
HEART					
Genotype	**n**	**concentration**	**se**	**p_w-value**	**p_m-value**
Wild type	3	0.6642	0.0619		
MitoQ	3	0.4675	0.0757	0.3316	
rd1/rd1	3	0.2579	0.0274	**0.0440**	
rd1/rd1 MitoQ	3	0.4632	0.1061	0.3875	0.3401
atrd1/atrd1	3	0.3288	0.0273	**0.0480**	
atrd1/atrd1 MitoQ	3	0.4570	0.0840	0.3264	0.3951
Rho$^{-/-}$	3	0.4714	0.0718	0.3324	
Rho$^{-/-}$ MitoQ	3	0.7447	0.0417	0.6926	**0.0270**
rds/rds	3	0.9538	0.1623	0.3439	
rds/rds MitoQ	3	0.7447	0.0417	0.7080	0.2862
RETINA					
Genotype	**n**	**concentration**	**se**	**p_w-value**	**p_m-value**
Wild type	3	0.0841	0.0052		
MitoQ	3	0.0729	0.0111	0.6630	
rd1/rd1	3	0.0430	0.0029	**0.0253**	
rd1/rd1 MitoQ	3	0.0413	0.0044	**0.0274**	0.8603
atrd1/atrd1	3	0.0747	0.0125	0.6852	
atrd1/atrd1 MitoQ	3	0.0554	0.0076	0.1722	0.6186
Rho$^{-/-}$	3	0.0411	0.0023	**0.0235**	
Rho$^{-/-}$ MitoQ	3	0.0568	0.0081	0.1863	0.2151
rds/rds	3	0.0778	0.0046	0.6741	
rds/rds MitoQ	3	0.0809	0.0124	0.8735	0.8665

Table 11: Reduced glutathione concentrations in wild type and retinal degeneration mutants administered MitoQ

Reduced glutathione concentrations (μmol/g protein) were measured in liver, brain, heart and retina from wild type, retinal degeneration mutants (*rd1/rd1, atrd1/atrd1, Rho*$^{-/-}$ and *rds/rds*) and retinal degeneration mutants administered MitoQ (*rd1/rd1* MitoQ, *atrd1/atrd1* MitoQ, *Rho*$^{-/-}$ MitoQ and *rds/rds* MitoQ . The standard errors (se) and statistical significance compared with wild type (p_w-value) and with single retinal degeneration mutants (p_m-value) are shown. Statistical significant values (p_w or p_m<0.05) are highlighted in red.

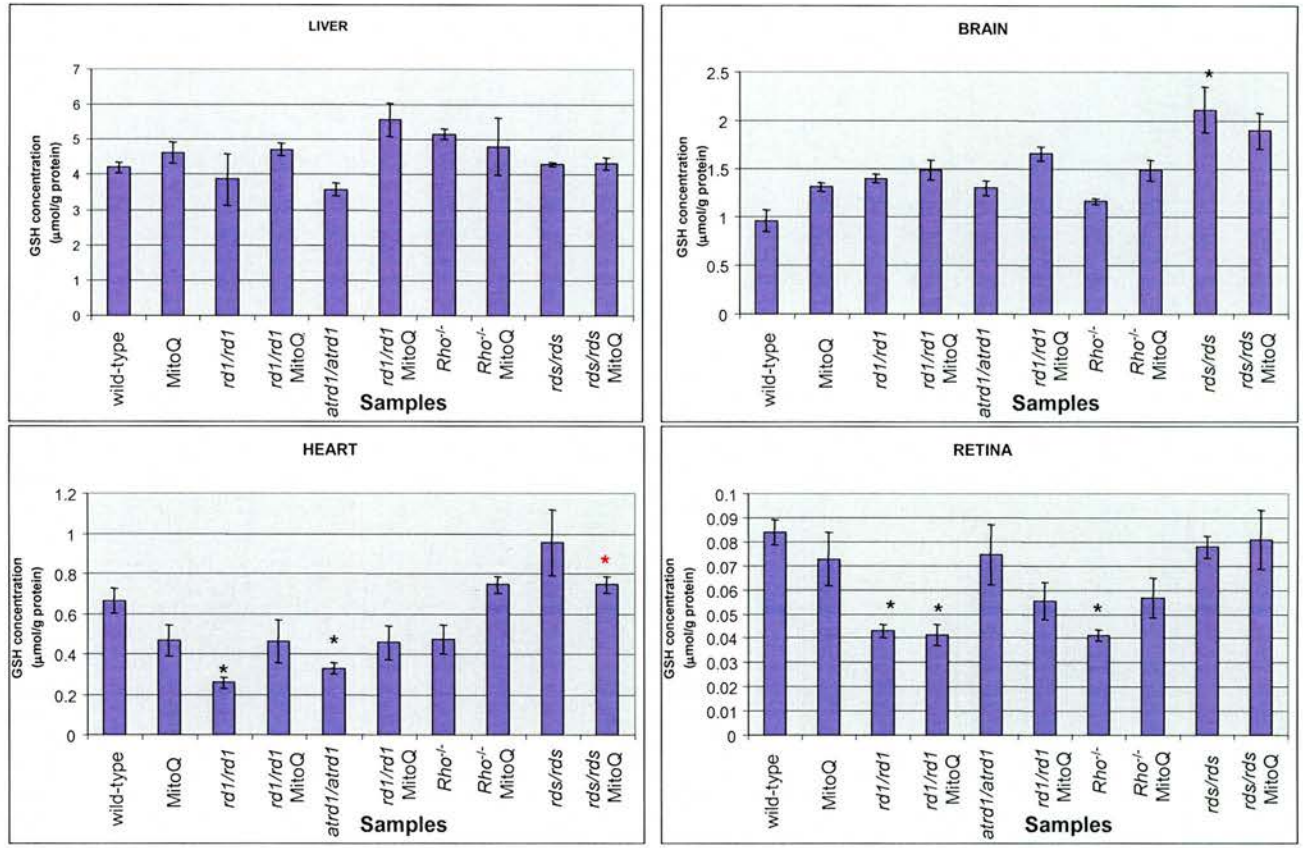

Figure 60: Reduced glutathione (GSH) concentrations in various tissues from wild-type and retinal degeneration mutants administered with MitoQ

GSH concentrations were measured in the liver, brain, heart and retina of retinal degeneration mutants treated with MitoQ. MitoQ administration had no effect on GSH concentrations in most samples. The GSH concentration was only significantly increased in *Rho*$^{-/-}$ heart upon antioxidant treatment. (* $p<0.05$, ** $p<0.01$, *** $p<0.001$ compared with wild-type (black) or with MitoQ-untreated retinal degeneration mutants (red))

rds/rds were treated with the ubiquinone analogue MitoQ, from conception until photoreceptor degeneration was complete. This is the first study in which MitoQ was orally administered to mice for a long period of time. In a previous *in vivo* study by Smith *et al.* (2003), administration of the drug at a concentration of 500 μM for 26 days was shown to have no side-effects to the animals. In Chapter 4 it was shown that retinal degeneration in the mutants is complete within between 3 weeks and 3 months of age, so it was necessary to confirm the safety of long-term oral administration of the antioxidant. Adult wild-type mice were therefore treated with a low (250 μM) or high (500 μM) dose of MitoQ for 3 months, during which period, the health of the animals was monitored daily. MitoQ administration, at either dose, had no side effects and the food consumption, weight gain and breeding capacity were unaffected by drug treatment. The possibility that neonatal survival was affected by MitoQ was considered, since some of the litters on either the low or high dose died shortly after birth. However, the absence of similar cases in consecutive wild-type and mutant litters did not support this possibility. It was therefore concluded that long-term oral administration of MitoQ at a 500 μM concentration was safe for the animals.

The uptake of MitoQ by whole retina and retinal mitochondria was investigated. This was carried out by using two chemically similar compounds, namely 4-iodobutyl-triphenylphosphonium (IBTP) and tritium-labelled MitoQ (^{3}H-MitoQ). Both compounds have been used for the same purpose by other investigators, and their uptake by isolated mitochondria, cells and some tissues has been shown (Kelso *et al.*, 2001; Lin *et al.*, 2002; Smith *et al.*, 2003). The IBTP results confirmed the uptake of mitochondrially-targeted antioxidants firstly by heart mitochondria after oral administration and secondly by isolated heart and liver mitochondria treated with the compound post-fractionation. The anti-IBTP antibody showed some non-specific binding, suggesting that different conditions or antibodies may be necessary to show uptake of IBTP by retina mitochondria after oral administration. Further experiments with ^{3}H-MitoQ showed uptake by several tissues, including retina. The mitochondrial uptake of ^{3}H-MitoQ was not investigated because this compound would not be retained in these organelles upon tissue fractionation and dissipation of the membrane potential. In summary, the mitochondrial uptake of MitoQ-like compounds was confirmed by use of

IBTP and their retina uptake was confirmed by the use of ^{3}H-MitoQ. These were sufficient indications for uptake of MitoQ by retina mitochondria.

The effect of MitoQ on wild-type and retinal degeneration mutants was assessed. Firstly, it was confirmed that administration of the drug was not compromising the structure or function of the retina, since no photoreceptor degeneration was evident in wild-type samples after administration of the antioxidant. In addition, the activity of complex I (CI) did not decrease and the GSH concentration remained constant at wild-type levels in MitoQ-treated wild-type samples. Although an increase in enzyme activity and GSH concentration would agree with administration of an antioxidant, the absence of these observations is not surprising. It is possible that in wild-type mice CI activity and GSH concentration are a maximum level which does not increase further.

Secondly, the retinal degeneration rates of *rd1/rd1*, *atrd1/atrd1*, *Rho*$^{-/-}$ and *rds/rds* mutants were assessed and MitoQ administration did not influence the rates of photoreceptor degeneration in any of the mutant samples. The failure of MitoQ to alter rates of retinal degeneration cannot be attributed to failure of the antioxidant to reach the target tissue, as its uptake by the retina was confirmed. Moreover, Adlam *et al.* (2005) demonstrated the antioxidant efficiency of MitoQ by orally administering the compound to rats and protecting heart function from ischemia-reperfusion injury. There are therefore two possible explanations for the failure to slow rates of degeneration. Firstly, the amount of administered MitoQ might not have been sufficient to reduce the rate of degeneration in the mutants. The results of the preliminary study, which confirmed the safety of long-term administration of 500 μM MitoQ, suggest that increased doses might also be safe to administer. Secondly, the fast degeneration rates, observed particularly in the *rd1/rd1* and *atrd1/atrd1* mutants, suggest that the mutations confer pathology of such severity that it is difficult to reverse.

At a biochemical level, MitoQ administration had some effect on enzyme activities and reduced glutathione concentrations. As expected, treatment with the antioxidant did not cause a change in any of the CS or CI activities in liver, brain and heart mutant samples. These were at wild-type levels in the absence of MitoQ and remained at the same levels after its administration. Similarly, the activity of

CS in all retina samples remained unchanged and similar to wild-type. MitoQ administration did not restore the previously observed decrease in CI activities in the retinal degeneration mutants, with one exception. In the *rds/rds* mutant, the activity of CI was significantly increased upon MitoQ treatment ($p=0.018$; $n=3$).

The fact that MitoQ administration did not change the rates of photoreceptor degeneration in the retinal degeneration mutants but ameliorated the loss of CI activity in the slower degeneration of *rds/rds* mice supports the possibility that the severity of the retinal degeneration mutation matters. Therefore, the administration of MitoQ to mutants in which the retinal degeneration progressed even more slowly might prove to be more fruitful.

To summarise, although the long-term oral administration of MitoQ at a concentration of 500 μM was shown not to be toxic to mice and there was some evidence of the uptake of the compound by retina mitochondria, it had no effect on the rates of photoreceptor degeneration in retinal degeneration mutants. The most promising result was the apparent partial rescue of the reduction in CI activity in the slowest mutant *rds/rds*, suggesting that further experiments to confirm and extend this result are justified.

CHAPTER 7

DISCUSSION

The main aim of this project was to determine the role of oxidative stress in retinal degeneration. The hypothesis that oxidative stress influences rates of degeneration was tested by crossing four mouse models for retinitis pigmentosa (RP) (*rd1/rd1*, *atrd1/atrd1*, *Rho*$^{-/-}$ and *rds/rds*) to heterozygous *Sod2*$^{+/-}$ knockout mice or by treating them with the mitochondrially targeted antioxidant, MitoQ. The rates of photoreceptor degeneration and levels of oxidative damage in the mouse models were assessed and changes in response to decreased *Sod2* expression or treatment with an antioxidant were investigated.

The hypothesis underlying this project assigns a general role to oxidative stress in retinal degeneration (Wright *et al.*, 2004). ROS production may or may not be directly implicated in either the generation or the pathology of retinal degeneration resulting from genetic mutations, but it is proposed to be indirectly implicated, regardless of the cause. Mutations in 40 genes have either been mapped or identified in RP (**Table 1**), each of which imposes a cellular stress, not always including oxidative stress, on photoreceptors and leads to apoptosis. The cellular redox state, which is cell type- and species-specific, can however influence the probability of cell death by apoptosis. The link between oxidative stress and apoptosis is based primarily on the dual role of mitochondria as both the major generators of oxidative stress and the mediators of the intrinsic apoptotic pathway, the principal mode of cell death in RP. The hypothesis therefore postulates that a change in the steady state level of ROS production, by experimentally altering the levels of antioxidant defences, would affect the probability of cell death in any given retinal degeneration, regardless of whether oxidative stress is primarily implicated in the disease.

The model supporting this hypothesis is diagrammatically presented in **Figure 61**. **Figure 61Ai** shows that in a homogeneous *population* of cells, the probability of apoptosis follows a normal bell-shaped distribution. A fixed cell death threshold (red dotted line) determines the proportion of apoptotic cells ($\mathbf{n_a}$). The mean probability of apoptosis can vary between different cell types and/or species, in such a way that the 'bell' shifts position along the x-axis and as a result the proportion of apoptotic cells $\mathbf{n_a}$ changes (**Figure 61Aii**). External insults, including genetic mutations and environmental effects may account for this shift. For example, the increased vulnerability of the photoreceptor cells

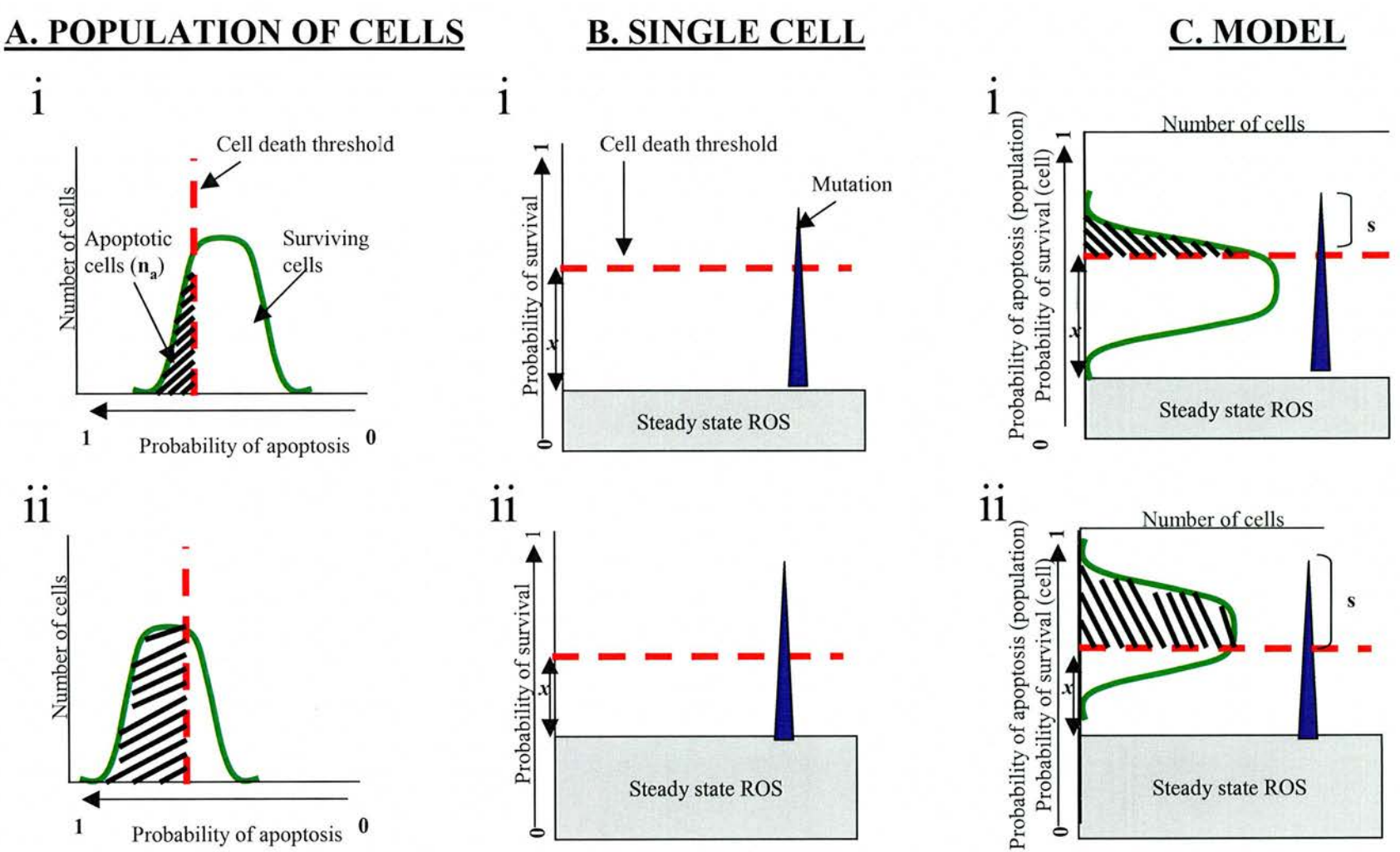

Figure 61: Schematic representation of retinal degeneration model

(Ai) In a population of cells, the probability of apoptosis follows a normal distribution. A fixed cell death threshold dictates the proportion of apoptotic cells ($\mathbf{n_a}$) in this population . **(Aii)** A shift in the mean probability of apoptosis affects $\mathbf{n_a}$. **(Bi)** A cell has an apoptotic threshold (red dotted line), a survival probability x, a probability of apoptosis $1\text{-}x$ and a given steady-state ROS production. Mutations (peaks) of different severity (peak height) are present in different neurodegenerations, some of which cross the apoptotic threshold and lead to cell death, while others are mild enough to go unnoticed. **(Bii)** Changes in the level of mitochondrial ROS production can influence the probability of apoptosis. **(Ci)** The combination of the mean probability of apoptosis of a population of cells (**Ai**) and of the probability of apoptosis and ROS production of single cells (**Bi**) shows how steady state ROS production can influence the degeneration of a population of cells. The rate at which degeneration occurs is a function of $\mathbf{n_a}$ and of mutation severity s.

attributed to increased PUFA concentration, high oxygen tension and light exposure, can result in an increased $\mathbf{n_a}$ in comparison to a population of liver cells that are not exposed to these sources of oxidative stress. **Figure 61Bi** shows the *single-cell* situation. A cell has an apoptotic threshold (red dotted line), a probability of survival ($\boldsymbol{x}$), a probability of apoptosis ($\boldsymbol{1-x}$) and a given steady state ROS production. Mutations (peaks) of different severity (peak height) may be present in the cell, and some may be severe enough to cross the apoptotic threshold, and lead to cell death, whereas others are mild enough to go unnoticed. There are different factors that can influence $\boldsymbol{x}$, including environmental, genetic and metabolic influences. One factor that has been shown to greatly influence cell survival is the steady state production of ROS, which are constitutively generated in mitochondria as a result of leaking electrons from the ETC. ROS formation has been inversely correlated with lifespan (Wright *et al.*, 2004), suggesting that increased production of free radicals increases the probability of apoptosis. Both the apoptotic threshold of a cell and its level of steady state mitochondrial ROS production are dependent on the type of cell and the species. Different cell types have a different susceptibility to 'external insults', which dictate their apoptotic thresholds, as mentioned above. As a result, exactly the same mutation expressed in two different cell types would not affect the survival of the two cells equally. Also, ROS production differs between species, so that, for example, mice have increased mitochondrial H_2O_2 production compared to cows (Sohal *et al.*, 1989; 1990). A photoreceptor cell therefore in two different species would have the same apoptotic threshold, as it is exposed to similar 'external insults', but the level of species-specific ROS production would affect its probability of survival when the same mutation or other cellular stress is present. The shift in the mean apoptotic probability of a population of cells and in the level of the cell apoptotic threshold, as determined by cell and species characteristics, are depicted in **Figure 61Aii** and **Bii**, respectively.

All these factors are summarised in **Figure 61Ci**, in which the probabilities of apoptosis and survival are overlaid on the y-axis, to illustrate schematically how ROS production could influence the rate of degeneration of a tissue.

A few points about the above model need to be clarified. Firstly, the cell death thresholds depicted in both the population of cells and in single cells are

virtually the same. The only difference lies in the fact that in the population of cells the cell death threshold is fixed and $\mathbf{n_a}$ changes in response to shifting of the mean apoptotic probability (the 'bell'). In contrast, in a single cell, the apoptotic threshold can shift in a cell type- and/or species-dependent manner. When however one focuses on a single cell type in a single species this apoptotic threshold is also assumed to be fixed. Therefore, a decreased apoptotic threshold implies both an increased single-cell probability of apoptosis and an increased proportion of a population of cells of doing so as well.

Secondly, although the probability axes have been overlaid and are on the same scale, from zero to one, they are used separately. A probability of apoptosis is used when referring to a population of cells, whereas a probability of survival is used when referring to a single cell.

Thirdly, steady state ROS production also influences the probability of apoptosis. In a single cell, whether a mutation causes it to cross the apoptotic threshold depends on the level of ROS production, which, if high enough, will lower $\boldsymbol{x}$ sufficiently to do so. The severity of the mutation is reflected by the height of the peak ($\boldsymbol{s}$). In a population of cells, where the apoptotic threshold is fixed, ROS production may shift the mean probability of apoptosis. The rate at which a population of cells degenerates depends both on the mean probability of apoptosis, which determines $\boldsymbol{n_a}$, and on the severity of the cell mutation, which determines s. In summary, the rate of degeneration of a homogeneous population of cells is a function of n_a and s, both of which are influenced by ROS levels. As shown in **Figure 61Cii**, increased ROS production can both shift the mean cell population probability of apoptosis and increase n_a or decrease the probability of cell survival x by 'elevating' the baseline of the mutation, which increases s.

In this project, the aim was to test the above hypothesis using a single species (mouse), a single cell type (photoreceptor cell) and four distinct genetic mutations (*Pde6b*^{rd1}, *Pde6b*^{atrd1}, *Rho* and *Prph2*^{rds}). All mouse photoreceptors are assumed to have the same apoptotic threshold and equal levels of steady state ROS production (**Figure 62A-2E**). What differs is the severity of the mutations present in the cell, which can be predicted based on published data.

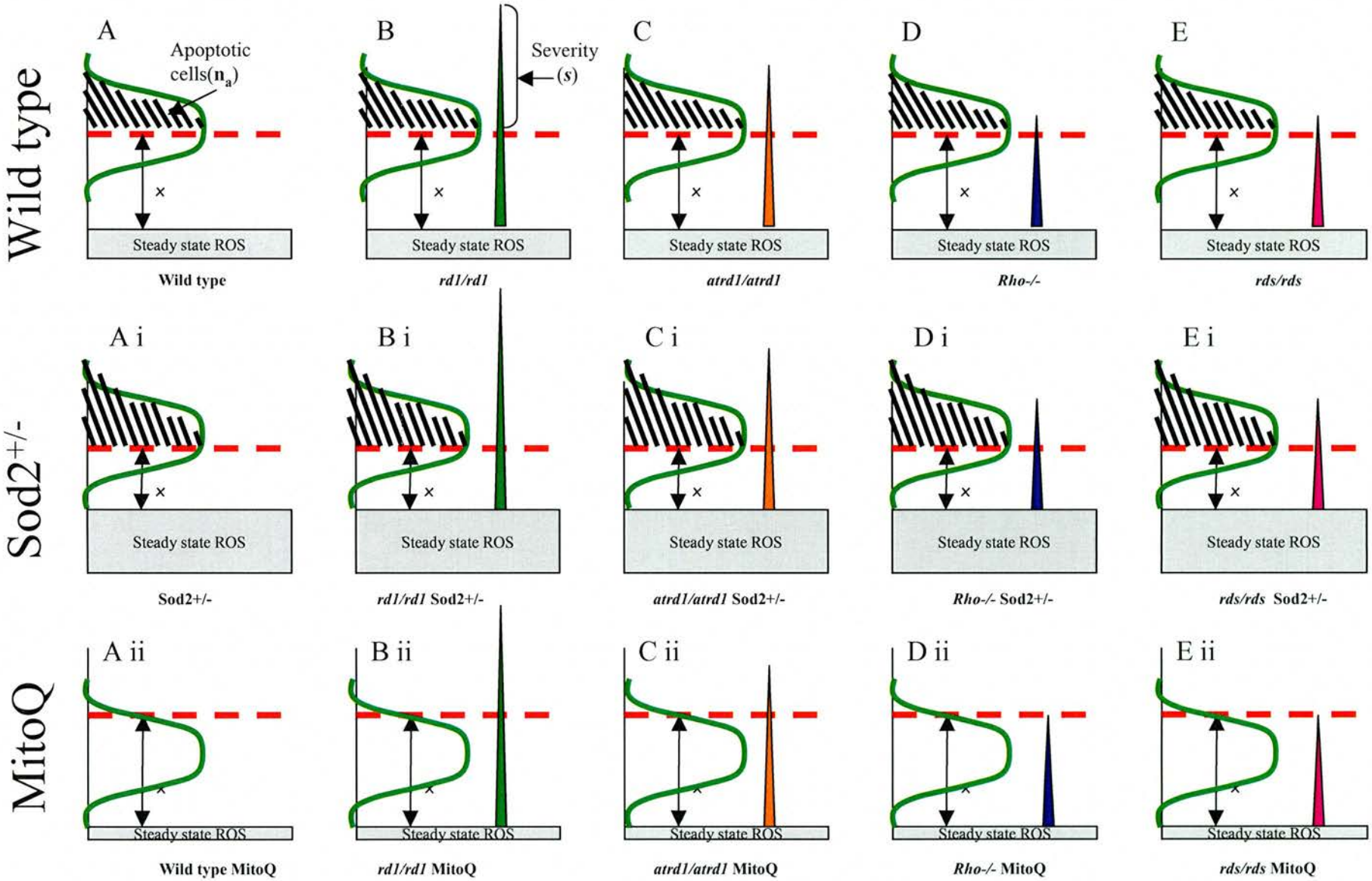

Figure 62: Schematic representation of the retinal degeneration model on the current project

A wild type photoreceptor cell **(A)** has a probability of survival ***x*** which depends on its steady state ROS production and on its apoptotic threshold. In a population of wild type cells the proportion of apoptotic cells $\mathbf{n_a}$ is determined by the cell death threshold. Four different mutations are separately expressed in photoreceptor cells; **(B)** *rd1/rd1*, **(C)** *atrd1/atrd1*, **(D)** *Rho-/-* and **(E)** *rds/rds.* They all exceed the apoptotic threshold of the photoreceptor cells, but because of their distinct severities (***s***) they lead to retinal degeneration at different rates. **(Ai)** Reduction in the expression of *Sod2* increases the steady state ROS production, lowers the probability of survival ***x*** and increases the proportion of apoptotic cells $\mathbf{n_a}$. In the mutants **(Bi-Ei)** this should result in increased rates of degeneration. Conversely, administration of the antioxidant MitoQ lowers the level of steady state ROS production **(Aii)** and this should slow the rates of degeneration in the mutants **(Bii-Eii)**

The rate at which a population of photoreceptor cells degenerate in each mutant is a function of the proportion of apoptotic cells in the population ($\mathbf{n_a}$) and of the severity of the genetic mutation (*s*) present in the cell. It follows that, with fixed thresholds and probabilities of apoptosis, that are specific to mouse photoreceptor cells, it is the mutation severities that determine degeneration rates in the mutants. The steady state ROS production was modified by either decreased Sod*2* expression (**Figure 62Ai-2Ei**) or MitoQ treatment (**Figure 62Aii-2Eii**). According to the model, increased oxidative stress in the mutants should increase the probability of apoptosis and speed up the rates at which photoreceptor cells degenerate. Similarly, exposure to the antioxidant MitoQ should reduce ROS production, and depending on the severity of the causal mutations, reduce the proportion of cells that cross the apoptotic threshold.

The results of the project are summarised in **Figures 63** and **64**. Briefly, rates of degeneration were estimated in each of the four mutants by both ONL analysis and TUNEL assays, and a comparison was made between the single retinal degeneration mutants, mutants crossed to *Sod2* heterozygous knockout mice and mutants treated with the antioxidant MitoQ. The genetic heterogeneity of retinal degeneration, discussed by Rivolta *et al.* (2002), was confirmed by the distinct degeneration rates observed in each of the mutants. Neither the rates of retinal degeneration nor the percentages of TUNEL-positive cells were altered in response to modified cellular redox states. Additionally, the levels of oxidative damage were assessed both by spectrophotometric enzyme assays and by reduced glutathione measurements. Signs of oxidative damage were detected in all four mutants, but their levels were not universally altered by modifying steady state ROS production. The decreased *Sod2* expression further compromised complex I activity in the homozygous *atrd1* mutant, while treatment with MitoQ ameliorated this enzyme's activity in the *rds/rds* mutant.

Distinct degeneration rates in the mutants

The rates at which the retinal degenerations proceeded in the four mutants were quite distinct, taking 3 weeks, 6 weeks, 3 months and 3 months to be completed in the *rd1/rd1*, *atrd1/atrd1*, *Rho*$^{-/-}$ and *rds/rds* mutants, respectively (**Figure 63,** left column). Similar rates of degeneration have been previously reported by

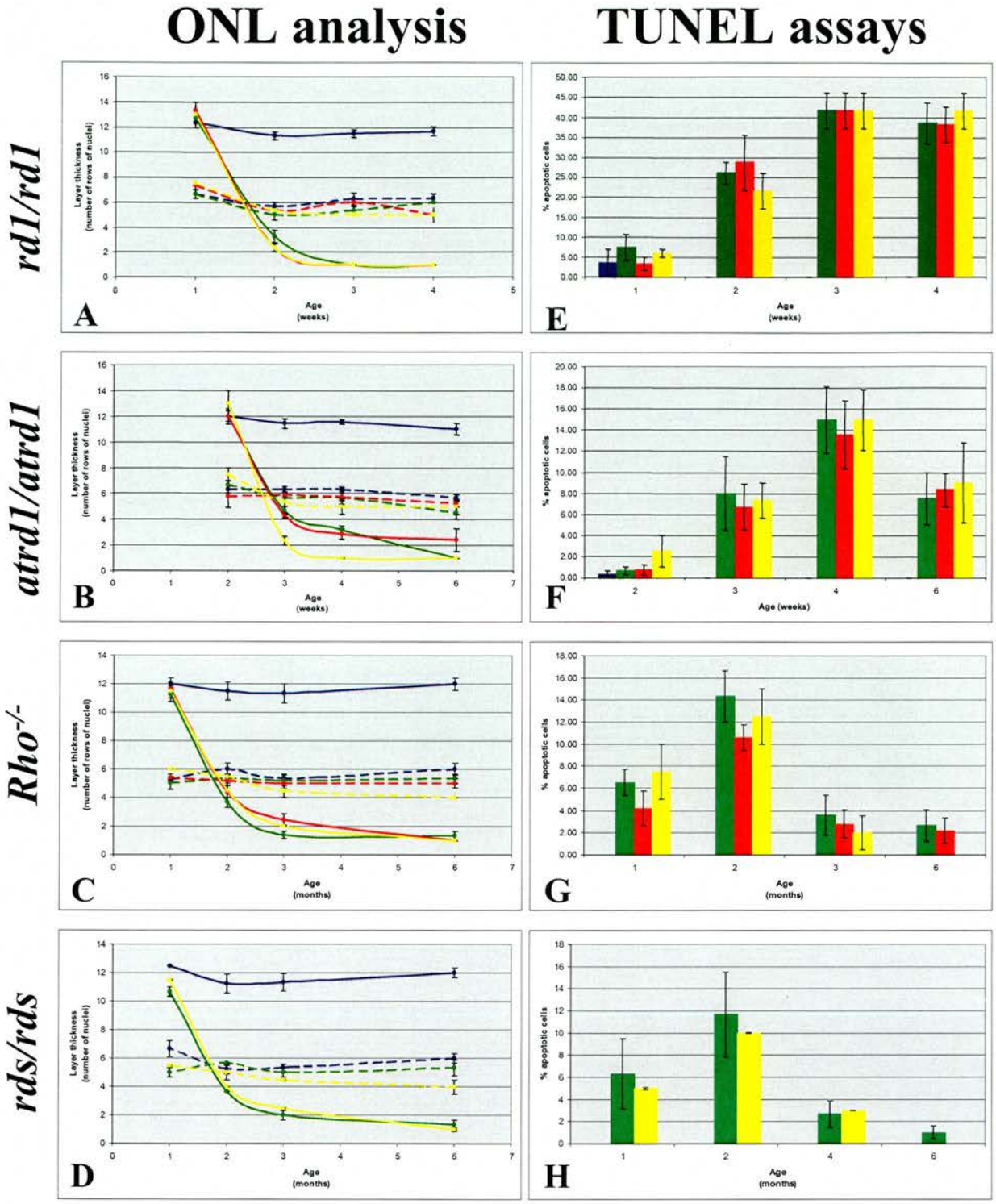

Figure 63: Summary results - Photoreceptor degeneration in retinal degeneration mutants

Photoreceptor degeneration was measured in (**A**, **E**) *rd1/rd1*, (**B**, **F**) *atrd1/atrd1* (**B**, **F**), (**C, G**) *Rho*$^{-/-}$ and (**D, H**) *rds/rds* mutants by (**A-D**) ONL analysis (ONL: solid lines,, INL: dotted lines) and (**E-H**) TUNEL assays. A comparison was made between wild-type samples (blue), single retinal degeneration mutants (green), mutants with decreased *sod2* expression (red) and mutants treated with MitoQ (yellow).

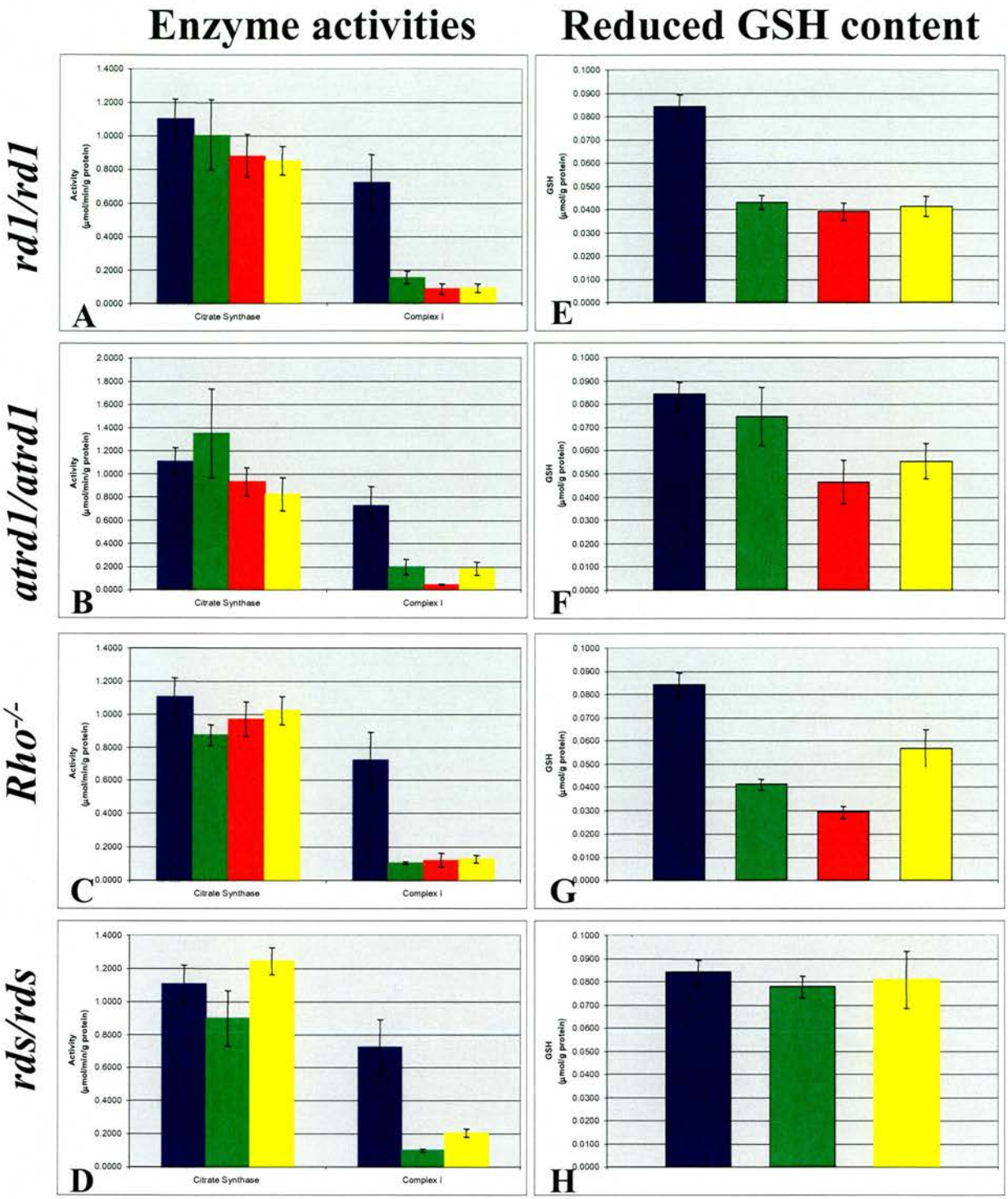

Figure 64: Summary results - Oxidative damage in retinal degeneration mutants

Oxidative damage was assessed in (**A**, **E**) *rd1/rd1*, (**B**, **F**) *atrd1/atrd1* (**B**, **F**), (**C, G**) *Rho*$^{-/-}$ and (**D, H**) *rds/rds* mutants by (**A-D**) spectrophotometric enzyme assays and (**E-H**) by measurements of reduced GSH contents. A comparison was made between wild type samples (blue), single retinal degeneration mutants (green), mutants with decreased *sod2* expression (red) and mutants treated with MitoQ (yellow).

Farber & Lolley (1974), Hart *et al.* (2005), Humphries *et al.* (1997) and Travis *et al.* (1991) for these muatnts. The results from the TUNEL assays (**Figure 63,** right column) were consistent with the ONL analysis results, confirming the estimated rates of degeneration. However, Portera-Cailliau *et al.* (1994) previously reported that in the *rd1/rd1* mouse the number of TUNEL-positive cells peaked at P14, compared with P21 in this study, while that in the *rds/rds* mouse did so at P18 and P30, compared with P14 here. Failure to observe exactly the same peaks of apoptosis in this project can be attributed to the time intervals over which samples were analyzed. These were probably not sufficiently tight to allow the detection of the precise peaks of apoptotic cell death. Nevertheless, the results were broadly very similar to those published by others.

Sod2 effects on retinal degeneration

Prior to analyzing the retinal degeneration double mutants, in which *Sod2* expression was halved, the retinal phenotype in the *Sod2* heterozygous null mutant was analyzed. An abnormal retinal phenotype was previously reported in $Sod2^{-/-}$ null mice at P20, but this did not include photoreceptor degeneration, possibly due to the early lethality of these animals (Sandbach *et al.*, 2001). In this project, $Sod2^{+/-}$ heterozygotes showed no signs of photoreceptor degeneration. As expected, all of the tissues assayed had decreased complex I activity (all $p<0.05$), and the GSH concentration was significantly reduced ($p<0.05$) by approximately 60% in the retina, brain and liver of these mice. Published studies have also reported reduced complex I activity and reduced GSH concentration in $Sod2^{+/-}$ mutants mutants (van Remmen *et al.* 1999). Although these results show a ubiquitous increase in oxidative stress in $Sod2^{+/-}$ mice, this was not sufficient to trigger photoreceptor apoptosis in these mutants. A direct effect of oxidative stress, caused by decreased *Sod2* expression on photoreceptor apoptosis was therefore excluded, arguing against the proposed model. In contrast to these results in the retina, a similar decrease in *Sod2* expression has been shown to increase apoptosis in other tissues. For example, the mitochondrial dysfunction observed in the heart of $Sod2^{+/-}$ heterozygotes is accompanied by an increased incidence of cardiomyocyte apoptosis (van Remmen *et al.*, 2001). This might suggest that basal steady state ROS production is higher in cardiomyocytes than in photoreceptor cells, so that the survival probability (***x*** in **Figure 61**) is lower in

these cells. Steady state mitochondrial H_2O_2 formation is high in heart relative to other tissues (Wright *et al.*, 2004), although the corresponding value for retina has not been published.

The retinal degeneration phenotype includes oxidative damage

The involvement of oxidative stress in the pathology of the retinal degeneration mutants analysed in this project has not previously been reported, except in the cases of *rd1/rd1* and *rds/rds*, where up-regulation of clusterin and ceruloplamsin, which are markers of oxidative stress, have been detected (Lohr *et al.*, 2006). In the present study, signs of oxidative damage were detected in all four mutants (**Figure 64,** left column). The observation that complex I activity was reduced only in the retinas of these models, and not in other tissues or in wild-type samples, while citrate synthase activity remained unchanged in all tissues, shows a direct effect of each mutation on increasing oxidative stress. Additionally, the retinal GSH concentration of *rd1/rd1* and $Rho^{-/-}$ mutants was significantly reduced compared to the wild-type ($p<0.05$) (**Figure 64,** right column).

A role for oxidative stress in retinal degeneration has been suggested before. The increased oxygen tension imposed by the choroidal blood flow, the high metabolic rate of the retina compared to other tissues which is shown by its elevated consumption of oxygen, and the high concentration of PUFAs, are three of the factors that render the wild-type retina prone to oxidative damage (Travis, 1998). It is therefore conceivable that the damaging effect of oxidative stress, even in wild-type photoreceptor cells, would be magnified in retinal degeneration mutants. Indeed, it has been suggested that the failure of *rds/rds* and *Rho* knockout mutants to form OS results in the proximity of the mitochondria to an increased pO_2, and hence to a possible increase in free radical production (Travis, 1998). Finally, although RP-type retinal degenerations primarily affect the survival of rod photoreceptors, cone photoreceptors also degenerate as a consequence and this has been shown to involve oxidative damage (Shen *et al.*, 2005). One possibility is that the decreased complex I activities reported in the mutants analysed are reflecting cone oxidative damage rather than rod damage. However, this is excluded, since the mouse retina is richer in rods and sample collection took place before complete retinal degeneration. If in the samples

assayed rods were oxidative damage-free their present majority should mask the cone damage.

Although oxidative damage has been previously reported in photoreceptor degeneration attributed to light exposure (Donovan *et al.*, 2001) and increased expression of genes implicated in oxidative stress has been detected in the *rd1/rd1* and *rds/rds* mutants (Lohr *et al.*, 2006), this is the first time that oxidative damage to complex I activity has been reported in these four retinal degeneration mutants. This implies post-translational damage to complex I subunits, perhaps including oxidation of thiols, nitration, nitrosylation and other changes, which could be investigated further by mass spectrometry.

Decreased *Sod2* expression and complex I activity

Decreasing the level of the antioxidant superoxide dismutase in the retinal degeneration mutants increased the level of oxidative damage only in the *atrd1/atrd1* mutant ($p=0.048$; $n=5$). This result was particularly unexpected given that complex I activity was already severly compromised in all the assayed tissues of the *Sod2* heterozygous knockout mouse. The difference in mutation severity between the *rd1/rd1* and *atrd1/atrd1* mutants, which is shown by their distinct rates of photoreceptor degeneration, may explain why only the slower (*atrd1*) degeneration shows a further change in complex I activity. The pathology of the *atrd1/atrd1* mutant has not been investigated in detail, since it was only recently generated by ENU mutagenesis (Thaung *et al.*, 2002). The causal mutation is in the *Pde6b* gene, which is the same as in the *rd1* mouse, suggesting that in the *atrd1* homozygous mouse there may also be an increase in cGMP levels, causing opening of cGMP-gated cation channels and an increase in the influx of cations, including Ca^{2+}. There is evidence that increases in Ca^{2+} can act as a trigger for cell death (Olshevskaya *et al.*, 2004). High outer segment Ca^{2+} has also been implicated as a causal factor in apoptosis in other retinal degenerations (Yuan *et al.*, 2003, Fain 2006). It seems however that in the homozygous *atrd1* mutant and not in the *rd1* mutant, despite the genetic mutation, additional oxidative damage is possible. If the proposed retinal degeneration model (**Figure 61**) is correct, it is not clear why decreased *Sod2* expression had no effect on photoreceptor degeneration in the $Rho^{-/-}$ mice and it would be interesting to know whether reducing Sod2 activity affects the *rds/rds* mutant. It was not however possible to

create an *rds/rds Sod2*$^{+/-}$ double mutant due to close linkage of *Sod2* and *Prph2* on mouse chromosome 17. If there is some residual activity of complex I, further change is only possible if it does not lead to massive cell death. The slower degeneration rate in *Rho*$^{-/-}$ compared to *rd1/rd1* and *atrd1/atrd1*, implies a milder mutation that could be more readily modified. The lack of a *Sod2* effect on complex I activity in this mutant suggests that the additional oxidative stress is insufficient to influence the rate of degeneration.

Decreased Sod2 expression and rates of photoreceptor degeneration.

Decreased *Sod2* expression had no effect on any of the rates of degeneration. There may be different explanations in each mutant. The *rd1/rd1* mutant is the fastest degenerating mutant, in which photoreceptors begin to degenerate before they are fully differentiated. The mutation seems to be of such a severity that it may not be possible to increase the rate of degeneration further. There may be a maximum for the function ($\mathbf{n_a} \times s$) that is consistent with some cell survival. The mutational damage may mask any additional stress introduced into the cell. Increased ROS however could result in a transition from apoptosis to necrosis, as the latter is associated with severe and acute insults. Future work using markers specific for necrosis would be interesting. In the *atrd1/atrd1* mouse, the retina also degenerates rapidly, although this mutant is not as severe as the *rd1/rd1* mutant. Despite the decrease in complex I activity in *atrd1* homozygotes, the decrease in Sod2 is not sufficient to affect the degeneration rate of this mutant. The lack of a further decrease in complex I activity in *Rho*$^{-/-}$ mice is consistent with the failure to change the degeneration rate in this mutant.

MitoQ administration and complex I activity

MitoQ had a positive effect on the *rds/rds* mutant by ameliorating its complex I activity ($p=0.018$; $n=3$). This both confirms the retinal uptake of the antioxidant and indicates that MitoQ is more likely to have a beneficial effect in mutants with slower rates of degeneration. The *rds/rds* mutant is the least severe mutant analyzed in this project, implying that there is a possibility for improvement of slower mutants such as *rds/+*. In contrast, homozygous *rd1* and *atrd1* mutants may be too severe and rapid for MitoQ to have an effect on oxidative damage.

The major question remains as to whether the rate of degeneration slows if targeted antioxidants completely restore complex I activity.

The beneficial effects of oral MitoQ administration at a concentration of 500 μM have previously been shown to decrease heart dysfunction, cell death and mitochondrial damage in ischemia-reperfusion (Adlam *et al.*, 2005). In particular, complex I activity was significantly ameliorated in heart samples treated with MitoQ in comparison to non-treated samples. It would therefore be expected that MitoQ administration at the same dose would have similarly beneficial effects in the retinal degeneration mutants assayed. Nevertheless, the issues of bioavailability and mitochondrial steady state concentration in the retina remain to be answered.

MitoQ administration and photoreceptor degeneration

There was no effect of MitoQ on rates of photoreceptor degeneration. In the cases of the *rd1/rd1* and *atrd1/atrd1* mutants, one explanation is again based on the severity of the mutations. In these mutants, in which photoreceptors start to degenerate shortly after birth, the achieved decrease in ROS production may not have been enough to influence the rate of photoreceptor cell death. This possibility is supported by the lack of a MitoQ effect on complex I activities. In the *Rho*$^{-/-}$ and *rds/rds* mice, the rates of degeneration were neither slowed nor reversed in response to MitoQ administration. The experimental set-up might account for the failure to detect any change in rates of degeneration. Samples were analyzed at monthly intervals until the degeneration was complete. Tighter time-points might have allowed the detection of subtle or short-lived changes in degeneration rates.

Modification of the redox state of the retina, by decreased *Sod2* expression or MitoQ administration, in general failed to alter levels of oxidative damage or degeneration rates. A number of questions are raised by this finding and their answers provide future directions for the project.

An issue that needs to be considered when analysing the numerical data collected in this study is that of statistical significance. Wacholder *et al.* (2004), in referring to molecular epidemiology studies, discussed the occurrence of false-positive

statistical findings and the limitations of declaring statistical significance based on a p-value alone. In addition to p-values, one has to ensure that the statistical power of an experiment, defined as the probability that one can detect an effect if there is really one, is sufficient and that multiple testing is also taken into consideration (Falconer & Mackay, 1996).

With respect to power, in this study, in most experiments we had appropriate sample sizes and sufficient power (0.80) to detect significant differences between wild-type and mutants at a false-positive rate of 0.05. However, what was not accounted for in this study was multiple testing, as different tissues and mutants were examined. As a result, it is possible that some of the significant findings are false-positives due to multiple testing. This could explain the presence of some unexpected statistically significant findings. For example, altered enzyme activities in retinal degeneration mutant heart, brain and liver samples were unexpected, given that the disease phenotype is confined to the retina. To determine whether these are true findings, future projects should include verifying the observed results.

Experimental design – number of oxidative stress markers

ROS are able to attack DNA, proteins and lipids and there are different markers for assessing the level of oxidative damage to each of these classes of molecules. As discussed in Chapter 3, various immunohistochemical methods were attempted but oxidative damage was eventually assessed only by two markers: the activity of the oxidative stress-sensitive complex I and the levels of GSH. It is possible that genetically decreasing Sod2 to 50% of wild-type level and oral administration of MitoQ at a concentration of 500 μM are indeed effective in altering the redox state of the retina. Failure to see more evidence of these effects could be attributed to an insufficient number of markers of oxidative damage in this project. Therefore, before reaching a conclusion as to the efficiency of these experimental approaches in modifying oxidative damage, using additional markers may be essential.

Mitochondrial DNA is prone to oxidative damage and there are different methods for detecting and assessing the extent of this damage. One way that was attempted was to perform cytochemical COX/SDH assays, as discussed in

Chapter 3. Although COX deficient photoreceptors have been detected in aged human samples (Barron *et al.*, 2001), COX-negative photoreceptor cells were not detected in any mouse mutants analysed in this project. This could be attributed to either the inefficiency of this method to detect mtDNA damage in photoreceptor cells or the absence of COX-deficient photoreceptors in the particular samples. An additional and more robust method for detecting oxidative mtDNA damage is screening for mtDNA mutations. Recently, Bender *et al.* (2006) showed that in substantia nigra neurons from both aged controls and patients with Parkinson's disease there was an increased incidence of somatic mtDNA deletions, often associated with respiratory chain deficiency. It would therefore be interesting to investigate the levels of oxidative damage-induced mutations in mtDNA in retinal degeneration models by sequencing. However, the increased mutation rate of mtDNA and its multiple heteroplasmic copies in the cell, render this approach experimentally challenging. Whether decreased *Sod2* expression in models of retinal degeneration or treatment with MitoQ would have an effect on the levels of detected mtDNA mutations is uncertain.

Since cone degeneration has been shown to involve oxidative damage (Shen *et al.*, 2005), it would also be interesting to measure cone function in retinal degeneration models and to try to modify them by experimentally altering the redox status of the cells. Cone degeneration is a secondary feature of the RP phenotype and takes significantly longer than rod degeneration to be completed. Using cone-specific markers, like wheat germ agglutinin, in conjunction with ONL analysis and/or TUNEL assays, one could follow the rate of cone degeneration. However, measuring enzyme activities and GSH contents in cone cells would be extremely challenging given the reduced number of these photoreceptor cells in mouse retinas.

Finally, in war it is always beneficial to know one's enemy, in this case the exact nature and levels of the ROS generated. The high reactivity of ROS with their target molecules complicates experimental methods for measuring ROS levels in a cell, which is the reason why the levels of oxidative stress are indirectly estimated. Although the various types of free radical species give rise to different types of cell damage, knowing the main damaging ROS in the retina and the nature this damage, would improve attempts at preventing it. Therefore, it would be useful to measure ROS in the retina. The markers 2'-7'-

dichlorofluorescein diacetate (DCFDA) and dihydroethedium have been used *in vitro* to assess production of hydrogen peroxide and superoxide anion respectively (Qi *et al.*, 2005). Also, attempts to measure HNE and MDA adducts in lipids and indicators of nitrosature stress were unsuccessful but warrant further investigation. Application of such markers to retinal samples from both wild-type and retinal degeneration mutants would shed further light on the level and type of oxidative stress we have attempted to modify.

Experimental design – choice of retinal degeneration mutants

Another reason for not finding a general effect of redox state modification on levels of oxidative damage and rates of degeneration could be the choice of mutants analyzed.

It is possible that the decreased expression of *Sod2* and the oral administration of MitoQ, at the levels applied in this project, would have an effect on mutants with slower rates of degeneration. None of the treatments had any effect on the fast degenerating *rd1* mutant, implying that the mutation in this mouse line is so severe that detrimental or beneficial changes in redox state are masked so that this is an inappropriate model to test the proposed hypothesis. The observation that MitoQ administration ameliorated the activity of complex I in the *rds/rds* mutant might be an indication that this antioxidant would be beneficial to slower degenerating mutants. The $Prph2^{+/rds}$ (Kedzierski *et al.*, 2001) and retinitis pigmentosa GTPase regulator (*Rpgr*) knockout (Hong *et al.*, 2004) mutants, in which photoreceptor degeneration takes a year to be completed, are examples of retinal degeneration mutants in which reduced Sod2 levels and/or Mito Q treatment may have an effect. The results from these experiments will shed more light on the efficiency of the experimental approaches in altering levels of oxidative damage and rates of degeneration.

The hypothesis tested supports the proposal that, irrespective of a direct causal role for oxidative stress in photoreceptor cell death, constitutive ROS production influences the probability of cell death. The complex I data suggests that oxidative stress directly influences the disease phenotype in all four models, which makes it difficult to dissociate this direct effect from an indirect one on rates of apoptotic cell death. Attempts to modify constitutive mitochondrial ROS production in a cell might be masked by an increase in ROS production caused by

the disease itself. If a substantial increase in oxidative stress is part of the disease pathology, it could overwhelm attempts to increase or decrease ROS production by genetic or pharmacological means. This could explain why none of the four mutants responded to the experimental treatments. In order to influence rates of degeneration, it may be necessary to modify the redox state in mutants causing little or no signs of direct oxidative damage.

Experimental design – dosage effects

The lack of a universal effect of either increased or decreased oxidative stress on rates of photoreceptor degeneration or detectable oxidative damage may be explicable in quantitative terms. The level of Sod2 in the mutants might not have been sufficiently low to increase steady state ROS production. The expression of *Sod2* however could not be genetically decreased by more than 50% as complete loss of Sod2 activity confers a lethal phenotype (Li *et al.*, 1995). It would therefore be interesting to repeat the experiments using mice where the *Sod2* null genotype is confined to the retina. Generation of a conditional retina-specific *Sod2* knockout mouse would ensure a long enough lifespan to allow a more significant increase in constitutive ROS production.

Similarly, the lack of an effect of MitoQ on rates of degeneration might be attributed to its administered dosage. Previous *in vitro* and *in vivo* work has demonstrated the antioxidant capacity of MitoQ. Smith *et al.* (2002) compared various methods of drug administration at different doses and showed that oral administration of MitoQ at a 1 mM concentration had no toxic effects on the animals for at least 26 days. This was not the case however for concentrations above 2 mM. In this project, where MitoQ was orally administered for a period of several months, the maximum concentration assessed was 500 μM. A preliminary study confirmed that oral administration of MitoQ at a concentration of 500 μM was efficiently taken up by different tissues. This confirmed the suitability of the method of administration and showed that intra-venous or intra-peritoneal injection was unnecessary. The preliminary study also demonstrated that the administered 500 μM concentration of MitoQ for a period of at least 3 months was not toxic to the animals. This suggests that higher concentrations of the antioxidant could be orally administered, in the expectation of exerting a more

efficient effect on rates of degeneration. Further analysis of ^{3}H-MitoQ would clarify the metabolic fate of this drug.

The complexity of both ROS production and the cellular antioxidant machinery highlights the multifactorial nature of oxidative stress. Although there are differences in the reactivity of different free radicals, oxidative damage cannot be attributed to a single reactive molecule. Hydroxyl radicals are the most reactive ROS whose generation follows that of superoxide anions and hydrogen peroxide. Similarly, the importance of cellular antioxidant mechanisms and enzymes varies, and the antioxidant status of a cell depends on the concerted action of different antioxidants. It is conceivable therefore that to efficiently affect the redox state of a cell, one might need to modify the level of more than one antioxidant system. Although published data suggests that either a 50% Sod2 decrease or treatment with MitoQ are effective on their own *in vivo*, it is possible that they should be coupled with modifications in other participants of the antioxidant machinery. Decreased *Sod2* expression in the heterozygous null mouse could be accompanied by a decrease in the levels of catalase and/or glutathione peroxidase, both of which detoxify the Sod2-generated superoxide anions. Alternatively, the joint over-expression of *Sod2* and catalase, as carried out by Schriner *et al.* (1999) to extend lifespan in mice, with or without MitoQ supplementation, might be required to reduce constitutive ROS production sufficiently to slow rates of degeneration. In this way, a more effective increase or decrease in ROS production would be evident. Similarly, the protective effect of MitoQ in terms of protein oxidation might be more efficient if it were coupled with increased levels of an antioxidant that was working at the level of mitochondrial DNA or lipid peroxidation damage. For example, MitoVitamin E has been shown to scavenge endogenous oxidants (Siler-Marsiglio *et al.*, 2005) and to prevent cell death in FRDA cells treated with the glutathione-synthesis inhibitor BSO (Jauslin *et al.*, 2003) and so might provide a complementary strategy.

To conclude, in the *rd1/rd1*, *atrd1/atrd1*, *Rho*$^{-/-}$ and *rds/rds* mouse models of RP, photoreceptor degeneration occurs at different rates. Although a direct causative role of oxidative stress in RP was excluded, evidence for oxidative damage, reflected in decreased CI activity, was present in all of the mutants. The rates of photoreceptor degeneration however were not affected by changed antioxidant

levels, but CI activity was further reduced in *atrd1/atrd1 Sod2*$^{+/-}$ double mutants with decreased *Sod2* expression, and ameliorated in the *rds/rds* mutant upon MitoQ administration. The results obtained in this project do not fully support the predictions based on the proposed hypothesis. Future work on slower degenerating mutants will be required to further elucidate the role of oxidative stress in photoreceptor degeneration.

REFERENCES

Adlam V.J., Harrison J.C., Porteous C.M., James A.M., Smith R.A.J., Murphy M.P., Sammut I.A. (2005) Targeting an antioxidant to mitochondria decreases cardiac ischemia-reperfusion injury. The FASEB Journal 19: 1088-1095

Allan D.J., Harmon B.V., Kerr J.F.R. (1987) Cell death in spermatogenesis *In* Perspectives of mammalian cell death, p.229, (ed. C.S. Potten) Oxford University Press

Ames A. 3rd, Li Y.Y., Heher E.C., Kimble C.R. (1992) Energy metabolism of rabbit retina as related to function: high cost of Na+ transport, Journal of Neuroscience 12 (3): 840-853

Anderson S., Bankier A.T., Barrell B.G., de Buijn M.H., Coulson A.R., Drouin J., Eperon I.C., Nierlich D.P., Rpe B.A., Sanger F., Schreier P.H., Smith A.J., Staden R., Young I.R. (1981) Sequence and organisation of he human mitochondrial genome, Nature 290: 457-65

Andreassen O.A., Ferrante R.J., Dedeoglu A., Albers D.W., Klivenyi P., Carlson E.J., Epstein C.J., Beal M.F. (2001) Mice with a Partial Deficiency of Manganese Superoxide Dismutase Show Increased Vulnerability to the Mitochondrial Toxins Malonate, 3-Nitropropionic Acid, and MPTP, Experimental Neurology 167: 189–195

Andrews R.M., Griffiths P.G., Johnson M.A., Turnbull D.M. (1999) Histochemical localisation of mitochondrial enzyme activity in human optic nerve and retina, British Journal of Ophthalmoloy 83 (2): 231-5

Antunes F., Han D., Cadenas E. (2002) Relative contributions of eart mitochondria glutathione peroxidase and catalase to H_2O_2 detoxification in in vivo conditions, Free Radical Biology and Medicine 33 (9): 1260-1267

Arroyo J.G., Yang L., Bula D., Chen D.F. (2005) Photoreceptor apoptosis in human retinal detachement, Ophthalmology 139: 605-610

Asikainen T.M., Huang T.T., Taskinen E., Levonen A.L., Carlson E., Lapatto R., Epstein C.J., Raivio K.O. (2002) Increased sensitivity of homozygous SOD2 mutant mice to oxygen toxicity, Free Radical Biology and Medicine 32 (2): 175–186

Asin-Cayuela J., Manas A.B., James A.M., Smith R.A.J., Murphy M.P. (2004) Fine-tuning the hydrophobicity of a mitochondria-targeted antioxidant. FEBS Letters 571: 9-16

Aulak K.S., Koeck T., Crabb J.W., Stuehr D.J. (2004) Dynamics of protein nitration in cells and mitochondria, American Journal of Physiology. Heart and Circulatory Physiology 286: H30-H38

Aulak K.S., Miyagi M., Yan L., West K.A., Massillon D., Crabb J.W., Stuehr D. (2001) Proteomic method identifies proteins nitrated *in vivo* during inflammatory challenge, Proceedings of the National Academy of Sciences of the United States of America 98 (21): 12056-12601

Awasthi Y.C., Sharma R., Cheng J.Z., Yang Y., Sharma A., Singhal S.S., Awasthi S. (2003) Role of 4-hydroxynonenal in stress-mediated apoptosis signaling, Molecular Aspects of Medicine 24: 219-30

Baehr W., Falk J.D., Burga B.K., Triantafyllos J.T., McGinnis J.F. (1988) Isolation and analysis of the mouse opsin gene, FEBS Letters 238 (2): 253-256

Barbouti A., Doulias P.T., Nousis L., Tenopoulou M., Galaris D. (2002) DNA damage and apoptosis in hydrogen peroxide-exposed Jurkat cells: bolus addition versus continuous generation of H(2)O(2), Free Radical Biology and Medicine 33 (5):691-702

Barron M.J., Johnson M.A., Andrews R.M., Clarke M.P., Griffiths P.G., Bristow E., He L.P., Durham S., Turnbull D.M. (2001) Mitochondrial abnormalities in ageing macular photoreceptors, Investigative Ophthalmology and Visual Science 42 (12): 3016-22

Bascom R.A., Manara S., Collins L., Molday R.S., Kalnins V.I., McInnes R.R. (1992) Cloning of the cDNA for a novel photoreceptor membrane protein (rom-1) identifies a disk rim protein family implicated in human retinopathies, Neuron 8 (6): 1171-84

Baylor D.A. (1987) Photoreceptor signals and vision. Proctor lecture, Investigative Ophthalmology and Visual Science 28 (1): 34-49

Beal M.F. (2002) Oxidatively modified proteins in aging and disease, Free Radical Biology and Medicine 32 (9): 797-803

Beatty S., Koh H., Phil M., Henson D., Boulton M. (2000) The role of oxidative stress in the pathogenesis of age-related macular degeneration, Survey of Ophthalmology 45 (2): 115-34

Beck J.A., Lloyd S., Hafezparast M., Lennon-Pierce M. Eppug J.T., Festing M.F.W., Fisher E.M.C. (2000) Genealogies of mouse inbred strains, Nature Genetics 24: 23

Bender A., Krishnan K.J., Morris C.M., Taylor G.A., Reece A.K., Perry R.H., Jaros E., Hersheson J.S., Betts J., Klopstock T., Taylor R.W., Turnbull D.M. (2006) High levels of mitochondrial DNA deletions in substantia nigra neurons in aging and Parkinson disease, Nature Genetics 38 (5): 515-7

Benedetti A., Comporti M., Esterbauer H. (1980) Identification of 4-hydroxynonenal as a cytotoxic product originating from the peroxidation of liver microsomal lipids, Biochimica et Biophysica Acta 620 (2): 281-96

Bennaars-Eiden A., Higgins L., Hertzel A.V., Kapphahn R.J., Ferrington D.A., Bernlohr D.A. (2002) Covalent Modification of Epithelial Fatty Acid-binding Protein by 4-Hydroxynonenal *in Vitro* and *in Vivo*: Evidence for a role in antioxidant biology, The Journal of Biological Chemistry 277 (52): 50693-50702

Bereiter-Hahn J. and Voth M. (1994) Dynamics of mitochondria in living cells: shape changes, dislocations, fusion, and fission of mitochondria, Microscopy and Research Techniques 27 (3): 198-219

Berson E.L., Gouras P., Gunkel R.D. (1968) Progressive cone degeneration, dominantly inherited, Archives in Ophthalmology 80 (1) 77-83

Berson E.L., Gouras P., Gunkel R.D. (1968) Progressive cone-rod degeneration, Archives in Ophthalmology 80 (1) 68-76

Berson E.L., Gouras P., Gunkel R.D. (1968) Rod responses in retinitis pigmentosa, dominantly inherited, Archives in Ophthalmology 80 (1): 58-67

Berson E.L., Gouras P., Hoff M. (1969) Temporal aspects of the electroretinogram, Archives in Ophthalmology 81 (2): 207-214

Bevers E.M., Comfurius P., Dekkers D.W., Zwaal R.F. (1999) Lipids translocation across the plasma membrane of mammalian cells, Biochimica et Biophysica Acta 1439 (3): 317-30

Beyer R.E. and Ernster L. (1990) The antioxidant role of Coenzyme Q In Highlight of ubiquinone research (eds. G. Lenaz, O. Barnobei, M. Battino), London: Taylor & Francis

Bhagavan H.N. and Chopra R.K. (2006) Coenzyme Q10: Absorption, tissue uptake, metabolism and pharmacokinetics, Free Radical Research 40 (5): 445-453

Bilinski T., Krawiec Z., Liczmanski A. & LJtwinska J. (1985) Is hydroxyl radical generated by the Fenton reaction *in vivo*? Biochemical and Biophysical Research Communications 130: 533

Bishop A. and Andreson (2005) NO signalling in the CNS: from the physiological to the pathological, Toxicology 298: 193-205

Blackstone N.W. and Green D.R. (1999) The evolution of a mechanism of cell suicide, BioEssays 21 (1): 84-88

Bleazard W., McCaffery J.M., King E.J., Bale S., Mozdy A., Tieu Q., Nunnari J., Shaw J.M. (1999) The dynamin-related GTPase Dnm1 regulates mitochondrial fission in yeast, Nature Cell Biology 1 (5): 298-304

Blok J. and Loman H. (1986) Bacteriophage DNA as a model for correlation of radical damage to DNA and biological effects, Basic Life Sciences 38: 75-87

Borner C. and Monney L. (1999) Apoptosis without caspases: an inefficient molecular guillotine? Cell Death and Differentiation 6 (6): 497-507

Bove J., Prou D., Perier C., Przedborski S. (2005) Toxin-induced models of Parkinson's disease, NeuroRx 2 (3): 484-94

Bowes C., Li T., Danciger M., Baxter L.C., Applebury M.L., Farber D.B. (1990) Retinal degeneration in the rd mouse is caused by a defect in the beta subunit of rod cGMP-phosphodiesterase Nature 347 (6294): 677-680.

Brigelius-Flohe R. (1999) Tissue-specific functions of individual glutathione peroxidases, Free Radical Biology and Medicine 27 (9-10): 951-65

Brink J., Hovmoller S., Ragan C.I., Cleeter M.W., Boekema E.J., van Bruggen E.F. (1987) The structure of NADH:ubiquinone oxidoreductase from beef-heart mitochondria. Crystals containing an octameric arrangement of iron-sulphur protein fragments, European Journal of Biochemistry 166 (2): 287-94

Brouillet E., Jacquard C., Bizat N., Blum D. (2005) 3-Nitropropionic acid: a mitochondrial toxin to uncover physiopathological mechanisms underlying striatal degeneration in Huntington's disease, Journal of Neurochemistry 95 (6): 1521-40

Brown G.C. (2001) Regulation of mitochondrial respiration by nitric oxide inhibition of cytochrome *c* oxidase, Biochimica et Biophysica Acta 1504: 46-57

Brown G.C. and Borutaire V. (2004) Inhibition of mitochondrial respiratory complex I by nitric oxide, peroxynitrite and S-nitrosothiols, Biochimica et Biophysica Acta 1658: 44-49

Brown W.M., George M. Jr., Wilson A.C. (1979) Rapid evolution of animal mitochondrial DNA, Proceedings of the National Academy of Sciences of the United States of America 76 (4): 1967-71

Burkle A., Diefenbach J., Brabeck C., Beneker S. (2005) Ageing and PARP, Pharmacological Research 53: 93-99

Bursch W., Ellinger A., Gerner C., Frohwein U., Schulte-Hermann R. (2000) Programmed cell death (PCD). Apoptosis, autophagic PCD, or others? Annals of New York Academy of Sciences 926: 1-12

Busuttil R.A., Garcia A.M., Cabrera C., Rodriguez A., Suh Y., Kim W.H., Huang T.T., Vijg J. (2005) Organ-Specific Increase in Mutation Accumulation and Apoptosis Rate in CuZn-Superoxide Dismutase–Deficient Mice, Cancer Research 65 (24): 11271-5

Buttke L.M. and Sandstrom P.A. (1994) Oxidative stress as a mediator of apoptosis, Immunology Today 15 (1): 7-10

Calderwood S.K. (2005) Regulatory interfaces between the stress protein response and other gene expression programs in the cell, Methods 35: 139-148

Cande C., Cecconi F., Dessen P., Kroemer G. (2002) Apoptosis-inducing factor (AIF): key to the conserved caspase-independent pathways of cell death? Journal of Cell Science 115 (Pt 24): 4727-34

Carlsson L.M., Jonsson J., Edlund T., Marklund S.L. (1995) Mice lacking extracellular superoxide dismutase are more sensitive to hyperoxia,

Proceedings of the National Academy of Sciences of the United States of America 92: 6264-6268

Carmody R.J., McGowan A.J., Cotter T.G. (1999) Reactive oxygen species as mediators of photoreceptor apoptosis *in vitro*, Experimental Cell Research 248: 520-530

Carter-Dawson L.D. and LaVail M.M. (1979a), Rods and cones in the mouse retina. I. Structural analysis using light and electron microscopy, Journal of Comparative Neurology 188 (2): 245-262

Carter-Dawson L.D. and LaVail M.M. (1979b), Rods and cones in the mouse retina. II. Autoradiographic analysis of cell generation using tritiated thymidine, Journal of Comparative Neurology 188 (2): 263-72

Cassarino D.S. and Bennett J.P. Jr (1999) An evaluation of the role of mitochondria in neurodegenerative diseases: mitochondrial mutations and oxidative pathology, protective nuclear responses, and cell death in neurodegeneration, Brain Research, Brain Research Reviews 29 (1): 1-25

Chang G.Q., Hao Y., Wong F. (1993) Apoptosis: final common pathway of photoreceptor death in *rd*, *rds*, and rhodopsin mutant mice, Neuron 11: 595-605

Chinnery P.F. and Turnbull D.M. (1998) Mitochondrial medicine, QJM 91 (5): 375-5

Chinnery P.F. and Turnbull D.M. (2000) Mitochondrial DNA mutations in the pathogenesis of human disease, Molecular Medicine Today 6 (11): 425-32

Clane F.L. and Barr R. (1971) Determination of ubiquinones, Methods in Enzymology 18C: 137-165

Clarke G., Goldberg A.F., Vidgen D., Collins L., Ploder L., Schwarz L., Molday L.L., Rossant J., Szel A., Molday R.S., Birch D.G., McInnes R.R. (2000) Rom-1 is required for rod photoreceptor viability and the regulation of disk morphogenesis, Nature Genetics 25 (1): 67-73

Clarke G., Lumsden C.J., McInnes R.R. (2001) Inherited neurodegenerative diseases: the one-hit model of neurodegeneration, Human Molecular Genetics 10 (20): 2269-75

Coghlan J.C., Flitter W.D., Clutton S.M., Ilsley C.D., Rees A., Slater T.F., (1993) Lipid peroxidation and changes in vitamin E levels during coronary artery bypass grafting. The Journal of Thoracic and Cardiovascular Surgery 106: 268-74

Cohen A.I. (1983) Some cytological and initial biochemical observations on photoreceptors in retinas of rds mice, Investigative Ophthalmology and Visual Science. 24(7): 832-43.

Cohen A.I. (1984) Some contributions to the cell biology of photoreceptors, Investigative Ophthalmology and Visual Science. 24: 1354

Connell G., Bascom R., Molday L., Reid D., McInnes R.R., Molday R.S. (1991) Photoreceptor peripherin is the normal product of the gene responsible for retinal degeneration in the *rds* mouse, Proceedings of the National Academy of Sciences of the United States of America 88(3): 723-6

Cortina M.S., Gordon W.C., Lukiw W.J., Bazan N.G. (2005) Oxidative stress-induced retinal damage up-regulates DNA polymerase gamma and 8-oxoguanine-DNA-glycosylase in photoreceptor synaptic mitochondria, Experimental Eye Research 81 (6): 742-50

Crapo J.D., Oury T., Rabouille C., Slot J.W., Chang L.Y. (1992) Copper, zinc superoxide dismutase is primarily a cytosolic protein in human cells, Proceedings of the National Academy of Sciences of the United States of America 89 (21): 10405-9

De Haan J.B., Bladier C., Griffiths P., Kelner M., O'Shea R.D., Cheung N.S., Bronson R.T., Silvestro M.J., Wild S., Zheng S.S., Beart P.M., Hertzog P.J., Kola I. (1998) Mice with a homozygous null mutation for the most abundant glutathione peroxidase, Gpx1, show increased susceptibility to the oxidative stress-inducing agents paraquat and hydrogen peroxide, Journal of Biological Chemistry 273 (35): 22528-36

Del Rio D., Stewart A.J., Pellegrini N. (2005) A review of recent studies on malondialdehyde as toxic molecule and biological marker of oxidative stress, Nutrition, Metabolism & Cardiovascular Disease 15:316-328

Demant P., Ivanyi D., van Nie R. (1979) The map position of the *rds* gene on the 17th chromosome of the mouse, Tissue Antigens 13 (1): 53-5

Deterre P., Bigay J., Robert M., Pfister C., Khun H., Chabre M. (1986) Activation of retinal rod cyclic GMP-phosphodiesterase by transducin: characterization of the complex formed by phosphodiesterase inhibitor and transducin alpha-subunit, Proteins. 1(2): 188-93

Dib M., Garrel C., Favier A., Robin V., Desnuelle C. (2002) Can malondialdehyde be used as a biological marker of progression in neurodegenerative disease? Journal of Neurology 249: 367-374

Diefenbach J. and Burkle A. (2005) Introduction to poly(ADP-ribose) metabolism, Cellular and Molecular Life Sciences 62 (7-8): 721-730

Donovan M. and Cotter T.G. (2002) Caspase-independent photoreceptor apoptosis *in vivo* and differential expression of apoptotic protease activating factor-1 and caspase-3 during retinal development, Cell Death and Differentiation 9 (11): 1220-31

Donovan M. Carmody R.J., Cotter T.G. (2001) Light-induced photoreceptor apoptosis *in vivo* requires neuronal nitric-oxide synthase and guanylate cyclase activity and is caspase-3-independent, Journal of Biological Chemistry 276 (25): 23000-8

Doonan F., Donovan M., Cotter T.G. (2003) Caspase-independent photoreceptor apoptosis in mouse models of retinal degeneration, The Journal of Neuroscience 23 (13): 5723-5731

Dringen R. (2000) Glutathione metabolism and oxidative stress in neurodegeneration, European Journal of Biochemistry 267 (16): 4903

Dryja T. P., Hahn L. B., Cowley G. S., McGee T. L., and Berson E. L. (1991). Mutation spectrum of the rhodopsin gene among patients with autosomal dominant retinitis pigmentosa. Proceedings of the National Academy of Sciences of the United States of America 88: 9370-9374.

Dryja T. P., McGee T. L., Reichel E., Hahn L. B., Cowley C. S.,Yandell D. W., Sandberg M. A., and Berson E. L. (1990a). A point mutation of the rhodopsin gene in one form of retinitis pigmentosa. Nature 343: 364-366.

Dryja T. P., McGee T. L., Hahn L. B., Cowley C. S., Olsson J. E., Reichel E., Sandberg M. A., and Berson E. L. (1990b). Mutations within the rhodopsin gene among patients with autosomal dominant retinitis pigmentosa. The New England Journal of Medicine 323: 1302-1307.

Du Y., Smith M.A., Miller C.M., Kern T.S. (2002) Diabetes-induced nitrative stress in the retina, and correction by aminoguanidine, Journal of Neurochemistry 80: 771-779

Elchuri S., Oberley T.D., Qi W., Eisenstein R.S., Roberts L.J., Van Remmen H., Epstein C.J., Huang T.T. (2005) CuZnSOD deficiency leads to persistent and widespread oxidative damage and hepatocarcinogenesis later in life, Oncogene 24: 367-380

Ernster L. and Dallner G. (1995) Biochemical, physiological and medical aspects of ubiquinone function, Biochimica et Biophysica Acta 1271: 195-204

Esposito L.A., Kokoszka J.E., Waymire K.G., Cottrell B., MacGregot G.R., Wallace D.C. (2000) Mitochondrial oxidative stress in mice lacking the glutathione peroxidase-1 gene, Free Radical Biology and Medicine 28 (5): 754-66

Esposito L.A., Melov S., Panov A., Cottrell B.A., Wallace D.C. (1999) Mitochondrial disease in mouse results in increased oxidative stress, Proceedings of the National Academy of Sciences of the United States of America 96 (9): 4820-5

Esworthy R.S., Ho Y.S., Chu F.F. (1997) The Gpx1 gene encodes mitochondrial glutathione peroxidase in the mouse liver, Archives in Biochemisty and Biophysics 340 (1): 59-63

Fadok V.A., Henson P.M. (2003) Apoptosis: Giving phosphatidylserine recognition an assist—with a twist, Current Biology 13: R655-657

Fain G.L. (2006) Why photoreceptors die (and why they don't), BioEssays 28: 344-354

Falconer D.S. and Mackay T.F.C. (1996) Introduction to quantitative genetics, 4th edition, Prentice Hall

Fan B.J., Tam P.O.S., Choy K.W., Wang D.Y., Lam D.S.C., Pang C.P. (2006) Molecular diagnostics of genetic eye diseases. Clinical Biochemistry 39: 231-239

Farber D.B. and Lolley R.N. (1974) Cyclic guanosine monophosphate: elevation in degenerating photoreceptor cells of the C3H mouse retina, Science 186(4162): 449-51

Fariss R.N., Apte S.S., Luthert P.J., Milam A.H. (1998) Accumulation of tissue inhibitor of metalloproteinases-3 in human eyes with Sorsby's fundus dystrophy or retinitis pigmentosa, British Journal of Ophthalmology 82 (11): 1329-34

Forgione M.A., Weiss N., Heydricks S., Cap A., Klings E.S., Bierl C., Eberhardt R.T., Farber H.W., Loscalzo J. (2002) Cellular glutathione peroxidase deficiency and endothelial dysfunction, American Journal of Physiology. Heart and Circulatory Physiology 282 (4): H1255-61

Frank J., Pompella A., Biesalski H.K. (2000) Histochemical visualization of oxidant stress, Free Radical Biology and Medicine 29 (11): 1096-105

Frederick J.M., Krasnoperova N.V., Hoffmann K., Church-Kopish J., Ruther K., Howes K., Lem J., Baehr W. (2001) Mutant rhodopsin transgene expression on a null background. Investigative Ophthalmology and Visual Science 42(3): 826-33.

Freitas I., Griffini P., Bertone V., Bertone R., Fenoglio C., Milliery R., Vairetti M. (2002) *In situ* detection of reactive oxygen species and nitric oxide production in normal and pathological tissues: improvement by differential interference contrast, Experimental Gerontology 37 (4): 591-602

Frey T.G. and Mannella C.A. (2000) The internal structure of mitochondria, Trends in Biochemical Science 25 (7): 319-24

Fung B.K., Young J.H., Yamane H.K., Griswold-Prenner I. (1990) Subunit stoichiometry of retinal rod cGMP phosphodiesterase. Biochemistry 29(11): 2657-64.

Galy A., Roux M.J., Sahel J.A., Leveillard T., Giangrandei A. (2005) Rhodopsin maturation defects induce photoreceptor death by apoptosis: a fly model for rhodopsin Pro23His human retinitis pigmentosa., Human Molecular Genetics 14 (17): 2547-57

Gardner P.R., Nguyen D.H., White C.W. (1994) Aconitase is a sensitive and critical target of oxygen poisoning in culctured mammalian cells and in rat lungs, Proceedings of the National Academy of Sciences of the United States of America 91: 12248-52

Gardner P.R., Raineri I., Epstein L.B., White C.W. (1995) Superoxide radical and iron modulate aconitase activity in mammalian cells, The Journal of Biological Chemistry 270 (22): 13399-13405

Garriga P. and Manyosa J. (2002) The eye photoreceptor protein rhodopsin. Structural implications for retinal disease. FEBS Letters 528(1-3): 17-22.

Gavrieli Y., Sherman Y., Ben-Sasson S.A. (1992) Identification of programmed cell death in situ via specific labelling of nuclear DNA fragmentation, Journal of Cell Biology 119 (3): 493-501

Genova M.L., Pich M.P., Biondi A., Bernacchia A., Falasca A., Bovina C., Formiggini G., Castelli G.P., Lenaz G. (2003) Mitochondrial production of oxygen radical species and the role of coenzyme Q as an antioxidant, Experimental Biology and Medicine 228: 506-513

Germain M., Mathai J.P., McBride H.M., Shore G.C. (2002) Endoplasmic reticulum BIK initiates DRP1-regulated remodelling of mitochondrial cristae during apoptosis, EMBO Journal 24 (8): 1546-56

Gibson G.E., Sheu K.F., Blass J.P. (1998) Abnormalities of mitochondrial enzymes in Alzheimer disease, Journal of Neural Transmission 105 (8-9): 855-70

GOBASE at http://gobase.bcm.umontreal.ca/index.php

Godley B.F., Shamsi F.A., Liang F.Q., Jarrett S.G., Davies S., Boulton M. (2005) Blue light induces mitochondrial DNA damage and free radical production in epithelial cells, The Journal of Biological Chemistry 280 (22): 21061-6

Gonzalez P.K., Zhuang J., Doctrow S.R., Malfroy B., Benson P.F., Menconi M.J., Fink M.P. (1996) Role of oxidant stress in the adult respiratory distress syndrome: evaluation of a novel antioxidant strategy in a porcine model of endotoxin-induced acute lung injury, Shock Suppl.1 : S23-6

Gow A.J., Farkouh C.R., Munson D.A., Posencheg M.A., Ischiropoulos H. (2004) Biological significance of nitric oxide-mediated modifications, Amrican Journal of Physiology. Lung Cellular and Molecular Physiology 287: 262-268

Greaves L.C., Preston S.L., Tadrous P.J., Taylor R.W., Barron M.J., Oukrif D., Leedham S.J., Deheragoda M., Sasieni P., Novelli M.R., Jankowski J.A., Turnbull D.M., Wright N.A., McDonald S.A. (2006) Mitochondrial DNA mutations are established in human colonic stem cells, and mutated clones expand by crypt fission, Proceedings of the National Academy of Sciences of the United States of America 103 (3): 714-9

Green D.R. and Kroemer G. (2004) The pathophysiology of mitochondrial cell death, Science 305: 629

Green D.R. and Reed J.C. (1998) Mitochondria and apoptosis, Science 281 (5381): 1309-12

Green K., Brand M.D., Murphy M.P. (2004) Prevention of mitochondrial oxidative damage as a therapeutic strategy in diabetes, Diabetes 52 (Suppl. 1): 110

Griffith O.W. and Meister A. (1985) Origin and turnover of mitochondrial glutathione, Proceedings of the National Academy of Sciences of the United States of America 82 (14): 4668-72

Guimaraes C.A., Benchimol M., Amarante-Mendes G.P., Linden R. (2003) Alternative programs of cell death in developing retinal tissue, Journal of Biological Chemistry 278 (43): 41938-46

Hall D.H., Gu G., Garcia-Anoveors J., Gong L., Chalfie M., Driscoll M. (1997) Neuropathology of degenerative cell death in *Caenorhabditis elegans*, Journal of Neuroscience 17 (3): 1033-1045

Halliwell B. (1997) What nitrates tyrosine? Is nitrotyrosine specific as a biomarker of peroxynitrite formation in vivo? FEBS Letters 411: (2-3): 157-60

Halliwell B. and Gutteridge J.M.C. (1999) Free Radicals in Biology and Medicine, 3rd edition, Clarendon Press, Oxford.

Hansen J.M., Go Y.M., Jones D.P. (2006) Nuclear and mitochondrial compartmentation of oxidative stress and redox signalling, Annual Review of Pharmacology and Toxicology 46: 215-34

Hao W., Wenzel A., Obin M.S., Chen C.K., Brill E., Krasnoperova N.V., Eversole-Cire P., Kleyner Y., Taylor A., Simon M.I., Grimm C., Reme C.E., Lem J. (2002) Evidence for two apoptotic pathways in light-induced retinal degeneration, Nature Genetics 32 (2): 254-60

Hart A.W., McKie L., Morgan J.E., Gautier P., West K., Jackson I.J., Cross S.H. (2005) Genotype-phenotype correlation of mouse pde6b mutation, Investigative Ophthalmology and Visual Science 46(9): 3443-50.

Hawkins R.K., Jansen H.G., Sanyal S. (1985) Development and degeneration of retina in rds mutant mice: photoreceptor abnormalities in the heterozygotes, Experimental Eye Research 41 (6): 701-20

He L., Poblenz A.T., Medrano C.J., Fox D.A. (2000) Lead and Calcium Produce Rod Photoreceptor Cell Apoptosis by Opening the Mitochondrial Permeability Transition Pore, The Journal of Biological Chemistry 275 (16); 12175-12184

Heath-Engel H.M. and Shore G.C. (2006) Mitochondrial membrane dynamics, cristae remodelling and apoptosis, Biochimica et Biophysica Acta: Molecular Cell Research, In Press, Corrected Proof, Available online 13 March 2006

Herrero A. and Barja G. (1997) Sites and mechanisms responsible for the low rate of free radical production of heart mitochondria in the long-lived pigeon, Mechanisms in Ageing and Development 98 (2): 95-111

Ho Y., Magnenat J., Bronson R.T., Cao J., Gargano M., Sugawara M., Funk C.D. (1997) Mice Deficient in Cellular Glutathione Peroxidase Develop Normally and Show No Increased Sensitivity to Hyperoxia, The Journal of Biological Chemistry 272 (26): 16644-16651

Ho Y.S., Xiong Y., Spector A., Ho D.S. (2004) Mice lacking catalase develop normally but show differential sensitivity to oxidant tissue injury, The Journal of Biological Chemistry 279 (31): 32804-12

Hobson A.H., Donovan M., Humphries M.M., Tuohy G., McNally N., Carmody R., Cotter T., Farrar G.J., Kenna P.F., Humphries P. (2000) Apoptotic Photoreceptor Death in the Rhodopsin Knockout Mouse in the Presence and Absence of c-fos, Experimental Eye Research 71: 247-254

Hockenbery D.M., Oltvai Z.N., Yin X.M., Milliman C.L., Korsmeyer S.J. (1993) Bcl-2 functions in an antioxidant pathway to prevent apoptosis, Cell 75 (2): 241-51

Hong D.H., Pawlyk B.S., Adamian M., Li T. (2004) Dominant, gain-of-function mutant produced by truncation of RPGR. Investigative Ophthalmology and Visual Science 45 (1): 36-41

Huang T.T., Yasunami M., Carlson E.J., Gillespie A.M., Reaume A.G., Hoffman E.K., Chan P.H., Scott R.W., Epstein C.J. (1997) Superoxide-mediated cytotoxicity in superoxide dismutase-deficient fetal fibroblasts, Archives of Biochemistry and Biophysics 344 (2): 424-432

Huang T.T., Carlson E.J., Kozy H.M., Mantha S., Goodman S.I., Ursell P.C., Epstein C.J. (2001) Genetic modification of prenatal lethality and dilated cardiomyopathy in Mn superoxide dismutase mutant mice, Free Radical Biology and Medicine 31 (9): 1101-1110

Humphries M.M., Rancourt D., Farrar G.J., Kenna P., Hazel M., Bush R.A., Sieving P.A., Sheils D.M., McNally N., Creighton P., Erven A., Boros A., Gulya K., Capecchi M.R., Humphries P. (1997) Retinopathy induced in mice by targeted disruption of the rhodopsin gene, Nature Genetics 15(2): 216-9.

Humphries P., Kenna P., Farrar G.J. (1992) On the molecular genetics of retinitis pigmentosa. Science. 256 (5058): 804-8

Hussain A.A., Willmott N.J., Voaden M.J. (1992) Cyclic GMP and calcium: the internal messengers of excitation and adaptation in vertebrate photoreceptors, Vision Research 30(12): 1923-48

Hutton M., Lendon C.L, 2, Rizzu P., Baker1 M., Froelich S., Houlden H., Pickering-Brown S., Chakraverty S., Isaacs A., Grover A., Hackett J., Adamson J., Lincoln S., Dickson D. Davies P., Petersen R.C., Stevens M., de Graaff E., Wauters E., van Baren J., Hillebrand M., Joosse M., Kwon J.M., Nowotny P., Che L.K., Norton J., Morris J.C., Reed L.A., Trojanowski A., Basun H., Lannfelt L., Neystat M., Fahn S., Dark F., Tannenberg T., Dodd P.R., Hayward N., Kwok J.B.J., Schofield P.R., Andreadis A., Snowden J., Craufurd D.C.,

Neary D., Owen F., Oostra B.A., Hardy J., Goate A., van Swieten J, Mann D., Lynch T., Heutink P. (1998) Association ofmissense and59-splice-site mutations in *tau* with the inherited dementia FTDP-17, Nature 393: 702-205

Ingold K.U., Bowry V.W., Stocker R., Walling C. (1993) Autoxidation of lipids and antioxidation by alpha-tocopherol and ubiquinol in homogeneous solution and in aqueous dispersions of lipids: unrecognized consequences of lipid particle size as exemplified by oxidation of human low density lipoprotein, Proceedings of the National Academy of Sciences of the United States of America 90 (1): 45-9

Ischiropoulos H. (2003) Biological selectivity and functional aspects of protein tyrosine nitration, Biochemical and Biophysical Research Communications 305: 776–783

Izumi M., McDonald M.C., Sharpe M.A., Chatterjee P.K., Thiemermann C. (2002) Superoxide dismutase mimetics with catalase activity reduce the organ injury in hemorrhagic shock, Shock 18 (3): 230-5

Jacobson M.D. and Raff M.C. (1995) Programmed cell death and Bcl-2 protection in very low oxygen, Nature 374 (6525): 814-6

James A.M., Smith R.A.J., Murphy M.P. (2004) Antioxidant and pro-oxidant properties of mitochondrial Coenzyme Q, Archives of Biochemistry and Biophysics 423: 47-56

Jansen H.G. and Sanyal S. (1984) Development and degeneration of retina in *rds* mutant mice: electron microscopy. Journal of Comparative Neurology 224 (1): 71-84.

Jansen H.G., Sanyal S., De Grip W.J., Schalken J.J. (1987) Development and degeneration of retina in *rds* mutant mice: ultra-immunohistochemical localization of opsin, Experimental Eye Research 44(3): 347-61

Jauslin M.L., Meier T., Smith R.A.J., Murphy M.P. (2003) Mitochondria-targeted antioxidants protect Friedreich Ataxia fibroblasts from endogenous oxidative stress more effectively than untargeted antioxidants. FASEB Journal 17: 1972-4

Justice M.J., Noveroske J.K., Weber J.S., Zheng B., Bradley A. (1999) Mouse ENU mutagenesis. Human Molecular Genetics 8(10): 1955-63

Kane D.J., Sarafian T.A., Anton R., Hahn H., Gralla E.B., Valentine J.S., Ord T., Bredesen D.E. (1993) Bcl-2 inhibition of neuronal death: decreased generation of reactive oxygen species, Science 262 (5137): 1274-7

Katai N. and Yoshimura N. (1999) Apoptotic retinal neuronal death by ischemia-reperfusion is executed by two distinct caspase family proteases, Investigative Ophthalmology and Visual Science 40 (11): 2697-705

Kauppinen R. (1983) Proton electrochemical potential of the inner mitochondrial membrane in isolated perfused rat hearts, as measured by exogenous probes. Biochimica et Biophysica Acta. 725: 131-7

Kedzierski W., Nusinowitz S., Birch D., Clarke G., McInnes R.R., Bok D., Travis G.H. (2001) Deficiency of rds/peripherin causes photoreceptor death in mouse models of digenic and dominant retinitis pigmentosa. Proceedings of the National Academy of Sciences of the United States of America 98 (14): 7718-23

Kelso G.F., Porteous C.M., Coulter C.V., Hughes G., Porteous W.K., Ledgerwood E.C., Smith R.A.J., Murphy M.P. (2001) Selective Targeting of a Redox-active Ubiquinone to Mitochondria within Cells, Journal of Biological Chemistry 276: 4588-4596.

Kerr J.F.R., Searle J., Harmon B.V., Bishop C.J. (1987) Apoptosis *In* Perspectives of mammalian cell death, p 93, (ed. C.S. Potten) Oxford University Press

Kety S.S. and Schmidt C.F. (1948) The nitrous oxide method for the quantitative determination of cerebral blood flow in man: theory, procedure and normal values, Journal of Clinical Investigation 27 (4): 476-483

Kim D.Y., Won S.J.,Gwag B.J. (2002) Analysis of mitochondrial free radical generation in animal models of neuronal disease, Free Radical Biology and Medicine 33 (5): 715-723

Kim H.C., Bing G., Kim S.J., Jhoo W.K., Shin E.J., Bok Wie M., Ko K.H., Kim W.K., Flanders K.C., Choi S.G., Hong J.S. (2002) Kainate treatment alters TGF-beta3 gene expression in the rat hippocampus, Brain Research. Moleculer Brain Research 108 (1-2): 60-70

Kockx M.M., Muhring J., Knaapen M.W., de Meyer G.R. (1998) RNA synthesis and splicing interferes with DNA in situ end labelling techniques used to detect apoptosis, American Journal of Pathology 152 (4): 885-8

Koeck T., Stuehr D.J., Aulak K.S. (2005) Mitochondria and regulated tyrosine nitration, Biochemical Society Transactions 33 (6): 1399-1403

Kolb H. and Gouras P. (1974) Electron microscopic observations of human retinitis pigmentosa, dominantly inherited. Investigative Ophthalmology 13(7): 487-98

Koopman G., Reutelingsperger C.P.M., Kuijten G.A.M., Keehnen R.M.J., Pals S.T., van Oers M.H.J. (1994) Annexin V for Flow Cytometric Detection of Phosphatidylserine Expression on B Cells Undergoing Apoptosis, Blood 84 (5): 1415-1420

Koutsilieri E., Scheller C., Grunblatt E., Nara K., Li J., Riederer P. (2002) Free radicals in Parkinson's disease Journal of Neurology 249 (Suppl 2): II 1-5

Krasnianski A., Deschauer M., Neudecker S., Gellerich F.N., Muller T., Schoser B.G., Krasnianski M., Zierz S. (2005) Mitochondrial changes in skeletal muscle in amyotrophic lateral sclerosis and other neurogenic atrophies, Brain 128: 1870-1876

Kuhn H. and Borchert A. (2002) Regulation of enzymatic lipid peroxidation: the interplay of peroxidising and peroxide reducing enzymes, Free Radical Biology and Medicine 33 (2): 154-171

Laas A. and Sohal R.S. (1998) Electron transport-linked ubiquinone-dependent recycling of a-tocopherol inhibits autooxidation of mitochondrial membranes. Archives of Biochemistry and Biophysics 352: 229-236

Larsen K.E. and Sulzer D. (2002) Autophagy in neurons: a review, Histology and Histopathology 17 (3): 897-908

Larsson N.G. and Luft R. (1999) Revolution in mitochondrial medicine, FEBS Letters 455 (3): 199-202

LaVail M.M. (1983) Outer segment disc shedding and phagocytosis in the outer retina, Transactions of Ophthalmological Societies of the United Kingdom 103 (4): 397-404

Lebowitz R.M., Zhang H., Vogel H., Cartwright J., Dionne L., Lu N., Huang S., Matzuk M.M. (1996) Neurodegeneration, myocardial injury, and perinatal death in mitochondrial superoxide dismutase-deficient mice, Proceedings of the National Academy of Sciences of the United States of America 93: 9782-9787

Leeuwenburgh C., Hansen P., Shaish A., Holloszy J.O., Heinecke J.W. (1998) Markers of protein oxidation by hydroxyl radical and reactive nitrogen species in tissues of aging rats, American Journal of Physiology 274 (2 Pt 2): R453-61

Lem J., Krasnoperova N.V., Calvert P.D., Kosaras B., Cameron D.A., Nicolo M., Makino C.L., Sidman R.L. (1999) Morphological, physiological, and biochemical changes in rhodopsin knockout mice, Proceedings of the National Academy of Sciences of the United States of America 96(2): 736-41.

Leveillard T., Mohand-Said S., Lorentz O., Hicks D., Fintz A.C., Clerin E., Simonutti M., Forster V., Cavusoglu N., Chalmel F., Dolle P., Poch O., Lambrou G., Sahel J.A. (2004) Identification and characterization of rod-derived cone viability factor, Nature Genetics 36 (7): 755-9

Levine R.L., Garland D., Oliver C.N., Amici A., Climent I., Lenz A.G., Ahn B.W., Shaltiel S., Stadtman E.R. (1990) Determination of carbonyl content in oxidatively modified proteins, Methods in Enzymology 186: 464-78

Li Y., Huang T.T., Carlson E.J., Melov S., Ursell P.C., Olson J.L., Noble L.J., Yoshimura M.P., Berger C., Chan P.H., Wallace D.C., Epstein C.J. (1995) Dilated cardiomyopathy and neonatal lethality in mutant mice lacking manganese superoxide dismutase, Nature Genetics 11: 376-381

Li Y., Schlamp C.L., Poulsen G.L., Jackson M.W., Griep A.E., Nickells R.W. (2002) p53 regulates apoptotic retinal ganglion cell death induced by N-methyl-D-aspartate, Molecular Vision 8: 341-50

Liang Y., Fotiadis D., Maeda T., Maeda A., Modzelewska A., Filipek S., Saperstein D.A., Engel A., Palczewski K. (2004) Rhodopsin signaling and

organization in heterozygote rhodopsin knockout mice. Journal of Biological Chemistry 279(46): 48189-96

Lin T.K., Hughes G., Muratovska A., Blaikie F.H., Brookes P.S., Darley-Usmar V., Smith R.A.J, Murphy M.P. (2002) Specific Modification of mitochondrial protein thiols in Response to Oxidative Stress, Journal of Biological Chemistry 277: 17048-17056

Lindahl T., Satoh M.S., Porier G.G., Klungland A. (1995) Post-translational modification of poly (ADP-ribose) polymerase induced by DNA strand breaks, Trends in Biochemical Sciences 20 (10): 405-11

Liu C., Li Y., Peng M., Laties A.M., Wen R. (1999) Activation of caspase-3 in the retina of transgenic rats with the rhodopsin mutation s334ter during photoreceptor degeneration, Journal of Neuroscience 19 (12): 4778-85

Lledias F., Rangel P., Hansberg W. (1998) Oxidation of catalase by singlet oxygen, Journal of Biological Chemistry 273 (17): 10630-7

Lohr H.R., Kuntchithapautham K., Sharma A.K., Rohrer B. (2006) Multiple, parallel cellular suicide mechanisms participate in photoreceptor cell death Experimental Eye Research 83 (2): 380-389

Lolley R.N. (1972) Changes in glucose and energy metabolism *in vivo* in developing retinae from visually-competent (DBA-1J) and mutant (C3H-HeJ) mice, Journal of Neurochemistry 19 (1): 175-85

Lolley R.N., Farber D.B., Rayborn M.E., Hollyfield J.G. (1977) Cyclic GMP accumulation causes degeneration of photoreceptor cells: simulation of an inherited disease. Science 196(4290): 664-6

Lolley R.N., Rong H., Craft C.M. (1994) Linkage of photoreceptor degeneration by apoptosis with inherited defect in phototransduction, Investigative Ophthalmology and Visual Science 35 (2): 358-62

Lolley R.N., Schmidt S.Y., Farber D.B. (1974) Alterations in cyclic AMP metabolism associated with photoreceptor cell degeneration in the C3H mouse, Journal of Neurochemistry 22(5): 701-7

Louie J.L., Kapphahn R.J., Ferrington D.A. (2002) Proteasome function and protein oxidation in the aged retina, Experimental Eye Research 75 (3): 271-284

Lowry O.H., Roberts N.R., Lewis C. (1956) The quantitative histochemistry of the retina, Journal of Biological Chemistry 220 (2): 879-892

Ma J., Norton J.C., Allen A.C., Burns J.B., Hasel K.W., Burns J.L., Sutcliffe J.G., Travis G.H. (1995) Retinal degeneration slow (rds) in mouse results from simple insertion of a t haplotype-specific element into protein-coding exon II. Genomics. 28(2): 212-9

Maguire J.J., Wilson D.S., Packer L. (1989) Mitochondrial electron transport-linked tocopheroxyl radical reduction, Journal of Biological Chemistry 264 (36): 21462-5

Mannella C.A., Forte M., Colombini M. (1992) Towards the molecular structure of the mitochondrial channel, VDAC, Journal of Bioenergetics and Biomembranes 24 (1): 7-19

Mariotti C., Solari A., Torta D., Marano L., Fiorentini C., Di Donato S. (2003) Idebenone treatment in Friedreich patients: One-year-long randomised placebo-controlled trial, Neurology 60: 1676-1679

Martin S.J., Reutelingsperger C.E.M., McGahon A.J., Rader J.A., van Schie R.C.A.A., LaFace D.M., Green D.L. (1995) Early Redistribution of Plasma Membrane Phosphatidylserine Is a General Feature of Apoptosis Regardless of the Initiating Stimulus: Inhibition by Overexpression of Bcl-2 and Abl, Journal of Experimental Medicine 182 : 1545-1556

Matsui H., Lin L.R., Ho Y.S., Reddy V.N. (2003) The effect of up- and downregulation of MnSOD enzyme on oxidative stress in human lens epithelial cells, Investigative Ophthalmology and Visual Science 44 (8): 3467-75

Matthews R.T., Yang L., Browne S., Bail M. & Beal M. F. (1998) Coenzyme Q10 administration increases brain mitochondrial concentrations and exerts neuroprotective effects, Proceedings of the National Academy of Sciences of the United States of America 95: 8892-7

Matyszak M.K. and Perry V.H. (1995) Demyelination in the central nervous system following a delayed-type hypersensitivity response to *Bacillus Calmette-Gui Rin*, Neuroscience 64 (4): 967-977

McBride A.G., Borutaite V., Brown G.C. (1999) Superoxide dismutase and hydrogen peroxide cause rapid nitric oxide breakdown, peroxynitrite production and subsequent cell death, Biochimica et Biophysica Acta 1454: 275-288

McCarthy NJ,Whyte MKB, Gilbert CS and Evan GI (1997) Inhibition of Ced-3/ICE-related proteases does not prevent cell death induced by oncogenes, DNA damage, or the Bcl-2 homologue Bak, Journal of. Cell Biology 136: 215-227

Meagher E.A. and Fitzgerald G.A. (2000) Role of oxidation in artherosklerosis, Indices of lipid peroxidation in vivo: strengths and limitations, Free Radical Biology and Medicine 28 (12): 1745-50

Melov S. (2000) Mitochondrial oxidative stress, Physiologic consequences and potential for a role in aging, Annals New York Academy of Sciences 908: 219-225

Melov S., Coskun P., Patel M., Tuinstra R., Cottrell B., Jun A.S., Zastawny T.H., Dizdaroglu M., Goodman S.I., Huang T.T., Miziorkos H., Epstein C.J., Wallace D.C. (1999) Mitochondrial disease in superoxide dismutase 2 mutant mice,

Proceedings of the National Academy of Sciences of the United States of America 96: 846-851

Melov S., Doctrow S.R., Schneider J.A., Haberson J., Patel M., Coskun P.E., Huffman K., Wallace D.C., Malfroy B. (2001) Lifespan extension and rescue of spongiform encephalopathy in superoxide dismutase 2 nullizygous mice treated with superoxide dismutase-catalase mimetics, Journal of Neuroscience 21 (21): 8348-53

Melov S., Schneider J.A., Day B.J., Hinerfeld D., Coskun P., Mirra S.S., Crapo J.D., Wallace D.C. (1998) A novel neurological phenotype in mice lacking mitochondrial manganese superoxide dismutase, Nature Genetics 18 (2): 159-63

Meydani M. (1995) Vitamin E. Lancet 345: 170-5

Miller T.J., Schneider R.J., Miller J.A., Martin B.P., Al-Ubaidi M.R., Agarwal N., Dethloff L.A., Philbert M.A. (2006) Photoreceptor cell apoptosis induced by the 2-nitroimidazole radiosensitizer, CI-1010, is mediated by p53-linked activation of caspase-3, Neurotoxicology 27 (1): 44-59

Miyagi M., Sakaguchi H., Darrow R.M., Yan L., West K.A., Aulak K.S., Stuehr D.J., Hollyfield J.G., Organiscial D.T., Crabb J.W. (2002) Evidence that light modulates protein nitration in rat retina, Molecular & Cellular Proteomics 1.2: 293

Molday R.S. (1994) Peripherin/rds and rom-l: Molecular Properties and Role in Photoreceptor Cell Degeneration, Progress in Retinal and Eye Research 13 (1): 271-299

Montoya J., Gaines G.L., Attardi G. (1983) The pattern of transcription of the human mitochondrial rRNA genes reveals two overlapping transcription units, Cell 34 (1): 151-9

Moriya M., Baker B.N., Williams T.P. (1986) Progression and reversibility of early light-induced alterations in rat retinal rods, Cell and Tissue Research 246: 607-621

Mullen R.J. and LaVail M.M. (1976) Inherited retinal dystrophy: primary defect in pigment epithelium determined with experimental rat chimeras, Science 192: 799-801

Murphy M.P. and Smith R.A.J. (2000) Drug delivery to mitochondria: the key to mitochondrial medicine. Advanced Drug Delivery Reviews 41: 235-250

Mytilineou C., Krameri B.C., Yabutz J.A. (2002) Glutathione depletion and oxidative stress, Parkinsonism and Related Disorders 8: 385-7

Naash M.I., Hollyfield J.G., al-Ubaidi M.R., Baehr W. (1993) Simulation of human autosomal dominant retinitis pigmentosa in transgenic mice expressing a mutated murine opsin gene, Proceedings of the National Academy of Sciences of the United States of America. 90(12): 5499-503.

Nakagawa H., Ohshima Y., Takusagawa M., Ikota N., Takahashi Y., Shimizu S., Ozawa T. (2001) Functional Modification of cytochrome *c* by peroxynitrite in an electron transfer reaction, Chemical and Pharmacological Bulletin 49 (12): 1547-1554

Nathans J. and Hogness D.S. (1984) Isolation and nucleotide sequence of the gene encoding human rhodopsin, Proceedings of the National Academy of Sciences of the United States of America. 81(15): 4851-5.

Nijtmans L.G.J., Ugalde C., van den Heuvel L.P., Smeitink J.A.M. (2004) Function and dysfunction of the oxidative phosphorylation system, *In* Mitochondrial function and biogenesis, Topics in Current Genetics (eds. C.N. Koehrer and M.F. Bauer), Springer

Nir I., Agarwal N., Papermaster D.S. (1990) Opsin gene expression during early and late phases of retinal degeneration in rds mice, Experimental Eye Research 51(3): 257-67.

Noell W.K., Walker V.S., Kang B.S., Beman S. (1966) Retinal damage by light in rates, Investigative Ophthalmology 5: 450-473

Noor R., Mittal S., Iqbal J. (2002) Superoxide dismutase--applications and relevance to human diseases, Medical Science Monitor 8 (9); RA210-5

Nulton-Persson A.C and Szweda L.I. (2001) Modulation of mitochondrial function by hydrogen peroxide, Journal of Biological Chemistry 276 (26): 23357-61

Nunomura A., Perry G., Pappolla M.A., Wade R., Hirai K., Chiba S., Smith M.A. (1999) RNA Oxidation Is a Prominent Feature of Vulnerable Neurons in Alzheimer's Disease, The Journal of Neuroscience 19 (6): 1959-1964

Old S.L. and Johnson M.A. (1989) Methods of microphotometric assay of succinate dehydrogenase and cytochrome c oxidase activities for use on human skeletal muscle, Histochemical Journal 21: 545-555

Olshevskaya E.V., Calvert P.D., Woodruff M.L., Peshenko I.V., Savchenko A.B., Makino C.L. Ho Y., Fain G.L., Dizhoor A.M. (2004) The Y99C Mutation in Guanylyl Cyclase-Activating Protein 1 Increases Intracellular Ca2_ and Causes Photoreceptor Degeneration in Transgenic Mice, The Journal of Neuroscience 24 (27): 6978-6085

Olsson J.E., Gordon J.W., Pawlyk B.S., Roof D., Hayes A., Molday R.S., Mukai S., Cowley G.S., Berson E.L., Dryja T.P. (1992) Transgenic mice with a rhodopsin mutation (Pro23His): a mouse model of autosomal dominant retinitis pigmentosa. Neuron 9 (5): 815-30.

Op den Kamp J.A.F.(1979) Lipid asymmetry in membranes. Annual Reviews in Biochemistry 48: 47

Orr H.T., Lowry O.H., Cohen A.I., Ferrendelli J.A. (1976) Distribution of 3':5'-cyclic AMP and 3':5'-cyclic GMP in rabbit retina in vivo: selective effects of

dark and light adaptation and ischemia, Proceedings of the National Academy of Sciences of the United States of America. 73(12): 4442-5

Palade G.E. (1953) An electron microscope study of the mitochondrial structure, Journal of Histochemistry and Cytochemistry 1 (4): 188-211

Pardridge W.M. (2001) Brain drug targeting: the future of brain drug development. Cambridge University Press

Pardridge W.M. (2005) The blood-brain barrier: bottleneck in brain drug development. NeuroRx 2 (1): 3-12

Pastore A., Federici G., Bertini E., Piemonte F. (2003) Analysis of glutathione: implication in redox and detoxification, Clinica Chimica Acta 333: 19-39

Pepe I.M., Panfoli I., Cugnoli C. (1986) Guanylate cyclase in rod outer segments of the toad retina. Effect of light and Ca^{2+}, FEBS Letters 203 (10): 73-6

Perkins G., Renken C., Martone M.E., Young S.J., Ellisman M., Frey T. (1997) Electron tomography of neuronal mitochondria: three-dimensional structure and organization of cristae and membrane contacts, Journal of Structural Biology 119 (3): 260-72

Petersen D.R. and Doorn J.A. (2004) Reactions of 4-hydroxynonenal with proteins and cellular targets, Free Radical Biology and Medicine 37 (7): 937-945

Phillips J.P., Campbell S.D., Michaud D., Charbonneau M., Hilliker A.J. (1989) Null mutation of copper/zinc Superoxide dismutase in Drosophila confers hypersensitivity to paraquat and reduced longevity, Proceedings of the National Academy of Sciences of the United States of America 86: 2761–2765.

Pierce E.A. (2001) Pathways to photoreceptor cell death in inherited retinal degenerations, BioEssays 23(7): 605-18

Pitkanen S. and Robinson B.H. (1996) Mitochondrial complex I deficiency leads to increased production of superoxide radicals and induction of superoxide dismutase, Journal of Clinical Investigation 98 (2): 345-51

Portera Cailliau C., Sung C-H., Nathans J., Adler R. (1994) Apoptotic photoreceptor cell death in mouse models of retinitis pigmenosa, Proceedings of the National Academy of Sciences of the United States of America 91: 974-978

Pugh E.N. and Lamb T.D. (1990) Cyclic GMP and calcium: the internal messengers of excitation and adaptation in vertebrate photoreceptors. Vision Research 30(12): 1923-48

Qi X., Lewin A.S., Sun L., Hauswirth W.W., Guy J. (2004) SOD2 gene transfer protects against optic neuropathy induced by deficiency of complex I. Annals of Neurology 56 (2): 171-2

Rao R.V., Ellerby H.M., Bredesen D.E. (2004) Coupling endoplasmic reticulum stress to the cell death program, Cell Death Differentiation 11 (4): 372-80

Raza H., Robin M.A., Fang J.K., Avadhani N.G. (2002) Multiple isoforms of mitochondrial glutathione S-transferases and their differential induction under oxidative stress, Biochemical Journal 366 (1): 45-55

Reaume A.G., Elliot J.L., Hoffman E.K., Kowall N.W., Ferrante R.J., Siwek D.F., Wilcox H.M., Flood D.G., Beal M.F., Brown R.H. Jr, Scott R.W., Snider W.D. (1996) Motor neurons in Cu/Zn superoxide dismutase-deficient mice develop normally but exhibit enhanced cell death after axonal injury, Nature Genetics 13(1): 43-7.

Reddy V.N., Giblin F.J., Lin L.R., Dang L., Unakar N.J., Musch D.C., Boyle D.L., Takemoto L.J., Ho Y.S., Knoernschild T. (2001) Glutathione Peroxidase-1 Deficiency Leads to Increased Nuclear Light Scattering, Membrane Damage, and Cataract Formation in Gene-Knockout Mice, Investigative Ophthalmology and Visual Science 42 (13): 3247-55

Rego A.C., Santos M.S., Oliveira C.R. (2000) Glutamate-mediated inhibition of oxidative phosphorylation in cultured retinal cells, Neurochemistry International 36 (2): 159-66

Reme C., Grimm C., Hafezi F., Marti A., Wenzel A. (1998) Apoptotic cell death in retinal degenerations, Progress in Retinal and Eye Research 17 (4): 443-464

Reme C.E., Wolfrum U., Imsand C., Hafezi F., Williams T.P. (1999) Photoreceptor autophagy: effects of light history on number and opsin content of degradative vacuoles, Investigative Ophthalmology and Visual Science 40 (10): 2398-404

Remington S.J. (1992) Structure and mechanism of citrate synthase, Current Topics of Cellular Regulation 33: 209-29

RetNet at http://www.sph.uth.tmc.edu/Retnet/home.htm, provided in the public domain by the University of Texas Houston Health Science Center, Houston, TX

Rideout D.C., Calogeropoulou T., Jaworski J.S., Dagnino R., McCarthy M.R. (1989) Anticancer drug design 4: 265-280

Rivera M.C. and Lake J.A. (2004) The ring of life provides evidence for a genome fusion origin of eukaryotes, Nature 431 (7005): 152-5

Rivolta C., Sharon D., DeAngelis M.M., Dryja T.P. (2002) Retinitis pigmentosa and allied diseases: numerous diseases, genes and inheritance patterns, Human Molecular Genetics 11: 1219-27

Rodieck R.W. (1973) The Vertebrate retina: principles of structure and function, W.H. Freeman and Company

Rong Y, Doctrow S.R., Tocco G., Baudry M. (1999) EUK-134, a synthetic superoxide dismutase and catalase mimetic, prevents oxidative stress and attenuates kainate-induced neuropathology, Proceedings of the National Academy of Sciences of the United States of America 96 (17): 9897-902

Rose G., Passarino G., Franceschi C., De Benedictis G. (2002) The variability of the mitochondrial genome in human aging: a key for life and death? The International Journal of Biochemistry and Cell Biology 34: 1449-1460

Rosen D. R., Siddique T., Patterson D., Figlewicz D.A., Sapp P., Hentati A., Donaldson D., Goto J., O'Regan J.P., Deng, H.-X., Rahmani Z., Krizus A., McKenna-Yasek D., Cayabyab A., Gaston S. M., Berger R., Tanzi R. E., Halperin J.J., Herzfeldt B., Van den Bergh R., Hung W.-Y., Bird T., Deng G., Mulder D. W., Smyth C., Laing N. G., Soriano E., Pericak-Vance M. A., Haines J., Rouleau G. A., Gusella J. S., Horvitz H. R., Brown R. H., Jr. (1993) Mutations in Cu/Zn superoxide dismutase gene are associated with familial amyotrophic lateral sclerosis, Nature 362: 59-62

Rothstein J.D., Bristol L.A., Hosler B., Brown R.H., Jr., Kuncl R.W. (1994) Chronic inhibition of superoxide dismutase produces apoptotic death of spinal neurons, Proceedings of the National Academy of Sciences of the United States of America 91: 4155-4159

Rozen H. and Skaletsky H. (2000) Primer3 on the WWW for general users and for biologist programmers. Methods in Molecular Biology 132:365-86

Rustin P., Rotig A., Munnich A., and Sidi D. (2002) Heart hypertrophy and function are improved by idebenone in Friedreich's ataxia, Free Radical Research 36: 467-9.

Samali A., Zhiyotovsky B., Jones D., Nagata S., Orrenius S. (1999) Apoptosis: cell death defined by caspase activation, Cell Death and differentiation 6 (6): 495-6

Sambrook J., Fritsch E.F., Maniatis T. (1989) Molecular Cloning, A Laboratory Manual, 2nd edition, Cold Spring Harbour Laboratory, New York: Cold Sping Harbour

Sandbach J.M., Coscun P.E., Grossniklaus H.E., Kokoszka J.E., Newman N.J., Wallace D.C. (2001) Ocular pathology in mitochondrial superoxide dismutase (Sod2)-deficient mice, Investigative Ophthalmology and Visual Science 42: 2173-2178

Sanjuan-Pla A., Cervera A.M., Apostolova N., Garcia-Bou R., Victor V.M., Murphy M.P., McCreath K.J. (2005) A targeted antioxidant reveals the importance of mitochondrial reactive oxygen species in the hypoxic signaling of HIF-1a, FEBS Letters 579: 2669-2674

Sanvicens N., Gomez-Vicente V., Masip I., Messeguer A., Gotter T.G. (2004) Oxidative stress-induced apoptosis in retinal photoreceptor cells is mediated by

calpains and caspases and blocked by the oxygen radical scavenger CR-6. The Journal of Biological Chemistry 279 (38): 39268-39278

Sanyal S., De Ruiter A., Hawkins R.K. (1980) Development and degeneration of retina in rds mutant mice: light microscopy, Journal of Comparative Neurology 194 (1): 193-207.

Sanyal S., Fletcher R., Liu Y.P., Aguirre G., Chader G. (1984) Cyclic nucleotide content and phosphodiesterase activity in the rds mouse (020/A) retina, Experimental Eye Research 38 (3): 247-56.

Saretzki G., Murphy M.P., von Zglinicki T., (2003) MitoQ counteracts telomere shortening and elongates lifespan of fibroblasts under mild oxidative stress, Aging Cell 2: 141-3

Sarra G.M., Stephens C., de Alwis M., Bainbridge J.W., Smith A.J., Thrasher A.J., Ali R.R. (2001) Gene replacement therapy in the retinal degeneration slow (rds) mouse: the effect on retinal degeneration following partial transduction of the retina, Human Molecular Genetics 10 (21): 2353-61

Sarver A., Scheffler N.K., Shetlar M.D., Gibson B.W. (2001) Analysis of peptides and proteins containing nitrotyrosine by matrix-assisted laser desorption/ionization mass spectrometry, Journal of the American Society of mass spectrometry 12 (4): 439-48

Schalken J.J., Janssen J.J., de Grip W.J., Hawkins R.K., Sanyal S. (1985) Immunoassay of rod visual pigment (opsin) in the eyes of rds mutant mice lacking receptor outer segments, Biochimica et Biophysica Acta. 839 (1): 122-6.

Schapira A.H. (1999) Mitochondrial involvement in Parkinson's disease, Huntington's disease, hereditary spastic paraplegia and Friedreich's ataxia, Biochimica et Biophysica Acta 1410 (2): 159-70

Schmidt S.Y. and Lolley R.N. (1973) Cyclic-nucleotide phosphodiesterase: an early defect in inherited retinal degeneration of C3H mice, Journal of Cellular Biology. 57 (1): 117-23

Schriner S.E., Linford S.W., Jones M.E., Osborne B.A., Treuting P., Ogburn C.E., Emond M., Coskun P.E., Ladiges W., Wolf N., Van Remmen H., Wallace D.C., Rabinovitch P.S. (2005) Extension of murine life span by overexpression of catalase targeted to mitochondria, Science 308 (5730): 1875-6

Schwartz L.M., Smith S.W., Jones M.E., Osborne B.A. (1993) Do all programmed cell deaths occur via apoptosis? Proceedings of the National Academy of Sciences of the United States of America 90 (3): 980-4

Schwartz L.M., Smith S.W., Jones M.E.E., Osborne B.A. (1993) Do all programmed cell deaths occur via apoptosis? Proceedings of the National Academy of Sciences of the United States of America 90: 980-984

Scorrano L., Ashiya M., Buttle K., Weiler S., Oakes S.A., Mannella C.A., Korsmeyer S.J. (2002) A distinct pathway remodels mitochondrial cristae and mobilizes cytochrome c during apoptosis, Developmental Cell 2 (1): 55-67

Scovassi A.I. and Diederich M. (2004) Modulation of poly (ADP-ribosylation) in apoptotic cells, Biochemical Pharmacology 68: 1041–1047

Sennlaub F., Courtois Y., Goureau O. (2002) Inducible nitric oxide synthase mediates retinal apoptosis in ischemic proliferative retinopathy, Journal of Neuroscience 22 (10): 3987-93

Sentman C.L., Shutter J.R., Hockenbery D., Kanagawa O., Korsmeyer S.J. (1991) bcl-2 inhibits multiple forms of apoptosis but not negative selection in thymocytes, Cell 67 (5): 879-88

Shen J., Yang X., Dong A., Petters R.M., Peng Y., Wong F., Campochiaro P.A. (2005) Oxidative damage is a potential cause of cone cell death in retinitis pigmentosa, Journal of Cellular Physiologu 203: 457-464

Shepherd D. and Garland P.B. (1969) The kinetic properties of citrate synthase from rat liver mitochondria, Biochemical Journal 114: 597

Shibutani S., Takeshita M., Grollman A.P. (1991) Insertion of specific bases during DNA synthesis past the oxidation-damaged base 8-oxodG, Nature 349 (6308): 431-4

Sidman R.L. and Green M.C. (1965) Retinal degeneration in the mouse: location of the rd locus in linkage group XVIII, Journal of Heredity 6: 23-9

Siler-Marsiglio K., Pan Q., Paiva M., Madorsky I., Khurana N.C., Heaton M.B. (2005) Mitochondrially targeted vitamin E and vitamin E mitigate ethanol-mediated effects on cerebellar granule cell, Brain Research 1052: 202-211

Singh A.K. and Shichi H. (1998) A novel glutathione peroxidase in bovine eye. Sequence analysis, mRNA level, and translation, Journal of Biological Chemistry 273 (40): 26171-8

Sjostrand F.S. (1953) The ultrastructure of the inner segments of the retinal rods of the guinea pig eye as revealed by electron microscopy, Journal of Cell Physiology 42 (1): 45-70

Skulachev V.P. (2006) Bioenergetic aspects of apoptosis, necrosis and mitoptosis, Apoptosis 11 (4): 473-85

Skulachev V.P., Bakeeva L.E., Chernyak B.V., Domnina L.V., Minin A.A., Pletjushkina O.Y., Saprunova V.B., Skulachev I.V., Tsyplenkova V.G., Vasiliev J.M., Yaguzhinsky L.S., Zorov D.B. (2004) Thread-grain transition of mitochondrial reticulum as a step of mitoptosis and apoptosis, Molecular and Cellular Biochemistry 256-257 (1-2): 341-58

Slee E.A., Adrain C., Martin S.J. (1999) Serial killers: ordering caspase activation events in apoptosis, Cell Death and Differentiation 6 (11): 1067-74

Slee E.A., Harte M.T., Kluck R.M., Wolf B.B.,Casiano C.A., Newmeyer D.D., Wang H.G., Reed J.C., Nicholson D.W., Alnemri E.S., Green D.R., Martin S.J. (1999) Ordering the cytochrome c-initiated caspase cascade: hierarchical activation of caspases-2, -3, -6, -7, -8, and -10 in a caspase-9-dependent manner, Journal of Cell Biology 144 (2): 281-92

Smith R.A., Porteous C.M., Coulter C.V., Murphy M.P. (1999) Selective targeting of an antioxidant to mitochondria, European Journal of Biochemistry 263 (3): 709-16

Smith R.A., Porteous C.M., Gane A.M., Murphy M.P. (2003) Delivery of bioactive molecules to mitochondria *in vivo*, Proceedings of the National Academy of Sciences of the United States of America 100: 5407-12

Smith R.S., John S.W.M., Nishina P.M. (2002b) Posterior Segment and orbit, *In* Systematic evaluation of the mouse eye: anatomy, pathology and biomethods (ed. R.S. Smith), CRC Press

Smith R.S., Sundberg J.P., John S.W.M. (2002a) The anterior segment and ocular adnexae, *In* Systematic evaluation of the mouse eye: anatomy, pathology and biomethods (ed. R.S. Smith), CRC Press

Smulson M.E., Pang D., Jung M., Dimtchev A., Chasovskikh S., Spoonde A., Simnulan-Rosenthal C., Rosenthal D., Yakovlev A., Dritschilo A. (1998) Irreversible binding of poly(ADP)ribose polymerase cleavage product to DNA ends revealed by atomic force microscopy: possible role in apoptosis, Cancer Research 58 (16): 3495-8

Sohal R.S., Sohal B.H., Brunk U.T. (1990) Relationship between antioxidant defenses and longevity in different mammalian species, Mechanisms of Ageing and Development 53 (3): 217-27

Sohal R.S., Svensson I., Brunk U.T. (1990) Hydrogen peroxide production by liver mitochondria in different species, Mechanisms of Ageing and Development 53 (3): 209-15

Sohal R.S., Svensson I., Sohal B.H., Brunk U.T. (1989) Superoxide anion radical production in different animal species, Mechanisms of Ageing and Development 49 (2): 129-35

Soultanakis R.P., Melamede R.J., Bespalov I.A., Wallace S.S., Beckman K.B., Ames B.N., Taatjes D.J., Janssen-Heininger Y.M. (2000) Fluorescence detection of 8-oxoguanine in nuclear and mitochondrial DNA of cultured cells using a recombinant Fab and confocal scanning laser microscopy, Free Radical Biology and Medicine 28 (6): 987-98

Spierings D., McStay G., Saleh M., Bender C., Chipuk J., Maurer U., Green D.R. (2005) Connected to death: the (unexpurgated) mitochondrial pathway of apoptosis, Science 310 (5745): 66-7

Stadelmann C. and Lassmann H. (2000) Detection of apoptosis in tissue sections, Cell Tissue Research 301 (1): 19-31

Steinberg R.H. (1987) Monitoring communications between photoreceptors and pigment epithelial cells: effects of "mild" systemic hypoxia. Friedenwald lecture, Investigative Ophthalmology and Visual Science 28 (12): 1888-904.

Stone W.L., Farnsworth C.C., Dratz E.A. (1979) A reinvestigation of the fatty acid content of bovine, rat and frog retinal rod outer segments, Experimental Eye Research 28 (4): 387-97

Sung C.H., Makino C., Baylor D., Nathans J. (1994) A rhodopsin gene mutation responsible for autosomal dominant retinitis pigmentosa results in a protein that is defective in localization to the photoreceptor outer segment. Journal of Neuroscience 14 (10): 5818-33.

Sverko V., Balog T., Sobocanes S., Gayella M., Marotti T. (2002) Age-associated alteration of lipid peroxidation and superoxide dismutase activity in CBA and AKR mice, Experimental Gerontology 37 (8-9): 1031-9

Tan E., Wang Q., Quiambao A.B., Xu X., Qtaishat N.M., Peachey N.S., Lem J., Fliesler S.J., Pepperberg D.R., Naash M.I., Al-Ubaidi M.R. (2001) The relationship between opsin overexpression and photoreceptor degeneration, Investigative Ophthalmology and Visual Science 42 (3): 589-600.

Tartelin E.E., Bellingham J., Bibb L.C., Foster R.G., Haskins M.W., Gregory-Evans K., Gregori-Evans C.Y., Wells D.J., Lucas R.J. (2003) Expression of opsin genes early in ocular development of humans and mice, Experimental Eye Research 76: 393-396

Taylor R.W. and Turnbull D.M. (1997) Laboratory diagnosis of mitochondrial disease, In Organelle disease (eds. D.A. Applegarth, J.E. Dimmick and J.G. Hall), Chapman & Hall, London

Thaung C., West K., Clark B.J., McKie L., Morgan J.E., Arnold K., Nolan P.M., Peters J., Hunter A.J., Brown S.D., Jackson I.J., Cross S.H. (2002) Novel ENU-induced eye mutations in the mouse: models for human eye disease. Human Molecular Genetics 11(7): 755-67.

Tietze F. (1969) Enzymic method for quantitative determination of nanogram amounts of total and oxidised glutathione: Applications to mammalian blood and other tissues. Analytical Biochemistry 27: 502-522

Toda K., Bush R.A., Humphries P., Sieving P.A. (1999) The electroretinogram of the rhodopsin knockout mouse. Visual Neuroscience 16(2): 391-8.

Travis G.H. (1998) Mechanisms of cell death in the inherited retinal degenerations, American Journal of Human Genetics 62 (3): 503-8

Travis G.H., Brennan M.B., Danielson P.E., Kozak C.A., Sutcliffe J.G.(1989) Identification of a photoreceptor-specific mRNA encoded by the gene responsible for retinal degeneration slow (rds), Nature. 338(6210): 70-3.

Travis G.H., Sutcliffe J.G., Bok D. (1991) The retinal degeneration slow (rds) gene product is a photoreceptor disc membrane-associated glycoprotein, Neuron 6 (1): 61-70

Tsan M.F., White J.E., Caska B., Epstein C.J., Lee C.Y. (1998) Susceptibility of heterozygous MnSOD Gene-knockout mice to oxygen toxicity, American Journal of Respiratory Cell and Molecular Biology 19: 114-120

Uchida M., Hanai S., Uematsu N., Sawamoto K., Okano H., Miwa M., Uchida K. (2001) Genetic and functional analysis of PARP, a DNA strand break-binding enzyme, Mutation Research 477: 89-96

Ursini F., Maiorino M., Brigelius-Flohe R., Aumann K.D., Roveri A., Schomburg D., Flohe L. (1995) Diversity of glutathione peroxidases, Methods in Enzymology 252: 38-53

Van Nie R., Ivanyi D., Demant P. (1978) A new H-2-linked mutation, rds, causing retinal degeneration in the mouse. Tissue Antigens 12(2): 106-8

Van Remmen H., Ikeno Y., Haminlton M., Pahlavani M., Wolf N., Thorpe S.R., Alderson N.L., Baynes J.W., Epstein C.J., Huang T.T., Nelson J., Strong R., Richardson A. (2003) Life-long reduction in MnSOD activity results in increased DNA damage and higher incidence of cancer but does no accelerate aging, Physiological Genomics 16: 29-37

Van Remmen H., Salvador C., Yang H., Huang T.T., Epstein C.J., Richardson A. (1999) Characterisation of the antioxidant status of the heterozygous manganese superoxide dismutase knockout mouse, Archives of Biochemistry and Biophysics 363 (1): 91-97

Van Remmen H., Williams M.D., Guo Z., Estlack L., Yang H., Carlson E.J., Epstein C.J., Huang T.T., Richardson A. (2001) Knockout mice heterozygous for *Sod2* show alterations in cardiac mitochondrial function and apoptosis. American Journal of Physiology Heart and Circulation Physiology 281: H1422-H1432

Van Soest S., Westerveld A., de Jong P.T., Bleeker-Wagemakers E.M., Bergen A.A. (1999) Retinitis pigmentosa: defined from a molecular point of view, Survey of Ophthalmology 43 (4): 321-34

Wacholder A., Chanock S., Garcia-Closas M., El Ghormli L., Rothman N. (2004) Assessing the probability that a positive report is false: an approach for molecular epidemiology studies., Journal of National Cancer Institute 96 (6): 434-42

Wagner R., Ryda N. Uhl R. (1989) Calcium regulates the rate of rhodopsin disactivation and the primary amplification step in visual transduction, FEBS Letters 242 (2): 249-54

Wallace D.C. (2005) A mitochondrial paradigm of metabolic and degenerative diseases, aging, and cancer: a dawn for evolutionary medicine, Annual Review of Genetics 39: 359-407

Williams M.D., Van Remmen H., Conrad C.C., Huang T.T., Epstein C.J., Richardson A. (1998) Increased oxidative damage is correlated to altered mitochondrial function in heterozygous manganese superoxide dismutase knockout mice. The Journal of Biological Chemistry 273 (43): 28510-28515

Winkler B.S., Boulton M.E., Gottsch J.D., Sternberg P. (1999) Oxidative damage and age-related macular degeneration, Molecular Vision 5: 32

Wislocki G.B. and Sidman R.L. (1954) The chemical morphology of the retina, Journal of Comparative Neurology 101 (1): 53-99

Wolf B.B. and Green D.R. (1999) Suicidal tendencies: apoptotic cell death by caspase family proteinases, Journal of Biological Chemistry 274 (29): 10049-52

Wolf B.B. and Green D.R. (2002) Apoptosis: letting slip the dogs of war, Current Biology 12: R177-R179

Wolf B.B., Schuler M., Echeverri F., Green D.R. (1999) Caspase-3 is the primary activator of apoptotic DNA fragmentation via DNA fragmentation factor-45/inhibitor of caspase-activated DNase inactivation, Journal of Biological Chemistry 274 (43): 30651

Wright A.F., Jacobson S.G., Cideciyan A.V., Roman A.J., Shu X., Vlachantoni D., McInnes R.R., Riemersma R.A. (2004) Lifespan and mitochondrial control of neurodegeneration. Nature Genetics 36 (11): 1153-1158

Yakes F.M. and Van Houten B. (1997) Mitochondrial DNA damage is more extensive and persists longer than nuclear DNA damage in human cells following oxidative stress, Proceedings of the National Academy of Sciences of the United States of America 94 (2): 514-9

Yamada H., Yamada E., Ando A., Esumi N., Bora N., Saikia J., Sung C., Zack D.J., Campochiaro P.A. (2001) Fibroblast Growth Factor-2 Decreases Hyperoxia-induced photoreceptor cell death in mice. American Journal of Pathology 159 (3): 1113-20

Yang Y., Sharma R., Sharma A., Awasthi S., Awasthi Y.C. (2002) Lipid peroxidation and cell cycle signaling: 4-hydroxynonenal, a key molecule in stress mediated signaling, Acta Biochimica Polonika 50 (2): 319-336

Yang Y., Sharma R., Sharma A., Awasthi S., Awasthi Y.C. (2003) Lipid peroxidation and cell cycle signaling: 4-hydroxynonenal, a key molecule in stress mediated signaling, Acta Biochimica Polonika 50 (2): 319-336

Yang Z.W., Zheng T., Zhang A., Altura B.T., Altura B.M. (1998) Mechanisms of hydrogen peroxide-induced contraction of rat aorta, European Journal of Pharmacology 344 (2-3): 169-81

Yen H.C., Oberley T.D., Vichitbandha S., Ho Y.S., St.Clair S.K. (1996) The protective role of manganese superoxide dismutase against adriamycin-induced acute cardiac toxicity in transgenic mice, Journal of Clinical Investigation 98 (5): 1253-1260

Young R.W. (1984) Cell death during differentiation of the retina in the mouse, Journal of Comparative Neurology 229 (3): 362-73

Yuan J., Lipinski M., Degterev A. (2003) Diversity in the mechanisms of neuronal cell death, Neuron 40: 401-413

Zarkovic K. (2003) 4-Hydroxynonenal and neurodegenerative diseases, Molecular Aspects of Medicine 24: 293-303

Zarkovic N. (2003) 4-Hydroxynonenal as a bioactive marker of pathophysiological processes, Molecular Aspects of Medicine 24: 281-291

Zelko I.N., Mariani T.J., Folz R.J. (2002) Superoxide dismutase multigene family: a comparison of the CuZn-SOD (SOD1), Mn-SOD (SOD2), and EC-SOD (SOD3) gene structures, evolution, and expression, Free Radical Biology and Medicine 33 (3): 337-49

Zhang C., Shen J., Lam T.T., Zeng H., Chiang S.K., Yang F., Tso M.O.M. (2005) Activation of microglia and chemokines in light-induced retinal degeneration, Molecular Vision 11: 887-95

Zhang Y., Aberg F., Appelkvist E-L, Dallner G., Ernster L. (1995) Uptake of dietary coenzyme Q supplement is limited in rats, Journal of Nutrition 125: 446-453

Zhong L.T., Sarafian T., Kane D.J., Charles A.C., Mah S.P., Edwards R.H., Bredesen D.E. (1993) Bcl-2 inhibits death of central neural cells induced by multiple agents, Proceedings of the National Academy of Sciences of the United States of America 90 (10): 4533-7